ERRATA to

Some Physical Properties of Granite at High Pressure

and Temperature

by Ide van der Molen

pv, line 3	------------------	classical
pvi, line 6	------------------	granites; Yoder
p10, line 17	------------------	(6 percent melt),
p36, Fig. 4.2	------------------	Symbols are inadvertantly omitted from the legend and should be corrected to read 2976 (▼), 2847 (0), 2854 (◑), 2979 (●) and 3031 (■)
p62, line 2g	------------------	in (1) on
p102, line 10	------------------	or K, <- $\frac{4}{3}$ μ
p125, line 15	------------------	O'Connell; also p156, line 4 O'Connell
p131, line 29	------------------	Kern, in prep.).
p138, line 17	------------------	Liebermann et al. (1975); also p. R6, line 29 (1975)
p142, line 11	------------------	delete , after data
p145, line 4	------------------	attenuated
p154, Fig. 14.7	------------------	Voigt and Reuss bounds reversed.
p A4, bottom line	------------------	$\phi_o = 1 - \dfrac{\pi}{\sqrt{18}} = 0.26.$

SOME PHYSICAL PROPERTIES OF GRANITE AT HIGH PRESSURE AND TEMPERATURE

A thesis submitted for the degree of

DOCTOR OF PHILOSOPHY

at the

AUSTRALIAN NATIONAL UNIVERSITY
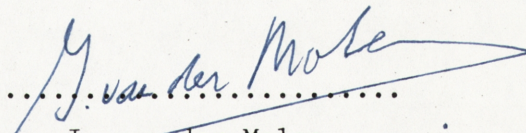
by

IDE VAN DER MOLEN

February 1979

<u>STATEMENT</u>

The work described in this thesis was carried out while I was a full-time research scholar in the Research School of Earth Sciences, at the Australian National University, during the period September, 1975 to February, 1979 with the exception of May and June, 1977.

Except where mentioned in the text or the acknowledgements, the research described in this thesis is my own.

No part of this thesis has been submitted to another university or similar institution.

....

I. van der Molen

Canberra, February, 1979.

ACKNOWLEDGEMENTS

PREFACE

One can study the earth without becoming involved with granite as one may appreciate German literature without reading Thomas Mann, or enjoy clasical music without having heard of J.S. Bach. A "granitoid" or granite *s.l.* is a granular igneous rock consisting of K-feldspar, quartz, plagioclase, minor amounts of mica or hornblende and accessory minerals. Granites occur in intrusions in a wide range of shapes and sizes, and form together with their gneissic counterparts the dominant rock type of the upper half of the continental crust. By nature of their importance and high degree of exposure at the surface, granites are also the most widely studied rocks. Tens of thousands of geologists have studied their petrology and mineralogy, their relationships with surrounding rocks in the field, their deformation structures, their ore content, their age, chemistry and possible origin. Geochemical studies both experimental and on natural granites, have put important constraints on the pressure and temperature during granite formation, on the composition of the source rock, on the melt-fraction of the magma and on the amount of mixing and unmixing during transport and emplacement. An increasing number of studies is devoted to physical and mechanical properties of granite, to its strength, permeability, heat- and electrical conductivity etc., and to its plastic deformation at high pressure and temperature. Further parameters of geophysical importance are the elastic properties of granite controlling the transmission of seismic waves, and other small recoverable deformations.

This thesis contains three experimental studies, each concerned with different physical properties of granite under high pressure and temperature conditions as pertaining at depth in the crust. The studies have in common the use of the same specimen material and the same experimental apparatus, but may – apart from some cross references between parts II and III – be read separately.

In part I (Chapters 1-8), I discuss the rheological properties of granite magma placing emphasis on the role of melt fraction. In spite of the wealth of data on granites there are no satisfactory answers to many simple questions related to their origin and emplacement: How does melt collect if it separates from its source rock, and what melt fraction is needed before a magma body develops a sufficiently high density contrast with its surroundings to rise at a geologically appreciable rate in the earth's gravitational field? To what extent is the rising of a magma body controlled

by the rheological properties of the surrounding material (highly unlikely
to be Newtonian as often assumed), and to what extent by rheological
properties of the magma itself? How do these properties vary if heat
exchange takes place with the surroundings during migration of the magma?
What strainrates and what stress-systems are involved and what volumes of
material? Such questions are not restricted to granites, Yoder (1976)
discussed some of them in relation to the generation of basaltic magma.
Geochemical and field studies alone cannot provide the answers. Indeed,
it would appear that a stage has been reached where the *general understanding
of magmatic processes* might be better advanced by study of the mechanical
aspects of the problem than by renewed mapping efforts, more measurements
of Rare Earth Element distributions or new detailed studies of simple
geochemical systems.[1] The determination of flow properties of partially-
melted granite is but a small contribution to answering the problems posed
above. However, the general conclusions from this study of deformation of
partially-melted granite (Chapters 7 and 8) are thought to be relevant also
in the wider context of general magmatic processes.

Part II (Chapters 9-12) deals with the thermal expansion of
granite over a range of confining pressures. A by-product of this study
is the confirmation of an effect which has been called the "shift of the
quartz $\alpha-\beta$ transition temperature" by its discoverer Kern (1978, in prep.).
The transition temperature of quartz in granite is found to increase
roughly three times more with confining pressure than in the case of single
crystals, because of stress inhomogeneities in the granite polycrystal.
A model for granite and an elastic theory are proposed which account for
both the magnitude of the "shift" and for the observation that the transition
in the polycrystal does not occur over a large range in temperature. The
prediction of the model for the maximum confining pressure at which cracks
may open in granite due to differential thermal expansion of the constituent
minerals is in good agreement with the experimental observations. The theory
may further be used to relate the small crack porosities, observed in igneous
rocks to volume changes of the constituent minerals during decompression and
cooling on the way to the surface. Possible practical application of the
thermal expansion data may be found in relation to the drilling of deep holes

---

[1] With apologies to those who have submitted proposals along these lines.

in the crust.

Part III (Chapters 12-14) may be read as a progress report on the development and testing of a specimen assembly with which the velocity of compressional - and shear waves through specimens of natural crystalline rocks can be measured at high pressure and temperature with the ultrasonic pulse transmission method. Preliminary results for dry and water saturated granite are presented and discussed in Chapter 14. The study has a bearing on the interpretation of seismic wave velocities through crustal rocks and some progress is made in understanding the factors controlling the temperature and pressure dependence of the elasticity of granite. It is argued however, that the large effect of cracks on velocity as observed in experiments, limits the direct application of the measurements to geophysical problems. The stress inhomogeneities caused by differential thermal expansion of the constituent minerals of granite persist over the period of an experiment and keep cracks open against the confining pressure, and cause the quartz α-β "shift" (part II). In natural rocks, for geological periods at high lithostatic pressure and high temperature, stress inhomogeneities will tend to relax, cracks will be closed in the absence of a pore fluid and there will be no shift of the quartz α-β transition.

SOME PHYSICAL PROPERTIES OF GRANITE AT HIGH PRESSURE AND TEMPERATURE

TABLE OF CONTENTS

PART I

EXPERIMENTAL DEFORMATION OF PARTIALLY-MELTED GRANITE

ABSTRACT

Control of melt fraction (up to 25 volume percent) by addition of different amounts of water to granite has facilitated a series of constant strainrate-, creep-, and cycle experiments at 800°C, 300 MPa, to study the rheological properties of partially-melted granite. Subsequent microscopic study of the deformed specimens reveals that under these conditions, most of the uniform deformation prior to macroscopic shear failure is accomplished by the concurrent operation of three distinct mechanisms: i) melt redistribution into films perpendicular to the least compressive stress, ii) relative movement of grains, and iii) axial fracturing of grains - the latter occurring even at low differential stress. At low melt fractions the deforming rock tends to take up melt by a mechanism of dilatancy pumping. The observed rheological behaviour is discussed in terms of simple models of rigid and elastic grains with a viscous fluid filling the interstices, and a dilatancy hardening relationship is derived for the case of hexagonally close-packed spheres. The strength of the partially-melted rock at $10^{-5}s^{-1}$ is found to decrease gradually from about 250 MPa at 5 volume percent melt to about 60 MPa at 15 percent melt, and then to drop rapidly to less than 1 MPa at 24 percent melt. The critical melt fraction separating granular - framework - controlled flow behaviour from suspension-like behaviour is deduced to be approximately 30 to 35 volume percent. The relevance of these results to natural conditions involving partially-melted rocks is discussed.

Chapter 1

THE PROBLEM

1.1   Introduction

Geological processes in the earth's crust and mantle often involve rocks that are melted in some degree, ranging from complete or extensive melting in igneous rocks to a small fractional melting in some migmatites. The generation, transport, differentiation and emplacement of magmas are important examples of such processes.   On a larger scale, flow of partially-melted peridotite with low melt fraction is commonly believed to take place within the asthenosphere.   In all these situations a knowledge of the mechanical properties of partially-melted rock is of importance in understanding the dynamics and structural aspects.

The physically most important property of partially-melted rock is its two-phase nature of solid crystals and a viscous melt.[1]   The present study explores the rheological behaviour of such mixtures as a function of melt fraction, placing particular emphasis on the influence of low degrees of partial melting, and the results of an experimental study on the deformation of partially-melted granite with melt fractions up to 25 volume percent will be presented.

The relevance of such a study to petrological and geophysical problems has been indicated above.   More generally, the understanding of the rheological behaviour of mixtures of solid grains and a viscous pore fluid has applications in a variety of fields.   As examples may be given the fields of ceramics (hot-glass ceramics), chemical engineering (slurrie flow), soil mechanics (stability and strength of wet soils, liquefaction), metallurgy

---

[1]Particularly in magmas at or near to the surface of the earth a third phase may originate in the form of gases leaving the melt under influence of reduced pressure.   This "vesiculation" may affect flow properties of magmas markedly (*e.g.* Shaw *et al.*, 1968) but will not be further considered in this thesis.

(partially-melted alloys), glaciology (temperate glaciers with water as a pore fluid) and sedimentology (debris flow, turbidity currents, bedload transport etc.). A comprehensive review of all the relevant literature from such fields is beyond the aim of this thesis. Reference to authors working in different disciplines will be made at appropriate places in the text.

1.2 Scope of behaviour in partially-melted rock

A large range of flow behaviour can be expected between the endmembers of completely solid and completely melted rock. However, for discussion it is convenient to define two rheological regimes within this range. The first regime is one of suspension-like behaviour in which the crystals or groups of crystals can pass one another during volume-constant flow without becoming "locked-up", and in which the flow properties are largely controlled by the viscosity of the suspending melt and the fraction of suspended material. In the second regime crystals and groups of crystals interlock in the undeformed state or after a small deformation, and further deformation at constant volume can only be achieved with fracturing or plastic deformation of the grains. The latter regime will be called granular framework-controlled, since here the flow behaviour will be influenced more by the rheological properties of the interlocking solids than by that of the melt.

A large rheological contrast may be expected between the two regimes, the transition occurring around *a critical melt fraction*. This critical melt fraction or, for systems other than partially-melted rock, critical fluid fraction can be conveniently defined as the fluid fraction at which the flow stress for volume-constant deformation at a given strain-rate changes most rapidly with fluid fraction, that is at the inflection in the curve in Figure 1.1.

1.3 Behaviour at melt fractions above the critical

Over the range of strainrates in which measurements have been done completely melted rocks behave as ideal Newtonian fluids, the viscosity of which depends on the chemical composition of the melt and on the temperature (e.g. Bottinga and Weill, 1972; Scarfe, 1973). The amount of water in the melt strongly affects the viscosity, especially in the case of siliceous melts (Sabatier, 1956; Shaw, 1963, 1965, 1972; Burnham, 1964;

5.

Figure 1.1   Distinction of two rheological regimes and definition of
a critical fluid fraction.
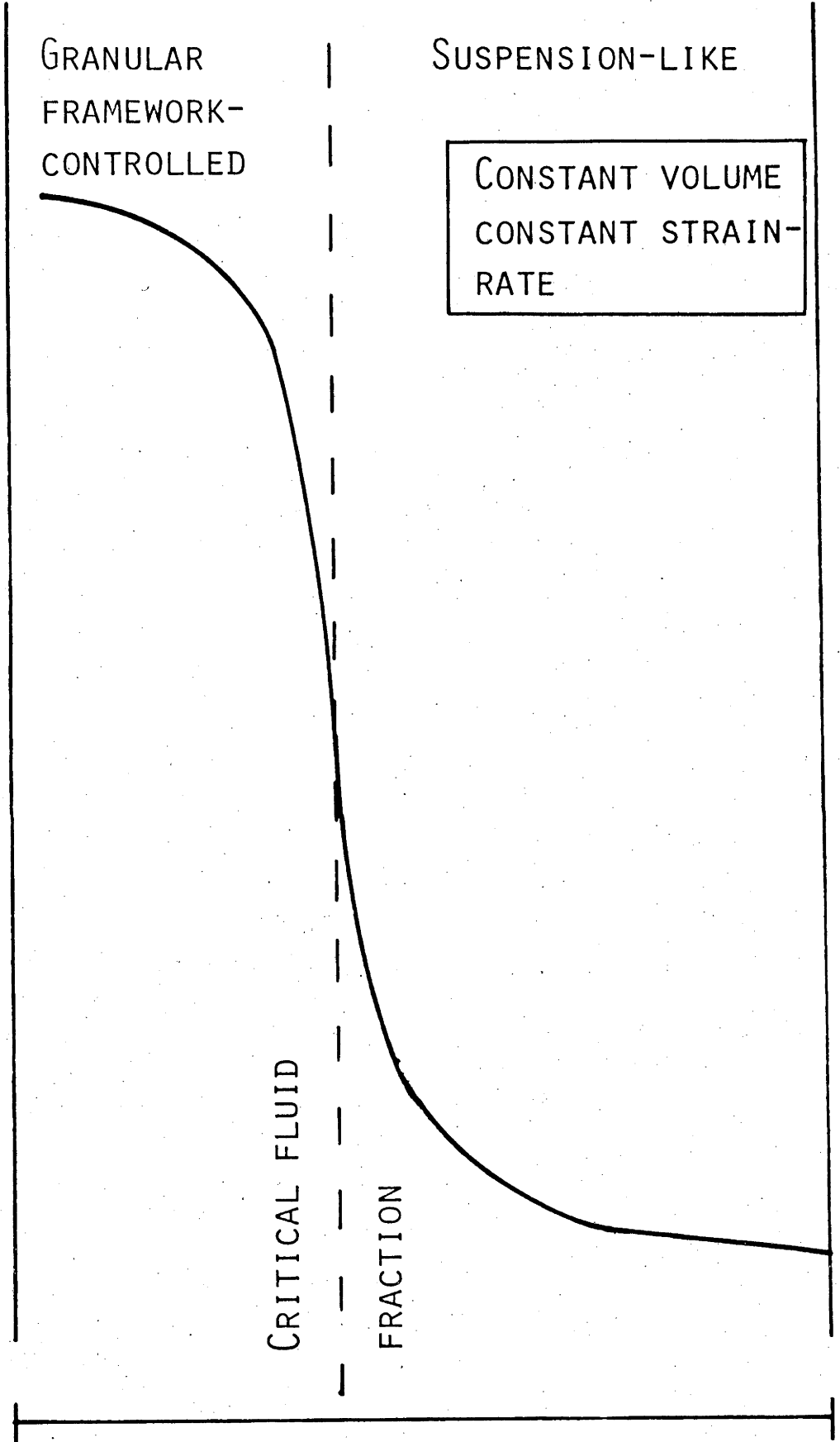
Scarfe, 1973). Consequently pressure has an important indirect influence on the viscosity of siliceous melts through controlling the amount of water and other volatiles, that are dissolved in the melt (e.g. Whitney, 1975; Winkler, 1974), although for a given bulk chemical composition the intrinsic influence of pressure is not appreciable except at very high pressures (>2GPa[1]; see Waff, 1975; Kushiro, 1976; Kushiro *et al.*, 1976).

To estimate the viscosity of melt-crystal suspensions the theoretical and empirical results for "relative viscosity" from studies on suspensions of rigid, neutrally buoyant spheres in a viscous fluid can be applied, if the viscosity of the melt and the fraction of suspended material are known. Relative viscosity is defined as the ratio between the viscosity of the suspension and that of the suspending fluid. Shaw (1965) and Arzi (1978 a) based extrapolations on the theoretical results of Roscoe (1952); in this thesis use will be made of the recent review of Jeffrey and Acrivos (1976) on the subject.

However, not all suspensions are known to behave as ideal Newtonian fluids at all strainrates or all fractions of suspended solids (e.g. Van Wazer *et al.*, 1963). Whether deviation from ideal Newtonian behaviour is observed depends in many cases on the precision of the measurements, and whether such a deviation is important depends on the type of problem for which rheological parameters are to be used. In the latter connection, behaviour approaching that of an ideal Bingham fluid, in which no flow occurs below a yield stress while the strainrate is linearly related to stress above the yield value, has been observed in magmas under natural conditions by Shaw *et al.* (1968) and Sparks *et al.* (1977). The measured values for the yield strength are of the order of 100 Pa, depending somewhat on the melt fraction. Yielding behaviour has also been observed in the laboratory by Shaw (1969) and Murase and McBirney (1973); for a discussion of the rheological measurement of yield stresses see Shaw (1969). Bingham behaviour would explain naturally observed features such as the flow morphology of lava (Johnson, 1970; Hulme, 1974) and xenolith transport in magma (Sparks *et al.*, 1977) more satisfactorily than ideally viscous behaviour.

---

[1]Throughout this thesis the Pascal is used as the unit of pressure or stress: 1 MPa = 10 bars, 1 GPa = 10 kbar. For a table of conversion factors to other units of stress see Hobbs *et al.* (1976, p. 3).

1.4   Estimate of critical melt fraction

To date no single set of rheological experiments exists covering
the full range of fluid fractions indicated in Figure 1.1. The critical
melt fraction therefore has to be estimated theoretically or to be deduced
from trends observed at fluid fractions lower or higher than the critical
fraction itself. Later in this thesis (Chapter 7) a combined approach
is attempted by comparing experimental results for partially-melted
granites on the low melt fraction side with relative viscosity results
for granitic melt suspensions on the high melt fraction side. Here
the value for the critical melt fraction will be discussed in the light
of the existing literature, and the expected effects of grainsize and
grainshape variation will be indicated.

Arzi (1978 a) considered the problem in some detail, although
values as high as 50 volume percent melt are quoted, his estimate of a
"rheological critical melt percentage" is "a non zero value, probably
within the range of 20 ± 10 percent". This estimate is based on the
model of Roscoe (1952) for the relative viscosity of suspensions of
uniform spherical grains which approaches infinity when the *closest packing
density* corresponding to 26 percent porosity is approached. The effect
of grain angularity is to increase this number somewhat. The effect of
a large range in sizes of spheres is to reduce it. However, the value
corresponding to the closest packing density is likely to be unrealistic,
since the packing must be somewhat looser in order that the particles can
move past each other in a sustainable constant-volume flow without "locking-
up" through interference.

It would appear to be more realistic to take as a critical fluid
fraction for mobility as a suspension the porosity value corresponding to
the *random packing density* for uniform spheres, that is 38 or 39 volume
percent (Morgenstern, 1963; Jeffrey and Acrivos, 1976). This figure is
supported by the following observations on granular materials and suspensions:
(1) For granular materials, the appropriate measurements are those of
      critical void ratio, the quantity used in soil mechanics to specify
      the degree of packing at which the granular mass can be deformed
      without volume change in drained tests (Terzaghi and Peck, 1967,
      p. 94); when extrapolated to zero effective confining pressure,
      the critical void ratio corresponds in principle to the critical
      fluid fraction defined here. In general the fluid fraction at the

critical void ratio is approximately equal or slightly less than the porosity corresponding to the minimum bulk density as determined in a pouring test (see various observations in Selig and Ladd, 1973). Thus, at the minimum bulk density for uniform glass spheres, the porosity is 42-43 percent (Brand, 1973; Dickin, 1973), and the critical void ratio determined in shear tests at minimal effective confining pressure corresponds to a porosity of 40 percent for uniform steel balls and 42 percent for uniform glass balls (Roscoe *et al*., 1958). The critical void ratio for uniform fine sand corresponds to a porosity of 44-45 percent, as determined by zero volume change in triaxial and shear tests at minimum effective confining pressure (Cornforth, 1973) or by liquefaction tests (Castro, 1969; Durham and Townsend, 1973). The latter figure is slightly higher than for steel and glass balls, probably reflecting some departure from spherical shape of the sand grains since the porosity at minimum bulk density also increases with increasing angularity in grain shape (Dickin, 1973; Holubec and D'Appolonia, 1973; Youd, 1973).

(2) A critical melt fraction between 35 and 45 percent for material with approximately equant grains is also suggested by the hydrostatic experiments of Arndt (1977) on melt separation in crushed garnet lherzolite. Over the time of the experiment no melt separation occurred in a specimen melted to 35 percent, whereas one fifth of the melt had separated out by gravitational settling of the crystals in a specimen melted to 55 volume percent.

(3) In the case of dense suspensions (see review by Jeffrey and Acrivos, 1976), empirical formulae have been fitted to the dependence of viscosity on concentration and the extrapolation of these formulae to infinite viscosity also yields in principle a value of the critical fluid fraction. For example observations by Krieger on suspensions of spherical particles, taken at the limit where Brownian movement and electrical effects are unimportant, have been extrapolated to infinite viscosity to give a critical fluid fraction of 32 percent (Jeffrey and Acrivos, 1976).

(4) The maximum phenocryst concentration found at the centers of flow differentiated basic dikes and sills of moderate width varies between 50 and 70 percent, the phenocryst concentration dropping gradually to values close to zero at the margins of the intrusion.

This phenomenon has been ascribed to the "Bagnold Effect", a mechanism of grain dispersive pressure acting between suspended phenocrysts during flow and leading to concentration in the center of a conduit where shear rates during emplacement of magmas are lowest (e.g. Komar, 1972 a and b, 1976; Barrière, 1976). In the present context it is important to note that the phenocryst concentration does not exceed 50 to 70 percent, again indicating a major change in rheological properties of magmas around 40 percent melt fraction.

The values of critical fluid fraction deduced from determinations of critical void ratio in granular masses may be too high on account of frictional effects, and the value from extrapolated viscosity of suspensions may be too low on account of the contact interferences between particles not being fully effective yet in the range of fluid fractions studied (greater than 50 percent) and so not being fully reflected in the empirical formulae used for extrapolation. These observations support the conclusion that for uniform spheres the geometrical boundary between mobility and immobility in an incompressible fluid medium lies approximately at the fluid volume fraction of 38-39 percent. However, the observations of Chong *et al.* (1971) on the influence of mixed particle sizes on the viscosity of suspensions, and the observation that the maximum porosity decreases with increasing range of grain sizes (Dickin, 1973; Youd, 1973) suggests that this critical fluid fraction will decrease quite markedly with the introduction of a wide range of grain sizes, although that effect could be mitigated in some degree by increased angularity of grain shape.

Finally it seems appropriate to point out that the estimates of critical melt fraction presented above are essentially based on a change in rheological behaviour when approached from the high melt or fluid fraction-side. The proper definition of critical melt fraction related to stress changes over the transition interval between the suspension-like and granular framework-controlled regimes is given in Section 1.2 and Figure 1.1. It may be concluded that the critical melt fraction in equigranular partially melted rock will lie close to, but somewhat below, 38 - 39 percent.

1.5   Behaviour at melt fractions below the critical

1.5.1   Previous work

Uniaxial deformation of partially-melted dolerite and micro-granodiorite was studied by Murrell and Chakravarti (1973). However, in such experiments with unsealed specimens, pores and cracks can open up and lead to early cohesive failure in a way that would not occur at depth in the earth. To avoid this limitation, specimen jacketing and confining pressure must be used. Preliminary experiments of such a kind were done by Murrell and Ismail (1976) who deformed two jacketed partially-melted granodiorite specimens to 5 and 8 percent shortening strain at 670^0 and 720°C respectively at confining pressures of 450 MPa and a strainrate of $10^{-5} s^{-1}$. Earlier Ave'Lallemant and Carter (1970) had observed local partial melting in a lherzolite deformed in solid medium apparatus at 1500 MPa confining pressure; they noted that the zones of melt tended to be oriented parallel to the maximum compressive principal stress. Arzi (1978 a and b) experimentally deformed three partially-melted granite specimens at 860^0 (6 percent melt) 960^0 (12 percent melt) and 1020^0C (17 percent melt) but gives little experimental detail. The results were expressed as "effective viscosities" respectively 10^8, 10^8 and 10^6 times higher than the viscosity of the melt.

1.5.2   Two important factors

The experimental work at low melt fractions is thus rather limited. To predict the rheological behaviour, comparison could again be made with other fields. An analogy with wet sands, see for instance the textbook on soil mechanics by Lambe and Whitman (1969), would indicate that a partially-melted rock with a low melt fraction, in which the crystals behave as rigid-brittle grains, will tend to increase in volume during deformation (dilatancy) when grains climb over one another to overcome interlocking, and that localized deformation in the form of shear failure, rather than bulk flow, may be expected. Two factors however may make an *a priori* comparison of partially-melted rock with a wet sand improper.

(1)   *Melt distribution*.   In a wet sand the grains are not coherent, the fluid occurs in a tortuous interconnected pore-system between the grains. Geometrically there are other possibilities for melt distribution : melt could be interconnected in films at all or most grainboundaries, or occur at grain edges only, conversely it

could be distributed in isolated globular inclusions within an essentially solid matrix.

(2) *Deformation mechanism within the solid.* Under normal conditions for wet soils, sand grains behave essentially as rigid material, they may undergo small elastic deformations or fracture when local stresses on the grains are high. However, it is not clear that this will also be the mechanism of deformation within the crystals at low stresses, and at the high temperatures associated with partial melting in rocks. The grains could again behave essentially rigid-brittle, but they could also change their shape plastically through a diffusion controlled mechanism or by dislocation processes operating within the grains.

These two factors are expected to seriously influence the rheological properties of partially-melted rocks. I will return to them in Chapter 8, when discussing the application of experimental results to geological problems.

1.6   Outline of Part I

The background of the problem having been set out above, a study will now be presented covering the experimental deformation of partially-melted granite with melt fractions less than the critical value. In order to study the role of melt fraction proper most deformation experiments were done under standard conditions of 300 MPa confining pressure, 800^0C after 100 minutes heating prior to deformation.

Chapter 2 describes the experimental technique and the precision of measurement. In Chapter 3 the specimen material is described, together with the methods by which different amounts of melt are obtained and recognised. The stress-strain results and the microscopical observations for partially-melted specimens which were deformed under standard conditions are given in Chapters 4 and 5 respectively. Experiments for which the experimental technique differed from the standard procedures outlined in other chapters, are grouped together in Chapter 6. The experimental results are summarised and extensively discussed in Chapter 7, before an attempt is made in the final chapter to apply them to geological problems.

Chapter 2

EXPERIMENTAL TECHNIQUE

2.1 Introduction

The reason that the rheology of partially-melted rock with low melt fractions has thus far received only limited attention from experiment- alists is not to be sought in lack of interest or imagination, but rather in the substantial experimental difficulties which have to be overcome before meaningful tests can be performed. The high temperature viscometer technique used by Shaw (1969), to study the flow behaviour of melt-crystal suspensions cannot be applied to rocks with low melt fractions, because even at low rates of deformation substantially high differential stresses, not accessible to a viscometer are required. Specimen jacketing and a confining pressure have to be used in order to prevent the formation of voids during deformation. To measure bulk rheological properties of a natural crystalline rock, specimens with a diameter at least 10 times the grain size and a length preferably twice the diameter, have to be used (e.g. Jaeger and Cook, 1976). To obtain melting uniformly throughout the specimen, a high constant temperature has to be achieved. Thus, fairly large volumes have to be kept under constant pressure and temperature during an experiment. For partially-melted rocks differential stresses less than 100 MPa have to be readily measurable, the latter requirement making the Griggs solid medium apparatus (Griggs, 1967; Tullis and Yund, 1977), most commonly used for deformation of rocks at high temperatures and high pressures, less ideal for the measurement of flow stresses in partially-melted rocks. The present experiments were performed in a high temperature, high pressure deformation apparatus using argon gas as a pressure medium (Paterson, 1970, 1977).

2.2 Assembly

Cylindrical specimens of 10 mm diameter, 20 mm length were dried for at least 24 hours at 110°C and then sealed dry or with a measured amount of added water into the assembly shown in Figure 2.1. The jacket was copper tubing of 0.25 mm wall thickness, and platinum discs of 0.025 mm thickness were placed between the specimen and the molybdenum endpieces to prevent sticking after the run. The assembly was weighed before and after runs to check for leaks.

13.

Figure 2.1   Specimen assembly.

Mo ENDPIECE

Mo SEALING RING

Pt SPACER

Cu JACKET

SPECIMEN

ADDED WATER

10 MM
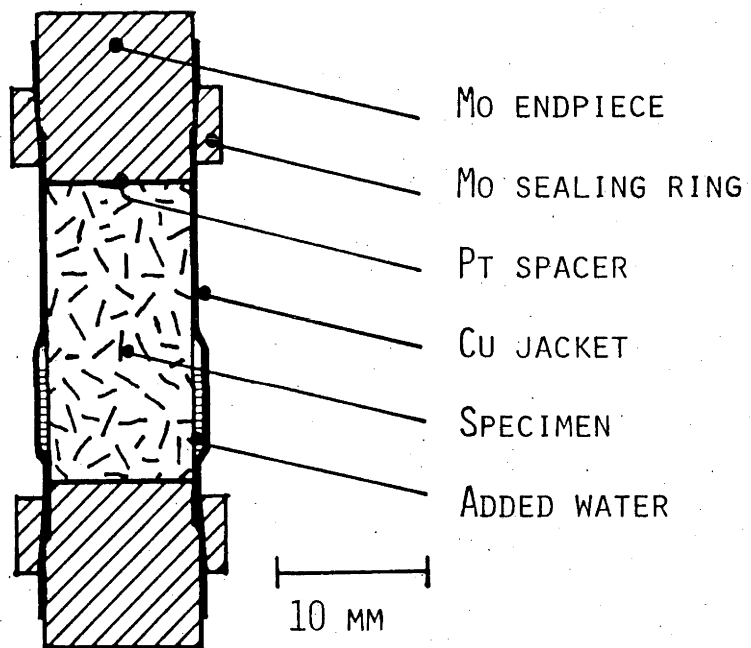
2.3 The measurement of pressure

A detailed description of the pressure system is given by Paterson (1970). The required gas pressure is maintained by a 1:16 oil-gas intensifier. The gas pressure, measured by a Manganin resistance gauge directly exposed to the gas inside the bomb, is recorded on a strip chart; control contacts in the recorder automatically actuate the intensifier when the gas pressure drops below the required setting due to leakage. When there is very little leakage the pressure may exceed the required setting during temperature rise due to the thermal expansion of the gas, in such a case the pressure was controlled manually with a release valve on the intensifier. The confining pressures thus obtained are believed to be precise within 5 MPa.

2.4 The measurement of temperature

Temperatures were recorded during the runs with two platinum, platinum - 13 percent rhodium thermocouples placed 8 and 18 mm above the specimen within the hollow loading piston, the nearer thermocouple also being used as control thermocouple for the furnace temperature controller since the temperature at this position is within 20°C of the temperature within the specimen itself. The required power ratio in the two furnace zones for minimum temperature gradient within the specimen was adjusted on the basis of the temperature difference between the two thermocouples, the required difference being known from calibration runs with a hollow dummy specimen in which the complete temperature profile in specimen and piston was determined. The specimen temperature is believed to be known within 10°C and the temperature variation along the specimen also to be less than this.

2.5 The measurement of differential stress

Differential stress in the specimen was obtained from the axial load, measured with an internal load cell and recorded on a strip chart after correcting for cross-section increase of the specimen, on the assumption of homogeneous deformation at constant volume; the internal load cell was calibrated in terms of measured shortening of a helical steel spring, the spring constant of which had been determined in a commercial testing machine. When the differential stress in the specimen is below 50 MPa the load carried by the copper jacket becomes significant and

correction was made for this in determining the stress. This correction is based on the results of J.A. McDonald (pers. comm.), for the constant strainrate deformation of copper in the present apparatus. The values used for jacket-load correction at 800°C, 300 MPa are indicated in Figure 2.2. The load supported by the copper jacket becomes of the same order as that supported by the specimen, when the stress is about 1 MPa, which sets this as a lower limit to the strength of specimens of high melt fraction that can be studied readily with the present arrangements. Conversely, the detectable strength of the copper jacket enabled me to determine the displacement at which the loading piston touched very weak specimens, and to determine the change in length of the specimen. The sensitivity of stress measurement is approximately 0.2 MPa, but larger uncertainties arise because of the jacket load correction.

2.6 The measurement of strain

Cross-head displacement was measured with a linear variable differential transformer (LVDT), recorded simultaneously with the load on the same strip chart, and corrected for elastic distortion in the loading assembly in order to give specimen shortening, expressed as engineering strain. The elastic distortion was determined using a dummy specimen of Kennametal K165 with a high Young's Modulus of $\sim$200 GPa at 800°C, such that, at the loads used, the measured displacements as in Figure 2.3, could be entirely attributed to elastic length changes in the loading assembly. Strain differences of 5×10^{-4} in the specimen can be distinguished within one run, while strain determinations can be repeated from one run to another within about 2×10^{-3}, the additional uncertainty here arising from such factors as difference in specimen seating.

2.7 Testing procedures

All experiments reported here were done at 300 MPa confining pressure and 800°C, unless stated otherwise. The hydrostatic confining pressure was applied first, then the temperature was raised to 800°C, typically in 45 minutes, about one third of this time being spent above the solidus temperature, 670°C, of the granite plus water system at this pressure (Winkler, 1974). The specimens were then held under hydrostatic conditions at 800°C for a further 100 minutes to allow melting to occur before straining. At the end of the run, cooling from 800°C to 670°C took about 5 minutes in all cases.

Figure 2.2   Load carried by the copper jacket for various strainrates
              at 800°C, 300 MPa. Based on measurements of J.A. McDonald.
              The figure represents the linear approximations used for
              the jacket correction.

$10^{-3}s^{-1}$

$10^{-4}s^{-1}$

$10^{-5}s^{-1}$

$10^{-6}s^{-1}$

$10^{-7}s^{-1}$

LOAD (KG)

STRAIN (PERCENT)
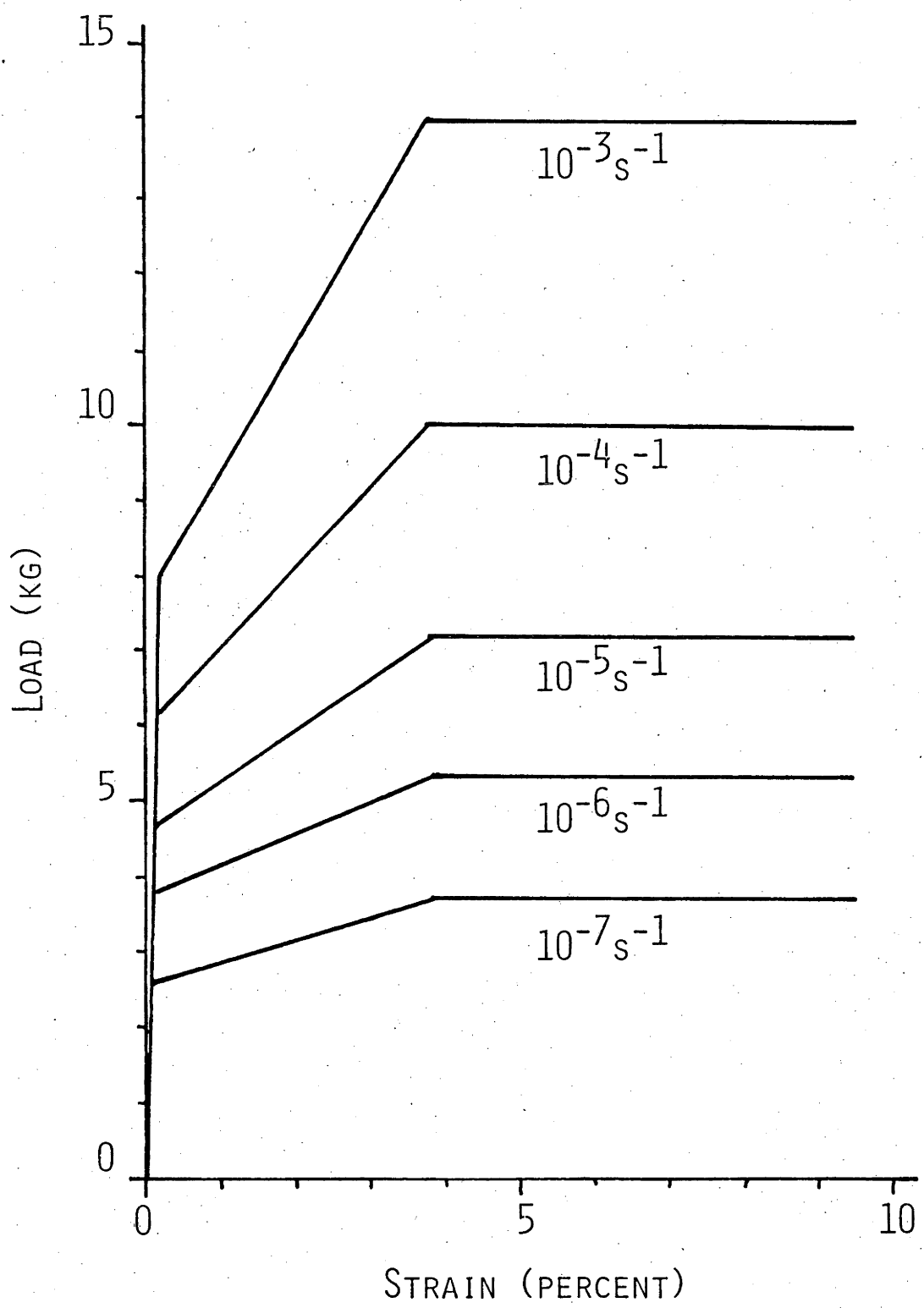
Figure 2.3   Displacement correction for elastic distortion of the
loading assembly of the apparatus at $800°C$, 300 MPa.
The upper abscissa indicates the overestimate in
strain for a specimen of 20 mm initial length which
would be made without this correction.
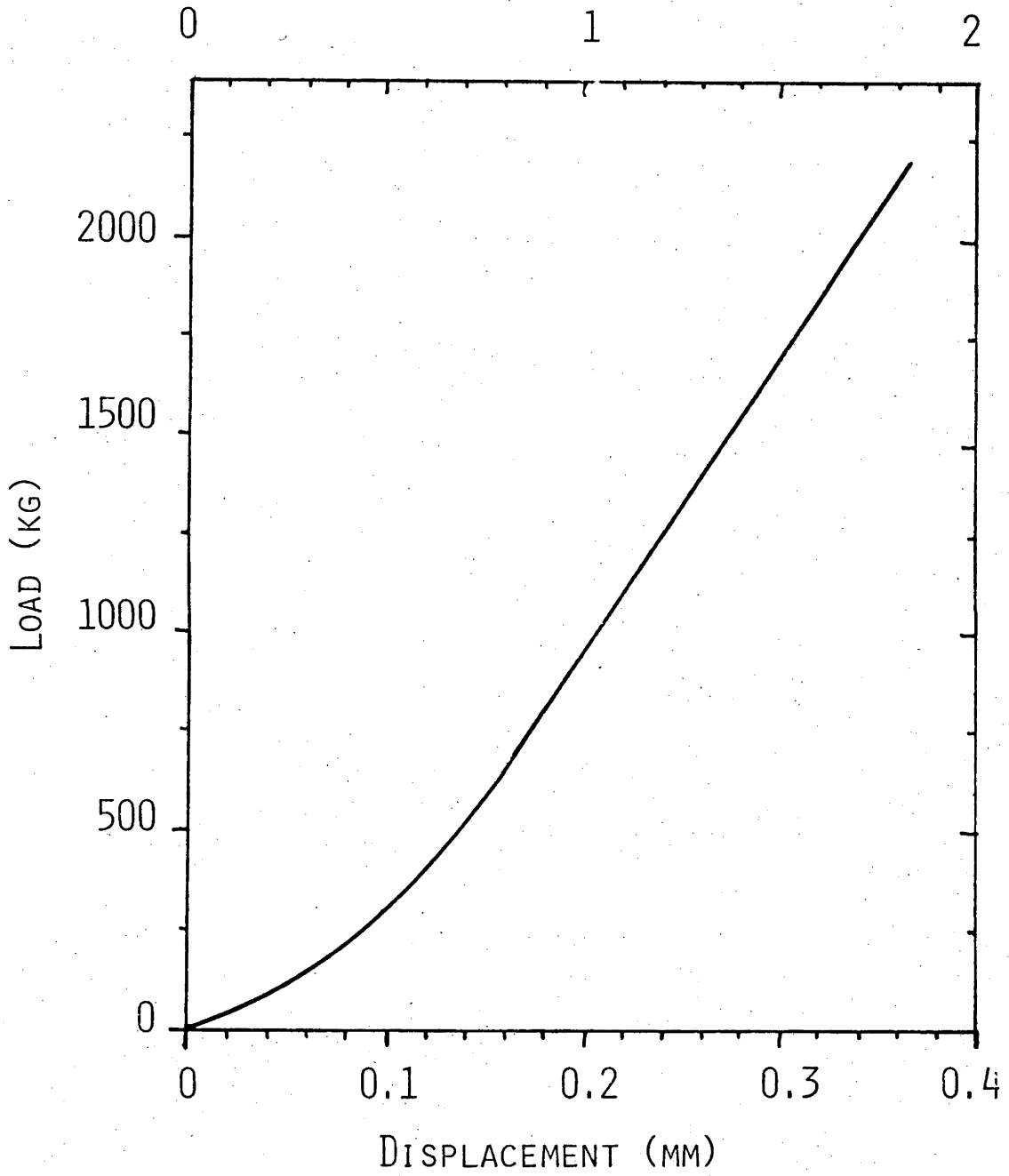
Three kinds of tests were performed:

(1) In *constant strainrate* tests, the loading piston was advanced at a constant rate; when stress changes gradually with strain, or when stress remains constant, this results in a constant engineering strainrate in the specimen. In view of the corrections which have to be applied to the displacement at high loads for the elastic distortion of the loading assembly (Figure 2.3), a constant rate of piston advancement results in a change in strainrate within the specimen, if large stress differences occur over small intervals in strain, as in the case of failure of the specimen. In practice, however, this gives few serious problems. The reported strainrates were determined as the average between zero and final strain, the actually observed strainrates do not differ more than a factor of two from this average value, except in the case of catastrophic failure.

(2) *Creep tests* were done by advancing the loading piston at a constant rate until the load corresponding to the required stress level on the specimen was attained. Constant stress was then maintained by manually varying the rate of piston advancement, and letting the load rise slightly with increasing strain, in accordance with calculations for cross-sectional increase of the specimen assuming volume constant deformation.

(3) In *cycling tests* the specimen was deformed at a constant rate of $10^{-5}s^{-1}$ in all cases to a given stress, after which the piston was backed off by hand, and part of the strain recovered in a time dependent fashion before a subsequent cycle of the same kind was performed. The load was either reduced abruptly to zero, after which the time dependent strain recovery was measured by repeatedly · touching the specimen, or the load was reduced gradually by withdrawing the piston in small steps whereby an unloading curve could be obtained. The precision of the time measured after load removal is not better than 2 seconds.

2.8 Microscopy and photography

After each run the specimen was recovered by carefully removing the copper jacket and the endpieces. In most cases this could be done without damaging the specimen, the quenched melt holding the grains of the specimen together; only in those runs where a sharp shear had occurred

some grains would spill off from the outside of the failure zone. The cores were then potted in epoxy resin and sectioned through the center, parallel to the axis of the core. The orientation of thin sections in specimens with localized failure zones was taken parallel to the core axis, and perpendicular to the plane of the failure zone. High quality polished thin sections ot 30μ thickness were subsequently studied optically using a Leitz microscope with an Orthomat photographic attachment.

Chapter 3

SPECIMEN MATERIAL AND THE FORMATION OF MELT

3.1 Introduction

The flow behaviour of partially-melted rock in the granular framework - controlled regime will not only be influenced by the rheological properties of the individual crystals making up the framework, but also by the spatial arrangements of those crystals, by the nature of their contacts, and by other factors defining the microstructure of the aggregate. It seemed necessary therefore, to use for specimen material a *natural* fine grained rock. Granite, having the lowest eutectic melting temperature in the presence of water, was chosen to facilitate experimenting and because it is the most common crustal igneous rock, which particularly in areas of high grade regional metamorphism, can be shown to be derived from the country rock by partial melting, also called anatexis or migmatisation (e.g. Mehnert, 1968; Winkler, 1974).

3.2 Specimen material

All specimens were cored from a single block of Delegate aplite (N.S.W., Australia). This is a fine grained granitic rock (0.5 mm average, 1 mm maximum grain size), containing roughly equal amounts of quartz (31 percent), plagioclase (31 percent) and K-feldspar (35 percent), and 3 percent biotite. The K-feldspar is slightly altered. The rock appears isotropic and uniform in hand specimen but a faint pink spotting is revealed on a polished slab, due to the K-feldspar being slightly concentrated in clusters of 5 mm size. This heterogeneity was not recognized initially, but it may account for some of the scatter in stress-strain results since its scale is comparable to that of the specimens.

3.3 The kinetics of melting in natural granite under experimental conditions

In this study a melt phase has been produced with the aid of added water. The extreme sluggishness of the reactions producing melt in oven-dry granite, just above its solidus is well known to experimental petrologists, who resort to the use of very fine powders and heating times of several weeks, in order to achieve equilibrium (*e.g.* Brown and Fyfe, 1970; Whitney, 1975; see also Johannes, 1978, for a discussion of the

attainment of geochemical equilibrium in melting experiments in granitic
systems). Mehnert *et al.* (1973) and Arzi (1978-b) previously studied
the kinetics of melt formation in natural fine grained granitic rocks
in the presence of excess water at temperatures at and above the solidus.
They found that an initial stage of approximately 1 hour of rapid melting
inside a specimen is followed by a very slow increase in internal melt
fraction with time, related to the diffusion of water from a source
external to the specimen, via a melted margin at the specimen – water
source interface into melted grainboundaries within the specimen (Arzi,
1978-b). Apparently, the melting rates in the presence of free water are
high, while those in its absence are low, that is when all water directly
available has dissolved into the melt, the rate of melting slows down,
even when geochemical equilibrium would require higher amounts of water-
undersaturated melt, or when more water for saturated melting can be
tapped through diffusion from outside the specimen.

After the initial melting stage, time does not influence the
melt fraction appreciably over a period of several hours, the time scale of
the present experiments. Thus, the amount of melt which forms inside the
specimen is determined mainly by two factors:

(1)   The amount of water needed to saturate the melt under the pressure-
       temperature conditions of the experiment.

(2)   The amount of water which can reside within the specimen in
       voids and cracks before melting starts.

It therefore becomes possible to control the amount of melt formed by
adding different amounts of water, and to perform rheological experiments
at effectively constant amounts of melt after an initial melting period.
If more water is added than can be accommodated within the specimen at
the pressure-temperature conditions of the experiment, an external melt
film develops in between the specimen and the jacket (Figure 2.1). Such
external melt films can be drawn into the specimen during deformation, as
will be shown below, whereby in deformed samples higher internal melt
fractions can be reached than the maximum possible in hydrostatic experiments.
It will be shown that the results for melt fractions in hydrostatic
experiments (Section 3.5) and deformation experiments (Section 3.6) can
be fully explained by a model for water-saturated melting, based on factors
(1) and (2) which is worked out in detail in Section 3.7.

Bulk geochemical equilibrium is not reached in the present experiments, due to their short duration and the kinetic factors outlined above. The composition of the aplite is very close to that of the minimum melting or eutectic composition in the granite system of quartz, plagioclase, K-feldspar and water. At 300 MPa the solidus of this system lies at approximately 670°C and very high degrees of melting, depending somewhat on the amount of added water, but in excess of 50 percent, would therefore represent the equilibrium condition at 800°C (see for instance Winkler, 1974; Whitney, 1975). The composition of the melt phase in the experiments is thought to be constantly close to the water-saturated granitic minimum composition; the rheologically important physical properties of the melt, its viscosity and compressibility are therefore taken to be constant at 800°C and 300 MPa, irrespective of the amount of melt.

3.4 The measurement of melt fraction

A detailed description of the microstructures developed during melting will be given in Chapter 5, here only those factors which are relevant to the determination of melt fraction will be discussed. Upon quenching after a run, melt transforms into an isotropic glass, which can be recognised under the optical microscope with crossed polarizers from the anisotropic minerals, while use of a gypsum plate can facilitate the recognition of melt from crystals in extinction position by a different colour of second order red (Arzi, 1978-b). With polarizers parallel the glass has a faint purplish colour of unknown origin, and a low relief with respect to the minerals. Occassionally resin occurs in cracks between the grains, because it is used to pot the specimen before thin sectioning. Distinction of glass from resin is difficult but possible through the yellowish colour of the resin and its slight anisotropy ("chickenpox texture").

The fractions of melt formed inside specimens with added water during the experiments at 800°C, 300 MPA confining pressure were determined by point-counting the glass visible in 30 micron polished thin sections. Sufficient points were counted to ensure reproducibility within 0.3 percent, but systematic errors arising from difficulties such as the detection of thin glass films in inclined grainboundaries, will make the uncertainty rather larger than this. Small amounts of glass, too small to determine

point-counting, were also visible locally at grainboundaries in specimens
to which no water had been added. Since the biotite in these was still
unaltered and since a weight loss of 0.25 weight percent occurs upon
heating to 800°C at atmospheric pressure, (see Table 3.1, p.28) it is
thought that some melt is formed with water released from the dehydration
of alteration products of K-feldspar or from desorption of strongly
adsorbed water. It will be assumed hereafter that this 0.25 percent weight
loss is made up entirely of such water and that the total water available
to form melt is the sum of this amount and that of the added water.

3.5 Results for hydrostatic experiments

The amount of melt formed within specimens heated under hydro-
static conditions remains less than 10 volume percent regardless of the
amount of available water (Figure 3.1, open symbols). No glass was
observed on the surface of specimens with 0 or 0.25 weight percent added
water, while a thin discontinuous film was observed with 0.5 percent added
water; however, with 1 percent or more added water a shining thick
continuous film was present indicating that the amount of melt formed
could no longer be accommodated within the accessible pore space in the
specimens. The amount of melt within the specimens did not increase
appreciably with time in periods of heating from 100 to 300 minutes. These
observations are consistent with an estimate of what the accessible pore
space is at 800°C, 300 MPa confining pressure, as determined by water
absorption and density measurements on preheated dry specimens, (see
Section 3.7).

3.6 Results for deformation experiments

The amounts of melt present in specimens after deformation are
also shown in Figure 3.1 (closed symbols), there again being no consistent
increase in melt fraction with time for any amount of added water. The
deformation took between 3 and 400 minutes and was preceeded by 100 minutes
heating under hydrostatic conditions. It is seen that, except in the case
of 0.25 weight percent added water, the amount of melt within the specimens
is greater than after hydrostatic heating, notably so with 1 percent or
more added water where the amount of melt is double. Except at the highest
water contents the amount of melt within the specimen is now equal to what
would be expected if all the available water were used to form water

Figure 3.1   Melt percentage within specimens as a function of
weight percent water.   The dashed lines indicate
the expected amounts of melt for deformed and
undeformed specimens from the model discussed in
Section 3.7.
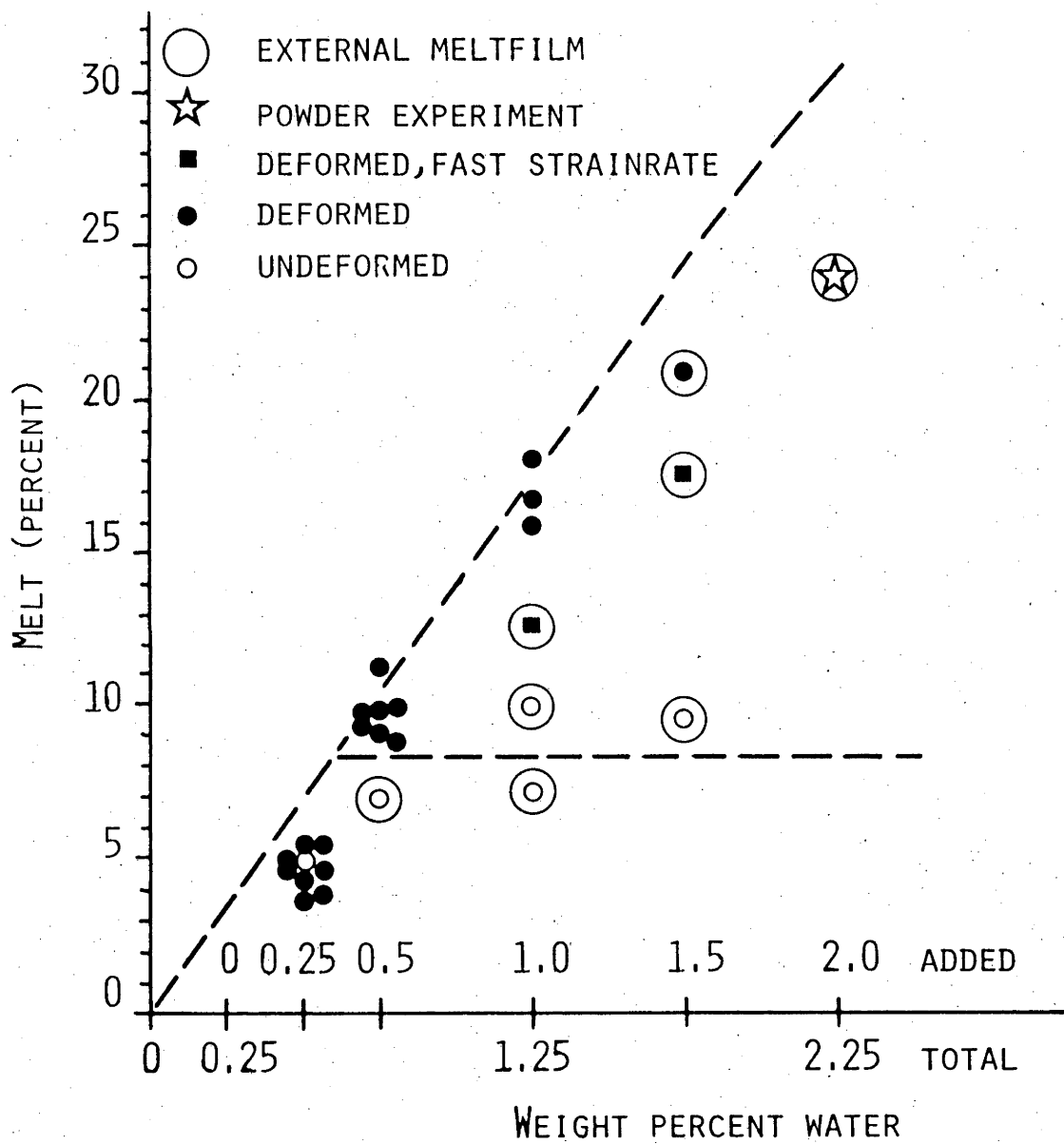
saturated granitic melt (Section 3.7). Evidently, during deformation dilation of the specimen contributes additional intercrystalline space within which all the water-rich fluid tends eventually to be accommodated. The results given in Figure 3.1 for specimens to which 0.5 percent water or more was added, are all for large strains (>5 percent). Figure 3.2 shows however, that the increase in melt fraction with straining, is a gradual one, and that during the first few percent of strain it is 1.5 to 2 times the strain. There appear to be upper limits to the increase in the amount of melt which can be achieved in this fashion, and to the strainrate for which it is effective. Thus, a slow strainrate run to 10 percent strain on a specimen with 1.5 percent added water, resulted in 21 percent melt rather than the theoretically possible 24 percent, and a shining melt film was observed on the outside of the specimen, and two fast strainrate runs at 10^{-4} to $10^{-3} s^{-1}$ on specimens to which 1.5 and 1.0 weight percent water respectively were added also showed melt films on the outside of the specimen and considerably less melt than expected was found inside. These results are indicated by square symbols in Figure 3.1.

3.7 Estimation of water absorption and melt formation

The amount of melt formed inside a specimen has been shown to depend on the amount of water added, the amount of water needed to saturate the melt at the temperature pressure conditions of the experiment, and the pore space available inside the specimen. This idea is worked out quantitatively below.

3.7.1 Total porosity

The initial total porosity of the rock is difficult to determine accurately, but an estimate can be made from the measured bulk density of 2.57 g/cm^3, and the mean density of the constituent minerals of 2.63 g/cm^3, the latter being obtained from the measured volume fractions (reported in Section 3.2) and the mineral densities given in Robie et al., 1966 (quartz 2.648, oligoclase, 2.646, K-feldspar 2.551 and biotite 2.8 g/cm^3). The bulk density has been determined from the oven-dry weight and the volume obtained from micrometer measurements made on diamond cored cylinders. In this way the total porosity is estimated to be initially 2.3 ± 0.1 percent.

Figure 3.2   Melt percentage within specimens as a function of strain in experiments at $10^{-5}s^{-1}$ strainrate. The dashed lines indicate the amounts of melt expected from the model discussed in Section 3.7. The dotted line represents an increase in melt fraction by a factor of 1.5 times the strain.
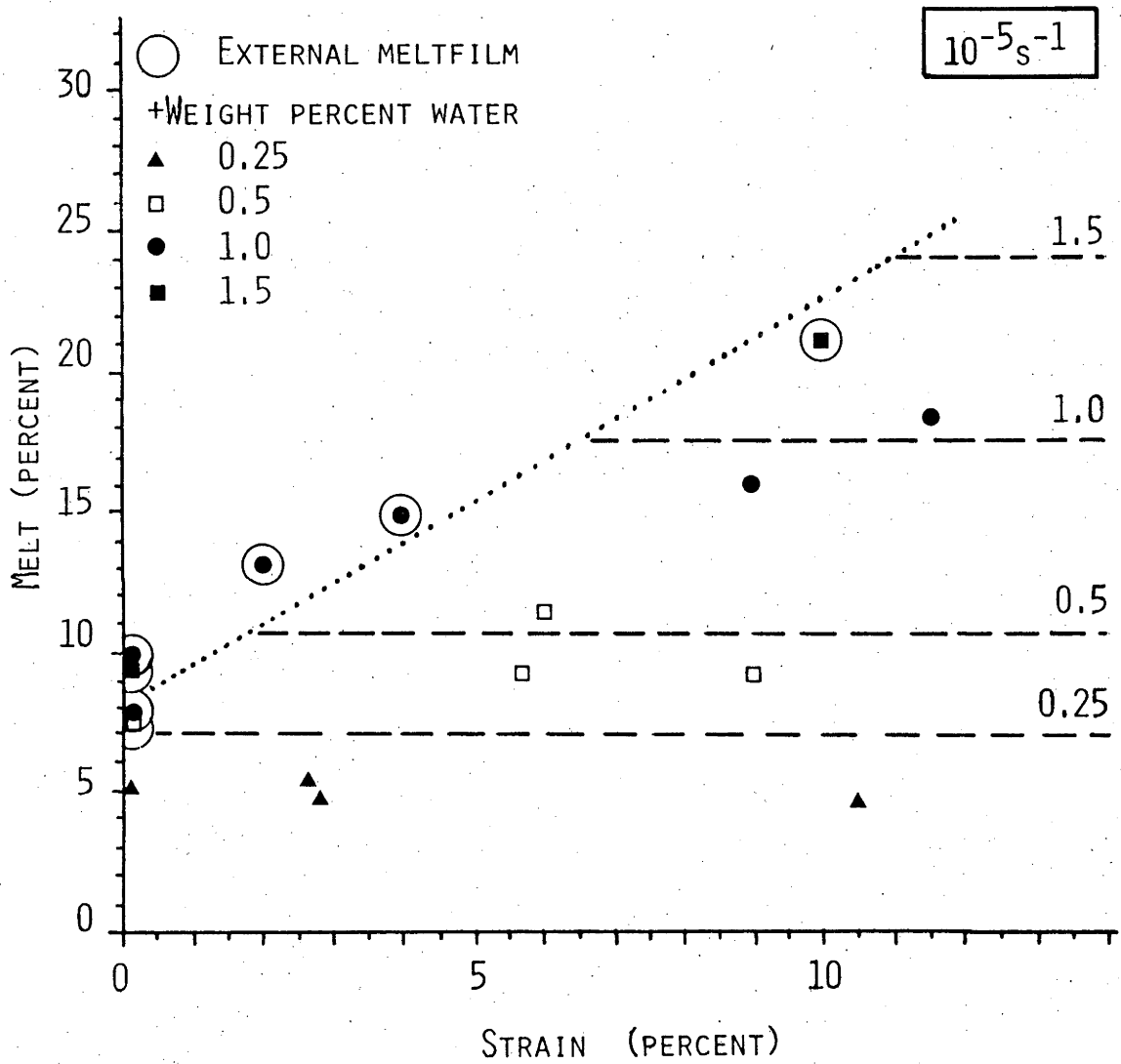
However, when a specimen is heated at low effective confining pressure a dilation occurs, which can be attributed to the formation of new cracks in response to internal stresses arising from inhomogeneous and anisotropic thermal expansion of the grains.

This effect can be measured directly as a decrease in bulk density and using the same method described above the total porosity after heat treatment can be calculated (Table 3.1). A small weightloss, discussed in Section 3.3, is observed after heating at 1 atmosphere; this is also included in Table 3.1. The increase in total porosity can also be calculated independently of weight and weight changes from volume measurements alone, and the results are seen to be in good agreement with the increases in total porosity as determined from bulk density measurements (Table 3.1).

3.7.2   Accessible and inaccessible porosity

Water absorption has been measured at room temperature and pressure in order to determine the porosity accessible to a fluid permeating the specimen from the surface. Measurements were made after oven drying and then after a cycle of heating to temperatures up to 800°C using the same specimens as for the total porosity determination. The weight of water taken up was determined by reweighing the specimens after immersion in water over-night following evacuation to 10^{-2}–10^{-3} torr; excess water on the outside of the specimen being removed with a paper tissue just before weighing. The volume of water taken up by the specimen was then calculated and is expressed as accessible porosity (Table 3.1). Interesting aspects of these results are that there is an exceptionally large increment in porosity between 500°C and 600°C, attributable to cracking associated with the α-β quartz transition, and that the accessible porosity is consistently lower by about 1.5 percent than the estimated total porosity. The latter indicating that the increase in total porosity with heating, as calculated from volume measurements, is entirely attributable to the increase in accessible porosity and that presumably the inaccessible porosity, remaining unchanged, consists of small pores within grains which are not intersected by the intragranular and grain-boundary cracking. The small equant pores within plagioclase observed by Sprunt and Brace (1974) and Montgomery and Brace (1975) may be examples of such inaccessible pore space.

Table 3.1   Weight and porosity changes in two sets of Delegate aplite
            specimens determined after heating for 1 hour at various
            temperatures.

Temperature °C	110	400	500	600	700	800
weight loss %	–	0.06	0.13	0.17	0.25	0.23
	–	0.05	0.13	0.18	0.24	0.25
total porosity %	2.3	2.6	2.9	3.9	4.1	4.3
(density measurement)	2.3	2.6	2.8	3.7	3.9	4.4
total porosity increase %	–	0.2	0.5	1.5	1.6	1.9
(volume measurement)	–	0.3	0.4	1.2	1.4	2.1
accessible porosity %	0.8	1.1	1.2	2.3	2.4	2.6
(water absorption)	0.8	0.9	1.3	2.2	2.4	2.8

Table 3.2   Maximum saturated melt from available water.

Added water (weight percent)	0	0.25	0.5	1.0	1.5	2.0
Available water (weight percent)	0.25	0.5	0.75	1.25	1.75	2.25
Estimated melt (volume percent)	3.5	7	10	17	24	31

3.7.3   Estimated water take-up at 800°C

I assume that the accessible porosity is the same at 800°C, 1 atmosphere, as subsequently measured at room temperature. I further assume that the same accessible pore space develops at high pressure, provided the pore pressure is equal to the applied confining pressure[1]. Actually water will start to react with granite to form melt at the solidus temperature of 670°C at 300 MPa, but this effect can be neglected since the water take-up is the same as at 800°C, 300 MPa, due to the difference in accessible pore space and water densities cancelling out (see below).

Under these assumptions it follows that the 1.02 cm^3 of Delegate aplite weighing 2.57 g/cm^3 dry will take-up a maximum of 0.015 g of water at 800°C, 300 MPa, taking a water density of 0.548 g/cm^3 (Burnham *et al.*, 1969); that is, the water content of the saturated rock will be 0.6 weight percent at 800°C, 300 MPa water pressure. The same result is obtained if interpolated values for accessible porosity and water density at 670°C, 300 MPa are used. It is possible that the accessible porosity at 800°C, 300 MPa, is slightly overestimated due to the pressure sensitivity of the quartz α-β transition temperature, but on the other hand the lower viscosity of water under these conditions than at ambient conditions may lead to a somewhat greater accessibility of pore space. I therefore take 0.6 weight percent as the best estimate of the maximum amount of water that can be expected to be taken up within the rock at 800°C, 300 MPa, with an uncertainty of perhaps + 0.1.

3.7.4   Estimated and observed melt fraction at 800°C, 300 MPa

The 0.015 g of water estimated above as the maximum taken up by 2.57 g of rock at 800°C, 300 MPa will form 0.193 g of melt if the water-saturated melt contains 8 weight percent of water similar to the value given by Winkler (1974); that is, the expected melt content would be 7.5 weight percent. Taking the melt to be about 10 percent less dense than the rock (Daly *et al.*, 1966; Bottinga and Weill, 1970), and neglecting the differences in compressibility, the expected volume fraction of melt is therefore between 8 and 9 percent, provided the water available is not less.

---

[1]For an experimental confirmation of these assumptions see Part II of this thesis, Chapter 9.

than 0.6 weight percent. If the rock dilates during deformation so as to accommodate all the added water in the experiment, then the corresponding amounts of water saturated melt to be expected are shown in Table 3.2.

These predictions are also shown by the dashed lines in Figure 3.1, where they are in good general agreement with the observed results. Some of the deviations from predicted behaviour have already been described in Section 3.6.

Chapter 4

STRESS-STRAIN OBSERVATIONS

4.1   Introduction

As outlined in Chapter 1 the previous work on the deformation of partially-melted rock with low melt fractions is rather limited. In a first approach to the problem of the role of melt fraction in influencing rheological properties it was therefore felt necessary to keep as many variables as possible constant and only change the amount of melt from one run to another by adding different amounts of water. The stress-strain results for such standard experiments are described in this chapter, and the corresponding microscopical observations in Chapter 5.

4.2   Constant strainrate tests

Using the assembly described in Chapter 2, stress-strain curves were determined at constant strainrate of 10^{-6} to $10^{-3} s^{-1}$ at 800°C on specimens to which amounts of water from zero to 1.5 weight percent had been added (Figures 4.1-a-e). The broken line also included in Figure 4.1-a corresponds to the elastic deformation (Young's Modulus 50 GPa) to be expected for an unmelted granite from extrapolation to these conditions (Birch, 1966). An unsealed dry specimen failed to a cohesionless powder at a stress of 60 MPa and strain of 1.2 percent under conditions otherwise the same as for Figure 4.1-a.

The sealed specimens were cohesive after the runs, except for a few loose grains at localized failure zones. The specimens with zero and 0.25 percent added water showed sharply defined shear zones. With 0.5 percent added water, specimens deformed beyond the stress maximum also showed localized shears, but in those strained less than about 6 percent the deformation was macroscopically uniform except for slight barrelling. With more added water, the specimens became similarly barrelled or wide shear zones were formed.

There was considerable variation in stress-strain behaviour within each group, especially within the group with 0.25 percent added water. The variation does not obviously correlate with differences in strainrate when less than 1.0 percent water is added (Figures 4.1-b and c), although a differential strainrate experiment (broken line in Figure 4.1-c) shows

Figure 4.1-a-e. Stress-strain curves for constant strainrate
experiments. Strainrate in units of $10^{-5}s^{-1}$.
The dashed line in Figure 4.1-a represents a
Young's modulus of 50 GPa, the dotted line an
unconfined run. The dashed curve in Figure 4.1-c
is a differential strainrate run. For further
details see Table 4.1.

(a) +0 w.% H₂O graph: Differential Stress (MPa) vs Strain (percent), showing curves labeled 26 × 10⁻⁵ s⁻¹, 1.0, and 0.6, with inflection point marker.

(b) +0.25 w.% H₂O graph: Differential Stress (MPa) vs Strain (percent), curves labeled 9.9 × 10⁻⁵ s⁻¹, 5.8, 2.4, 29, 0.3, 0.7, 0.9.

(c) +0.5 w.% H₂O graph: Diff. Stress (MPa) vs Strain (percent), curves labeled 0.9 × 10⁻⁵ s⁻¹, 0.8, 14, 0.4, 1.0, 2.0, 7.9, 0.5.

(d) +1.0 w.% H₂O graph: Diff. Stress (MPa) vs Strain (percent), curves labeled 82 × 10⁻⁵ s⁻¹, 9.1, 1.7, 1.0.

(e) +1.5 w.% H₂O graph: Diff. Stress (MPa) vs Strain (percent), curves labeled 48 × 10⁻⁵ s⁻¹, 1.0.

Table 4.1 Constant strainrate tests.

Run No.	Strainrate	Melt Fraction	Stress Maximum		Inflection		Max Slope
	x 10^{-5} s^{-1}	%	Stress MPa	Strain %	Stress MPa	Strain %	GPa
Zero added water							
2922	26	<3	255	3.0	135	1.4	13.5
2837	1.0	<3	277	2.5	135	1.2	17.3
0.25 percent added water							
2924	29	3.4	177	3.2	100	1.6	7.6
3040	9.9	4.3	301	4.8	153	1.6	12.4
2992	5.8	3.7	318	3.8	140	1.3	12.7
2993	2.4	4.7	259**	10.5	132	1.8	6.5
2939	0.9	4.8	100	2.3	54	1.2	4.6
2942	0.7	5.3	108	2.3	60	1.1	5.3
2937	0.3	5.4	155	3.6	89	1.8	5.1
0.5 percent added water							
2859	14	10.0	100**	7.6	40	1.8	2.3
2841	7.9	10.0	66	5.3	25	1.6	2.0
2844	2.0	11.3	77**	5.7	35	2.0	2.0
2946	1.0	9.0	93	8.8	38	1.5	2.8
2835	0.8	8.9	99**	5.8	47	2.3	2.3

Table 4.1 Constant strainrate tests. (ctd)

Run No.	Strainrate x $10^{-5}s^{-1}$	Melt Fraction %	Stress Maximum Stress MPa	Stress Maximum Strain %	Inflection Stress MPa	Inflection Strain %	Max Slope GPa
0.5 percent added water (ctd).							
2938	0.4		-	-	43	1.9	2.9
	*0.9	9.9	114	6.8	-	-	-
2839	0.5	9.3	53**	5.7	27	2.2	1.1
1.0 percent added water							
3029	82	12.1	107	8.3	46	2.8	2.3
3023	9.1	16.8	59	7.8	20	1.5	1.8
2961	1.7	15.9	34	7.8	11	2.2	0.7
3026	1.0	18.2	35	9.3	13	2.6	0.7
3107	1.5	13.2	14**	2.2+	-	-	-
3108	1.5	14.9	27**	4.0+	11	2.3	1.5
1.5 percent added water							
3095	48	17.5	31	4.0	15	2.2	1.0
3059	1.0	21.0	5.3	5.9	3.0	3.0	0.2

* differential strainrate experiment. ** highest stress, no stress drop observed.

+ small strain experiment, quenched under stress.

the flow stress to be strainrate dependent in a given specimen. At high water contents (Figures 4.1-d and e) a clear dependence on strainrate is noted, and therefore I attribute the erratic behaviour at lower water contents to a specimen variability that is obscuring the normal strainrate sensitivity in many cases.

Despite the scatter just noted, the following major trends can be discerned:

(1) In no case is a steady state reached; the stress is always strongly dependent on the strain, except for relatively small strain intervals at the larger water contents.

(2) The stress-strain curves have a conspicuous inflected or S-shape up to a stress maximum, after which a stress drop occurs. The stress at the inflection is roughly half the maximum stress, while the strains at the inflection and at maximum stress increase, and the sharpness and magnitude of stress drop decrease, as the amount of water is increased. The maximum slope of the stress-strain curve also decreases with increasing amount of water (Figure 4.1, Table 4.1).

(3) A strainrate sensitivity is only clearly revealed in the case of 1 and 1.5 percent added water (Figure 4.1-d and e). A simple reading of these figures suggests very roughly a doubling of the stress level for one decade of increase in strainrate, but the strainrate sensitivity for a given melt fraction is somewhat less than this because the specimens tested at the highest strainrates also had the lowest melt fractions (Table 4.1).

4.3   Creep tests

Five creep experiments were done at 800°C, 300 MPa in which the strain was measured as a function of time at constant stress, as shown in Figure 4.2. The total strains achieved were greater by 1-2 percent, than those plotted since the latter were measured from the point of reaching the final load and do not include the deformation during the initial loading at a constant strainrate of about $4 \times 10^{-5}s^{-1}$. As might be expected from the constant strainrate tests, the amount of creep strain in a given time increases with amount of added water (and hence melt fraction) and with the applied stress.

Figure 4.2   Creep experiments.   The right-hand side of the
figure represents the strain histories; the left-
hand side shows the corresponding strainrate
histories.   The numbers above the curves give the
stress in MPa.
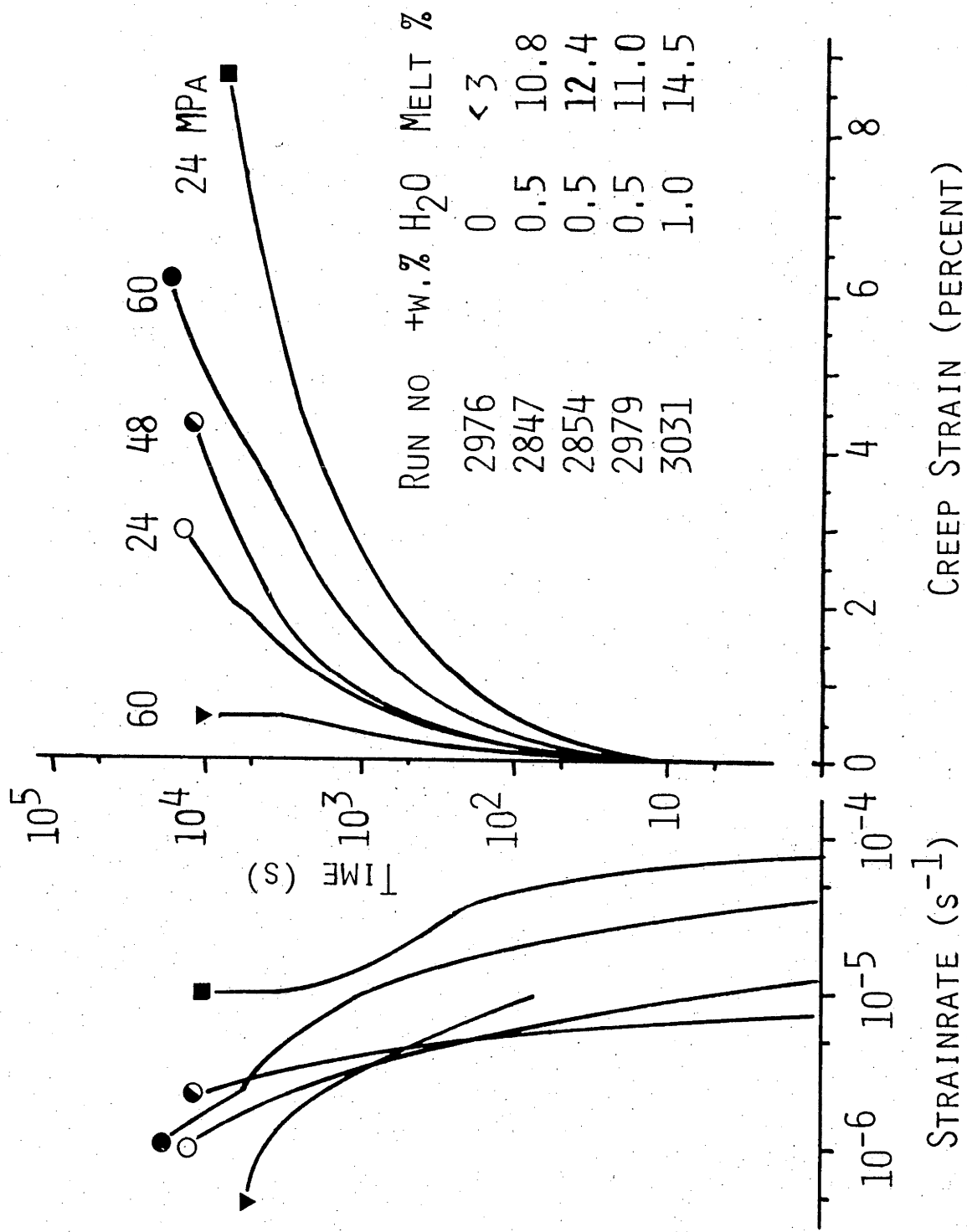
RUN NO	+w.% H_2O	MELT %
2976	0	<3
2847	0.5	10.8
2854	0.5	12.4
2979	0.5	11.0
3031	1.0	14.5

24 MPA

60 48 24 60

CREEP STRAIN (PERCENT)

TIME (S)

10^5 10^4 10^3 10^2 10

STRAINRATE (s^{-1})

10^{-4} 10^{-5} 10^{-6}

The strainrate histories are shown at the left of Figure 4.2. In general, an Andrade, (time$^{1/3}$) transient creep law is very roughly obeyed. In the cases of zero and 0.5 percent added water, the departures from such a law are mainly towards a logarithm of time law, as indicated by downward curvature in the strainrate plot. Only in the case of 1 percent added water is there an approach to steady state creep for a strain interval of about 2.5 percent towards the end of the run (*c.f.* the corresponding constant strainrate experiments).

4.4   After-effects and cycling tests

On the release of the load at the end of a constant strainrate test, there is both an immediate recovery of strain and a subsequent recovery that continues with time at a decaying rate. The same behaviour is observed repeatedly when the specimen is deformed in further stages to higher strains. These effects are shown in Figures 4.3-a-d, for cycling tests on specimens with zero, 0.25, 0.5 and 1.0 percent added water. Only a weak indication of time dependent elastic recovery is noticed in the specimen with no added water (Figure 4.3-a), but in all cases with added water in which the quantities of melt are measurable, the duration of strain recovery after load removal is seen to be between 100 and 1000 seconds (Figures 4.3-b-d), but at least half of the total recoverable strain appears in the first 15 to 20 seconds after load removal. The unloading curves are steep initially but show marked non-linearity particularly at low stress levels. It is also noteworthy, that in cyclic straining the initial slope in each stress cycle is very low, indicating that the immediate reversal of the strain also requires very low stresses.

In all cases with added water the total amount of recovered strain greatly exceeds what would be expected for a uniform elastic unloading of an entirely solid rock. This excess is tabulated as ε^* in Table 4.2 under the assumption of a Young's Modulus of 50 GPa for the solid rock. The quantity ε^* is very small for specimens with zero added water, indicating nearly solid unloading behaviour, but in all cases where water was added the additional strain is 0.3 percent or more, irrespective of the amount of melt, of the magnitude of the stress or strain, or of previous cycling. Also given in Table 4.2, are the "relaxed unloading modulus", $E_{relaxed}$, calculated from the stress at maximum strain and the total amount of strain recovered at zero stress, and the "unrelaxed unloading modulus",

Figure 4.3-a-d.   Cycling experiments. The upper half of the
             diagrams represents the stress-strain curves for
             loading and step-wise unloading (open symbols);
             the last stress measurement before removal of
             the load is indicated by a closed symbol. The lower
             half represents strain recovery as a function of time
             from the moment of load removal. The dashed line
             in Figure 4.3-a represents a Young's modulus of 50
             GPa. For further details see Table 4.2.
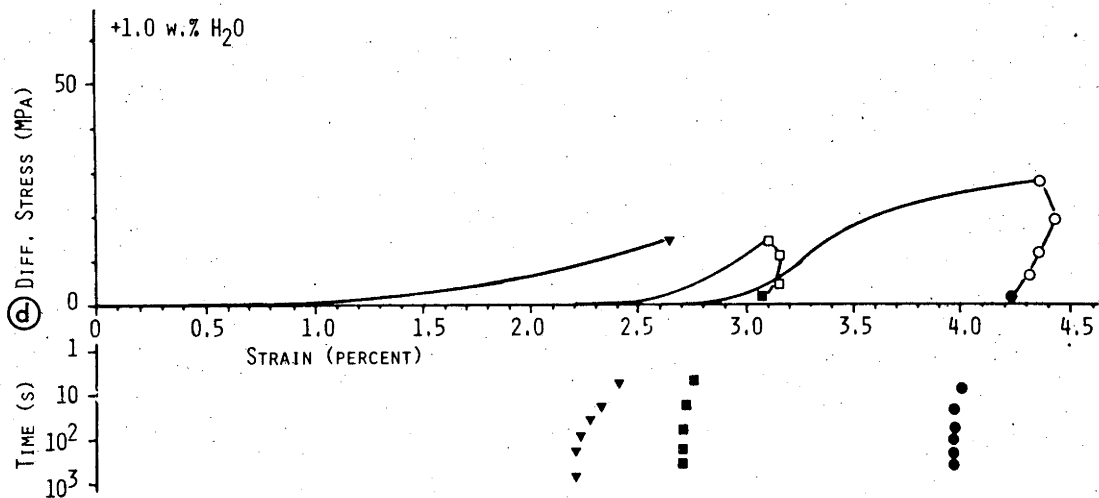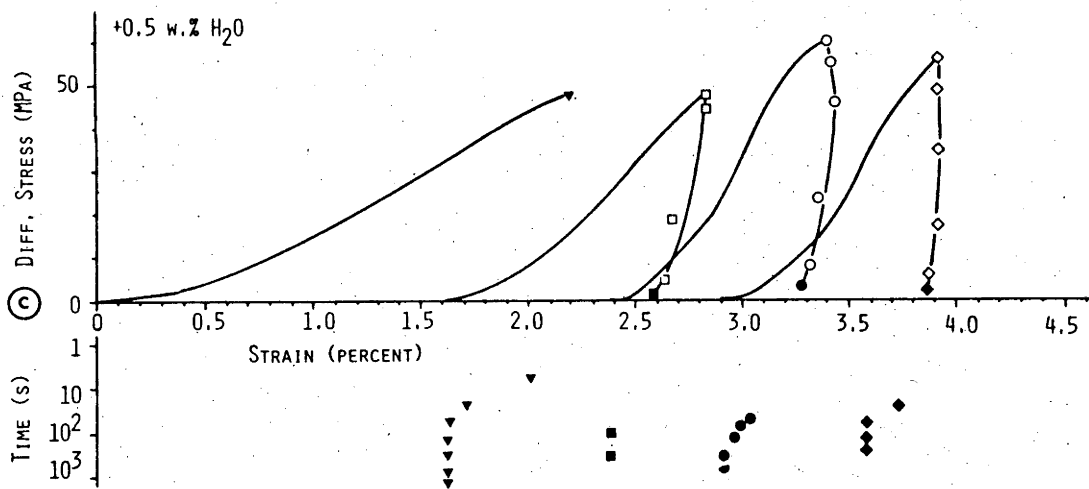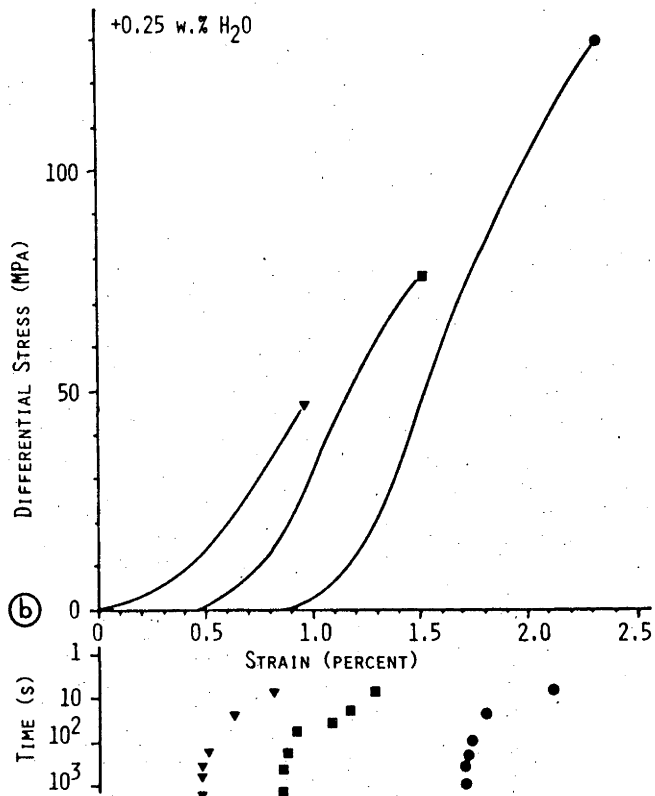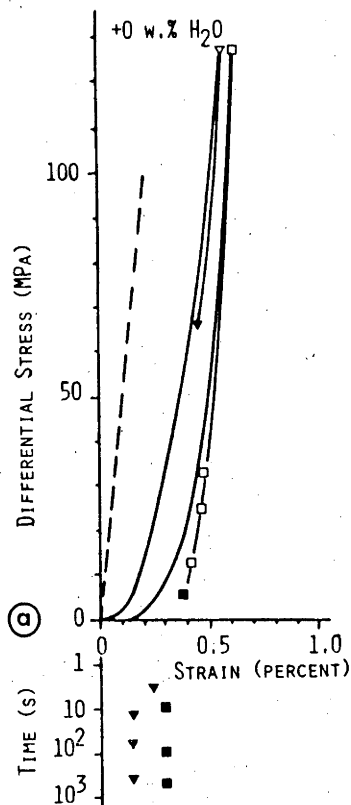
Table 4.2   Cycling tests.

Run No.	+H_2O w %	Melt %	Cycle	ε^* %	$E_{relaxed}$ GPa	$E_{unrelaxed}$ GPa
3106	zero	<3	1	0.17	30	+)
			2	0.16	39	53
3066	0.25	5	1	0.40	10	+)
			2	0.52	11	+)
			3	0.37	21	+)
3073	0.5	10	1	0.48	8	+)
			2	0.36	10	22
			3	0.43	9	31
			4	0.27	10	66
3109	1.0	15	1	0.42	3	+)
			2	0.41	2	12 Ø)
			3	0.43	4	9 Ø)

+) not recorded   Ø) complicated by creep

$E_{unrelaxed}$, calculated as the secant modulus from the stress at maximum strain to the point of lowest detectable stress during unloading. Because of the small stress-strain intervals over which these moduli are determined the precision cannot be better than roughly a factor of 2. Nevertheless, some clear trends are revealed. The relaxed modulus is seen to decrease with increasing amounts of added water and counted melt percentage, while the unrelaxed modulus is not obviously dependent on melt fraction where recorded.

In another experiment with 0.5 weight percent added water, after reaching a stress of 60 MPa at 3.0 percent strain, the piston was retracted abruptly to a position corresponding to roughly half the expected total recoverable strain. For 15 seconds no load was registered, then the growing specimen came into contact with the piston again, and the load rose from zero to a level corresponding to 5 MPa in 140 seconds and remained there for the next 1000 seconds, slightly relaxing to 3.7 MPa. After retracting the piston, further strain recovery occurred until a total strain of 2.0 percent was reached after about 300 seconds. In this case ϵ^* has the high value of 0.9 percent.

Chapter 5

MICROSCOPICAL OBSERVATIONS

5.1   Introduction

In this chapter the microstructural observations on partially-
melted granite specimens will be presented: first for the hydrostatic case,
then for the deformed specimens to illustrate the modifications in
microstructure which occur during deformation and to gain an impression of
the mechanisms which are operating during deformation in these experiments.

The methods by which quenched melt can be recognized in thin
section have been described in Chapter 3, together with some of the
difficulties encountered when melt films are very thin and not inclined
at a high angle to the plane of the thin section. Thus it is not possible
to positively identify an unmelted grain boundary under the microscope.
To determine the degree of wetting of grainboundaries by melt, I have
therefore adopted the procedure of counting the fraction of grain boundaries
in which melt can be seen to occur.

5.2   Hydrostatic experiments

The microstructure of the Delegate aplite after heating for 100
to 300 minutes hydrostatically at 800°C, 300 MPa with added water is in
general similar to that observed and illustrated for other granites with
added water by Mehnert *et al.* (1973), Büsch *et al.* (1974) and Arzi (1978-b).
The principal features are:

(1)   Melt has formed throughout the specimen at triple point junctions of
        quartz, plagioclase and K-feldspar, along quartz-plagioclase and
        quartz-K-feldspar grainboundaries, and to a lesser extent along
        plagioclase-K-feldspar grainboundaries and where identical minerals
        are in contact. The melt films at the boundaries have random
        orientations and there are no differences in film thickness between
        the center and the outside of the specimen.

(2)   Although most melt films have a fairly constant thickness it is also
        noted that, particularly at low melt fractions, melt appears to
        occur in some grainboundaries in channels separated by bridging
        contacts from one grain to another. A full gradation exists
        from such boundaries which seem to be filled with melt only locally

to those separated by more or less planar films. A sawtooth-like contact is often found between melt film and a feldspar grain when the cleavages of the feldspar are inclined to the orientation of the melt film.

(3)   The fraction of grainboundaries observed to bear melt was determined to be more than 90 percent for 10 volume percent melt and to decrease to 84 and 63 percent for 7 and 5 percent melt respectively. These fractions are larger than reported by Arzi (1978-b). The observed decrease is at least in part due to the increased difficulty of recognizing thinner melt films with decreasing melt fraction. I therefore conclude that the rock is substantially disaggregated as a result of this wide spread presence of melt at grainboundaries.

(4)   Melt also occurs in cracks in all minerals including cleavages in feldspars (*c.f.* Mehnert *et al.*, 1973). These cracks are more common than in the starting material and are randomly oriented.

(5)   Inclusions of quartz in feldspar or of feldspar in quartz have melt rims, and radial and concentric cracks in the host are melt-filled (Figure 5.1).

(6)   Biotite grains are entirely black or show black rims in thin section owing to an overgrowth of a dehydration phase (*c.f.* Büsch *et al.*, 1974), and the melt rims around altered biotites are slightly wider than around other minerals.

(7)   There is some undulatory extinction in the quartz and deformation twinning in the plagioclase similar to that in the starting material. No recrystallization is observed; there are some "nests" of the size of normal grains consisting of fine square shaped plagioclase grains, but these are also found in the starting material. These observations apply for all amounts of water, only the thickness of melt films increasing with amount of water.

From the short time for melt formation and the absence of gradients in melt fraction through the specimen it is concluded that water occurs throughout the specimen in cracks and grainboundary cavities at the beginning of melting since the diffusivity of water through granite melt once formed is low (of the order of $10^{-7} cm^2 s^{-1}$ under experimental conditions, Shaw, 1974; Arzi, 1978-b). The increase in crack density can be ascribed to effects of

Figure 5.1   Radial and concentric cracks filled with melt
around inclusion of quartz in plagioclase. Hydro-
static experiment; melt appears as black isotropic
glass, crossed polarizers.

Figure 5.2   Preferential alignment of melt films in grain-
boundaries and cracks parallel to the maximum
compressive stress, indicated by arrows. (Run.
No. 2841).

Figure 5.3   Axial fractures in quartz grains, filled with melt
(Run. No. 2841).
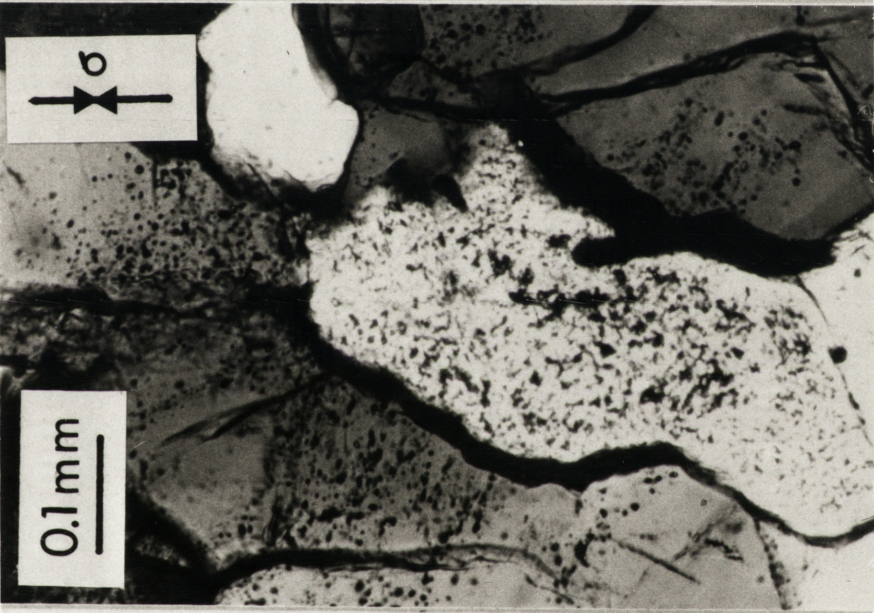
differential thermal expansion of the minerals under conditions of low effective confining pressure.

As noted earlier, no biotite reaction was seen in specimens to which no water had been added although the conditions are above the solidus of dry biotite granite (Brown and Fyfe, 1970). On the other hand biotites alter in specimens with added water. Evidently the dehydration reaction of biotite is accelerated in the presence of water or water-rich melt.

5.3 Deformation experiments

In deformed specimens in which no macroscopic shear-failure occurred, the microstructure described above is modified uniformly throughout the specimen in two main respects:

(1) The density of intragranular microfractures is much greater, even at the lower differential stresses. The new fractures are statistically parallel to the specimen axis and the maximum compressive principal stress and so will be described as "axial fractures". They are filled with melt (Figures 5.2, 5.3 and 5.4). Differential movement on these fractures and on grainboundaries is sometimes evident from the position and shape of grain fragments (Figure 5.3) or, in the case of plagioclase, from the offset in deformation twins (Figure 5.4). The axial fracturing of the grains is similar to that observed by Gallagher *et al.* (1974) in sand. Melt filled axial fractures appear to occur preferentially through the centers of grains.

(2) There is now a strong trend for melt films to be reduced in thickness or removed from grainboundaries and cracks at a high angle to the maximum compressive principal stress while the melt film thickness in grainboundaries and cracks in a more axial orientation has increased (Figure 5.2). This feature is observed in all specimens in spite of the increase in total melt fraction in specimens to which more than 0.25 weight percent water has been added, but becomes less pronounced in the specimens with the highest melt fractions. I did not observe any clear difference between the melt film distributions in specimens which were allowed to relax before cooling and those cooled to temperatures below the solidus while the differential stress was maintained.

Figure 5.4   Offset on axial fractures in plagioclase grain.
              Note also the crossing fractures in the quartz
              grain above (*c.f.* Gallagher *et al.* 1974). (Run No.
              2835).

Figure 5.5   Sharp, anastomsoing shear with gouge in dry specimen
              deformed to 8.5 percent strain. Note intensive axial
              fracturing around shear zone. (Run. No. 2922).

Figure 5.6   Wide, ill defined shear characterized by moderate
              grain size reduction and melt enrichment in a run
              with 18 percent melt deformed to 11.5 percent strain.
              (Run. No. 3026).
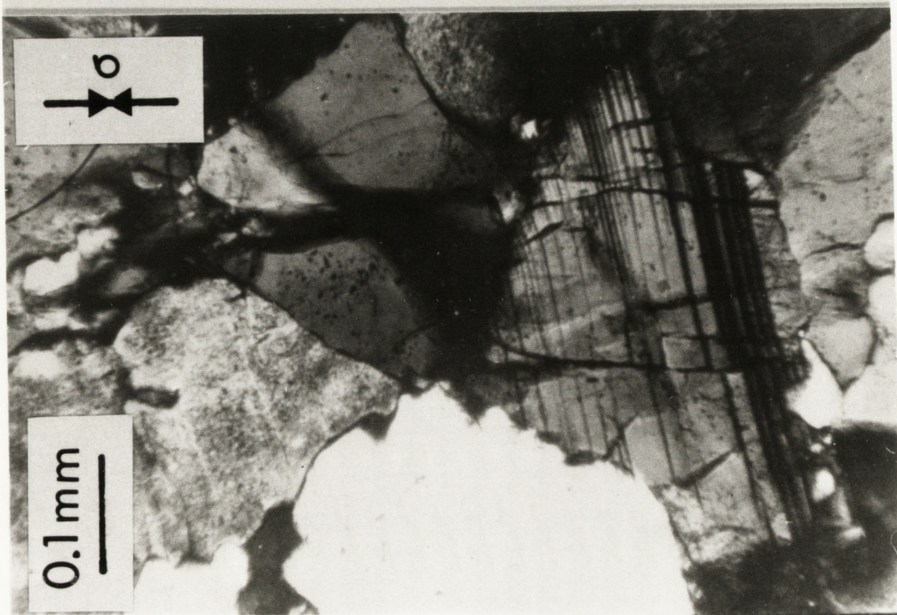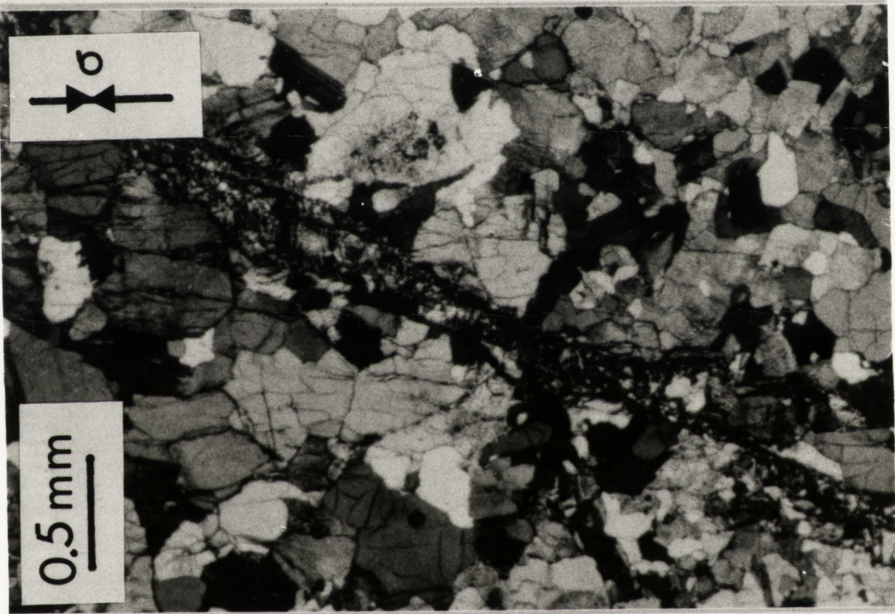
Specimens taken beyond a stress maximum showed the following types of localized deformation features:

(1)   In specimens to which no water has been added and which contain very little melt a sharp shear zone of about 100 μ width and containing gouge crosses the specimen at 30° to the axis (Figure 5.5). Locally pinch and swell occurs along the shear. Axially-fractured grains are found throughout the specimen but occur preferentially in a zone of 2 mm width around the shear.

(2)   In contrast, specimens to which 1.0 or 1.5 weight percent water has been added, and which contain more than 15 volume percent of melt, show only ill defined inclined shear zones of 2-4 mm width in which grain size reduction is slightly more intensive than elsewhere (Figure 5.6); gouge is seen only very locally over the length of a few grains. It would appear that most of the deformation has occurred by widespread melt redistribution and cataclastic flow.

(3)   Specimens to which 0.25 and 0.5 percent water has been added show intermediate microstructures. The variability of stress-strain results for specimens with 0.25 percent added water is reflected in their microstructures. Thus specimens which failed at relatively low stresses and strains have sharp 30° shear zones with gouge, as in runs without added water, while those which failed at higher stresses have conjugate shears or shears at a high angle to the axis (even 50° and 70°) and a high degree of axial fracturing outside the shear zone. In specimens with 0.5 percent added water shear zones occurred at angles from 30° to 50° and part of such a shear may be narrow and gouge bearing with a zone of intensive axial fracturing around it, while another part may be solely a wide zone of melt filled fractures.

There is little evidence of intragranular plastic strain in the specimens, although the presence of some strain features in the starting material, as noted above, confuses the issue slightly. The only clear indication of plasticity induced in the experiments is given by an occassional altered biotite grain which is kinked or smeared out in a shear zone. In a few cases, K-feldspar grains show an S-shaped extinction not observed in specimens subjected to hydrostatic pressure only, but in view of the electron microscope observation of Tullis and Yund (1977) that undulatory extinction can arise from submicroscopic fracturing, one should be cautious in interpreting this effect as evidence of crystal plasticity.

No features were observed that suggested preferential melting at highly stressed contacts according to Riecke's pressure melting mechanism (Riecke, 1895; Paterson, 1973).

Chapter 6

MISCELLANEOUS EXPERIMENTS

6.1   Introduction

All deformation experiments described above were done at 800°C
after 100 minutes under hydrostatic conditions on specimens assembled in
the same way. In this chapter I have grouped together a number of experiments
in which the procedures followed were different. In Section 6.2, the effect
of a higher melt fraction than can be obtained in standard experiments, is
explored by assembling powdered granite with added water. The effect of
changing the temperature in otherwise standard experiments is described
in Section 6.3. In the final section of this chapter, I will describe the
testing and confirmation of a theoretical relationship which allows
calculation of the stresses needed to expell viscous melt from between two
grains approaching one another during compression. Discussion of the results
is deferred to Chapter 7.

6.2   Powder experiment

In the experiments with solid specimens, it has been shown that
the initial melt fraction is limited to less than 10 volume percent, and it
would appear that even when additional surficial melt is drawn into the
specimen during deformation a limit of about 25 volume percent may be set
by the circumstance that the strength falls to a negligibly low level at
this amount. In an attempt to explore the behaviour at larger melt
fractions, another approach was therefore made, beginning with a specimen
of compacted powder having a high initial porosity.

Some of the Delegate aplite was crushed and sieved to separate
a 400-1200 μ diameter fraction. A suitable amount of this fraction was
compacted in a 10 mm diameter pellet press to 200 MPa before sealing with
2.0 weight percent of added water into the same assembly as before (Figure
2.1). The porosity of the pellets was about 40 percent as determined from
bulk density.

Following the same pre-heating and testing conditions as before
(100 minutes at 800°C, 300 MPa) a constant strainrate experiment was carried
out to 12 percent shortening, at a strainrate of $10^{-4}s^{-1}$. In spite of this
high strainrate, the load measured during deformation could be entirely

attributed to that supported by the copper jacket, showing that the flow stress in the partially-melted specimen was very low - less than 1 MPa.

The deformation was fairly uniform as shown by the overall shape of the jacket which was straight although buckled on a fine scale. A thin section made after the experiment showed only about 24 volume percent of melt distributed within the specimen instead of the 31 percent expected for 2 weight percent of added water (Table 3.2, Figure 3.1), and a layer of glass was observed on the outside of the specimen. There was a bimodal grain size distribution, thought to result partially from crushing during pellet pressing (an effect previously found in analogous experiments on olivine: P.N. Chopra - private communication).

6.3 Experiments at various temperatures

6.3.1 Creep test during a temperature cycle

Figure 6.1 represents the results for a creep experiment on a specimen with 0.5 weight percent added water at 48 MPa differential stress, during a temperature cycle between 500°C and 800°C at 300 MPa confining pressure. The temperature history is shown in Figure 6.1-b : at 500°C stress was applied first, then the temperature was raised gradually to 800°C in approximately half an hour and the creep strain was recorded for almost 2 hours before the temperature was lowered again to 500°C in half an hour, followed by unloading. Throughout the run constant stress was maintained by driving the loading piston backwards or forwards to comply with the creep strain in the specimen and thermal length changes in both the specimen and the loading assembly.

Figure 6.1-a shows the strain history. Correction was made for length changes in the loading assembly with temperature, as established in a calibration run on a dummy specimen with known thermal expansion. No correction was made for thermal length changes in the specimen. A rough measure of the linear thermal expansion of granite between 500°C and 800°C under low effective confining pressure but 48 MPa differential stress can therefore be obtained from the figure. It is seen that the strain in the specimen decreases by $\sim 3 \times 10^{-3}$ during 300°C increase (A-B) and increases $\sim 4 \times 10^{-3}$ during 300°C decrease (C-D). Neglecting creep effects during temperature changes a linear thermal expansion coefficient of the order $10^{-5}°C^{-1}$ is obtained. This value is in reasonable agreement with (although

Figure 6.1-a, b. Creep during a temperature cycle between 500°C
and 800°C at 300 MPa confining pressure and 48 MPa
differential stress. Figure a, gives the amount of
strain as a function of time, figure b, the temper-
ature history. The strains are calculated assuming
the initial length at 500°C to be equal to that at
ambient conditions. The "strain differences" between
A and B, and C and D are caused by length changes in
the specimen with temperature.

(a) Run 2864 + ½ w.% H_2O 48 MPa

STRAIN (PERCENT)

C D

UNLOADING

A B

LOADING

0 60 120 180

(b)

TEMP. (°C)

B C

800

700

A

SOLIDUS

600

500

D

0 60 120 180

TIME (MINUTES)
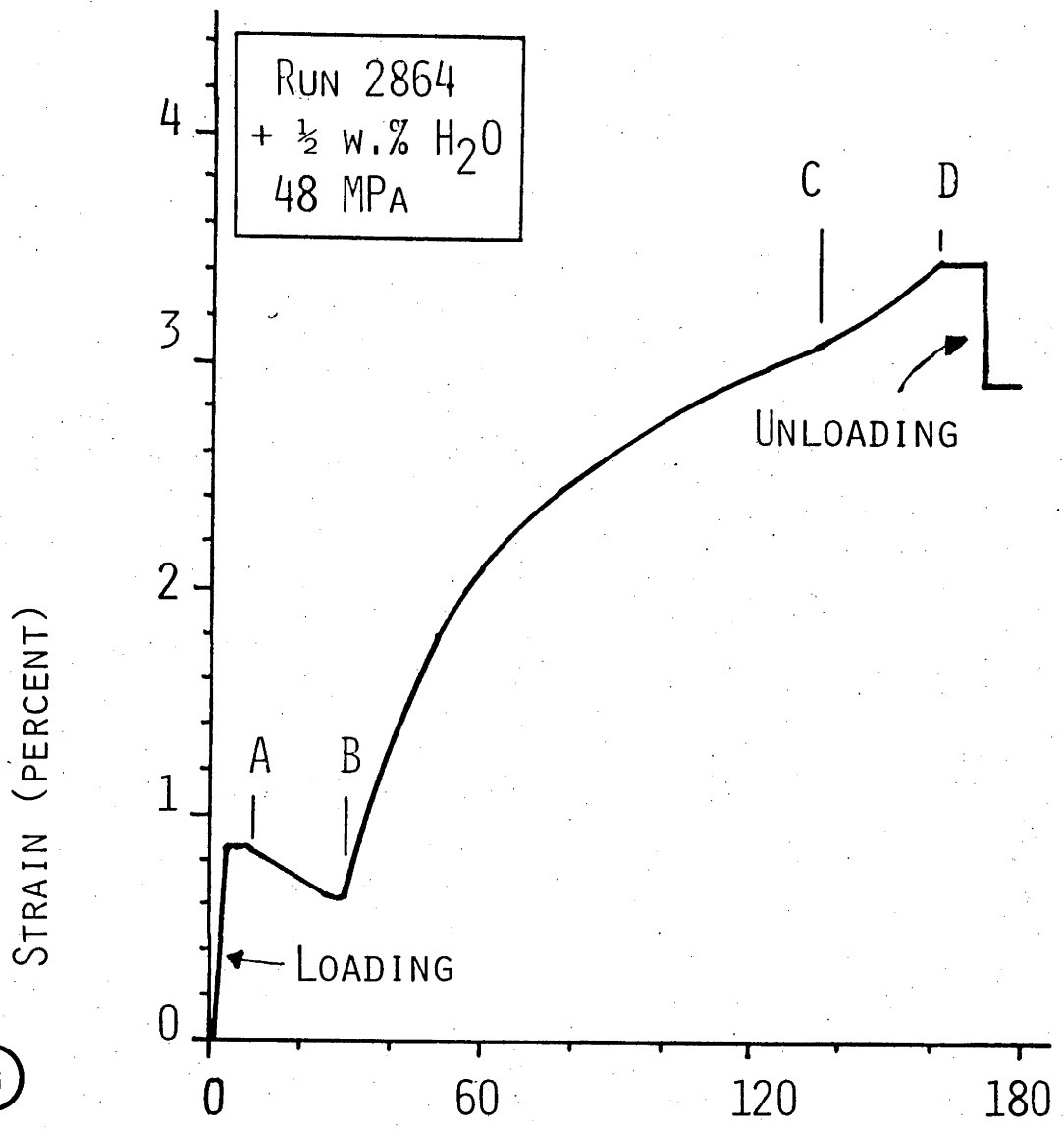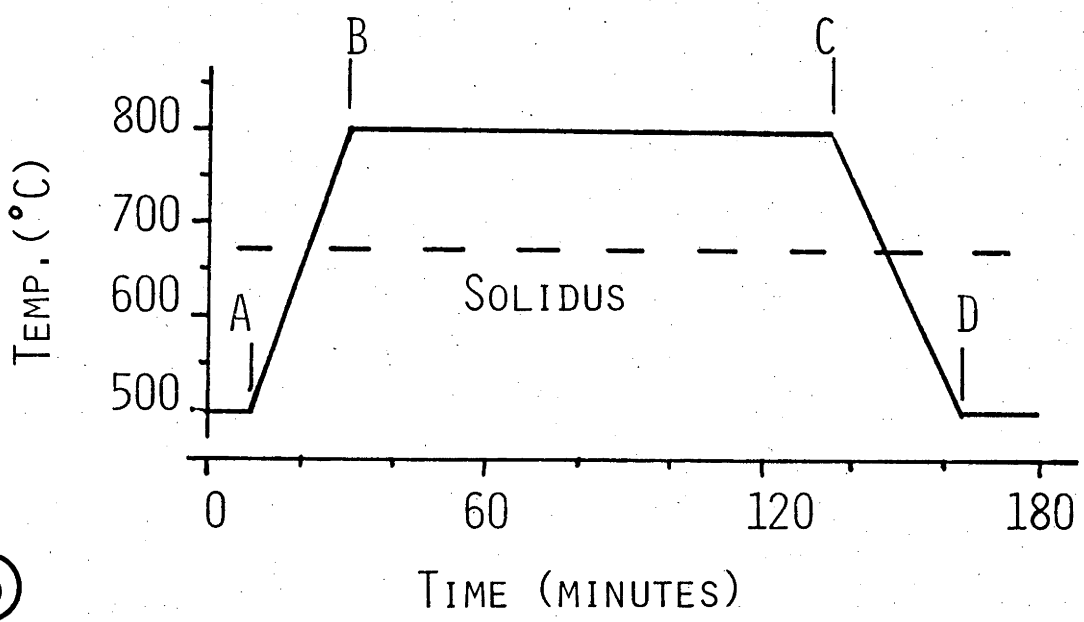
slightly lower than) the more precise measurements of thermal expansion in the presence of a pore fluid under 300 MPa hydrostatic confining pressure, presented in Part II (Chapter 9.4.4). If the apparent difference is real the effect could be ascribed to the differential stress preventing the opening of cracks in the axial direction plus possible creep effects.

The initial deformation at 500°C is essentially elastic : creep is not recorded immediately when the solidus is exceeded at 670°C but becomes noticable at 800°C. This delay in the onset of creep presumably reflects unfavourable melting kinetics and perhaps also decreasing melt viscosity associated with the increasing temperature. At 800°C creep occurs at a rate decreasing from $\sim 10^{-5} s^{-1}$ to $10^{-6} s^{-1}$, initially at an increasing melt percentage. Experience from other runs at 800°C (Chapter 3) would suggest that the melt fraction remained constant after an hour or so at the finally observed value of 11 volume percent. Another experiment at 25 MPa differential stress gave similar results. However, the complicated corrections needed to analyse the data and the uncertainty about the state of melting reduce the precision and usefulness of this type of experiment.

6.3.2 Creep and cycle test at three different temperatures

A specimen with 0.5 weight percent added water was taken to 300 MPa and 800°C, and kept under hydrostatic conditions for 100 minutes prior to performing a constant strainrate test ($5 \times 10^{-5} s^{-1}$) by advancing the loading piston at a constant rate until a differential stress of 60 MPa was reached. Subsequently a creep test was performed at this stress level for a period of 1 hour. After that, the piston was withdrawn and the specimen allowed to relax for 5 minutes before the temperature was decreased to 750°C in another 5 minutes. The specimen was then kept under hydrostatic conditions at 750°C for 20 minutes, followed by a constant strainrate test to the same differential stress of 60 MPa and one hour creep at that stress. In a third, fourth and fifth cycle similar experiments were performed on the same specimen at 800°C, 850°C and 800°C, using the same period under hydrostatic conditions prior to deformation, the same piston advancement rate, the same creep stress and the same creep period, the same time for relaxation after unloading, and the same time to change temperature by 50°C. The results for this complicated experiment which lasted more than 10 hours are indicated in Figure 6.2.

Stress-strain results are indicated in Figure 6.2-a. Correction was made for length changes in the loading system with temperature and

Figure 6.2-a,b. Creep and cycle test at three different temper-
atures, 800°C, 750°C and 850°C, at 300 MPa confining
pressure and 60 MPa differential stress. Figure -a
gives the stress-strain curves for five cycles with one
hour of creep in each cycle. The downward arrows
indicate unloading; to obtain elastic strains the
last point of each cycle has been compared with the
first point of the next. Figure -b gives the
loading -, creep-, elastic- and permanent strains of
each cycle. For further explanation see text.
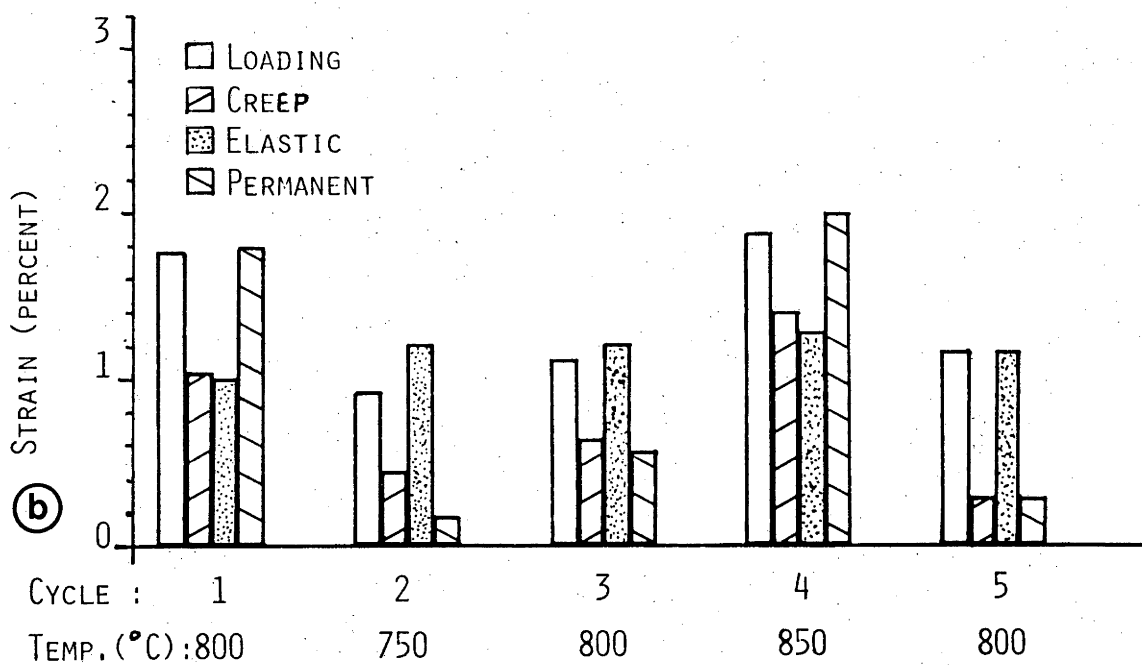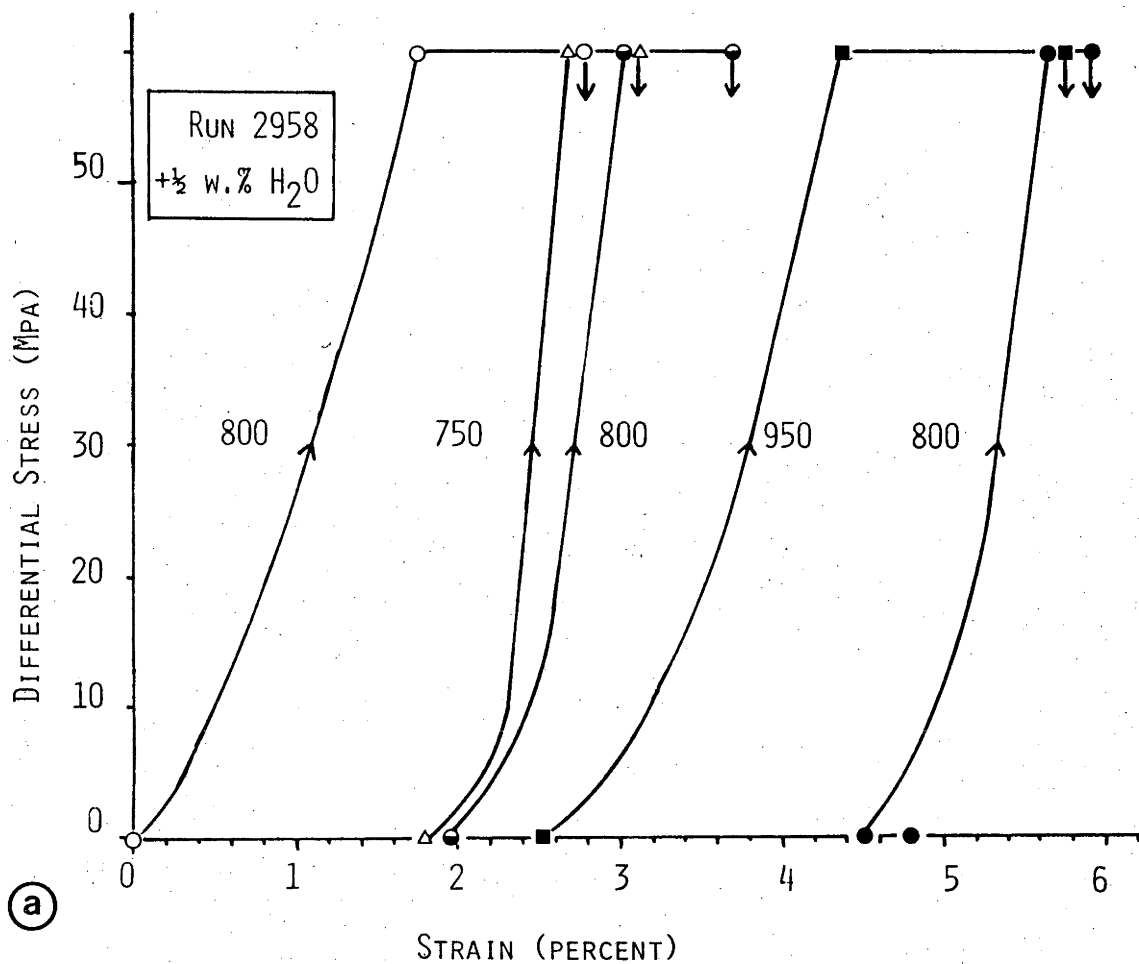
differential stress. In Figure 6.2-b, I have indicated the amounts of strain during loading to 60 MPa, the creep strain in 1 hour, the elastically recovered strain and the permanent strain for each cycle as obtained from Figure 6.2-a. The elastic strain represents the strain recovered between the removal of differential stress with unloading at the end of a cycle and the application of differential stress in the next. The permanent strain is the difference between the initial strain at the beginning of a cycle and the initial strain at the beginning of the next. The measurements of loading strain and creep strain are made at constant temperature and are believed to be correct within 10^{-3} (compare Chapter 2.6). The permanent and elastic strains are calculated from measurements at different temperatures and depend on a correction, the results are therefore believed to be somewhat less precise.

The following features can be observed:

(1)   On the scale of precision of the present experiments the elastic recovery does not change with the number of the cycle, or with the temperature. The viscosity of the granitic melt however changes by a factor of ~6 over the 100°C temperatures interval covered (see Shaw, 1972). As expected the relaxed unloading modulus (Chapter 4.4) is independent of melt viscosity. An $E_{relaxed}$ of 5 GPa is indicated, a somewhat low value compared to those listed in Table 4.2 Another experiment with a high amount of relaxed strain is described in Chapter 4.4. It is not known what causes this variation between specimens.

(2)   By comparing cycles 1, 3 and 5 at 800°C it is seen that during the first cycle part of the finally observed permanent strain is induced during loading and part during creep. In subsequent cycles most of the permanent strain is induced during creep, while the loading strain is elastically recovered. The amount of creep strain per hour decreases with increasing cycle number and increasing total strain. The latter observation is in good agreement with the results of creep experiments described in Chapter 4.3.

(3)   Increasing temperature increases the amount of strain per cycle. By comparing cycles 2, 3 and 4 in Figure 6.2-b it is seen that the permanent strain per cycle increases by a factor of ~3 per 50°C, in spite of the trend noted under (2).

(4)   At 750°C, more strain is recovered elastically than induced
       during loading. This indicates that part of the creep strain
       can be recovered elastically afterwards. Such an effect is not
       noted for the cycles at higher temperatures.

The counted melt fraction was 14 volume percent, 3 to 4 percent
higher than for deformation experiments at 800°C, with 0.5 weight percent
added water (Figure 3.1). This difference may be partly explained by the
unusually long run period, but could also be caused by the higher temperature
of 850°C during the present run, because the melt rate in granite with
added water increases with temperature as demonstrated by Mehnert *et al.*
(1973). The large strains at 850°C may therefore indicate an increase
in melt fraction, but it is noticed that the deformation in the subsequent
cycle at 800°C agrees well with the trend obtained from previous cycles.

6.4   Melt expulsion experiment

The microscopical observations presented in Chapter 5 indicate
that melt films originally at a high angle to the highest macroscopic
differential stress are pushed out during shortening and that the expelled
melt enters grainboundaries and cracks oriented at a smaller angle to
the axial stress. The forces needed to expell melt from between two grains
approaching at a constant rate are strongly dependent on the grain size and
the melt film thickness, and to a lesser extent on the approach velocity
and the melt viscosity. In Appendix 1, the following relationship is
derived from the work of Bowden and Tabor (1950, p. 274):

$$\sigma = 1.5 \, \frac{\eta V}{h^3} \cdot R^2 \qquad \text{c.g.s.} \qquad (1)$$

where σ is the stress needed to bring two rigid, cylinders of radius R
together in the axial direction at a constant velocity V by expelling a
fluid film of thickness h and viscosity η from between them. The geometry
is shown in Figure A.1.1 in Appendix 1. A similar relationship was applied
by Bowden and Tabor to the case of a hammer hitting an anvil covered by a
thin fluid film with a low viscosity. Here a simple test will be described
demonstrating the validity of (1) during conditions of low approach velocity
and high melt viscosity as they pertain during deformation tests on partially-
melted granite.

A composite specimen consisting of two cylinders of Anita Bay dunite (each 9 mm in length and 9.93 mm in diameter) separated by a disc of 1.23 mm thickness and 9.93 mm diameter of petrographic microslide glass was jacketed in thin Cu-tubing and sealed off with Mo-endpieces and rings, as used in the standard assembly of Figure 2.1. This assembly was then taken up to 300 MPa confining pressure and 900°C and deformed axially in compression. During the experiment the rate of piston advancement V was kept constant at 2 x 10^{-5} cm per second, R and the initial thickness h_o were known from the micrometer measurements prior to the experiment such that σ and h could be determined from the load and displacement chart. The viscosity of the glass under these conditions is not known, but if it is comparable to that of other common glasses at 900°C and atmospheric pressure a value of close to 10^7 Pascal second (10^8 Poise) may be expected (D. Burmann - glassblower, private communication). The test of (1) consists in determining η from the known variables during a compression test. From (1) we have:

$$^{10}\log\eta \ = \ ^{10}\log\sigma + 3\,^{10}\log h - \,^{10}\log(1.5VR^2) \qquad (2)$$

where all quantities are expressed in c.g.s. For each set of σ and h values the same result should be obtained for η and this value has to be reasonably close to the expected value of $\sim 10^7$ Pascal second.

In evaluating the experimental results correction was made for the elastic distortion of the apparatus, but not for the load carried by the Cu-jacket during deformation, nor for any strain which did occur in the dunite specimens. The omission of the jacket correction leads to an overestimate of the load carried by the melt at low loads, and therefore (2) will give too high values for the viscosity of the melt. Neglecting the strain in the dunite specimens at high loads results in an underestimate of h and therefore (2) will give too low values for the viscosity.

The results for the experiment are presented in Table 6.1. It is seen that for stress values between 2 and 50 MPa reasonably constant viscosity values of 6 x 10^6 to 9 x 10^6 Pascal seconds are obtained, in satisfactory agreement with the expected value. At stresses lower than 2 MPa the influence of the Cu-jacket is appreciable in good agreement with the magnitude of the jacket corrections presented for 800°C in Chapter 2.5. The measurement of h becomes increasingly less precise towards higher loads in view of its decreased magnitude and the higher apparatus distortion correction (Chapter 2.6). Nevertheless, it can be concluded that deformation

Table 6.1   Determination of melt viscosity during an expulsion
experiment.

σ(MPa)	h(μ)	η(x 10^6Pa s)
0.6	1000	85
0.9	630	30
2.0	290	6.4
2.4	280	7.2
3.0	250	6.4
4.4	220	6.2
6.3	200	7.2
9.8	180	7.9
18.2	160	9.1
31.0	130	8.9
39.0	120	9.1
46.8	110	8.3
49.0	100	6.6
63.1	80	4.2
117.5	55	2.6
150.3	<10	<0.02

of dunite under these conditions becomes significant at stress levels above 50 MPa.

Microscopical examination of the thin section made after the experiment revealed that the glass disc had been reduced in thickness from 1.23 mm to 20 to 40 μ during the test. Most expelled melt had collected at the circumference of the contact, however some melt-filled intergranular axial fractures of several 100 μ in length were seen to originate from the contact film thinning out progressively into the dunite specimens on either side. The occurrence of these axial fractures close to the center, rather than at the margins of the specimen is likely to reflect the parabolic pressure gradient existing in the fluid during uniaxial compression, varying from a value of 2σ at the center to 0 at the margins (see Appendix I). The observation of melt-filled axial fractures through the center of grains in deformed partially-melted granite (Chapter 5) is recalled in this context.

Chapter 7

DISCUSSION

7.1   Summary of results

The observations described above give the following general
picture. In the first 100 minutes under hydrostatic conditions at 800°C
melt is formed at grainboundaries and triple point junctions. The amount
of melt within the specimen depends on the amount of water that can enter,
and is in good agreement with expectations, based on measurements of
accessible pore space and water saturated melting. In a hydrostatic
experiment the maximum water take-up is 0.6 weight percent giving rise to
8 to 10 volume percent melt; any extra added water resides between the
specimen and the jacket and causes melting there. During deformation this
external film is drawn into the specimen.

The stress-strain curves of the partially-melted rock have in
common a generally sigmoidal shape but the details change substantially
with increasing melt fraction, especially beyond about 10 volume percent.
With less than 10 percent of melt there is only a slightly developed
initial toe, and the slope soon becomes quite steep (up to 17 GPa slope,
about one third of the elastic slope for unmelted granite) and the stress
maximum is usually followed by a relatively sharp fall associated with the
formation of a sharply defined shear failure. With greater than 10 percent
of melt, the initial toe becomes much more pronounced, the maximum slope
and peak stress become much lower and occur at larger strains, and there
is a less marked fall after the flatter maximum, while the deformation
becomes more homogeneously distributed throughout the specimen. When the
melt fraction reaches about 25 percent the maximum stress has fallen to an
undetectable level, below 1 MPa. In no case is steady state behaviour
manifested over a substantial strain interval, an aspect that is further
emphasized by the creep observations which suggest almost entirely transient
creep behaviour associated with some sort of exhaustion mechanism.

Some strainrate sensitivity is observed. For experiments at 800°C
the maximum slope of the stress-strain curves during loading is found to
increase somewhat with increasing strainrate for melt fractions exceeding
10 volume percent. The maximum stress reached during constant strainrate
experiments is rather insensitive to strainrate as is shown in Figure 7.1
for the various melt fractions studied. An ideally Newtonian fluid would have

Figure 7.1   Maximum differential stress versus strainrate for various melt fractions. Note the low strainrate sensitivity. Star indicates powder experiment.
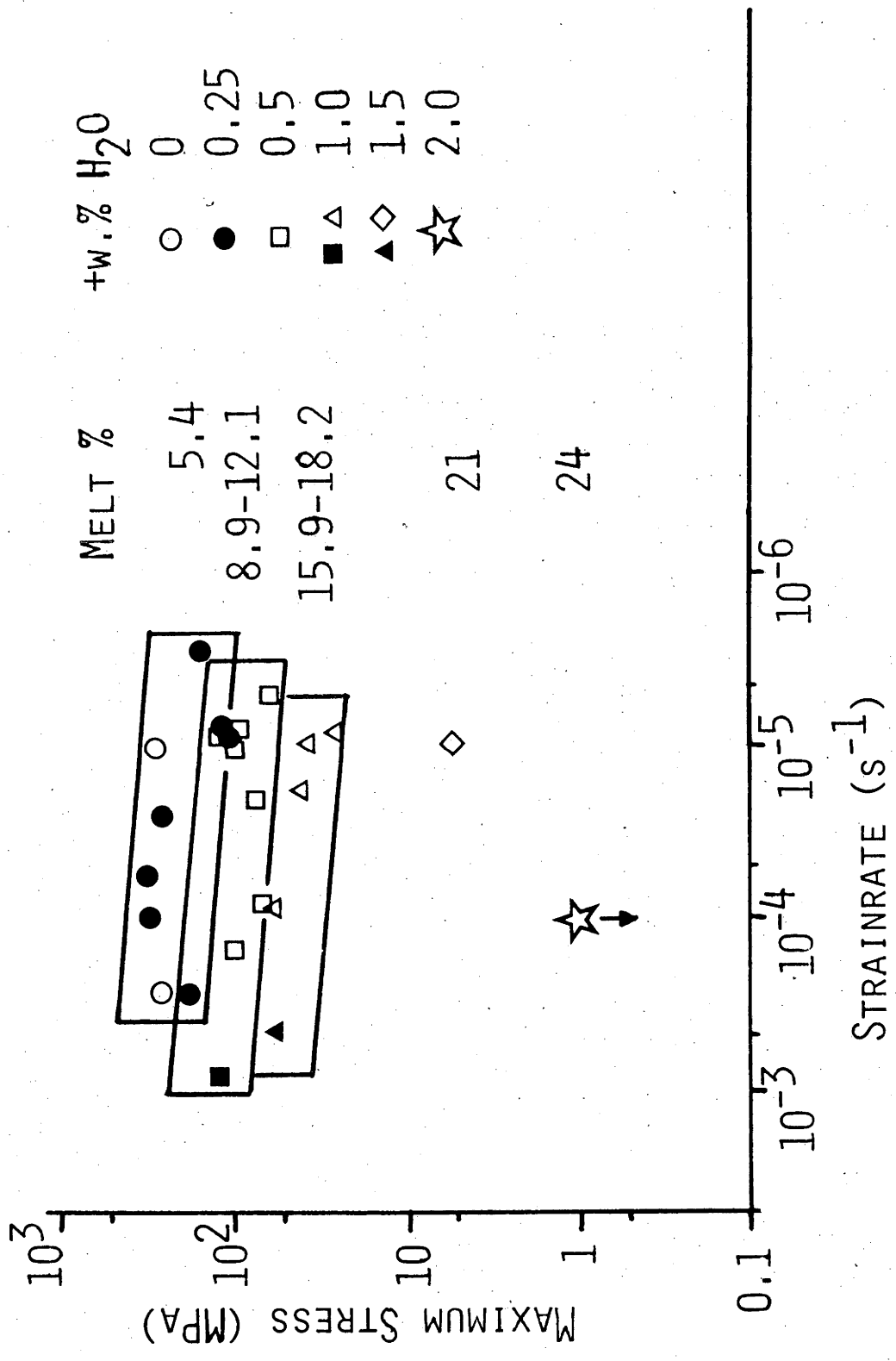
a slope of -1 on such a plot, whereas the results here are seen to give
a slope closer to -0.1, suggesting only a minor contribution of the viscous
melt to rate sensitivity of the maximum stress. In view of the absence
of a steady state and the low rate sensitivity, expression of these results
in terms of "effective viscosities" is not warranted.

The effects of temperature are not explored in detail in this
study. The preliminary results of Chapter 6.3.2 suggest that the relaxed
unloading modulus of partially-melted granite is uninfluenced by temperature
between 750°C and 850°C. The maximum slope of the stress-strain curves
during loading decreases with increasing temperature, while the creeprate
for a given stress increases.

The microscopical observations point to there being two predominant
and complementary processes contributing to the deformation. Firstly, there
is movement of melt, it being transferred from grainboundaries and cracks
inclined steeply to the applied axial stress into those inclined at low
angles, as well as being drawn into the specimen from surface films. Secondly,
there is fracturing of many grains and relative movement of the grains or
their fragments. Melt films, are detected at the majority of grainboundaries,
even with low melt fractions, indicating that the initial polycrystalline
solid has been largely disaggregated into an assemblage of grains with
negligible cohesion between them.

7.2 Outline of the discussion

The two-phase nature of partially-melted rock has been stressed
throughout this study. In the following discussion I will attempt to analyse
the deformation characteristics of granite with melt in terms of simple two-
phase models suggested by the microscopical observations. It will be pre-
sumed that the material is completely disaggregated and may be considered
as a jacketed assemblage of separated particles with viscous fluid in the
interstices. Compressive and shear forces can therefore be transmitted
between particles in the models, but not tensile forces.

Melt expulsion and elastic and brittle deformation of grains,
as well as sliding between grains, occur concurrently during one deformation
increment. Such processes will be considered in isolation in the following
sections. Relevant, but perhaps somewhat unrealistic assumptions will be
made about the shape and the physical properties of the grains, or about
the distribution of melt films in order to illustrate specific aspects.

Thus, I will move freely from one two-phase model taking the particles as rigid and cylindrical to evaluate melt expulsion from between grainboundaries, to another model considering the grains to be rigid and spherical to evaluate dilatational aspects, to yet another model in which the elastic unloading effects are analyzed by considering spherical elastic particles.

It is convenient to separate the various conceivable aspects of the rheological behaviour into three groups as discussed in Sections 7.3 to 7.5, although in practice a great deal of overlap can be expected.

In the final section of the discussion the concept of the critical melt fraction, introduced in Chapter 1, will be taken up again, using the experimental data of this study for the lower melt fractions and the findings of suspension studies for the higher fractions.

7.3   Consolidation aspects

Under this heading are grouped the aspects of behaviour that probably predominate in the initial concave upwards part of the stress-strain curve. They involve the movement together of the grains to form a closer packed assemblage, small distortion of this assemblage, and the concomittant movement of fluid relative to the particles. One can distinguish the following specific effects.

7.3.1   Initial compaction

In the initial stages of straining, the grains will be moved generally towards each other in the direction of shortening, squeezing out intervening melt, until a continuous framework of contacts is established that can support compressive differential loading. In doing so, melt will be squeezed into interstices inclined more nearly parallel to the loading direction, and there will be some tendency towards a denser packing of grains with movement of melt into the annular space between jacket and specimen. If the melt were initially uniformly distributed around the grains, the shortening strain associated with this initial compaction could amount to roughly one-third of the melt fraction, but in practice it is likely to be considerably less on account of the observed non-uniform melt film thickness.

The stress on two cylindrical grains needed to expell a flat melt film from between them is calculated in Appendix I from the following equation derived from the work of Bowden and Tabor (1950):

$$\sigma = \frac{3}{8}\eta\dot{\epsilon}(\frac{d}{h})^3 \qquad\qquad (1),$$

where η is the viscosity and h the thickness of the melt film, d the grain-size and $\dot{\epsilon}$ the over all strainrate. That such an equation can be applied to the case of slow approach velocity or low strainrate, and high melt viscosity has been demonstrated in Chapter 6.4. The results of the calculation (Table A.1.1) indicate that the stress during a constant strainrate experiment becomes significant on the scale of precision of the present apparatus, that is $\sigma > 1$MPa, if the melt film films perpendicular to the shortening direction are between 1 and 10 μ in thickness. Subsequently stress rises rapidly in a non-linear fashion with further melt expulsion to values much higher than actually reached in any of the experiments. A flat melt film of constant thickness has been assumed in the calculation above. The effect of different melt film shapes may be evaluated qualitatively. If the faces of the approaching grains are parallel but curved, the distance to which each unit of melt has to travel before it is expelled from between the grains increases, for the same initial melt film thickness and grain diameter. The rate of shear in the melt is thereby increased such that higher stresses may be expected than calculated for flat melt films. If on the other hand, the approaching faces of grains are not parallel, the stress needed for expulsion during constant strainrate compression will be less than in the parallel cases considered when the faces diverge towards the perimeter of the grains, and more when they converge towards the perimeter.

The present analysis suggests that deformation of individual grains during axial compression of partially-melted granite may start before the grains are in physical contact with each other across intervening melt films (see also Bowden and Tabor, 1950). The strainrate sensitivity and the temperature sensitivity of the maximum slope of the stress-strain curves during loading, noted in Section 7.1, may be caused to some extent by the dependency of σ in (1) or η and $\dot{\epsilon}$.

7.3.2   Dilatancy hardening

So long as the grains remain intact further straining beyond the initial compaction can only be achieved by the grains sliding or rolling over each other. Since the compacted granular assemblage will have a fairly high density of packing, higher than would correspond to the critical melt fraction defined in Chapter 1.2, this further deformation will involve dilatancy. The amount of dilation can be expected to be of the order of

the shortening strain ε (see Appendix 2). If the initial porosity is ϕ_o the dilantancy can be expressed as a volumetric strain of the order of $\frac{\varepsilon}{\phi_o}$ in the pore space. Thus if the pore space is filled with an expansible fluid of bulk modulus $\tilde{K}$, and the specimen is sealed so that no fluid moves in or out of it, then the pore pressure drop Δp accompanying the dilatancy will be of the order $-\frac{\tilde{K}\varepsilon}{\phi_o}$.

By analogy with models of hard spheres (Appendix 2), the additional uniaxial stress σ on the sealed specimen needed to bring about a dilation involving a pressure drop Δp in the pore fluid will be, in the absence of friction:

$$\sigma = -C'\Delta p \qquad (2),$$

where C' is a constant having a value of about 1 to 4. Therefore, we can expect the dilatancy hardening relation to be:

$$\sigma = \frac{C\tilde{K}\varepsilon}{\phi_o} \qquad (3)$$

where C is a constant of order unity to ten. For example, with 10 percent melt the slope of the stress-strain curve associated with dilatancy hardening would be expected to be between $10\tilde{K}$ and $100\tilde{K}$. With a value of the order of 10 GPa for the bulk modulus of silicate melt (Murase and McBirney, 1973) this slope is very steep, steeper in fact than the slope expected for the elastic distortion of unmelted granite with a Young's Modulus of 50 GPa, and so only very small amounts of strain and dilation will be associated with such a homogeneous distortion of the packing assemblage of rigid grains at the stress-levels observed. Even if the pore pressure drop according to equation (2) led to the release of some water, the bulk modulus of which would be about 0.5 GPa at 800°C, 300 MPa pressure (Burnham *et al.*, 1969), the dilatancy hardening slope would not be markedly reduced in order of magnitude in view of the small volume of water likely to be released.

7.3.3   Influence of friction and viscosity

The dilatancy hardening just discussed arises from a balance between compressive contact forces between grains and a suction or pressure difference between the fluid and the region exterior to the sealed specimen. However, there will also be a frictional force component associated with the contact forces, which will augment the required differential stress. Further analogy with hard sphere models (Appendix 2) suggests that the

differential stress σ in (2) and (3) will be accordingly raised by a
multiplying factor of the order $\frac{1 + \mu}{1 - \mu}$ where μ is the coefficient of friction.
For μ = 0.5 a three-fold increase in σ is indicated, but the effect could
be smaller if the melt acted as a lubricant. When the viscosity of the
melt is sufficiently high relative to the local strainrates in the melt
films, the compaction will be significantly time-dependent, and the
compressive forces will be effectively transmitted between grains before
they come into direct contact. The compaction and dilatancy stages will
then overlap or be coupled in a rate dependent way. That is, instead of
a compaction straining at very low stresses being followed by a very steep
dilatancy hardening stage, one could expect in practice a concave upwards,
rate dependent, strain hardening curve of the type observed, in which the
stress level is determined by a combination of dilatancy hardening and
a viscous-frictional component reflecting viscous shearing resistance
in melt films separating grains as well as any normal contact friction that
may arise.

7.3.4   Dilatancy pumping

So far I have not taken into account the presence of melt initially
in the annular space between specimen and jacket, in the cases with sufficient
water added to form melt fractions in excess of 8 to 10 percent. The pressure
differential associated with the dilatancy discussed in Section 7.3.2 will
cause this surficial melt being forced into the body of the specimen. As
this movement occurs additional pore space has to be made available simul-
taneously by further dilatation, calling for an additional shortening strain
of the same order of magnitude as the dilation itself. Thus during dilatancy
pumping of surficial melt a strain of the order of $\phi - 0.10$ can be expected,
where ϕ is the final melt fraction (Appendix 2). In practice the results in
Figure 3.2 indicate that the increase in porosity is related to the axial
strain by a factor 1.5 to 2; this factor is consistent with values of 3 and
smaller, predicted by models for contacting rigid spheres of equal and unequal
sizes (Appendix 2).

The effectiveness of dilatancy pumping will depend on the viscosity
of the melt and it is to be expected that, in analogy to the situation with
the validity of Terzaghi's effective stress-law in brittle fracture with
pore pressure (Brace and Martin, 1968; Ladanyi, 1970; Rutter, 1972), there
will be a critical strainrate above which the dilatancy pumping of a given
amount of melt will not be completed in the course of an experiment to a

given strain. This critical rate is evidently of the order of 10^{-4} to $10^{-3}s^{-1}$ for an initial melt fraction of about 10 percent, from the observations on melt fractions in the specimens with 1 and 1.5 weight percent added water at the faster strainrates (Table 4.1, Figure 3.1). The viscosity of the granitic melt phase saturated with 8 weight percent water at 800°C, 300 MPa (Winkler, 1974) can be estimated to be around 10^4 Pascal second (10^5 Poise) (Shaw, 1972). There may also be an upper limit to the amount of melt that can be drawn into the specimen prior to macro-scopic failure since in the specimen with 1.5 weight percent water, not all melt was drawn in during deformation, even at $10^{-5}s^{-1}$ strainrate to 10 percent strain, while the stress maximum occurred at about half that strain (Table 4.1, Figure 4.4-e).

7.4 Flow aspects

7.4.1 Yielding

As the differential stress rises, a stage is eventually reached at which there is, in a macroscopic sense, some sort of yielding in the specimen to give rise to the bending-over of the stress-strain curve beyond the inflection. There is no evidence in the present experiments that this yielding involves plastic yielding of the grains themselves or any significant amount of *pressure melting* of the grains. Rather, the yielding would appear to consist of an increased facility of the relative movement of grains, closely associated with intragranular fracturing. Thus the yielding can be viewed as the initiation of, or perhaps a preliminary transient phase leading to a granular flow process, that may be continued to indefinitely large strains.

7.4.2 Flow

Sustainable granular flow involves the exchange of neighbours during the relative movement of the grains, which will incur dilation if the melt fraction is less than the critical amount. However, it has already been argued that the dilation, apart from that associated with dilatancy pumping of excess melt, remains small. Therefore, since the grains of the partially-melted rock do not depart markedly from an equant shape or have a great range in sizes, it cannot be expected in the light of the factors reviewed in Chapter 1, that indefinitely continued flow is possible with the initial microstructure unless the melt fraction approaches 40 percent. At melt

fractions of 20-25 percent and less, large strains can only be expected if fracturing of grains occurs so as to introduce a greater range in particle size and so reduce the critical melt fraction (it is presumed that the effect of fracturing in broadening the grain size distribution will outweigh its effect in increasing the angularity of particles; in any case the latter effect is probably kept minimal by the tendency to wear off the asperities, as observed in another context by Karabelas, 1976). Two questions of interest now arise:

(1)   Although the specimen with 24 percent melt exhibited negligible strength in the present experiments the maximum strain reached was only of the order of 10 percent. It is therefore not clear whether this flow is sustainable to large strains since at least 50 percent strain is needed for a single neighbour exchange; moreover, there are some microscopical indications that the flow is not stable. On the other hand, the sharp decline in strength beyond 15 percent melt fraction suggests that a fully mobile state is being approached at 25 percent melt fraction.

(2)   In the specimens with 15 to 20 percent melt, grains are extensively fractured in spite of the low macroscopic stresses. This observation supports the view that the mobility is dependent on the fracturing for lowering the critical melt fraction through increasing the range of grain sizes. The occurrence of fracturing at stresses of a few MPa points to high stress concentrations at grain contacts (see also Section 7.5), but the fracturing of grains may also be facilitated to some extent by a stress-corrosion effect involving the water present in the melt (c.f. Scholz, 1972; Martin, 1972). The absence of an obviously high strainrate sensitivity of the flow stress is evidence for the fracturing being the rate controlling factor rather than the viscosity of melt films in the cases where the flow stress is readily measurable.

7.4.3   Stability

It is generally observed in the experiments that with continued deformation the stress eventually begins to fall and, probably more or less simultaneously, a localized shear develops. That is, the deformation eventually becomes unstable under uniformly applied loading. Such an instability under approximately constant volume conditions is attributable

either to a lack of work hardening or to an insufficient strainrate
sensitivity of the flow stress (Hart *et al.*, 1975; Hart, 1976). Since
the flow of partially-melted granite is relatively insensitive to strainrate,
the stability or instability of flow is presumably dependent on strain
hardening, in this case arising from the increasing resistance to relative
movement and fracturing of the grains. The shear instability would then
represent some sort of local weakening during straining. The occurrence
of some localization of shearing even in the cases of relatively high melt
fractions, where the stress-strain curve can no longer be determined suggests
again that here also grain interference and fracturing are largely controlling
the behaviour rather than the viscosity of the melt because the latter, if
controlling, would give a high strainrate sensitivity and tend to stabilize
the flow.

7.5   Aspects of unloading

Further light is thrown on the factors underlying the mechanical
behaviour of the partially-melted granite by consideration of the observed
after effects, especially of the non-linear unloading behaviour and the
time dependence (Chapter 4.4).

7.5.1   Non-linear unloading behaviour

This behaviour is similar to that observed for other cracked or
granular materials after compression and is commonly ascribed to non-linear
elastic effects at contacts between curved surfaces or to elastic and
frictional effects at cracks and grainboundaries (e.g. Walsh, 1965; Biot,
1973; Warren and Anderson, 1973; Jaeger and Cook, 1976, p. 400). In the
present case, there are three possible sources of driving force for the
reverse strain : the pore pressure drop associated with dilatancy hardening,
surface energy effects and the elastic stresses in the granular framework.
The first two effects seem unlikely to be important because, respectively,
only very small strains are associated with the dilatancy hardening effect
at the stress levels observed according to the considerations of Section
7.3.2, and it is not obvious that there are any substantial changes in
melt-solid interfacial areas during unloading (the microscopical observations
support this conclusion). Elastic distortion of the granular framework,
however, would account for the observed effects.

It is not feasible to model exactly the elastic behaviour of the granular framework during unloading without a detailed description of the three-dimensional contact structure. However, markedly non-linear behaviour like that observed in unloading could be expected for two reasons:

(1)   As a result of some rounding of grains during partial melting and of disturbance of the original packing by relative displacement in the deformation, it can be expected that the contacts will be essentially of the nature of Hertzian contacts between curved surfaces. The non-linearity of the force-displacement relationship at such contacts is well known (e.g. Landau and Lifshitz, 1959, p.30) and will be reflected in macroscopic non-linear behaviour.

(2)   The non-linearity of the elasticity will be made more marked by a tendency for the number of contacts to change with the load.

Calculations with simple models of spherical grains and one Hertzian contact between each neighbouring pair indicate that elastic strains of the order of the observed unloading strains can be accounted for (Appendix 3). The calculation in Appendix 3 also shows that very high stresses, of the order of one thousand times the macroscopic stress, are predicted at the contacts, giving an explanation for the widespread cracking observed in the grains; furthermore, the stresses tend to be higher the smaller the radius of curvature, giving a greater tendency for cracking the smaller grains and thereby increasing the range of grain sizes and facilitating the transition to liquid-like behaviour discussed previously.

The Hertzian equations of Appendix 3 are not strictly correct at high values of stress and strain. Nevertheless the occurrence of axial fractures in partially-melted granite deformed at low macroscopic differential stress of 1-10 MPa, as well as in specimens deformed at higher stresses, may be attributed to the high stress concentration at non-parallel contacts. The plastic yield strength of the constituent minerals of granite is likely to be exceeded prior to the occurrence of brittle failure, but evidence of extensive plasticity is lacking in the present experiments. High plastic deformation rates would be required locally at contacts to completely prevent an elastic build-up of high contact stress. This requirement is clearly not met during the constant strainrate experiments on partially-melted granite. Some crystal plasticity is likely to have occurred at contacts, but this is not visible under the optical microscope.

7.5.2 Time dependence

Accompanying the elastic rebound in the granular framework there will be non-uniform changes in the intergranular spaces, requiring accommodating movement of melt. The time dependence in the after effect can then be expected to arise from the viscous resistance to this movement of melt, especially at sites where the solid surfaces are in close proximity, as in cracks or slightly-open grainboundaries. However, representation of the effects by a conventional linear spring and dashpot model would be inadequate because of the non-linearity required of the spring and the wide range of relaxation times to be expected for flow in cavities of different aspect ratios. Qualitatively, the unrelaxed modulus would derive from elastic unloading displacements in the granular framework which involve negligible displacement of the melt, while the relaxed modulus refers to complete elastic unloading with accompanying redistribution of melt.

7.6 Critical melt fraction of granite at a strainrate of $10^{-5}s^{-1}$

In Chapter 1, two rheological regimes were distinguished in the melting interval, a framework-controlled regime at low melt fractions and a suspension-like regime at high melt fractions, separated by a transition regime in which the stress needed to deform the partially-melted rock at a given rate changes dramatically. The critical melt fraction was defined as the fluid fraction for which the stress changes most rapidly as a function of melt fraction.

In Figure 7.2, I have plotted the maximum stress reached during constant strainrate compression ($10^{-5}s^{-1}$) of partially-melted granite, as obtained from Figure 7.1, against the melt fractions counted in thin section under the microscope. It should be emphasized that the indicated stress does not represent "flow stress" since steady state has not been observed for $10^{-5}s^{-1}$ for any of the melt fractions studied. For comparison, the stress for plastic flow for dry-unmelted granite at higher confining pressures for a strainrate of $10^{-6}s^{-1}$, derived from Tullis and Yund (1977), is also shown. The line depicting increasing strength with decreasing melt fraction at high degrees of melting has been calculated for $\dot{\varepsilon} = 10^{-5}s^{-1}$ using a melt viscosity of 10^4 Pascal second (10^5 Poise) and assuming the trend in relative viscosity of fluids with added uniform spheres as established by suspension experiments (Jeffrey and Acrivos, 1976). Below 50 percent fluid fraction no unequivocal measurements are available but a

70.

Figure 7.2   Maximum differential stress and flow stress as a
function of melt fraction for a strainrate of $10^{-5}s^{-1}$
The upper curve gives the results from this study,
the star indicates the powder experiment. The lower
curve shows the relative viscosity for suspensions
with a fluid viscosity of 10^4 Pascal seconds
(Jeffrey and Acrivos, 1976); the horizontal arrows
indicate the influence of mixed grain size on this
curve. Also shown is the range of results for
plastic flow of Westerly granite at high confining
pressures, 700°C – 900°C and $10^{-6}s^{-1}$ (Tullis and
Yund, 1977). The critical fraction is between 30
and 35 volume percent melt.
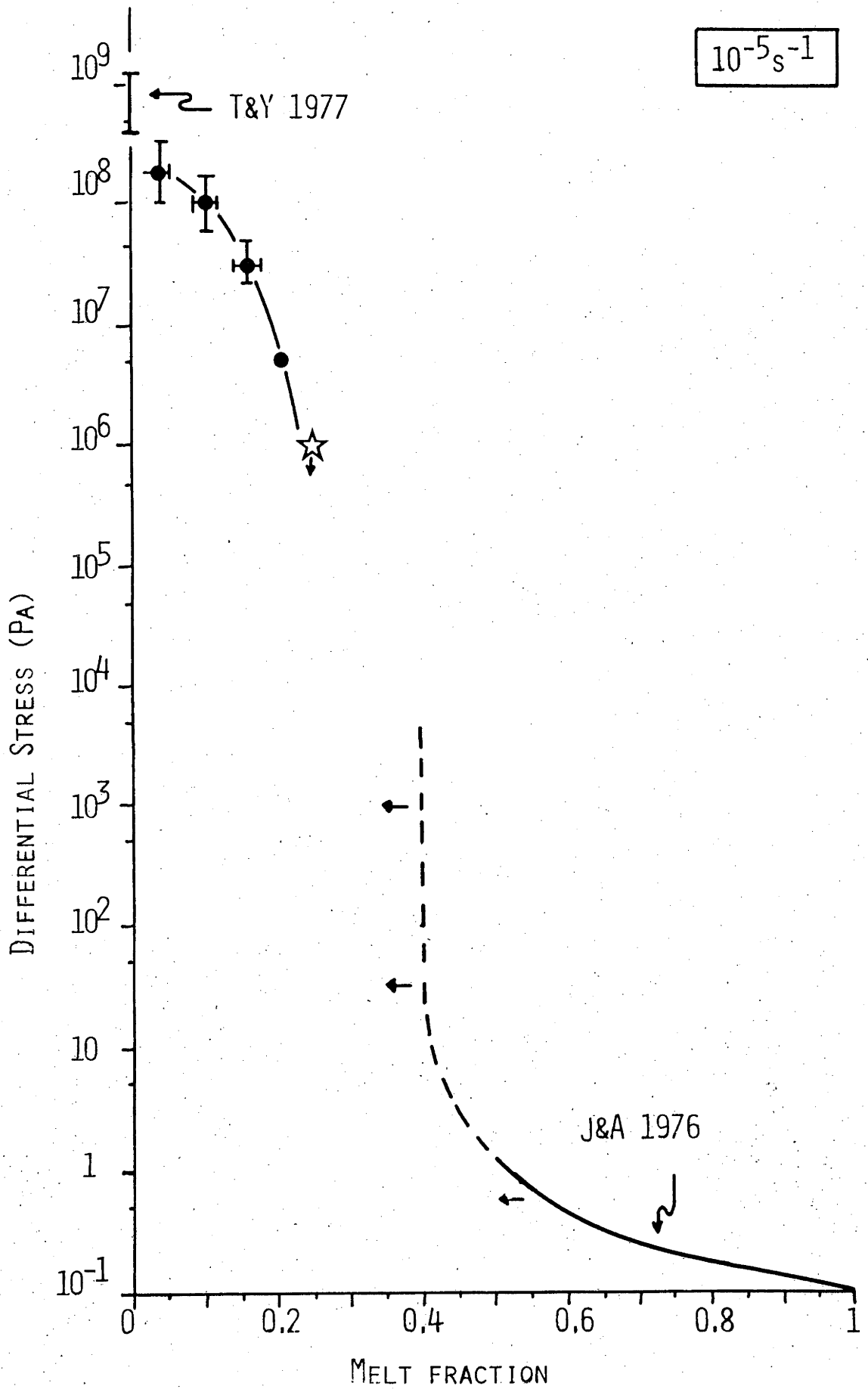
very rapid increase to indefinitely large stress values for *rigid* grains
is predicted by extrapolation formulae. When a range of particle sizes
is introduced this line should move somewhat towards lower melt fractions,
as shown by arrows. For a further discussion of these factors see Chapter
1.4. the line for higher melt fractions represents "flow stress", because
a steady rate of deformation is obtained after some initial changes when
a constant stress is applied to suspensions (Jeffrey and Acrivos, 1976).

I conclude form Figure 7.2 that the critical melt fraction in
granite for a strainrate of $10^{-5}s^{-1}$ is fairly well bracketed at a value of
30 - 35 volume percent. This is in excellent agreement with the expected
value of somewhat below 38 - 39 percent, deduced in Chapter 1.4. The
slightly lower value may reflect the grainsize variation caused by the
fracturing of grains during deformation of the aggregate. Up to 15 volume
percent melt, the stress decreases gradually in the granular framework-
controlled regime; with further increase in melt fraction the stress
drops dramatically if the critical melt fraction is approached. Similarly,
the flow stress increases rapidly below fifty percent melt when the critical
melt fraction is approached from the high melt fraction side.

Chapter 8

APPLICATION

8.1 The problems of extrapolation to natural conditions

8.1.1 Deformation mechanism in the solid grains

Although the temperature and pressure in the experiments are similar to those in the crust where partial melting of granitic material is thought to occur, it is not clear that the mechanisms of flow are the same in the two cases, since the experiments are necessarily conducted at high strainrates and high stresses.

It is therefore not clear to what extent extrapolation to geological conditions is justified. The question of mechanism is fundamental but is particularly difficult to resolve because the commonly observed recrystallization of crystalline igneous rocks previously deformed in a partially-melted state (Berger and Pitcher, 1970) tends to obscure any evidence of plastic or brittle deformation in the grains.

At least three types of potential behaviour in rocks with small melt fractions, as in migmatites or in a partially-melted upper mantle, can be envisaged:

(1)   Deformation by relative movement of grains with interference between grains being accommodated by grain fracturing, as observed in the experiments.

(2)   Deformation by relative movement of grains in which diffusion within the melt provides the accommodation mechanism and is rate controlling.

(3)   Deformation involving plastic flow within the grains; flow by dislocation movement within grains could lead to maintenance of large contact areas between grains through localized yielding at points of stress concentration and provide the rate controlling step.

These three distinct possibilities will be discussed in turn below.

By analogy with the experiments on partially-melted granite reported here, and with the observations of soil mechanics (e.g. Lambe and Whitman, 1969; see also Chapter 1.5.2) it may be expected that a steady state flow regime will not be attainable in the earth for the first type

of behaviour, as local shear zones will tend to develop. Differential movement, interference and fracture need not be restricted to the scale of individual grains in a partially-melted rock. Groups of crystals with melt in between them may act as interfering and breakable entities on any scale. Similarly the fluid phase in between these entities need not be completely melted, but may contain a fraction of crystals, as long as there is a large difference in flow properties between the "fluid-like" and "solid-like" elements of the system. This idea is applied to the agmatic structure of migmatites in Section 8.2.

If diffusion along grainboundaries is the rate controlling step, the onset of melting can be expected to increase the flowrate for a given stress, or to decrease the flow stress for a given rate (Stocker and Ashby, 1973). Once melt has formed and a fast diffusion path has become available however, it seems unlikely that the rate of deformation for a given stress will rise appreciably with a further increase in melt percentage until the critical melt fraction is approached. Increases in strainrate over this interval are expected to be caused by the increase in average contact stress with increasing fluid fraction. Frank (1965) has proposed a model for the deformation of aggregates with fluid in which by continual rearrangement of grains during flow a small number of highly stressed contact points is maintained, the yielding at which determines the flowrate; such a model might apply to hot-glass ceramics (James and Ashbee, 1975). It is difficult to assess whether such a mechanism can be operative in a rock with a very small melt fraction (<5 volume percent), but it may be expected that non-coaxial deformation histories, in which the orientations of contacts between grains change continuously with respect to the macroscopic differential stress will favour effects as described by Frank's model.

The experiments of Auten *et al.* (1974) and Auten and Gordon (1975) suggest that the introduction of a melt phase will have only a minor effect on the creep rate for a given stress if the rate controlling mechanism is dislocation creep in the solid grains. Auten and co-workers studied the uniaxial (unconfined) compressive creep of a eutectic alloy, Al-2at. percent Ga, at temperatures just below and just above the solidus of 27°C. At lower temperature Ga occurs in the grainboundaries of aluminium grains which deform by dislocation creep, at higher temperatures ∿1 volume percent melt forms at the grainboundaries while the deformation mechanism in the solid grains remains dislocation creep. Apart from a small transient upon melting,

likely to be associated with the expulsion of melt and the removal of any asperities from grainboundaries at a high angle to the compressive stress, they found no increase in steady state creep rate. This result has been quoted by Nicolas and Poirier (1976) and Goetze (1977) to point out that the zone of low flow strength, thought to occur under the lithosphere – this zone is often equated to the low velocity layer and the high attenuation layer – does not necessarily have to be caused by partial melting. Such caution seems justified in view of the experimental results and the widespread acceptance that the dominant flow mechanism in the upper mantle involves dislocation processes. However, one aspect has to be considered before the results on this alloy can be extrapolated to cover upper mantle conditions. Aluminium has a face-centered cubic structure and a sufficient number of independent slip systems to meet the Von Mises criterion for coherent plastic deformation with complete compatibility at grainboundaries in a polycrystal (Paterson, 1969). The presence or absence of a small melt fraction in grainboundaries does therefore not exert a large influence because compatibility is no problem in the unmelted state. Olivine, the dominant mineral in the upper mantle, has only three independent slip systems (e.g. Goetze and Kohlstedt, 1973). Coherent plastic flow in olivine polycrystals by dislocation mechanisms can still occur if the Von Mises criterion is somewhat relaxed (Paterson, 1969). The presence of an easily redistributed melt phase at grainboundaries provides a way of relaxing the requirement of complete compatibility at grainboundaries, and it is therefore expected that deformation of partially-melted olivine-rich rocks by dislocation creep will be facilitated by the presence of a melt phase, but how much is not known. Apart from this effect it would appear that the presence of a melt in rocks deforming by dislocation processes will not change the flow rate for a given macroscopic differential stress to any great extent. That is, unless the local contact stresses at the grainboundaries are raised such that a change towards a higher strainrate mechanism in the solid grains can occur (compare Stocker and Ashby, 1973).

8.1.2   Melt distribution

As stressed in Chapter 3.3, the fine grained granite with melt is not in geochemical equilibrium when the deformation experiments are performed. Similarly structural equilibrium of the melt distribution has not been achieved in the experiments lasting a few hours. The distribution of melt appears to be governed by pre-existing cracks and grainboundaries in which

water occurred prior to melting (Chapter 5). In equilibrium the distribution depends on the interfacial energies of the melt against the grainboundaries and of the grainboundaries against one another, as well as on the total amount of melt present (e.g. Smith, 1948). It has commonly been assumed that wetting of grainboundaries by melt in partially-melted rocks in equilibrium under hydrostatic conditions is more or less complete. Arguments presented in favour are such experimental observations on natural rocks as given in this thesis and by Mehnert *et al.* (1973), and the microstructures obtained in geochemical equilibrium studies in which crystals are formed during cooling and melt is found to wet grainboundaries.

The assumption of complete wetting is currently being questioned and it is argued that the periods used in the experiments quoted in favour have been insufficient to reach textural equilibrium. In a recent pair of papers Bulau and Waff (in prep.) consider the thermodynamical constraints on equilibrium melt distribution, and present experimental evidence that 1-2 volume percent of basaltic melt in an olivine rock at hydrostatic pressure is distributed at grainedges only, while melt films are absent from grainboundaries. Taking their argument to the extreme, it would appear that complete wetting may only be expected if every grain has the shape of a sphere, that is, at 26 volume percent melt and higher for a uniform grain size, or at lower fractions for a large range in grain sizes (compare Chapter 1.4). The effect of differential stress on the equilibrium distribution of melt is not known. A dynamic equilibrium will be achieved if the deformation, and therefore the microstructure, reaches a steady state.

8.2 Application of the critical melt fraction concept to geological problems

Despite the uncertainties about the relevant mechanisms and the melt distribution, the present experiments help to bring into focus some general questions connected with flow in partially-melted rocks in nature.

The concept of a critical melt fraction representing the threshold of suspension like behaviour, introduced earlier, is clearly of considerable practical importance in connection with the mechanical response of partially-melted rock bodies in tectonic environments. The nature of the dramatic fall in flow resistance occurring at this melt fraction can be deduced from Figure 7.2. The general form of this curve is expected to remain valid under geological conditions even if the mechanisms of flow at lower melt fractions

are modified, as will be argued below.

Temperature rises over the melting interval of a natural rock; in general this will result in a decrease of flow stress for a given strain-rate in both the melt and the solid fraction irrespective of what deformation mechanism is operating in the grains. The chemistry of the meltphase changes over the melting interval, generally from silicic towards more basic compositions, which apart from the temperature effect will also cause a lowering in melt viscosity. The strainrate sensitivity of solids is in general lower than that of a viscous melt. Commonly strainrate sensitivity is expressed in terms of a stress exponent n such that $\dot{\varepsilon} \sim \sigma^n$. Viscous fluids have an exponent of $n = 1$, the brittle deformation of solids on the other hand is rather insensitive to strainrate (high n-values), while for plastic deformation of rocks and minerals due to dislocation processes n-values of 3-5 have been obtained. Only at very low stresses and strain-rates have n-values close to 1 been obtained for crystalline solids (e.g. Stocker and Ashby, 1973; Ashby and Verrall, 1977). Now reconsider Figure 7.2, for the right hand side of the diagram, that is at melt fractions exceeding the critical, a drop of one decade in strain rate will result in a drop of one decade in stress for all strainrates. On the other hand, a drop in strainrate of one order of magnitude will result in only a small drop in stress on the left side of the diagram since deformation is still in the brittle field, compare also Figure 7.1. With further decrease in strainrate different deformation mechanisms will start operating in the solid fraction in the granular framework-controlled regime, but the difference in stress level on the left and the right of a diagram such as Figure 7.2 will continue to increase until the rate sensitivity of the deformation mechanism in the solid has reached an n-value of 1, beyond which the difference will remain constant. From the discussion in Section 8.1.1, and from the arguments presented in Chapter 1.4 and those given here, it is concluded that the general distinction between a suspension-like regime and a granular framework-controlled regime will be enhanced under geological conditions of lower stress and lower strainrate. It is felt that the critical melt fraction will not change appreciably, because there will be large stress differences between the stress needed to deform suspensions at a certain rate and corresponding granular aggregates at the same rate, irrespective of the mechanism of deformation operating in the solids. The factor determining the value of the critical melt fraction is therefore essentially a geometrical one. It may be expected that the

critical melt fraction for partially-melted rock will lie between 30 and 40 volume percent melt for all strainrates, including geological ones.

The observed tendency to localized shear failure at low melt fractions is likely to be most relevant where deformation rates are relatively high and it may provide a partial explanation for deep seated earthquakes (*c.f.* Raleigh and Paterson, 1965). More generally, field evidence in deformed igneous bodies points to widespread occurrence of instabilities in the form of "healed" shear zones and offsets of dikes (reviewed by Berger and Pitcher, 1970) and of the agmatic or breccia structure of migmatites (e.g. Mehnert, 1968). The observations of Hoffmann (1977) are of particular interest in illustrating the large rheological contrast with relatively small change in melt fraction around the critical value, and possible unstable behaviour on the low melt fraction side. He showed by geochemical equilibrium studies that granite intruding granodiorite in the Damara Belt of South West Africa may have had 50 to 55 percent melt at the time of intrusion while the host had 30 percent melt, explaining "the ambivalent characteristics of the Salem Granodiorite acting like blocks and being agmatically brecciated at a large scale, but also mingling with the Red Granite at sharp edges".

8.3   Some other applications

Another aspect of behaviour of geological interest is the relative movement of melt and solid components of the rock. Apart from gravitational settling, relative movement of small fractions of melt may also occur in response to deformation but the nature of the behaviour will depend on whether the system is effectively "open" or "closed" ("drained" or "undrained" in soil mechanics terms). The experiments represent a situation that is closed on the larger scale but within which relative movement between specimen and surrounding melt layer can occur. The dilatancy pumping effect observed is in fact opposite to the effect postulated by Shaw (1969) as a response to deformation, namely, that shear will tend to "knead" melt from a partially-melted rock. The latter effect is more likely to occur in an open situation where there is also a large gradient in the hydrostatic component of the stress, introducing an additional filter-pressing effect. In discussing the extraction of a melt fraction in geological situations it is therefore necessary to specify the mechanical situation in more precise terms than is commonly done.

Both in closed and open situations, local redistribution of melt films in grainboundaries and cracks may also be of practical significance. Thus, a tendency for the melt films to be oriented normal to the least principal compressive stress may contribute to anisotropy in elastic wave velocities in the upper mantle (Schlue and Knopoff, 1976; Bamford and Crampin, 1977).

PART II

A NOTE ON THE THERMAL EXPANSION OF GRANITE

AT HIGH PRESSURE AND ON THE ASSOCIATED SHIFT

IN THE α-β TRANSITION OF QUARTZ

ABSTRACT

Measurements are presented of volume changes in granite during room temperature compression followed by temperature increase to 900°C at 100, 200 and 300 MPa confining pressure. Comparison with thermal expansion and compressibility data for the constituent minerals allows changes in porosity to be estimated. Under confining pressure, porosity is found to decrease with heating to 200°C through expansion of the minerals into cracks which are thought to be related to the geological cooling history of the rock. Between 200°C and 840°C porosity increases as a result of differential thermal expansion of the constituent minerals, but crack opening is increasingly suppressed at higher confining pressures. Extrapolation of the results indicates that differential thermal expansion can no longer cause crack opening in dry granite at confining pressures in excess of 450 MPa. The quartz α-β transition temperature in granite is marked by a kink in the thermal expansion curve of the rock, and it is found to increase by 60°C-72°C per 100 MPa confining pressure, as opposed to the published value of 26°C per 100 MPa for single crystals of quartz. An elastic theory based on the classic work of Eshelby (1957) is advanced, which allows calculation of the stresses and strains in and around a spherical inclusion in a matrix of different thermal expansion and compressibility resulting from changes in confining pressure and temperature. The theory together with a simple model for cracked granite accounts semiquantitatively for the observations of thermal expansion of granite and the effect of confining pressure thereon, and for the observed α-β transition temperatures for quartz, if it is assumed that grainboundaries have zero tensile strength. Three possible focusing effects have been identified which cause the α-β transition of all individual quartz grains in granite to occur at the same temperature: i) the internal pressure of quartz grains cannot exceed three times the confining pressure applied to the granite as a whole, ii) the finite yield strength of the matrix decreases with increasing temperature, and iii) although counteracted to some extent by increased compressibility, the large increase in the volumetric thermal expansion of quartz grains at temperatures just below the α-β transition, and the pressure sensitivity of that transition cause larger pressure rises in those grains with initially lower internal pressures.

Chapter 9

INTRODUCTION AND EXPERIMENTS

9.1   Introduction

The velocities of compressional elastic waves propagating through
dry natural crystalline rocks are known to be sensitive to the state of
microcracking of the material.   Graphs of ultrasonically determined V_p versus
confining pressure show a rapid, non-linear increase in velocity from 1
atmosphere to 100-200 MPa, beyond which the increase becomes smaller and
more linear with pressure (*e.g.* Birch, 1960; Kern, 1978; part III of this
thesis).   The first stage is associated with the progressive closure of
microcracks by confining pressure, whereas the second is thought to reflect
the intrinsic pressure sensitivity of the crackfree material.   However,
Christensen (1974) has shown that a small part of the change in V_p at room
temperature and higher pressures, up to 1000 MPa, may still be caused by a
further closure of, presumably more equant, pores.

The last ten years have seen rapid progress in the experimental
determination of temperature derivatives of V_p for natural rocks at pressures
between 100 and 1000 MPa and temperatures up to 750°C.   For references see
Table 12.1 in part III. V_p has been shown to decrease gradually with
increasing temperature for a wide variety of rocks.   Interpretation of these
results is made difficult by the fact that part of the observed decrease
is caused by the reopening of old cracks or the opening of new cracks at
high temperature against the confining pressure.   This effect is ascribed
to the differential expansion of the constituent minerals of the rock
(Ramananantoandro and Manghnani, 1978; Kern, 1978).   The minimum pressure
needed to prevent the opening of cracks was estimated to be ~100 MPa per
100°C by Kern (1978).

Notable exceptions to the rule of a gradual decrease in V_p with
increase in temperature are provided by quartzite and other quartz-bearing
rocks such as granite and granulite.   Fielitz (1971, 1976) was the first to
demonstrate experimentally that V_p at pressure in such rocks, decreases
markedly from its room temperature value to a sharp low at the quartz α-β
transition temperature, followed by a rapid rise to higher velocities with a
further increase in temperature.   Fielitz further demonstrated the observed
behaviour to be in good agreement with the Voigt-Reuss-Hill average for a
quartz polycrystal calculated from the known changes in the elastic compliances

for single crystals of quartz at the α-β transition.

Studies of granite and granulite (Kern, 1978, in prep.) have revealed the same feature but here the lowest V_p occurs at a higher temperature than the single crystal quartz α-β transition temperature corresponding to the applied confining pressure. Kern concluded that the observed low in V_p is associated with the quartz α-β transition, but that the "shift" towards higher temperatures must be due to stress inhomogeneities caused by the different thermal expansion coefficients of the constituent minerals of granite and granulite.

9.2 Purpose and organization of the present note

Knowledge of the degree of crack opening is essential for an understanding of the observed variations in P-wave velocities under conditions of confining pressure and high temperature. In this chapter, I will describe the results of an experimental study on the thermal expansion of a fine grained granite at confining pressures of 100, 200 and 300 MPa and temperatures up to 900°C. Comparison of the observations with a hypothetical crack-free granite allows estimation of porosity changes as a function of pressure and temperature. It will be shown that the α-β transition of quartz in granite is reflected by the bulk volumetric expansion of the rock. Independent measurements are therefore obtained for the shift of the quartz α-β transition temperature in granite. Small differences exist, but in general the results confirm those obtained by Kern (1978, in prep.) with the aid of P-wave velocity measurements.

The remainder of this note will be devoted to a *quantitative* interpretation of the observed effects. For this purpose, Chapter 10 gives an analysis of the elastic field due to an ideally elastic spherical inclusion in a matrix of different ideal elasticity. The theory is based on the work of Eshelby (1957), and allows calculation of the elastic field changes which result from thermal expansion or contraction of an inclusion relative to a matrix maintained at a constant confining pressure.

The experimental results of Chapter 9 will then be discussed in terms of the theory in Chapter 11. In view of the major simplifying assumptions which have to be made to make the theoretical results applicable to the case of a real granite, the observations are surprisingly well predicted by a model based on the theory.

9.3 Specimen material, experimental procedure and data reduction

The specimen material used for the thermal expansion experiments is Delegate aplite, a finegrained isotropic and equigranular granitic rock, consisting out of roughly equal amounts of quartz (31 percent), plagioclase (31 percent) and K-feldspar (35 percent) and a minor amount of biotite (3 percent). The material and specimen assembly have been described in detail in part I, Chapters 3 and 2 respectively.

Experiments were performed in the high-pressure, high-temperature deformation apparatus using argon gas as a pressure medium (Paterson, 1970, 1977). General descriptions of the apparatus and of the experimental procedures have been given in Chapter 2. Here, only aspects of particular interest to the measurement of compression and thermal expansion will be described.

Length changes of the specimen were calculated from differences in "touch-point" displacements as recorded on the load-displacement strip chart. Touch-points were determined by advancing the loading piston onto the specimen until the internal load cell, which is placed in the anvil under the specimen, recorded a load of 10 kg. The piston was then backed off and the same procedure repeated three more times to ensure that a reproducible measurement was made. The variation in touch-point displacement thus determined for each single reported measurement was never more than 0.004 mm, the equivalent of 2×10^{-4} linear strain in the specimens of 20 mm length.

Changes of touch-point displacement with pressure and temperature are affected by length changes in the pressure bomb, the anvil, the piston and the specimen endpieces, as well as by length changes in the specimen. The necessary correction was carefully determined with a dummy specimen of the same dimensions as the granite specimens to be used, and for which the thermal expansion and compressibility were accurately known. This correction was subtracted from the total changes in touch-point displacement to yield the length changes of the granite specimens. Prior to the first measurement at 1 atmosphere and room temperature the specimen was touched twice with a force of 100 kg to ensure good seating of the specimen assembly onto the anvil, and of the endpieces onto the specimen. It is estimated that the results for length changes thus obtained are precise within 0.02 mm, the equivalent of 10^{-3} linear strain of the specimens, for all temperatures and pressures reported. Temperature is believed to be known within $10°C$ for the

whole specimen, and pressure within 5 MPa for the set of experiments reported.

Experiments have been performed at 100, 200 and 300 MPa confining pressure. First length changes were measured at room temperature during compression, then the temperature was raised at an average rate of 3°C per minute. Before each measurement, temperature was kept constant for 5 minutes, to allow the specimen to equilibrate. Equilibration periods of up to 1 hour were used by Cooper and Simmons (1977) in their experiments on the thermal expansion of granite at atmospheric pressure. On the scale of precision of the present experiments, I have not been able to note time dependent effects between 1 and 20 minutes at constant temperature. Measurements were made at intervals of 50°C to 100°C at lower temperatures, but more frequently around the α-β transition temperature of quartz. Conversion of linear strains to volumetric strains has been done on the assumption of isotropic volume changes through multiplication by a factor of 3.

9.4   Experimental results

9.4.1   Compression at room temperature

The measured compression for Delegate aplite at room temperature is shown in Figure 9.1-a for three dry runs to 100, 200 and 300 MPa, and for one "wet" run to 300 MPa in a specimen with 0.7 weight percent or 1.8 volume percent added water. For comparison, Figure 9.1-b shows the compression of water (Burnham *et al.*, 1969) and of quartz, plagioclase (oligoclase) and K-feldspar (microcline) as given by Birch (1966). The dashed line marked "granite" in this figure represents the compression of a hypothetical, crack free granite at room temperature. The compression of this "granite" has been calculated by assuming that it has a compressibility equal to one-third of the sum of the volumetric compressibilities of quartz, oligoclase and microcline.[1] In the hypothetical case these is no effect due to differential volumetric or linear compression of the constituent minerals.

---

[1] Reuss' assumption about the compressibility of a polycrystal has been followed here. The differences resulting from taking Voigt's assumption, or calculating the Voigt-Reuss-Hill average, (*e.g.* Watt *et al.*, 1976), are small and do not affect the arguments presented here.

Figure 9.1-a   Compression of wet and dry granite at room temper-
                ature.   The dashed line indicates a possible decrease
                in compressibility for the highest pressure.

Figure 9.1-b   Compression of water (Burnham *et al.*, 1969) and of
                the constituent minerals of granite at room temper-
                ature (Birch, 1966).   The dashed line represents a
                hypothetical crackfree granite consisting of
                equal proportions of quartz, oligoclase and microcline
                (Reuss average).

PRESSURE (MPA)

(a) WET, DRY, ERROR

(b) OLIGOCLASE, MICROCLINE, "DRY GRANITE", QUARTZ, H_2O
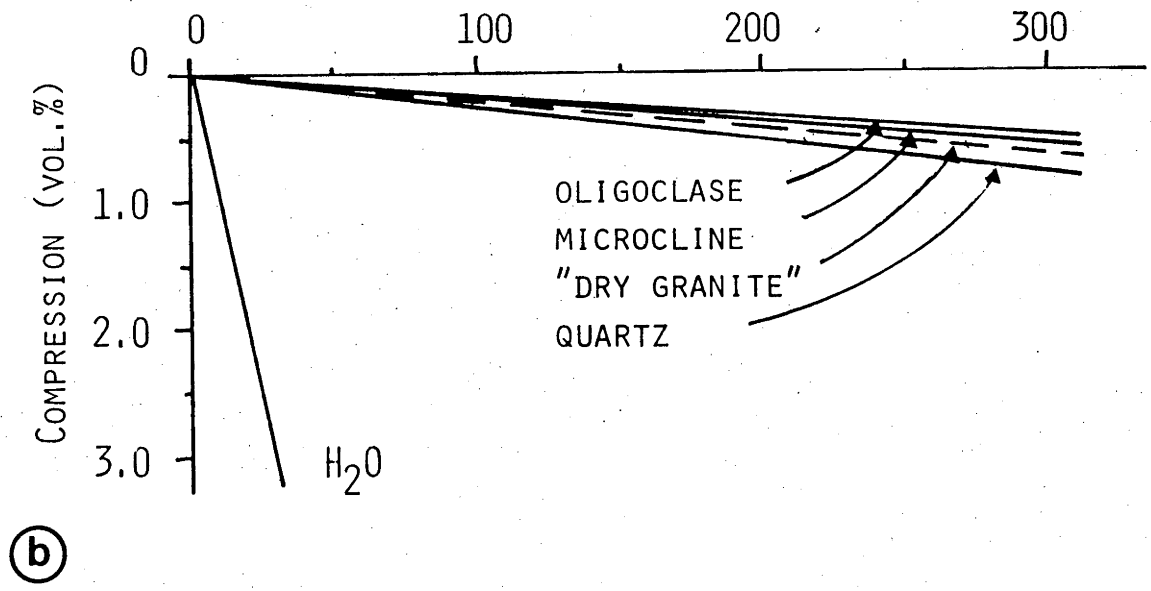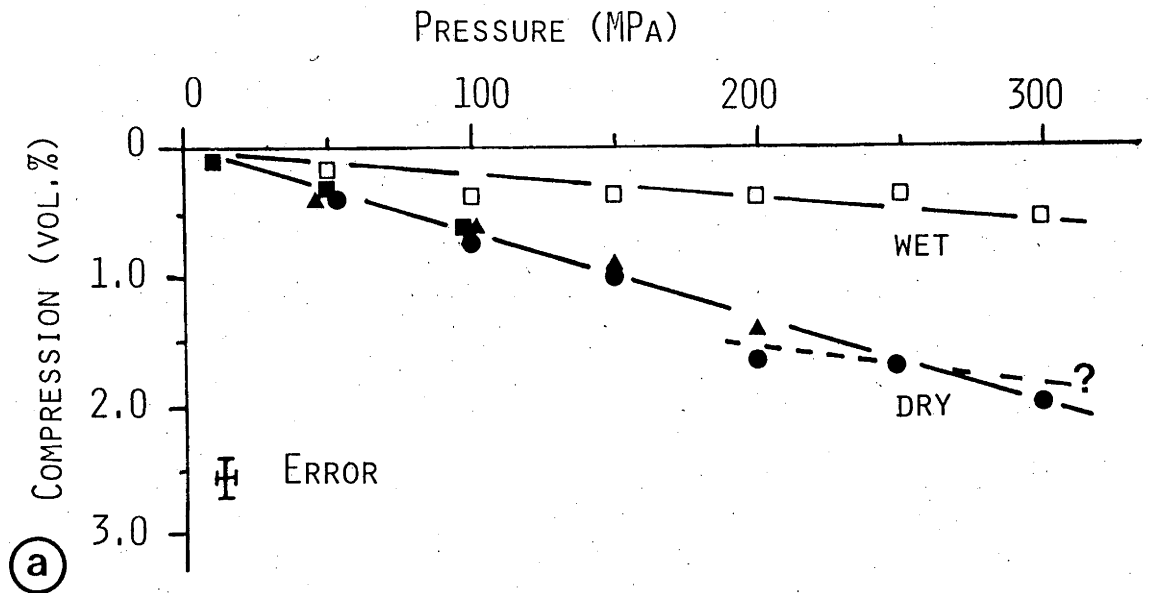
The compression of a similar hypothetical "wet granite" with 1.8 volume percent H_2O and equal fractions of quartz, oligoclase and microcline has also been calculated. Despite the high compressibility of water the result does not differ much from that for dry "granite" because of the small volume fraction of water present. In fact, its compression coincides virtually with that of real quartz; to avoid a confusion of lines this has not been shown in Figure 9.1-b.

The results for the compression of dry hypothetical granite and for real dry Delegate aplite are notably distinct. At 100 MPa a difference is noted of ~0.5 volume percent, and at 200 and 300 MPa of 0.7 to 1.0 and ~1.3 volume percent respectively. It is recalled here that the specimen material possesses a total porosity of ~2.3 volume percent at ambient conditions, part of which is made up of small spherical pores inside grains, and part of which consists of crack shaped cavities mainly at grainboundaries. An accessible porosity of 0.8 volume percent, associated with grainboundary cracks has been measured in water absorption tests (Chapter 3, Table 3.1). Comparison of these porosity values with the differences in volumetric compression, noted above, indicate that a large part, but not all of the total porosity of Delegate aplite is removed by the application of 200-300 MPa confining pressure. Probably most of the accessible porosity is removed at ~200 MPa.

The measured average compressibility of dry granite between 1 atmosphere and 300 MPa is, from Figure 9.1-a, ~0.7 percent per 100 MPa, with a possible reduction to a value closer to 0.25 percent per 100 MPa, at the highest confining pressure. The former value is in good agreement with the measured compressibility of other granites at low confining pressure (e.g. Brace, 1965), although a wide range of values exists (Birch, 1966). The latter value agrees well with the compressibilities of other natural granites at a few hundred MPa confining pressure (Birch, 1966), and with the compressibility of 0.21 percent per 100 MPa for the hypothetical "granite" of Figure 9.1-b.

The results for the wet specimen of Delegate aplite on the other hand are, on the scale of precision of the measurements, not significantly different from the results for a hypothetical "wet granite" with the same amount of added water. It is concluded that part of the excess added water (1.8 volume percent) has entered into the accessible porespace (0.8 volume percent), thereby preventing the closure of cracks.

9.4.2   Estimated expansion at 1 atmosphere

The expansion of specimens at atmospheric pressure to high
temperatures cannot be measured with the present apparatus and furnace
arrangement.   An estimate of the expansion of Delegate aplite to 800°C
at 1 atmosphere is made in Figure 9.2.   In Figure 9.2-a the volumetric
thermal expansions of the constituent minerals of granite are shown (data
from Skinner, 1966).   Quartz has a steep, non-linear thermal expansion
curve up to the α-β transition temperature after which the expansion
coefficient becomes slightly negative.   Oligoclase and microcline experience
smaller, gradual, and almost equal expansions up to 1000°C.   The dotted line
in Figure 9.2-a represents the thermal expansion of a dry *hypothetical*
"granite" which has a coefficient of expansion equal to the average of
those for real quartz, oligoclase and microcline.[1]   Again in the hypothetical
case there is no effect due to differential expansions of the constituent
minerals.   The *changes* in porosity observed at room temperature after heating
in a muffle furnace are obtained from Table 3.1 (Chapter 3), and the average
is represented in Figure 9.2-b.   An admittedly crude estimate of the thermal
expansion of Delegate aplite at 1 atmosphere is now obtained by adding the
curve for porosity changes of the lower figure to the curve for the
hypothetical granite of the upper figure.   The result is represented by a
dashed line in Figure 9.2-a.   Uncertainties in the estimate arise from the
assumption that there is no change in porosity in unjacketed specimens
during cooling from the highest temperature reached, from the porosity
measurements themselves and from the uncertainties in the temperature
measurements for the muffle furnace used (~20°C).   I have failed to find
examples in the literature of the expansion of other granites at 1 atmosphere
to temperatures exceeding the quartz α-β transition.   The estimated result
for Delegate aplite at 400°C is in good agreement with the accurate measure-
ments of thermal expansion in various granites at 1 atmosphere to 400°C
by Cooper and Simmons (1977).

9.4.3   Expansion at pressure in dry specimens

The measured compression and thermal expansion of dry specimens
of Delegate aplite with respect to 20°C and 1 atmosphere are shown in Figure

---

[1] This is also a Reuss-averaging assumption.   The remarks made earlier
(footnote p. 84) apply here as well.

Figure 9.2-a   Atmospheric thermal expansion of the constituent

minerals of granite (after Skinner, 1966; solid lines),

of a hypothetical crack free granite consisting

of equal proportions of these minerals (Reuss average;

dotted line), and of real granite (estimated; dashed

line).

Figure 9.2-b   Porosity increase of granite at 1 atmosphere as a

function of temperature. The bar indicates the

spread of the data at higher temperatures (Table 3.1).

(a)

QUARTZ

"DRY GRANITE"

MICROCLINE

OLIGOCLASE

EXPANSION (VOL.%)

5.0
4.0
3.0
2.0
1.0
0

(b)

SPREAD

POR. INCR. (VOL.%)

2.0
1.0
0

TEMPERATURE (°C)

0   200   400   600   800   1000
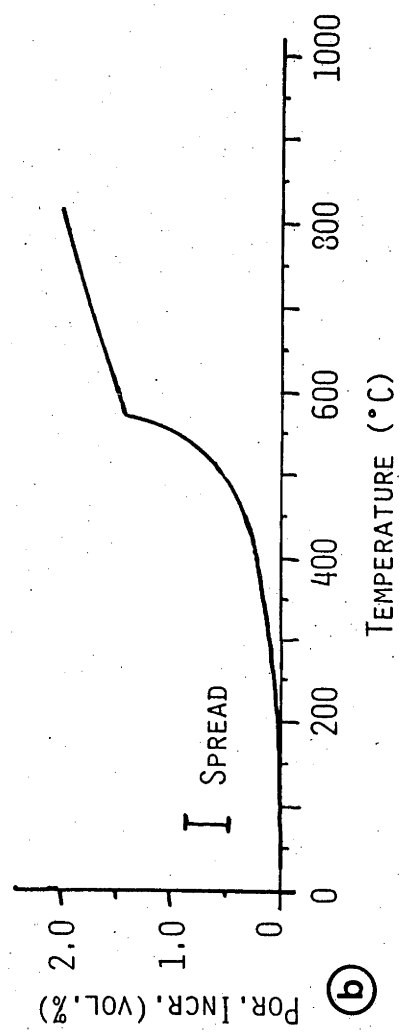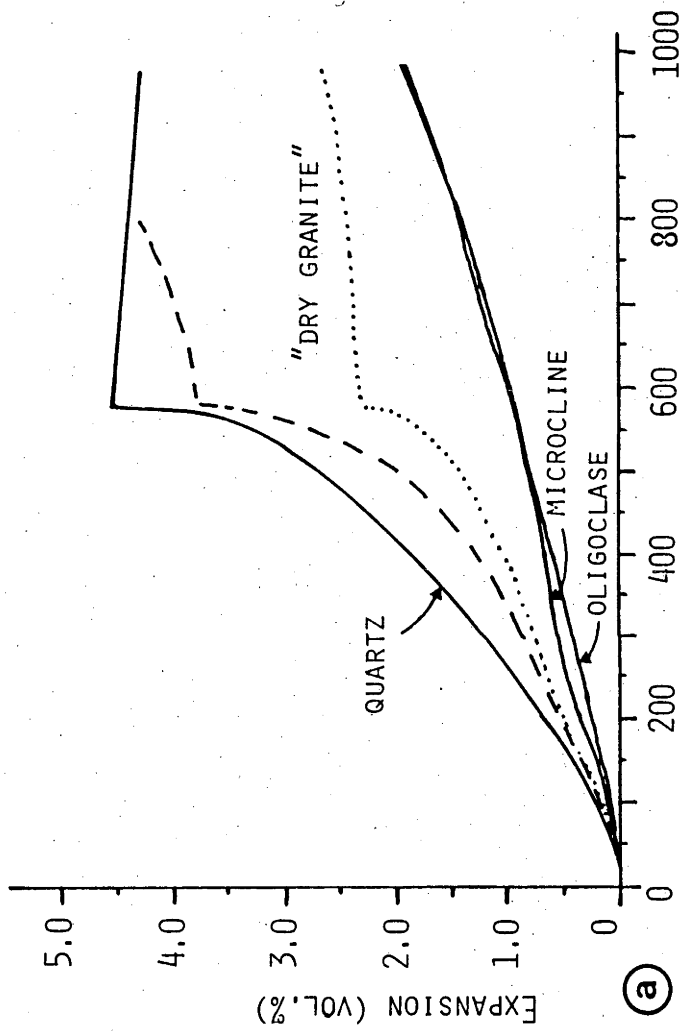
Figure 9.3   Thermal expansion of dry granite at 100, 200 and 300

MPa confining pressure.   The marked kinks in the

expansion curves are associated with the α-β trans-

ition of quartz.   The dashed line represents the

estimated atmospheric expansion of granite.
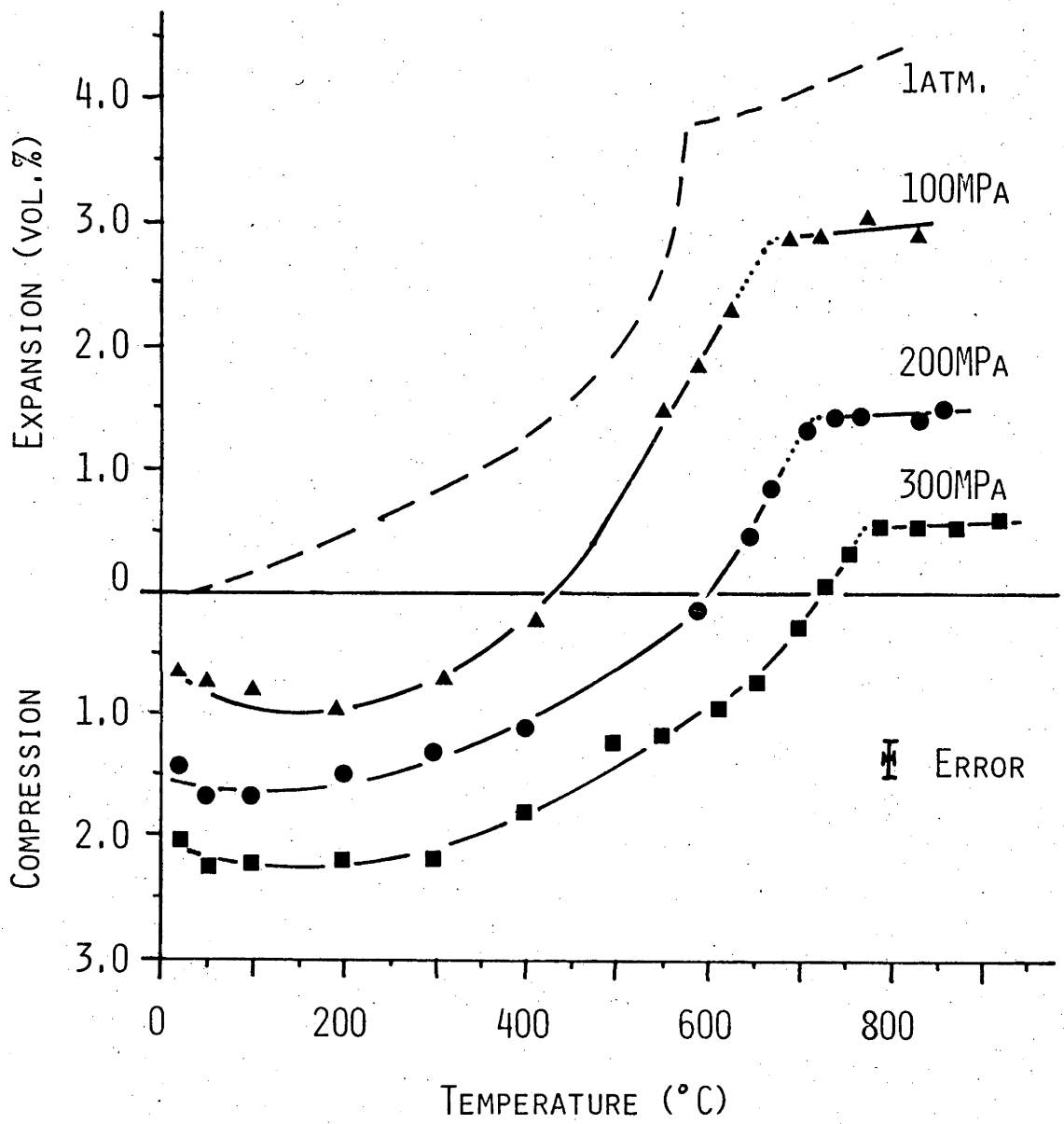
9.3 for 100, 200 and 300 MPa confining pressure. The estimated thermal expansion at 1 atmosphere is shown by a dashed line for comparison. Similar measurements were presented by Kern (1978, in prep.) for granite and granulite to lower temperatures. There is good general agreement between the two sets of data.

Several important conclusions may be drawn from this diagram, these will be discussed in turn below.

i. Shift in the quartz α-β transition temperature

All curves are characterized by a sharp kink which is associated with the α-β transition of quartz. The temperature interval in which the transition occurs is estimated from Figure 9.3, and shown against confining pressure in Figure 9.4 by solid symbols. The α-β transition temperature for single crystals of quartz increases by ~26°C per 100 MPa confining pressure from 573°C at 1 atmosphere (e.g. Coe and Paterson, 1969; Koster van Groos and Ter Heege, 1973). This effect is shown by a solid line in Figure 9.4. The temperature intervals in which the quartz α-β transition occurs in the fine grained granite are displaced to considerably higher temperatures than the single crystal α-β transition temperatures corresponding to the same confining pressures. The results of Kern (in prep.) based on observations of the P-wave velocity minimum in a cubic anvil apparatus are reproduced here by open boxes. Some discrepancy is noted between the two data sets, particularly at the highest pressures. The dashed line in Figure 9.4 represents the prediction of a model which will be discussed in Chapter 11.

ii. Decreasing porosity with temperature increase to 200°C

In section 9.4.1 it was concluded that much of the porosity of Delegate aplite becomes closed by the application of 100 to 300 MPa confining pressure. Figure 9.3 shows that at pressure the volume of the rock remains constant, or even decreases somewhat between 20°C and 200°C. A similar effect is observed by Kern (in prep.) for granite and granulite to 200°C at 200 MPa. The constituent minerals of these rocks expand over this temperature interval and it is therefore concluded that more of the porosity is closed at 200°C and pressure than at 20°C and the same pressure. The magnitude of the porosity change cannot be exactly calculated because there are no measurements of the volumetric thermal expansions of the individual constituent minerals at pressure. It will be assumed however, here as well as in later sections of this study, that the magnitude of the

Figure 9.4   The quartz α-β transition temperature in granite as a
              function of confining pressure. The pressure
              dependence of $T_{\alpha-\beta}$ for single crystals of quartz is
              also indicated. The dashed line represents the
              model discussed in Chapter 11.
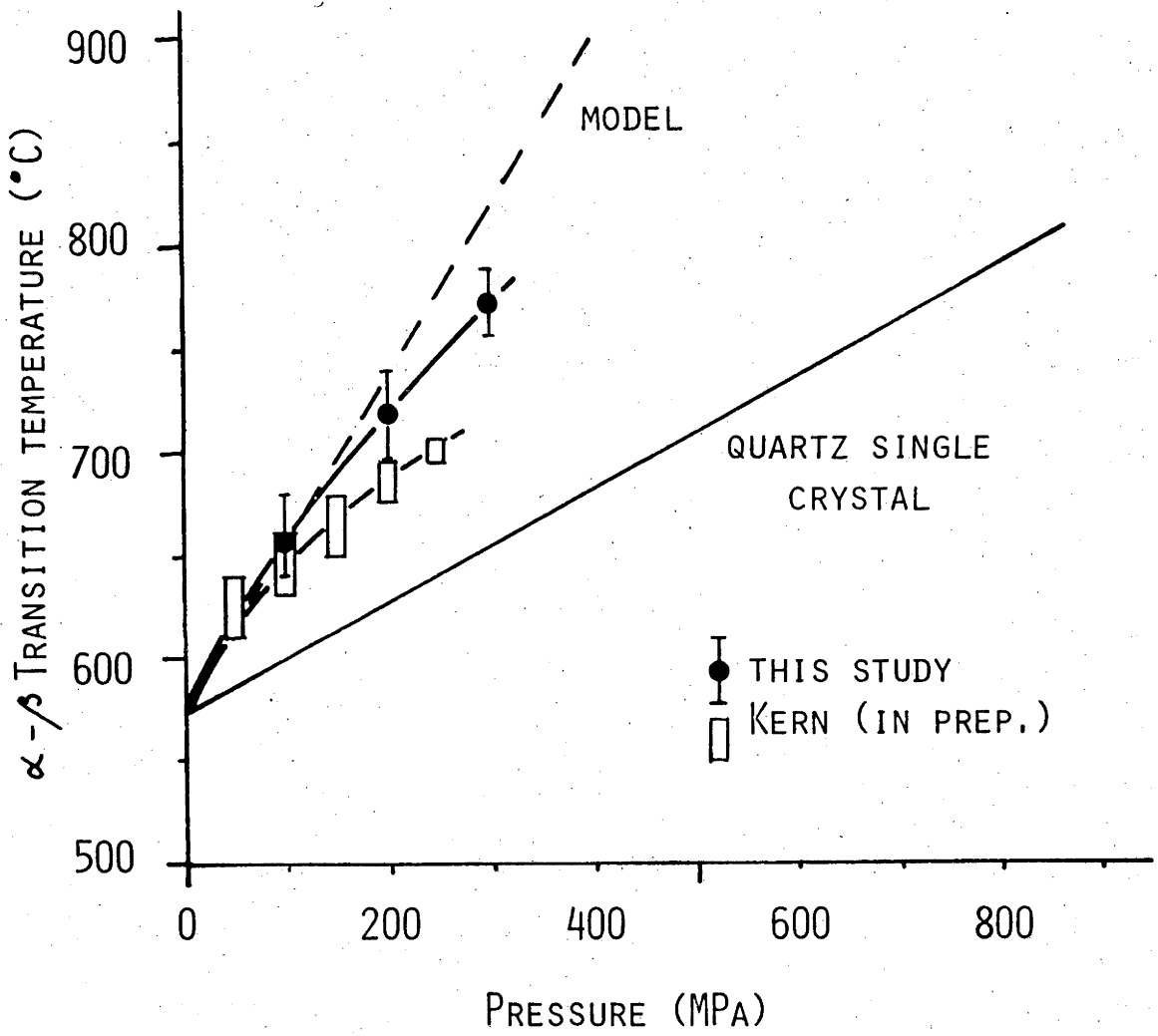
volumetric expansion at 1 atmosphere represents an upper bound to the
possible thermal expansion of the constituent minerals at higher confining
pressures. There is an indication in the work of Koster van Groos and
Ter Heege (1973) that the large increase of the thermal expansion coefficient
of quartz at 1 atmosphere towards the α-β transition temperature may become
less at high confining pressures. The assumption made above would be in
accordance with this possible change. The ~0.5 percent volume increase of
the hypothetical "granite" of Figure 9.2-a between 20°C and 200°C at 1
atmosphere is therefore taken as the maximum possible volume increase of the
constituent minerals of Delegate aplite at confining pressure over the same
temperature range. Combining this result with the observations of Figure
9.3 it is concluded that there is a decrease in porosity during heating from
20°C to 200°C at 100, 200 and 300 MPa pressure, but that it cannot be more
than 0.5 to 0.8 volume percent.

Part of the decrease in porosity may be due to a higher efficiency
of the confining pressure in closing cracks at higher temperature through
plastic flow or elastic softening of the minerals. However, in view of
the low temperature of 200°C, the moderate pressures and the short time
scale of the experiments, both effects are thought to be small. It would
seem more likely that the porosity decrease is caused by the differences in
the thermal expansion coefficients of the constituent minerals and by
the nature of the cracks and their geometry in the material. Nur and
Simmons (1970) demonstrated that the occurrence of cracks in igneous rocks
which are exposed at the surface of the earth may be ascribed to differential
volume changes of their constituent minerals during the geological cooling
and depressurisation history of the rock. I suggest, that the reverse effect
operates during the 200°C temperature rise in the experiments, that is, part
of the crack porosity which originated due to differential contraction in the
earth during cooling, becomes closed again with differential thermal expansion
in the experiments. The thermal expansion of minerals into pre-existing cracks
during heating of granite at atmospheric pressure has been demonstrated
by Cooper and Simmons (1977).

iii.   Increasing porosity at high temperatures

From Figure 9.3, it is seen that the volume of dry Delegate aplite
increases between 200 and 840°C by ~ 4.0, ~3.6, ~3.0 and ~2.6 volume percent
respectively for 1 atmosphere, 100, 200 and 300 MPa pressure. An upper bound
to the thermal expansion of the constituent minerals at pressure over this

temperature interval is given by the 2.0 volume percent increase of the dry
hypothetical granite of Figure 9.2-a, between 200°C and 840°C. The *minimum*
increases in porosity for the specimen material at 1 atmosphere, 100, 200
and 300 MPa over this temperature interval are therefore found to be ~2.0,
~1.6, ~1.0 and ~0.6 volume percent respectively. It is concluded that
cracks can open up against the applied confining pressures but that this
becomes increasingly difficult at higher values of the confining pressure.
If the minimum increase were to be the same as the real increase the
observed trend would suggest that there can be no more opening of cracks
at pressures higher than ~450 MPa. If the real increase were to be somewhat
higher, a higher maximum pressure would be obtained, for which the opening of
cracks is possible against the confining pressure.

The temperature chosen for comparison is 840°C, because it lies
above the temperature for the quartz $\alpha-\beta$ transition in the specimen material
at all pressures studied. The volumetric expansion of the rock is very
small or zero above the transition, both in the specimen material and in the
hypothetical "granite" used for comparison.

Thus, the porosity of Delegate aplite is expected to rise gradually
from above 200°C until the $\alpha-\beta$ transition of quartz takes place. At even
higher temperatures, the porosity may remain constant, or even decrease
somewhat if the contraction of quartz at 1 atmosphere beyond the transition
(Figure 9.2-a) also occurs at pressure. The expansion coefficients observed
above 200°C are initially somewhat lower than for the theoretical granite.
The decrease in porosity from 20°C to 200°C may therefore continue to higher
temperatures than 200°C before the increase in porosity to 840°C takes place.
The lack of compressibility data at temperature and of thermal expansion
data at pressure prevent a detailed calculation of the development of porosity
as a function of temperature. Further complications arise from the stress in-
homogeneities which occur on the scale of grains in the granite during thermal
expansion. Discussion of these factors is deferred to Chapter 11.

9.4.4   The effect of a pore fluid

Figure 9.5 represents the thermal expansion of Delegate aplite
at 300 MPa for a dry, and for a wet specimen with 0.7 weight percent, or
1.8 volume percent added water. An estimated extra 0.25 weight percent
water is released from within the rock upon heating to 800°C (Chapter 3,
Table 3.1). For comparison, the estimated expansion at atmospheric

Figure 9.5   Comparison of the thermal expansion of wet and dry
grainte at 300 MPa confining pressure. The dashed
line represents the estimated atmospheric expansion
of granite. The possibility of a kink in the curve
for wet granite is supported by the occurrence of a
marked kind around that temperature in a run at
300 MPa where argon gas occurred as a pore phase
(not shown in the figure).
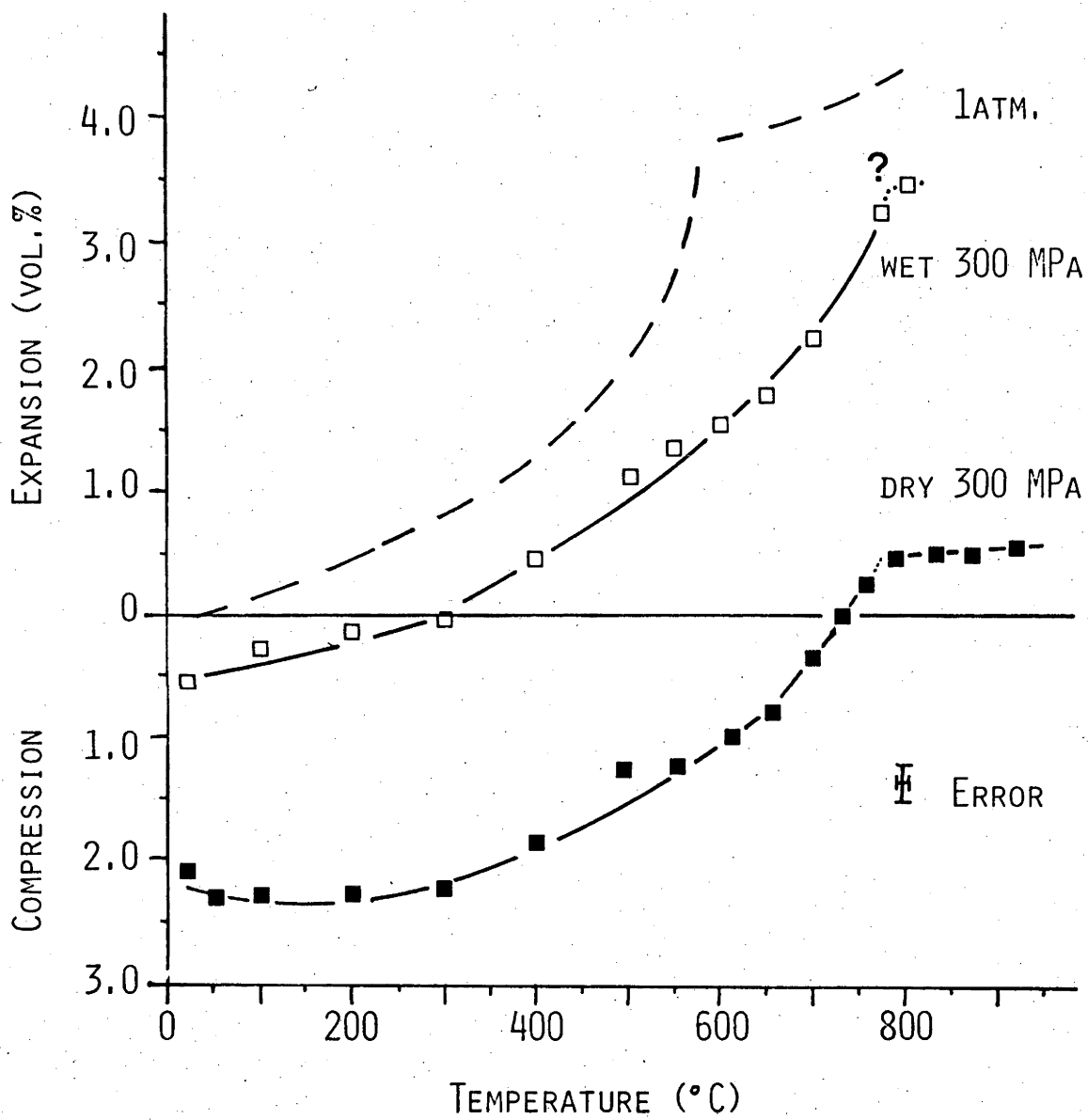
pressure is shown by a dashed line in Figure 9.5. No measurements were made beyond 800°C for the wet experiment, it is concluded however, from the absence of a marked kink in the thermal expansive curve around 650°C, and a possible indication of a kink close to 800°C, that the α-β transition of quartz in granite with water as a pore fluid is shifted to higher temperatures than for single crystals of quartz, at the applied confining pressure (compare Figure 9.4). The issue is slightly confused by the fact that melting occurs in specimens of granite with water at 300 MPa above 670°C (Chapter 3). However, the same conclusion about pore fluid effects follows from an experiment (not represented in the figure), in which argon gas occupied the pore space within the specimen. During one run on dry granite at 300 MPa the copper sealing jacket punctured accidentally in such a way, that argon gas was able to enter the specimen. The run was characterized by similar volume increases as the wet case shown, (about 0.3 volume percent higher), but with a clear kink in the thermal expansion curve between 740°C and 800°C. These results suggest that the shift in the quartz α-β transition temperature noted for dry granite does also occur in the presence of a pore fluid, whether water or gas, and that the shift is of comparable magnitude.

Following the procedure used earlier by comparing the observed results for wet granite at 300 MPa with the hypothetical dry granite at 1 atmosphere, it can now be shown that there are no changes in porosity to 200°C. Similarly, the minimum increase in porosity from 200°C to 800°C, can be calculated to be ~1.7 volume percent. The total porosity at 800°C and 300 MPa is therefore much higher for the wet case than for the dry one. The initial total porosity in both cases is ~2.3 volume percent at room conditions. In the dry granite ~1.3 volume percent porosity has been removed by compression to 300 MPa at room temperature plus another unknown amount less than 0.6 volume percent by heating to 200°C prior to an increase by ~0.6 volume percent to 840°C. In the wet case there is no decrease in porosity during compression to 300 MPa and heating to 200°C. The total porosity of wet Delegate aplite at 800°C and 300 MPa is therefore calculated to be at least 4.0 volume percent. This result is in excellent agreement with the total porosity calculated from density measurements at room temperature for dry specimens which were heated in an atmospheric furnace to 800°C (Chapter 3, Table 3.1). The present experiments therefore confirm

the assumptions made in Chapter 3, about porosity at 800°C and 300 MPa in Delegate aplite with excess added water.[1]

---

[1] The effect of the quartz α-β transition on porosity is found to be somewhat different than assumed in Chapter 3, because of the observed shift, but this does not affect the calculations of total and accessible porosities at 800°C made in that chapter.

Chapter 10

ELASTIC THEORY

10.1 The elastic field of a spherical inclusion in a matrix subjected to hydrostatic pressure

Consider the following three dimensional problem in elasticity. A sphere of an ideally elastic isotropic material is surrounded by an infinite matrix of another ideally elastic isotropic material. Let the inclusion be "glued" to the matrix at the contact such that stresses can be transmitted even if they are tensional. In the reference state stress and strain are zero in both matrix and inclusion. Now a hydrostatic stress p is applied at infinity onto the matrix. What is the resulting state of stress and strain inside the inclusion, and in the matrix, both far away from – and close to the contact with the inclusion?

This problem has been solved by Eshelby (1957) for general ellipsoidal inclusions and for a general state of stress applied to the matrix. The problem considered above is a considerable simplification of the general case and a less complicated notation can be used.

Let the bulk modulus of the matrix be K and its shear modulus μ, and let the bulk modulus of the inclusion be K_1. We adopt a sign convention in which compressive stress and compressive pressure are positive, and in which expansive volumetric strain (dilatation) and elongation are negative, for example:

$$p \ = \ K.\Delta \quad ,$$

where Δ is volumetric strain.

The following relationships can now be derived from Eshelby's (1957) general equations [1]:

---

[1] Notice that there is a misprint on p. 390 of Eshelby (1957), the last term on the right hand side of the equation for ${}^1p_{il}$ has to be:

$$-\frac{1}{3} \cdot \frac{1+\sigma}{1-\sigma} \cdot \frac{2\mu}{3K} \cdot A \cdot p^A \cdot (n_i \, n_l - \frac{1}{3} \, \delta_{il}).$$

The volumetric strain of the inclusion is:

$$\Delta_1 = \frac{P}{K} \cdot \frac{3K + 4\mu}{3K_1 + 4\mu} \qquad (1).$$

The hydrostatic pressure in the inclusion is:

$$p_1 = p \cdot \frac{K_1}{K} \cdot \frac{3K + 4\mu}{3K_1 + 4\mu} \qquad (2).$$

The linear strain in the matrix at the contact in directions normal to the inclusion surface is:

$$\varepsilon_{c\perp} = \frac{p}{K} \left[\frac{1}{3} + \frac{2(K_1 - K)}{3K_1 + 4\mu} \right] \qquad (3).$$

The linear strain in the matrix at the contact in directions parallel to the inclusion surface is:

$$\varepsilon_{c//} = \frac{p}{3K} \left[\frac{3K + 4\mu}{3K_1 + 4\mu} \right]$$

$$\qquad (4).$$

$$= \frac{p}{K} \left[\frac{1}{3} - \frac{(K_1 - K)}{3K_1 + 4\mu} \right]$$

From (3) and (4) it is seen that the volumetric strain in the matrix at the contact is:

$$\Delta_c = \varepsilon_{c\perp} + 2\varepsilon_{c//} = \frac{p}{K} \qquad (5),$$

which is equal to the volumetric strain of the matrix infinitely far away from the inclusion.

The normal and tangential stresses in the matrix at the contact with the inclusion are:

$$\sigma_{c\perp} = p \cdot \frac{K_1}{K} \cdot \frac{3K + 4\mu}{3K_1 + 4\mu} = p \left[1 + \frac{4\mu (K_1 - K)}{K(3K_1 + 4\mu)} \right] \qquad (6),$$

and

$$\sigma_{c//} = p \left[1 - \frac{2\mu(K_1 - K)}{K(3K_1 + 4\mu)} \right] \qquad (7).$$

From (2) and (6) it is seen that the internal pressure of the inclusion equals the normal stress in the matrix at the contact. The requirement of a balance of forces across the contact is fulfilled. From (6) and (7)

it is seen that the "hydrostatic component" of the stress in the matrix at the contact is:

$$p_c = \frac{\sigma_{c\perp} + 2\sigma_{c/\!/}}{3} = p \qquad (8),$$

which is equal to the hydrostatic pressure in the matrix infinitely far away from the inclusion.

Equations (3) – (8) describe the state of stress and strain in the matrix at the contact with the inclusion; the volumetric strain and the pressure in the matrix infinitely far away from the inclusion have also been given. Intermediate states occur in between; the disturbance of the elastic strain field of the matrix due to the inclusion decays with distance r from the inclusion as $\frac{1}{r^3}$ (compare Eshelby (1957) equation 2.18).

We will now determine the conditions for which during compression ($p>0$) the hydrostatic pressure in the inclusion and the normal or the tangential stress in the matrix become tensional. In the case considered here, $K>0$, $\mu>0$, $\mu = \frac{3K(1-2v)}{2(1+v)}$, where v is the Poisson ratio of the matrix, and $- 1<v<\frac{1}{2}$ (Jaeger, 1969, p. 57). For holes in the matrix $K_1 = 0$, for inclusions more compressible than the matrix $0<K_1<K$ and for inclusions less compressible than the matrix $K_1>K$. Thus in the present case, where all the strain in the inclusion is caused by the applied compressive pressure p we also have the condition $K_1 \geq 0$. For reasons which will become apparent in Section 10.2, we will also consider when tensional stresses would develop if it were possible that $K_1<0$. From (2) and (6) it is seen that:

$$p_1 = \sigma_{c\perp} < 0 \quad \text{if:}$$

$$\frac{4\mu(K_1 - K)}{K(3K_1 + 4\mu)} < -1 \qquad (9\text{-a}).$$

The possible range of K_1 values in accordance with this inequality is given as a function of the Poisson ratio of the matrix in Figure 10.1-a. It is seen that:

$$p_1 = \sigma_{c\perp} > 0 \quad \text{if:}$$

$$K_1 > 0 \quad \text{for:} \qquad (9\text{-b}).$$

$$-1<v<\frac{1}{2}$$

Figure 10.1-a Values of the effective or equivalent bulk modulus
of the inclusion, as a function of the Poisson
ratio of the matrix, for which tensional normal
stresses between matrix and inclusion are possible.

Figure 10.1-b Values of the effective or equivalent bulk modulus
of the inclusion, as a function of the Poisson
ratio of the matrix, for which tensional tangential
stresses in the matrix are possible. For an explan-
ation of the term "effective or equivalent bulk
modulus" see Section 10.2.

TIMES K

μ

$\dfrac{6\mu K}{2\mu - 3K}$

POISSON
RATIO

$-\dfrac{4}{3}\mu$

$\dfrac{6\mu K}{2\mu - 3K}$

6
5
4
3
2
1
0

0.5

-0.5

-1

0
-1
-2
-3
-4

(b)

TIMES K

μ

POISSON
RATIO

$-\dfrac{4}{3}\mu$

6
5
4
3
2
1
0

0.5

-0.5

-1

0
-1
-2
-3
-4

(a)
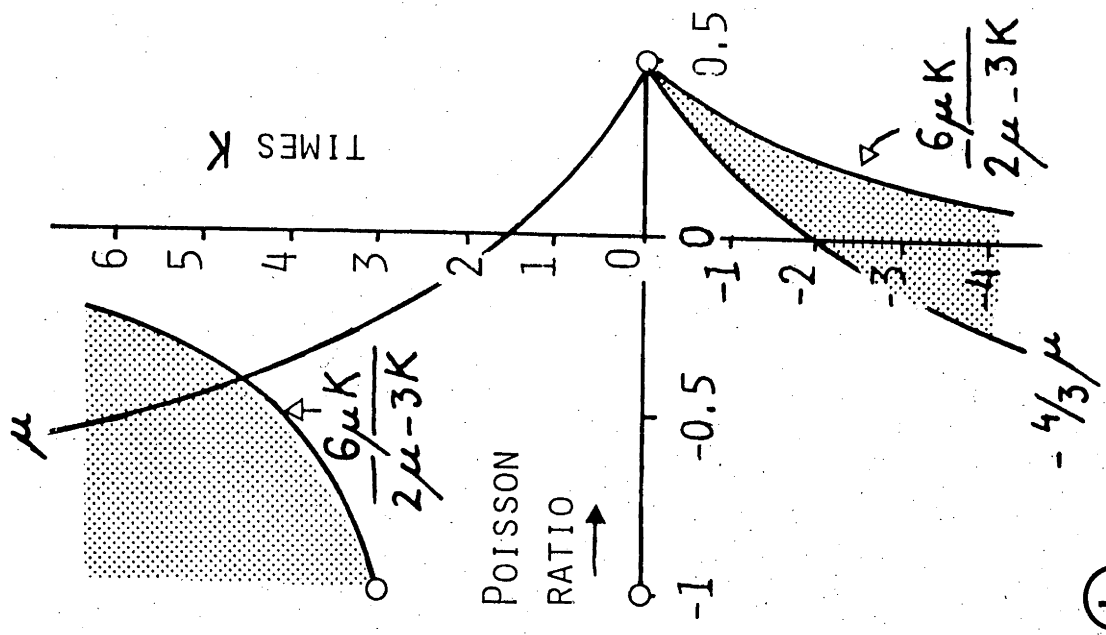
In the present case the pressure in the inclusion and the normal stress in the matrix will always be compressive during compression, unless the inclusion is a hole when - trivially - the pressure of the inclusion and the normal stress in the matrix at the contact are zero.

It is also seen that <u>if it were possible that $K_1 < 0$</u>:

$$p_1 = \sigma_{c\perp} < 0 \quad \text{if:}$$
$$-\frac{4}{3}\mu < K_1 < 0 \text{ for:} \qquad\qquad (9\text{-}c).$$
$$-1 < v < \tfrac{1}{2}$$

Next we determine the conditions under which the tangential stress in the matrix becomes tensional during compression ($p > 0$). From (7) it is seen that:

$$\sigma_{c//} < 0 \quad \text{if:}$$
$$\frac{2\mu \ (K_1 - K)}{K \ (3K_1 + 4\mu)} > 1 \qquad\qquad (10\text{-}a).$$

Substitution of inequality (10-a) into (6) or (2) indicates that (10-a) is equivalent to:

$$\sigma_{c//} < 0 \quad \text{if:}$$
$$p_1 = \sigma_{c\perp} > 3p \qquad\qquad (10\text{-}b).$$

Tensional tangential stress is developed in the matrix if the pressure in the inclusion exceeds three times the compressive pressure applied to the matrix. The possible range of K_1 values in accordance with inequalities (10-a) and (10-b) is given as a function of the Poisson ratio of the matrix in Figure 10.1-b. It is seen that:
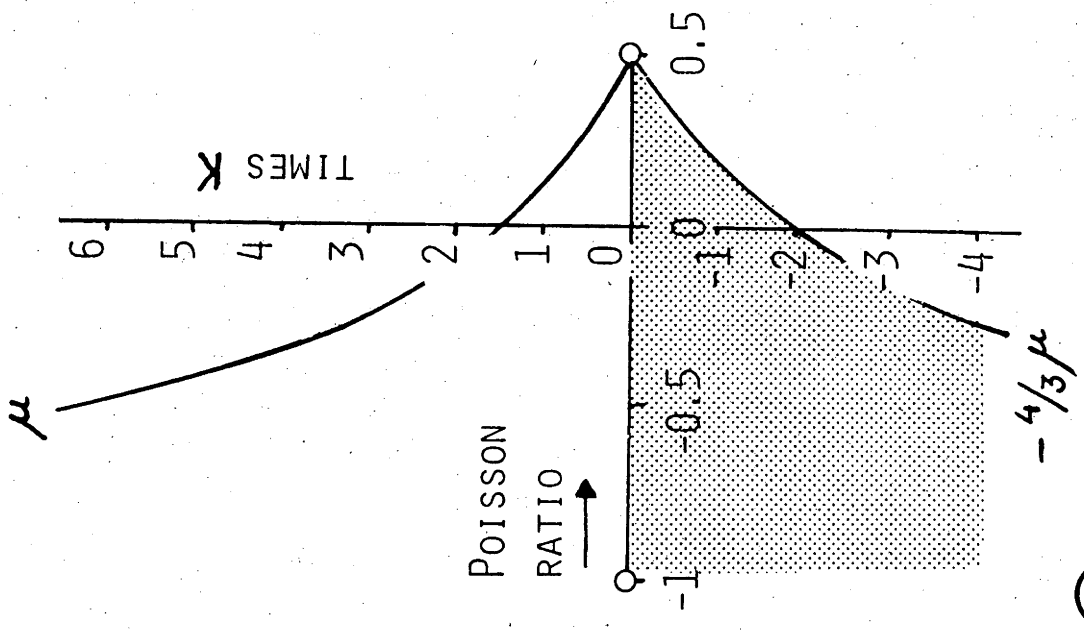
$$\sigma_{c//} < 0 \quad \text{if:}$$
$$K_1 > \frac{6\mu K}{2\mu - 3K} \text{ for:} \qquad\qquad (10\text{-}c).$$
$$-1 < v < 0$$

Thus in the present case the tangential stress in the matrix can only become tensional during compression for the (rare) case of a negative Poisson ratio of the matrix, and then only if $K_1 \gg K$.

We notice however, that <u>if it were possible that $K_1 < 0$</u>, tensional tangential stresses could also develop for a positive Poisson ratio of the matrix during compression provided any of the following conditions is met (Figure 10.1-b):

$$\sigma_{c//} < 0 \quad \text{if:}$$

$$K_1 > \frac{6\mu K}{2\mu - 3K} \quad \text{for} \quad -1 < v < 0 \quad (10\text{-}c)$$

$$\text{or} \quad K_1 < -\frac{4}{3} \quad \text{for} \quad -1 < v < 0$$

$$\text{and} \quad \sigma_{c//} < 0 \quad \text{if:} \quad (10\text{-}d).$$

$$-\frac{4}{3}\mu > K_1 > \frac{6\mu K}{2\mu - 3K} \quad \text{for} \quad 0 < v < \tfrac{1}{2}$$

$$\text{and} \quad \sigma_{c//} < 0 \quad \text{if:}$$

$$K_1 < -2K \quad \text{for} \quad v = 0.$$

10.2 Effect of a volumetric strain in the inclusion which is not caused by the applied pressure

All equations used thus far were already present in some form or another in Eshelby (1957). The inclusion described in the previous section underwent a volumetric strain Δ_1 by the application of a pressure p to the matrix and the resulting pressure in the inclusion, p_1, is given by $K_1 \Delta_1$.

We now wish to consider the situation where an included sphere of originally the same size, and with a bulk modulus K_2 undergoes the same volumetric strain:

$$\Delta_2 = \Delta_1 \qquad (11),$$

and develops the same inclusion pressure:

$$p_2 = p_1 \qquad (12),$$

but where a part Δ_2^* of the strain Δ_2 is not caused by the application of a pressure p. Such a "pressure-free" part of the inclusion strain may

be brought about, for example, by differential thermal expansion of matrix and inclusion during a temperature change.

Provided the initial sizes of the inclusions are the same and provided (11) and (12) are met, the new inclusion can replace the old one, described in the previous section, without altering the state of stress and strain in the matrix, or the pressure and the total strain in the inclusion.

Equation (12) is ensured if:

$$K_2 \quad (\Delta_2 - \Delta_2^*) = K_1\Delta_1 \qquad\qquad (13),$$

and from (1), (11) and (13) it follows that:

$$\Delta_2 = \frac{p}{K} \cdot \frac{3K + 4\mu}{3K_1 + 4_\mu} = \frac{K_2}{K_2 - K_1} \cdot \Delta_2^* \; . \qquad (14).$$

From (14) we solve for K_1 and obtain:

$$K_1 = K_2 \; [\; \frac{\frac{p}{K}(3K + 4\mu) - 4\mu\Delta_2^*}{\frac{p}{K}(3K + 4\mu) + 3K_2\Delta_2^*} \;] \; . \qquad (15).$$

The expression on the right hand side of (15) may now be considered as the "effective" or the "equivalent" bulk modulus of the inclusion. That is, the bulk modulus that would be required by the inclusion if the total inclusion strain Δ_2 and the inclusion pressure p_2 were to be caused by the application of a confining pressure p to the matrix.

Substitution of (15) into (1)-(8) now allows one to express the states of stress and strain inside the inclusion and in the matrix at the contact with the inclusion in terms of the elastic constants K and μ of the matrix, the applied pressure p and the bulk modulus K_2 of the inclusion material plus its "pressure-free" strain Δ_2^*. The resulting relationships are somewhat cumbersome and not represented here.

From (15) we note that, while $K_2 \geq 0$ (the bulk modulus of the new inclusion material can again not be negative), it is now possible for the "equivalent" bulk modulus to become negative for certain combinations of the values of μ, K, K_2 and Δ_2^*. It is for this reason that we have considered negative values for K_1 in the previous section. From a combination of Figures 10.1-a and b it can now be seen that for positive Poisson ratios of the matrix tensional stresses will exist during compression

when $K_1 < 0$. (It should be remarked however, that for no value of v can $K_1 = -\frac{4}{3}\mu$ because substitution of that into (15) would imply that $K_2 = -\frac{4}{3}\mu$, in contradiction with the requirement that $K_2 \geq 0$.)

Substitution of (15) into (9-c) allows us to calculate the value of the pressure-free strain Δ_2^* needed to cause tensional normal stress in the matrix, as well as a state of hydrostatic tension in the inclusion during compression of the matrix by a pressure p. It is found that:

$$p_2 = \sigma_{c\perp} < 0 \quad \text{if:}$$
$$\Delta_2^* > p \left(\frac{3}{4\mu} + \frac{1}{K}\right) \quad \text{for:} \tag{16},$$
$$-1 < v < \tfrac{1}{2}$$

where it should be remembered that volumetric contractions are taken positive with the sign convention used. The situation described by (16) can arise if there is a contraction of the inclusion relative to the matrix which is not caused by the applied confining pressure, but for instance by differential thermal expansion of matrix and inclusion during a temperature rise. Equation (16) is independent of the bulk modulus of the inclusion as would be expected.

Substitution of (15) into (10-c) and (10-d) now allows us to calculate the values of Δ_2^* needed to cause tensional tangential stress in the matrix during compression by a pressure p. It is found that:

$$p_2 = \sigma_{c\perp} > 3p \quad \text{and} \quad \sigma_{c/\!/} < 0 \quad \text{if:}$$
$$\Delta_2^* < p \left(\frac{1}{K} - \frac{3}{2\mu} - \frac{3}{K_2}\right) \quad \text{for:} \tag{17},$$
$$-1 < v < \tfrac{1}{2}$$

where it should be remembered that volumetric expansions are taken negative with the sign convention used. For positive Poisson ratios of the matrix the situation described by (17) may arise if there is a volumetric expansion of the inclusion relative to the matrix which is not caused by the applied compressive pressure, but for instance by differential thermal expansion of matrix and inclusion during a temperature rise.

10.3 Examples

10.3.1 Pressure differences during isothermal compression and during a temperature rise at constant confining pressure

Firstly, we calculate the stresses which develop in and around an inclusion during room temperature compression. Let there be zero stress and zero strain in the matrix and in the inclusion at room temperature and atmospheric pressure. It is further assumed that the Poisson ratio of the matrix $v = 0.25$, so that $\mu = \frac{3}{5}K$. This relationship is closely obeyed by many rock-forming minerals (*e.g.* Birch, 1966). It is easily seen that (2), (6) and (7) now reduce to:

$$p_i = \sigma_{c\perp} = p \left(\frac{9K_i}{5K_i + 4K}\right)$$

$$= p \left(\frac{9B}{5B + 4B_i}\right) \tag{18},$$

and

$$\sigma_{c//} = p \left(\frac{3K_i + 6K}{5K_i + 4K}\right)$$

$$= p \left(\frac{3B + 6B_i}{5B + 4B_i}\right) \tag{19},$$

where the subscript i now refers to the inclusion and no subscripts to the matrix. B and B_i are the compressibilities of the matrix and the inclusion.[1]

Numerical examples of (18) and (19) are given in Table 10.1. For compressibilities of the inclusion and matrix materials I have chosen those of real quartz (0.02706 per 100 MPa) and plagioclase (0.0179 per 100 MPa) at room temperature as given by Birch (1966). The extreme cases for which the inclusion is a hole ($B_i = \infty$) or incompressible ($B_i = 0$) are also shown in Table 10.1. It is understood, that neither quartz nor plagioclase are elastically isotropic. To emphasize that only the volumetric differential compression of these two minerals is considered, I have used quotation marks.

---

[1] The letter B has been chosen instead of the more conventional β for compressibility to avoid confusion with α and β-quartz.

Table 10.1   Stresses in and around an inclusion in an infinite matrix
during isothermal compression by a pressure p.

	$p_i = \sigma_{c\perp}$	$\sigma_{c//}$
Inclusion is incompressible	1.800 p	0.600 p
"Plagioclase" in "quartz"	1.177 p	0.912 p
"Quartz" in "plagioclase"	0.815 p	1.093 p
Inclusion is a hole	0.000 p	1.500 p

It is seen from Table 10.1 that considerable differences may exist between the pressure applied to the matrix and that inside the inclusion if their compressibilities are not the same.

Substitution of (15) into (18) yields:

$$p_i = \frac{K_i (9p - 4K\Delta_i^*)}{5K_i + 4K} = \frac{9pB - 4\Delta_i^*}{5B + 4B_i} \qquad (20),$$

where subscript i again refers to the inclusion material. This formula allows us to calculate the change in the internal pressure of the inclusion if the "pressure-free" strain Δ_i^* of the inclusion is increased from 0 to Δ_i^*. For expansion of the inclusion relative to the matrix ($\Delta_i^* < 0$) we get:

$$0 > \delta p_i = -4\Delta_i^* \cdot \frac{K_i K}{5K_i + 4K}$$

$$= -4 \frac{\Delta_i^*}{5B + 4B_i} \cdot \qquad (21).$$

That is, the increase in pressure of the inclusion is independent of the magnitude of the confining pressure p provided Δ_i^*, B and B_i are independent of the confining pressure, and provided B and B_i are independent of temperature.

For example let the thermal expansion of a "quartz" inclusion relative to a "plagioclase" matrix be 0.25 volume percent. Then the internal pressure of the "quartz" inclusion rises by 55.6 MPa. Comparison with Table 10.1 shows that now for $p = 300$ MPa the internal pressure of the inclusion is the same as the applied confining pressure. For lower values of p the inclusion pressure has risen above the confining pressure and for higher values of p it is still below that.

10.3.2 Tensional stresses during thermal expansion at pressure

In this example I investigate the effect which the confining pressure has on the amount of relative thermal expansion Δ_i^* needed to cause tensional normal stress between the matrix and the inclusion, or tensional tangential stress in the matrix. Again taking zero strain in matrix and inclusion at room conditions, and assuming $v = 0.25$ it is easily seen that (16) and (17) reduce to:

$$p_i = \sigma_{c\perp} < 0 \quad \text{if:}$$

$$\Delta_i^* > p \cdot \frac{9}{4}B \tag{22},$$

and $\quad p_i = \sigma_{c\perp} \geq 3p \quad$ and $\quad \sigma_{c/\!/} < 0 \quad$ if:

$$\Delta_i^* < -p \left(\frac{3}{2} B + 3B_i \right) \tag{23}.$$

Two examples are shown in Figure 10.2-a, for elastically isotropic materials which have the same compressibilities as real quartz and real plagioclase. A "plagioclase" inclusion tends to develop a tensional stress normal to the contact with a "quartz" matrix under compression if the contraction of the inclusion relative to the matrix exceeds that by the line marked "plag" in "q". A tensional tangential stress develops in a "plagioclase" matrix if the expansion of a "quartz" inclusion relative to the matrix exceeds that by the line marked "q" in "plag".

Figure 10.2-b shows the difference in volume percent between the volumetric thermal expansions of real plagioclase and quartz at 1 atmosphere. The figure is obtained from Figure 9.2-a by subtracting the expansions of plagioclase from those of quartz. If the volumetric thermal expansion behaviour of Figure 10.2-b is attributed to the hypothetical (i.e. isotropic) inclusion and matrix materials in Figure 10.2-a, they may be compared. For instance at 200 MPa confining pressure a temperature rise to ~400°C is needed before tensional normal stresses develop across the boundary between a "plagioclase" inclusion and a "quartz" matrix. For the reverse case of a "quartz" inclusion in a "plagioclase" matrix the temperature will have to rise to ~520°C at 200 MPa before tensional tangential stresses develop in the matrix. It is also seen (dotted arrows in Figure 10.2) that given the differential thermal expansion behaviour of Figure 10.2-b, there cannot exist tensional stresses between "quartz" matrix and "plagioclase" inclusion if the confining pressure exceeds ~600 MPa. Similarly, the maximum confining pressure for which tensional tangential stress may develop in a "plagioclase" matrix around a "quartz" inclusion is reached at ~340 MPa.

The calculations presented above are for a temperature-insensitive compressibility value of "quartz". The compressibility of real quartz is known to increase with temperature towards the α-β transition at 1 atmosphere (Coe and Paterson, 1969; for details see also Chapter 11 and Figure 11.1).

Figure 10.2   Differential thermal expansion behaviour of quartz
and plagioclase and the pressures for which this
may lead to tensional stresses.

    a.   The absolute value of the pressure free strain Δ_i^*,
needed to cause tensional tangential stress in a
"plagioclase" matrix around a "quartz" inclusion,
or tensional normal stress between a "quartz"
matrix and a "plagioclase" inclusion, increases
with the confining pressure applied to the matrix.
With the sign convention used, the first case
represents negative and the second positive values
of Δ_i^*.

    b.   Relative volume change between quartz and plagio-
clase as a function of temperature at 1 atmosphere
(after Skinner, 1966). If the differential thermal
expansion behaviour of Figure -b is ascribed to the
hypothetical matrix and inclusion materials of
Figure -a, the maximum confining pressures for which
tensional stresses may arise due to differential
thermal expansion may be obtained in the manner shown
by the dotted arrows. (For further discussion see
text).
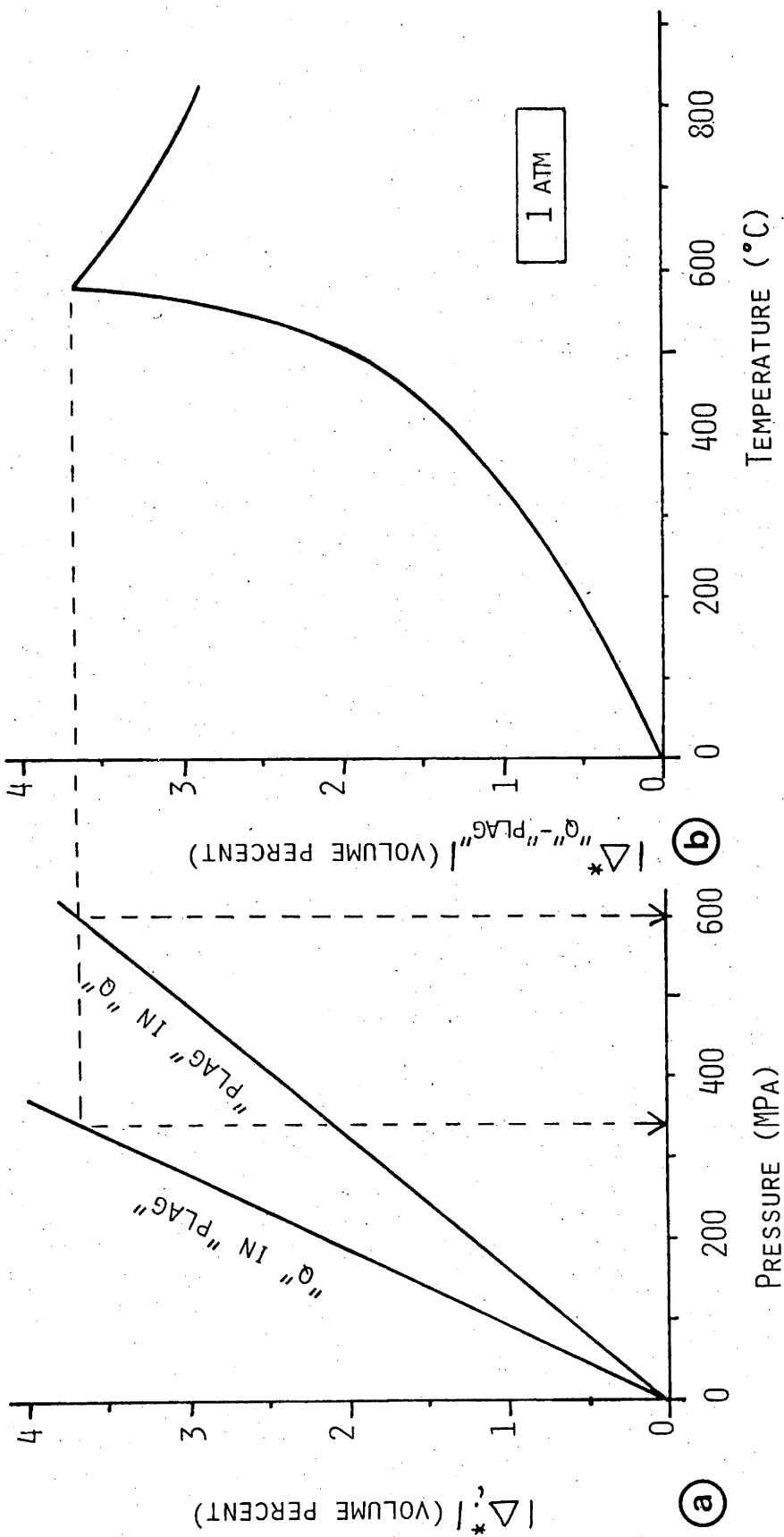
Furthermore, in the above calculations, the relative volumetric thermal expansion behaviour of "quartz" and "plagioclase" at pressure has been assumed to be constant and the same as that of real quartz and plagioclase at 1 atmosphere. In reality the effect of pressure is to shift the quartz α-β transition to higher temperatures (Chapters 9 and 11), and this spreads out the thermal expansion curve of Figure 10.2-b over wider temperature intervals.

Inspection of equations (22) and (23) and of Figure 10.2 indicates that both the elastic softening of quartz at temperatures approaching the α-β transition and the displacement of the transition to higher temperatures at pressure cooperate to <u>increase</u> the temperature intervals needed to produce tensional stresses at a given confining pressure. The softening of quartz will also tend to <u>decrease</u> the maximum confining pressure at which tensional stresses are possible at all. Values lower than the ~340 MPa for "quartz" in "plagioclase: and the ~600 MPa for "plagioclase" in "quartz" will therefore be obtained for the maximum confining pressures at which tensional stresses may develop, if the properties of matrix and inclusion are chosen such that they represent the properties of real quartz and plagioclase more closely.

CHAPTER 11

DISCUSSION

11.1 General

The experimental results of Chapter 9 indicate that volume changes
in natural granite under experimental conditions of moderate confining
pressures and increasing temperature are caused both by volume changes
of the constituent minerals, and by changes in the pore volume in between
them. In particular it has been shown that confining pressures of 100,
200 and 300 MPa are insufficient to prevent an increase in porosity during
a temperature rise from 200°C to 840°C. It has also been found that the
porosity increase over this temperature interval decreases as the confining
pressure is increased. From the trend at lower pressure, it is estimated
that porosity can no longer increase during a temperature rise to 840°C
if the confining pressure exceeds ~450 MPa.

The observations of Kern (1978, in prep.) on the shift of the
quartz α-β transition temperature in granite have, in general, been confirmed.
The shifts recorded in the present experiments are towards somewhat higher
temperatures than those reported by Kern, particularly so at the highest
confining pressures.

Qualitatively, the opening of pores in granite against a confining
pressure may be ascribed to the differential thermal expansion of the
constituent minerals. Differences in volume changes and shape changes
on the grain scale may lead to local tensional stresses, causing the opening
of pores in an aggregate which as a whole is held under confining pressure.
Similarly, the shift of the α-β transition of quartz in granite to higher
temperatures has been attributed qualitatively to stress inhomogeneities
within the crystalline aggregate (Kern, 1978, in prep.).

The experimental observations provoke the following questions:

i.   Why are confining pressures of 100 to 300 MPa insufficient to
     prevent the opening of pores during a temperature rise?

ii. What factors determine the magnitude of the observed shift in
     the quartz α-β transition temperature?

iii. Why is the α-β transition for quartzes in granite at pressure not
     spread out over a range of temperatures? Curves of V_p versus
     temperature show a very sharp minimum, not a broad low (see *e.g.*

Kern, 1978, in prep.), and the graphs of volume change versus
temperature presented in Chapter 9, exhibit a marked kink, not
a gradual change. If the shift in the α-β transition is caused
by stress inhomogeneities in the aggregate at pressure, what
causes those inhomogeneities in stress to be more or less the
same for all individual quartz crystals, such that sharp changes
may be observed in the bulk properties of the rock?

11.2 The inapplicability of the elastic theory to the case of a real granite.

Before using the results of the elastic theory presented in
Chapter 10 to solve the problems mentioned in the previous section, it seems
appropriate to emphasize the large differences between the realities of the
specimen material and the assumptions of the theory.

*The theory consideres only isotropic volume changes of matrix and
inclusion.* As such it is not directly applicable to the minerals quartz,
plagioclase and K-feldspar, because these are anisotropic, both in their
linear compressibilities (Birch, 1966) and in their linear thermal expansion
coefficients (Skinner, 1966). However, it seems reasonable to assume that
the bulk properties of the granite are governed by the differential volume
changes of the constituent minerals. Locally second order effects may
arise from the anisotropy of the minerals, but over the whole of the
specimen these tend to cancel out, since there is no preferred crystallo-
graphic orientation in the material studied. It is therefore believed that
the large effect which differential stress has on the α-β transition
temperature in single crystals of quartz (Coe and Paterson, 1969) will not
influence the transition temperature in a random polycrystal to any great
extent. The latter conclusion is strengthened by the observation of Kern
(in prep.) that there is no shift for the α-β transition temperature in
monomineralic quartzite at 200 MPa confining pressure.

The theory describes a spherical inclusion. The real granite is
more or less equigranular and the average grain shape is equant, but each
individual grain has an irregular angular surface. In thin section, curved
grainboundaries may be observed as well as straight and serrated ones,
and where three grainboundaries meet they can often be seen to make the
120° triple junction characteristic of crystalline rocks. An expanding
angular inclusion has a wedging effect on its surroundings and stress
concentrations arise in the matrix which do not occur in the case of a

spherical inclusion. The same remarks apply to inclusions which have a smooth surface but a non-spherical shape (for the general ellipsoidal inclusion see Eshelby, 1957). It may therefore be expected that the minimum thermal expansion, needed to produce tensional stresses in a surrounding matrix under confining pressure will be *smaller* in the case of non-spherical, than in the case of spherical inclusions. Similarly, it may be expected that the maximum confining pressure for which tensional stresses are possible (given a certain maximum differential expansion) will be *higher* in the case of non-spherical than in the case of spherical inclusions.

The theory considers an isolated inclusion in an infinite homogeneous matrix. The most serious differences between the theory and the real granite arise here. Occasionally, in granite an individual quartz grain may be completely surrounded by feldspar crystals, and less likely still an occasional feldspar grain may be completely surrounded by quartz crystals. But statistically the matrix around any grain consists of two-thirds feldspar (plagioclase + K-feldspar) and one-third quartz. If, in the real rock, quartz is viewed as the inclusion material and the feldspars are considered to make up the matrix, then there is a very high concentration of inclusions unlike the infinitely dilute concentration assumed in the development of the theory. In thin section contiguous quartz crystals are visible and the distance from one quartz crystal to the next in any direction is never more than 3 or 4 grain diameters. Moreover, the matrix around any quartz grain is full of discontinuities in the form of grainboundaries, pre-existing cracks, cleavages in feldspar and the small amount of biotite present in Delegate aplite. The presence of discontinuities in the "matrix" and the high concentration of quartz "inclusions" modify the homogeneous disturbance caused by a single inclusion in a flawless homogeneous matrix. There will be stress concentrations caused by the discontinuities and interferences of stress fields of "inclusions" close to one another. The resulting inhomogeneous stress field in the real rock is too complicated to calculate theoretically.

11.3 Application of the elastic theory to the case of a real granite

11.3.1 The model

Delegate aplite is viewed as a matrix of plagioclase and K-feldspar grains with spherical inclusions of quartz. The matrix contains grainboundaries and cracks which may be closed by a confining pressure. Closed grainboundaries and closed cracks are thought to have no effect on the transmission of compressional forces, but their tensile strengths are assumed to be zero. Each quartz inclusion is surrounded by several matrix grains, so there are matrix-grainboundaries perpendicular or at a high angle to the surface of each quartz inclusion.

First consider a quartz inclusion of the granite which is completely surrounded by feldspar grains at atmospheric conditions without open grainboundaries or cracks. A confining pressure p is applied and the temperature is increased. It has been shown in Chapter 10 (equations 10-b and 17) that tensional stress develops in the matrix tangential to the surface of the inclusion if the internal pressure of the inclusion exceeds three times the applied confining pressure. Once this pressure is reached in the quartz inclusion, as a result of resisted differential volumetric expansion of the inclusion relative to the matrix, the grainboundaries perpendicular to the contact will open up because they have zero tensional strength. Any further volumetric increase of the quartz inclusion relative to the matrix causes a further opening of the grainboundaries in the matrix, but the internal pressure in the inclusion remains $3p$.

If the whole granite consisted of such inclusions of quartz in a crack free matrix at room conditions, it would be predicted that cracks originate around all inclusions at the same temperature. For instance the example in Chapter 10.3.2 would indicate that this temperature will have a unique value above 520°C at 200 MPa confining pressure. Similarly, it would be predicted that the maximum confining pressure for which the formation of porosity due to differential thermal expansion of quartz inclusions and feldspar matrix is possible would be less than ~340 MPa.

Next consider a quartz inclusion of the granite which is again surrounded by feldspar grains, but this time with an open crack or grainboundary perpendicular to its surface at room temperature. Assume that the application of a confining pressure p at room temperature is just

sufficient to close this crack, that is, at a confining pressure p for the whole granite there is zero compressive stress across the crack perpendicular to the quartz inclusion. Even a small increase in temperature resulting in a volumetric increase of the quartz inclusion relative to the matrix now causes the reopening of this crack which was only just kept closed by the confining pressure. A crack perpendicular to another quartz inclusion, for which a fraction of p is sufficient for closure at room temperature, will require a larger relative expansion of the quartz inclusion, and therefore a larger interval in temperature for reopening while the granite is at a confining pressure p.

The progressive closing of more and more porespace in Delegate aplite by confining pressures up to 300 MPa has been demonstrated in Chapter 9.4.1. The above considerations would therefore predict a more or less gradual increase in porosity with increasing temperature provided the confining pressure is not too high to resist all opening of cracks. Because of the initial presence of cracks the maximum pressure for which crack opening is possible will be *higher* than the value of less than 340 MPa calculated above for the initially crack free case. The extrapolation of the experimental results for Delegate aplite indicates that the maximum pressure for crack opening in this material is of the order of 450 MPa.

11.3.2   Focusing effects

For any crack to open, a separative movement of the two faces of the crack must be possible. This will only be the case if the wider matrix around *the quartz inclusion plus the crack* allows such a differential movement to occur. The opening up of a crack allowed by the matrix may be expected to be limited, increasingly so at higher confining pressure because there will be fewer open pores available in the rock to accommodate displacive movements. During a temperature rise, the expanding quartz inclusion plus its crack will at some stage start to require more space from the wider matrix than available, and the internal pressure of the inclusion will start to rise while the crack is open. Eventually, the crack must open further or a new crack must be formed in the matrix if the internal pressure in the quartz inclusion reaches three times the applied confining pressure. For those cases where the confining pressure does not prevent the opening of cracks we may now make the following conclusion. At a given pressure p more quartz grains in granite reach an internal

pressure $3p$ if the temperature is increased. None of the quartz inclusions can reach an internal pressure exceeding $3p$. This I will call the first focusing effect. Because of the initial inhomogeneity of the granite there will still be a range of temperatures for which individual quartz crystals reach an internal pressure $3p$.

A second focusing effect arises from the temperature sensitivity of the finite yield strength of the matrix material which enables the existence of stress inhomogeneities. If the matrix were to behave as a fluid without a yield strength there could be no shear stresses, and therefore no pressure gradients in the matrix between individual inclusions of quartz. Irrespective of the non-elastic process by which yielding occurs in the matrix (through plastic flow, sliding on frictional contacts or brittle fracture of individual grains), it is likely that the yield strength at a given pressure decreases with increasing temperature. The maximum possible difference in internal pressure between nearby quartz inclusions will therefore be lower at high temperature than at low temperature.

It would appear that a third focusing effect may arise from the pressure sensitivity of the α–β transition of quartz, and the associated changes in its compressibility and expansion. The transition temperature of single crystals of quartz is known to increase by 26°C per 100 MPa pressure from 573°C at one atmosphere (*e.g.* Coe and Paterson, 1969; Koster van Groos and Ter Heege, 1973). In Figure 11.1-a, I have shown the changes in thermal expansion coefficient A and in volume compressibility B of quartz as a function of temperature towards the α–β transition at atmospheric pressure. The thermal expansion curve is calculated from the data of Skinner (1966) and the curve for compressibility from the compliance data for quartz as shown by Coe and Paterson (1969, Fig. 3). In the absence of compressibility data for single crystals of quartz at high pressure and temperature, or of thermal expansion data for high pressures, I will assume that similar changes occur at pressure as at 1 atmosphere, but that the changes are spread out over larger temperature intervals because of the pressure sensitivity of the α–β transition temperature. This assumption is shown schematically in Figure 11.1-b for two inclusions of quartz in granite under confining pressure. Due to stress heterogeneities in the aggregate inclusion 1 has a lower internal pressure than inclusion 2, and at a given temperature T, the first grain is therefore nearer to its α–β transition temperature than the second. An increase in temperature ΔT will now result in a larger volumetric expansion of the first grain than of

Figure 11.1   Thermal expansion coefficient and compressibility of
               quartz as a function of temperature and pressure.

          a.   Changes in the coefficient of thermal expansion
               (after Skinner, 1966) and volume compressibility
               of quartz (calculated from compliance data
               presented by Coe and Paterson, 1969), for atmospheric
               pressure and temperatures towards the α-β transition.
               Notice that the thermal expansion increases more
               rapidly for all temperatures.

          b.   (Schematic) Assumed influence of pressure (1 atmos-
               phere, left-hand curves, highest pressure right-hand
               curves) on the thermal expansion coefficient and the
               compressibility of quartz. Notice that, for any
               temperature interval ΔT and for any given pressure,
               the thermal expansion coefficient increases more
               rapidly with respect to its value at 100°C than
               the compressibility, and more so for low than for
               high pressure.
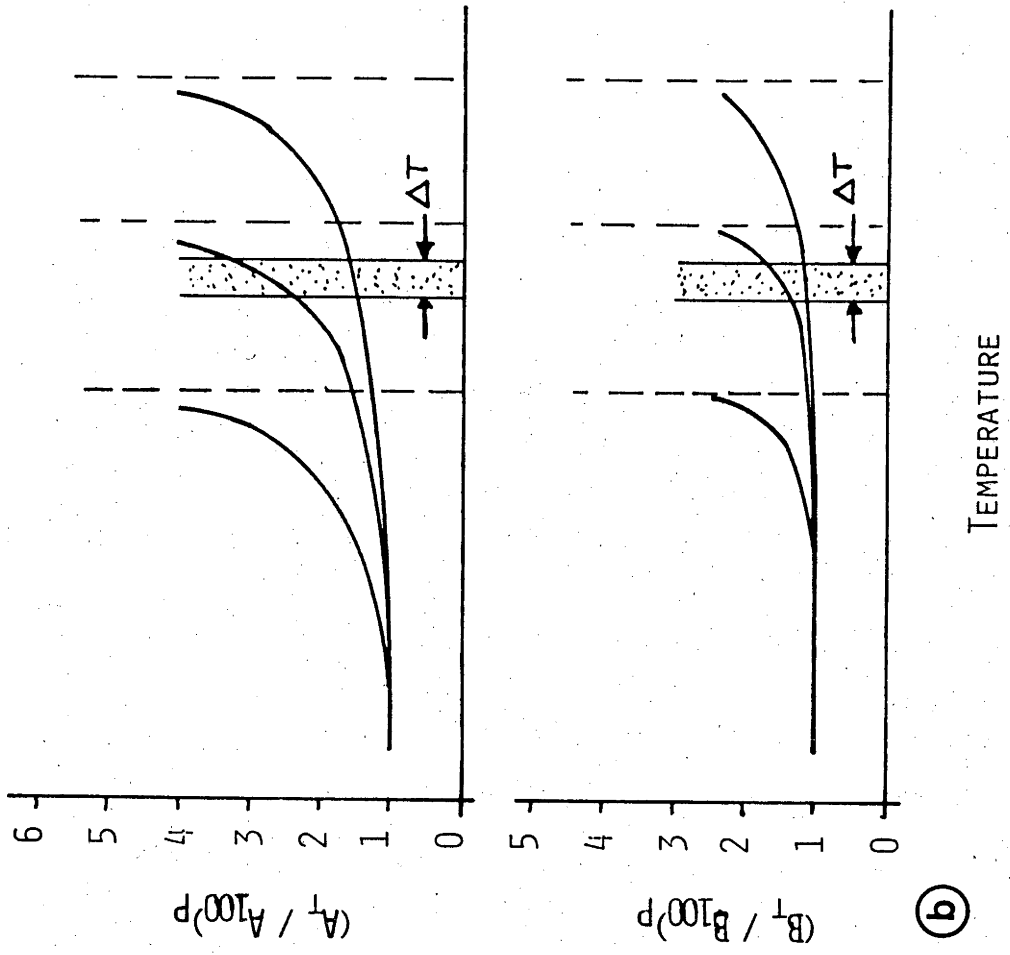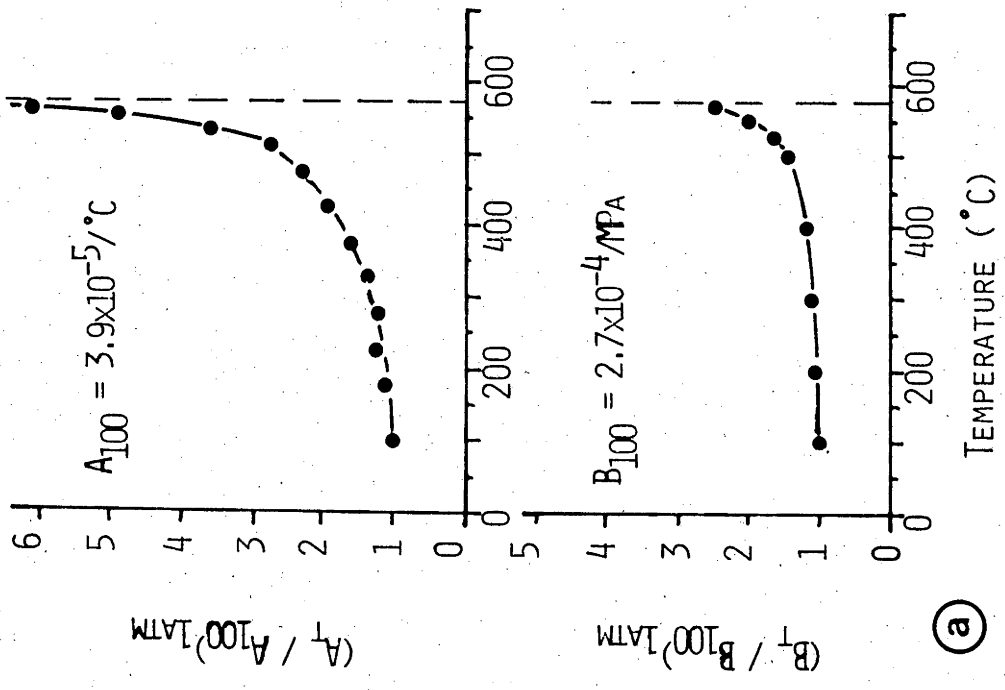
the second, but simultaneously the first grain will become much softer (its compressibility increases more) than the second. Because of the resistance of the matrix against expansion of the inclusion, the former effect will tend to produce a larger increase in internal inclusion pressure for the grain with the lowest initial p_i, but the softening effect will tend to favour a larger pressure increase in the grain with the highest initial value of p_i. Thus there are two competing processes operating in granite during a temperature rise both related to the pressure sensitivity of the quartz α-β transition temperature. The thermal expansion effect tends to minimise pressure differences between inclusions, but the softening effect tends to increase them.

Differentiation of equation (20) from Chapter 10 with respect to T at constant pressure yields:

$$(\frac{dP_i}{dT})_p = (\frac{(9p - 5p_i)\,(\frac{dB}{dT})_p - 4p_i(\frac{dB_i}{dT})_p - 4\,(\frac{d\Delta_i^*}{dT})_p}{5B + 4B_i} \qquad (24),$$

where the same notation and sign convention are used as in Chapter 10. I will assume that the compressibility changes of the matrix material feldspar are negligible compared to those of the inclusion material quartz. Now, since $- d_i\Delta^* = (A_i - A)dT$, we have:

$$(\frac{dP_i}{dT})_p = \frac{4(A_i - A)_p - 4p_i(\frac{dB_i}{dT})_p}{5B + 4B_i} \qquad (24\text{-a}).$$

Equations (24) and (24-a) reflect the competing effects mentioned in the discussion above. A low confining pressure favours high values of A_i (Figure 11.1-b) relative to A, and of course low values of p_i, both effects tending to produce high values of $\frac{dP_i}{dT}$ at low pressures. On the other hand at low pressures, $\frac{dB_i}{dT}$ (Figure 11.1-b) and B_i have high values and tend to make $\frac{dP_i}{dT}$ smaller at low pressure than at high pressure.

The lack of single crystal data prevents a quantitative analysis. It would appear however, that the changes in the first term of the numerator in equation (24-a) with changes in pressure outweigh the changes in the second term of the numerator, because these tend to cancel each other out, and to outweigh the changes in the denominator as well because B is relatively unaffected by pressure and temperature changes. In summary, I conclude from Figure 11.1, and from equations (24) and (24-a) that a focusing

effect related to the pressure sensitivity of the quartz α-β transition temperature is likely to operate in granite during temperature rises. The effectiveness of similar focusing effects has been demonstrated and discussed by Coe and Paterson (1969). They found a sharp α-β transition temperature in a hollow specimen of a single crystal of quartz, which was in a markedly heterogeneous state of stress at low temperature. Coe and Paterson argued that without the focusing effect operating during temperature increase the stress heterogeneity would have persisted and the α-β transition would have occurred at different temperatures for different parts of the crystal.

11.3.3   The shift of the quartz α-β transition temperature in granite

The focusing effects described above cooperate to make the internal pressure in all quartz inclusions of the model equal to three times the applied confining pressure at high temperatures, provided the confining pressure is not too high to prevent cracking. From the present model it would therefore be predicted that the α-β transition of quartz in granite occurs at a temperature which is the same as that for single crystals of quartz at three times the applied pressure. Or, stated otherwise, the model predicts that the α-β transition of quartz in granite increases by (3 x 26 =) 78°C per 100 MPa confining pressure from 573°C at 1 atmosphere. This is the dashed line in Figure 9.4. The experimental results of the present study indicate somewhat lower values of 60°C to 72°C per 100 MPa. In view of the major simplifying assumptions which were made for the model calculation, this is a surprisingly close agreement. In Section 11.2 it was concluded that the non-sphericity of inclusions tends to decrease the inclusion pressure for which tensional stresses arise in the matrix. The focusing related to cracking around inclusions will therefore be to a lower inclusion pressure than predicted for spherical grains, which may partly account for the observed discrepancy. The theoretical model fails to account for the difference between the present results and those of Kern (in prep.) which are also shown in Figure 9.4. The reason for this discrepancy is not known.[1]

---

[1] The rock types used in the two sets of experiments are similar, and so are the experimental procedures (Kern, priv. comm., 1979). The precision with which confining pressure may be determined in a cubic anvil apparatus (Footnote continued on following page.)

The evidence of Chapter 9.4.4 suggests that the absence or presence of a porefluid does not markedly alter the magnitude of the quartz α-β transition shift. This result is easily understood if it is realized that most of the surface area of a quartz inclusion expanding relative to its feldspar matrix will be in solid-solid contact with the matrix. If a pore phase is present, it will occur essentially in narrow cracks or tubular pores in the matrix at high angles to the surfaces of quartz inclusions. Even if normal contact stresses between the solid matrix and the inclusion are much higher than the applied confining pressure and the porefluid pressure, the quartz inclusions cannot relax their high internal pressures by expanding into these narrow pores or by any other non-elastic accommodating mechanism over the time interval of the experiments. The α-β transition of quartz would only occur at a temperature corresponding to the applied confining pressure and to the pore pressure if the expanding quartz inclusions were completely surrounded by porefluid. This may become the case if there is a large volume fraction of melt present at the grainboundaries of the rock (Part I), but occurs not in the experiments of Chapter 9 where there is only a relatively small grainboundary porosity filled with water or argon gas.

The α-β transition of quartz in granite is a good example of a physical phenomenon in a polycrystalline aggregate which does not follow Terzaghi's Effective Stress Law $(P_{eff} = P_{conf} - P_{pore})$. The "effective pressure" for the transition of quartz is near $3P_{conf}$, and is not influenced by porepressure. On the other hand, porosity changes due to differential thermal expansion of the constituent minerals, are seen to follow Terzaghi's Law more closely. The total amount of porosity formed at 300 MPa and 800°C in the presence of a porefluid is the same as that formed at 800°C and atmospheric pressure (Chapter 9.4.4).

---

at high temperatures is probably somewhat lower than in a gas apparatus. However, in view of the α-β transition temperature measured by Kern (in prep.) for quartzite at 200 MPa, corresponding to the α-β transition temperature for single crystals of quartz, the precisions of pressure and temperature determination in a cubic anvil apparatus are thought to be sufficiently high to conclude that there is a real discrepancy between the two data sets. Note that the deviation from the model at the higher pressures is the same for both (Figure 9.4).

11.4   Concluding remarks

The findings of this experimental and theoretical study can be
used to evaluate the results of other experimental studies. For example,
Kern (in prep.) found that the decrease in V_p at 200 MPa confining pressure
with increasing temperature towards the α-β transition of quartz is *larger*
for granite and granulite, containing only a fraction of quartz, than in
quartzite consisting entirely of quartz. In quartzite each crystal
has the same volumetric expansion and the creation of new pores at confining
pressure during a temperature rise will be small. In granite however, the
crack closure by compression to 200 MPa at room temperature is reversed
with increasing temperature due to differential volumetric expansion of
the constituent minerals. The associated changes in V_p are large, as they
are during room temperature compression (Chapter 9.1; Part III). The
net effect of crack opening plus intrinsic changes in the elasticity of the
constituent minerals in granite on V_p is therefore larger than the effect
of intrinsic changes in the elasticity of quartz which control V_p through
quartzite at the same confining pressure.

The above example serves as a warning against uncritical application
of experimentally obtained temperature derivatives of velocity through rocks
to geological and geophysical problems. In specimens under conditions of
a few 100 MPa confining pressure and 500°C - 800°C, stress inhomogeneities
may exist over relatively short experimental periods of a few hours to a
few days. It seems likely however, that inhomogeneities in the stress
field disappear by plastic flow or other non-elastic processes in rocks
which occur for geological time intervals at the same pressures and temper-
atures in the earth's crust. It would seem reasonable therefore to expect
no shift in the α-β transition of quartz in a granitic crust with a high
temperature gradient. Similarly, it may be expected that the opening of
cracks against a lithostatic pressure, due to differential thermal expansion
will be absent or minimal at deep levels in the crust in the absence of a
porefluid. The value of $(\frac{dV_p}{dT})_p$ to be expected for quartzite in the crust
is larger than for granite, and the velocity of P-waves through a dry
granitic crust is probably less sensitive to pressure and temperature than
experimental results would suggest.

Nur and Simmons (1970) first considered the origin of small
cracks in exposed igneous rocks in terms of a spherical inclusion model,
and showed that microcrack porosity is closely related to the presence of

quartz in many rocks. Their models fail to account for the simultaneous (and in the case of quartz *competing*) effects of decreasing pressure and temperature. They noted that "Tension could develop around grains for a limited range of values of elastic constants. Since the tensile strength of rocks is almost zero, cracks will appear instantaneously", but ascribed the general origin of cracks to the limited shear strengths of rocks and minerals in a way which is physically not entirely clear. Cracks can only open up through the action of tensile stress. If sufficiently precise single crystal data become available, the present theory should allow one, from a measurement of crack porosity, to place bounds on pressure and temperature conditions for which crack opening started in an intrusive rock on its way to the surface of the earth.

The measurements of thermal expansion at pressure may find practical application in relation to deep drilling in the crust. Plans are underway to drill deep holes to extract thermal energy from areas of high heat flow, or to dispose of radioactive waste in cooler, stable areas. The decompression (stress relief) and cooling at the end of a deep drill hole will result in the opening of cracks within the rocks and possible expansion into the drill hole, and the physical properties of the wall rock will change. Wang and Simmons (1978) recently showed that most of the crack porosity observed in cores of gabbro from 5.3 km depth in the Michigan basin can be ascribed to the stress relief factor.

The theory derived in Chapter 10 need not be restricted to the case of differential thermal expansion. The effect of any relative volume change of matrix and inclusion can be calculated. The equations could, for instance, be applied to calculate the instantaneous stress field developing around a spherical region undergoing rapid transformation in a lithospheric slab decending into the asthenosphere. As such the theory could contribute to an understnading of deep focus earthquakes. With the existing formulae derived by Eshelby (1957), the theory can be modified to cover the two dimensional problem of a cylindrical inclusion, and the case of a general three dimensional ellipsoidal inclusion. The effects of non-hydrostatic stress fields applied to the matrix, instead of hydrostatic confining pressure considered here, can also be obtained from Eshelby's equations.

The theory for an infinitely dilute concentration of inclusions plus the simple model presented are capable of predicting the observed thermal

expansion behaviour and the observed shift of the quartz α-β transition temperature in granite to a large extent, but some discrepancies are not accounted for. It is felt that a self consistent theory (*e.g.* Watt *et al.*, 1976), ascribing the average properties of granite to the matrix around each crystal, could remove some of these differences.

PART III

MEASUREMENT OF P- AND S- WAVES THROUGH DRY AND WET GRANITE
AT HIGH PRESSURE AND TEMPERATURE

ABSTRACT

An experimental assembly for the measurement of ultrasonic wave velocities through specimens of crystalline rock or single crystals, at simultaneous high pressure and temperature is described. Compressional-(V_p) and shear-(V_s) wave velocities for dry granite during room temperature compression to 300 MPa, and during temperature increase to 500°C at 100, 200 and 300 MPa confining pressure are presented and the dynamic elastic moduli throughout this range are calculated from the measurements. The effect on V_p of water as a porefluid in granite has also been measured over the same range in pressure and temperature, and it is found that the differences between the wet and dry specimens are closely related to differences in crack porosity and to the compressibility of water. The changes in the dynamic bulk modulus, shear modulus and Poisson ratio of dry granite with compression at room temperature are compared with the self-consistent model for the elasticity of cracked solids of O'Connel and Budianski (1974) and with the Voigt and Reuss moduli calculated for a hypothetical crack free granite. This comparison indicates an increase in the average aspect ratio (thickness : width) from ~1.8 x 10^{-2} to ~5 x 10^{-2} between 1 atmosphere and 50 MPa for the 13 percent decrease of the initial porosity of ~2.3 percent, pointing to the closure of the flattest cracks over this pressure interval. Between 50 and 300 MPa porosity decreases further to ~1.0 percent but the average aspect ratio of the cracks remains constant. It is emphasized that the pressure and temperature derivatives of V_p, V_s and the elastic parameters of dry granite as obtained from the experiments are strongly influenced by cracks which open against the confining pressure with increasing temperature (part II). The problems encountered in applying the experimental results to interpret the seismic velocity structure of the crust are discussed.

Chapter 12

INTRODUCTION

12.1 General

The theoretical prediction of elastic wave velocities and attenuation in imperfectly elastic crystalline materials containing cracks and pores, which may be open or filled with a viscous compressible pore fluid, has received a great deal of attention in recent publications (*e.g.* Anderson *et al.*, 1974; Kuster and Toksöz, 1974; O'Connell and Budiansky, 1974, 1977; and many others). An extensive literature recently reviewed by Paterson (1978), quoting more than 50 references, also exists on the experimental determination of these properties in real rocks of known composition and structure, with and without pore fluids and under varying conditions of temperature, pressure and non-hydrostatic stress.

The ultimate goal of these studies is to arrive at a better understanding and interpretation of the wealth of seismological data on elastic wave transmission through the earth, to obtain information about the state of stress, the microstructure, the degree of microfracturing or partial melting etc., in rocks at depth which can not be observed directly.

Pressure and temperature increase with depth in the earth, but until recently relatively little was known about the combined effect of temperature and pressure on the velocity of compressional and shear waves through natural rocks. Table 12.1 lists references to recent experimental work, references to earlier experimental work may be found in the papers mentioned. Many of the studies listed are primarily concerned with exploring the changes in velocities over the experimentally available range in pressures and temperatures, but some study specific aspects such as the influence of crystallographic preferred orientation on seismic anisotropy, or the influence of pore pressure on velocities. Such aspects are mentioned in the last column of Table 12.1.

12.2 Comparison of experimental techniques

The experiments listed in Table 12.1, have in common velocity determination with the "pulse transmission" or "time of flight" method, through rock specimens of a few centimeters length using transducers with natural frequencies around 1 MHz. Distinction into two groups of experiments

Table 12.1 Ultrasonic determination of V_p and V_s through natural rocks at simulatneous high pressure and temperature.

Reference	Rock types	$V_p - V_s$	P_{max}	T_{max}	Special aspects
Bayuk and Tedeyev (1974)	Granite, gabbro, diabase, serpentinite, gneiss, limestone.	V_p	400 MPa	450°C	-
Kroenke et al. (1976)	Variety of mafic and ultramafic rocks.	V_p	300 MPa	350°C	-
Spencer and Nur (1976)	Dry and wet granite.	V_p,V_s	500 MPa	500°C	Pore pressure effects.
Stewart and Peselnick (1977)	Wide variety of Franciscan rocks.	V_p	800 MPa	300°C	-
Ramananantoandro and Manghnani (1978)	Dunite	V_p	1000 MPa	500°C	Anisotropy
Fielitz (1971, 1976)	Quartzite, granite, gabbro, peridotite, norite, mon-zonite.	V_p,V_s	420 MPa	750°C	Velocity minimum in quartz bearing rocks.
Kern and Fakhimi (1975)	Peridotite, amphibolite, serpentinite, marble	V_p	200 MPa	700°C	Anisotropy
Meissner and Fakhimi (1977)	Granite, gneiss, metagabbro, peridotite	V_p	600 MPa	500°C	Anisotropy
Kern (1978)	Granite, granulite, amphi-bolite, peridotite.	V_p	600 MPa	700°C	Velocity minimum in quartz bearing rocks. Shift of the quartz α-β transition temperature.
Kern (in prep.)	Quartzite, single crystal quartz, granite, granulite.	V_p,V_s	400 MPa	750°C	Shift of the quartz α-β transition temperature.

Gas apparatus (rows 1–5)

Cubic anvil apparatus (rows 6–10)

can be made on basis of the method by which pressure is generated and on the position of the transducers relative to the specimen.

In the first group, internally heated gas apparatuses have been used with argon or nitrogen gas as a confining medium. Specimens have been sealed in thin metal jackets and transducers are placed directly onto the specimen or near to the specimen on endpieces. In this arrangement sending and receiving transducers are at pressure and temperature during the experiment. Transducer materials with high Curie temperatures are therefore required; Lithium Niobate crystals (Curie temperature ~1200°C) have been used successfully up to 500°C by Spencer and Nur (1976) and Ramananantoandro and Manghnani (1978). Several design problems must be overcome. Insulated and shielded transducer leads have to be brought into the high-pressure, high-temperature volume of the gas apparatus while maintaining a good pressure seal. Connections of leads to transducers and of transducers to specimen or endpiece have to be made inside the high pressure bomb, where space is at a premium. An advantage of this technique over the one described below is that the time of flight of a pulse through the specimen represents the major part of the travel time from one transducer to the other, such that only minor corrections are needed for the travel time through endpieces, and that velocity changes in the specimen can be easily detected. Another advantage is the high degree of precision with which a truly hydrostatic pressure can be generated and measured in a gas apparatus, while the sealing of the specimen with an impervious jacket allows the effect of pore fluids on elastic wave velocities to be studied. Spencer and Nur (1976) used an arrangement whereby the pore pressure could be controlled independently of the confining pressure and the temperature.

Experiments of the second group comprise those performed in a cubic-press apparatus with heated anvils. A state of near hydrostatic stress is arrived at by advancing six pistons in three mutually orthogonal directions onto unjacketed cube shaped specimens (Kern and Karl, 1969). Transducers are placed on the low temperature side of the pistons (e.g. Fielitz, 1971), and no special requirement of high Curie temperature is needed for the transducer material. The travel time of the pulses through the specimen at pressure and temperature is obtained by subtracting the calibrated time needed for a pulse to travel to and from the specimen through the pistons from the total time measured by the transducers. This technique, thus far only used in Germany for the present purpose, has been most successful in

obtaining a large number of velocity data for a wide variety of natural rocks at simultaneous high pressure and temperature (Table 12.1). P- and S- waves have been measured at 200 and 400 MPa by Fielitz (1971, 1976), and Kern (in prep.) at temperatures as high as 750°C.

12.3 Purpose and outline of the present study

Part III of this thesis may be read as a progress report on the development and testing of an experimental assembly with which P- and S- waves can be measured through natural rock specimens under varying conditions of pressure, temperature and non-hydrostatic stress in the gas apparatus built by Paterson (1970, 1977).

Aims in starting this project were:

1. To extend the work of Spencer and Nur (1976) on the effect of water as a pore fluid in granite on velocities at high pressure and temperature. To calculate the dynamic elastic parameters of granite from V_p and V_s, in particular to obtain pressure and temperature derivatives for Poisson's Ratio in dry granite, about which conflicting evidence has been recorded in the experimental literature (see Section 12.4).

2. To complement the observation on velocities through granite at temperatures around the quartz α-β transition, as measured in a cubic-press apparatus by Fielitz (1971, 1976) and Kern (1978, in prep). To advance the understanding of the shift in the quartz α-β transition temperature in granite, discovered by Kern.

3. To measure changes in velocities through granite with added water if the temperature is increased to values exceeding the solidus where a highly viscous, relatively incompressible meltphase develops at grainboundaries, replacing the highly compressible and low viscosity supercritical water occurring in cracks and pores at temperatures just below the solidus (Part I). To investigate whether the microstructural changes which were found to occur during deformation of partially-melted granite (Part I), are reflected by changes in ultrasonically measured velocities.

Not all these goals have been reached, essentially due to failure to obtain reliable velocity measurements at temperatures higher than 500°C. The problem of the shift of the quartz α-β transition temperature in granite has already been dealt with by measurement of the thermal expansion of

granite and a model has been proposed to explain the magnitude of the
observed shift (Part II). The Poisson ratio problem will be introduced
in Section 12.4, and in the last section of this chapter I will comment
on the expected effects of partial melting in granite on ultrasonically
measured velocities. Chapter 13 gives a detailed description of the
experimental assembly and a discussion of the measurement procedures, and
some suggestions will be given for improvement of the assembly. The
preliminary results obtained will be presented and discussed in the final
chapter.

12.4   The Poisson ratio problem

The Poisson ratio v of an ideally elastic isotropic material
is defined as the ratio of lateral extension to longitudinal shortening
in a cylinder under uniaxial compression. Values of v may vary between
$-1 < v < 0.5$ for different elastic materials (Jaeger, 1969, p.57). Values
close to 0.5 indicate that the uniaxial deformation of the material occurs
at approximately constant volume, while lower values of v imply volumetric
contraction. At $v = 0$ the volumetric strain equals the shortening strain
and for v values close to -1 the elastic contraction is close to three
times the shortening.

If it is assumed that crystalline rocks behave macroscopically as
ideally isotropic materials with respect to the small deformations
associated with the transmission of compressional and shear waves, then the
dynamic elastic paramters of the rocks may be obtained from concurrent
measurements of V_p and V_s:

$$K = \rho \left(V_p^2 - \frac{4}{3} V_s^2 \right) \qquad\qquad (1),$$

$$\mu = \rho \, V_s^2 \qquad\qquad (2),$$

and, since $v = (3K - 2\mu)/(6K + 2\mu)$:

$$v = \left[\left(\frac{V_p}{V_s}\right)^2 - 2 \right] / \left[2\left(\frac{V_p}{V_s}\right)^2 - 2 \right] \qquad\qquad (3),$$

where K, μ are the bulk modulus and the shear modulus and ρ is the density
of the rocks.

Nur and Simmons (1969) noticed that the Poisson ratio of dry

granite containing cracks may be very low, or even slightly negative at low confining pressure, but that the application of confining pressure closes most cracks, whereby K increases more rapidly than μ, such that values of v between +0.25 and +0.30 are obtained at pressures exceeding 50 MPa. The observation of Spencer and Nur (1976) on P- and S- wave velocities through dry granite at confining pressure indicate that v increases with increasing pressure, and that v increases with increasing temperature, more so at a confining pressure of 400 MPa than at 300 and 200 MPa. The results obtained by Fielitz (1971, 1976) and Kern (in prep.) on the other hand indicate an opposite effect of temperature on v at a given confining pressure in quartz-bearing rocks such as quartzite, granite and granulite (see Figure 14.9-c). Kern (in prep.) showed that v in quartzite at 200 MPa decreases from 0.12 at room temperature to -0.16 at the quartz α-β transition temperature, beyond which it increases rapidly to +0.21 over 50°C. A much smaller decrease in v, from 0.21 at room temperature to 0.16 at the α-β transition temperature of quartz was observed by Kern (in prep.) for granite and granulite. These results were already known from the experimental work of Fielitz (1971, 1976), who also showed the changes in P- and S- velocity with temperature in quartzite at 200 MPa to be in excellent agreement with the prediction of a Voigt-Reuss-Hill average calculated from the known changes in the elastic parameters of single crystals of quartz at 1 atmosphere. Fielitz' model calculation for V_p and V_s in quartzite would indicate a decrease in v from 0.12 at room temperature to -0.14 at the α-β transition followed by a rapid increase to high positive values at higher temperatures.

Knowledge of v in granite as a function of pressure and temperature is of importance for the interpretation of the structure of the earth's crust, in particular for the interpretation of crustal low velocity layers (e.g. Fielitz, 1971, 1976; Spencer and Nur, 1976; Kern, in prep.)). The discrepancy between the experimental results obtained in a gas apparatus and those obtained in a cubic press apparatus therefore warrants further investigation of the problem.

12.5 The effect of partial melting in granite on ultrasonically determined velocities

Although no measurements of V_p or V_s were obtained in the present study at temperatures high enough to cause partial melting in the granite, I will include some comments on the effects which may be expected.

It is noticed that granite is not an ideal material to study the effect of partial melting on P- and S- velocities. The results of Fielitz and Kern discussed earlier indicate that large changes in velocity, particularly in V_p, may be expected at temperatures in the vicinity of the quartz α-β transition. In granite at 300 MPa this transition occurs between 750°C and 800°C (Part II); any effects due to melting at temperatures exceeding the solidus of the system granite plus water, which is 670°C at 300 MPa (Part I), will therefore be superposed on those changes related to the quartz α-β transition and may be difficult to separate from them.

Upon melting in the system granite plus water, a highly compressible, low viscosity hydrous porephase is replaced by a relatively incompressible high viscosity melt at grainboundaries (Part I). Apart from effects of temperature on the elasticity of the matrix minerals, substantial changes may therefore be expected to be associated with the change in porefluid when the solidus temperature is exceeded. A self-consistent theoretical model for the viscoelastic properties of an isotropic, fluid-saturated cracked solid has been developed by O'Connell and Budiansky (1977). In principle this model enables calculation of the effect of the melting reaction in granite plus water on the velocity and attenuation of P- and S- waves.

Because of uncertainties in some of the input parameters for the calculation, particularly for the aspect ratios $(\frac{c}{a})$ and the crack densities ε, I will not include a detailed calculation of the expected effects of melting on P- and S- waves according to the model. All essential arguments leading to the following conclusions are presented by O'Connell and Budiansky (1977). *For an ultrasonic frequency of 10^6 Hz* it may be expected that melting in the system granite plus water leads to:

1. A change in the possible relaxation mechanism from fluid flow between cracks in the presence of water, to viscous relaxation in cracks in the presence of melt, or, depending on the average aspect ratio of the melted grainboundaries, to a situation where relaxation is no longer possible. In the latter case the effective elastic properties of granite plus melt would be almost indistinguishable from those for a crack free granite ("glued case" of O'Connell and Budiansky).

2. Such changes in relaxation mechanism would increase both V_p and V_s.

3. If granite plus melt corresponds to the "glued case", a marked
    improvement in the quality of the received signals for both P- and
    S- waves may be expected since the attenuation in the specimen will
    decrease upon melting. Dissipation of energy due to flow of water
    from one crack to another will occur at ultrasonic frequencies, but
    in the "glued case" no energy can be lost in deforming the melt.
    In the latter situation meltfilms are essentially not noticed by high
    frequency waves. Changes in meltfilm configuration, associated with
    the static deformation of partially-melted granite (Part I), will
    then not be reflected by changes in ultrasoncially determined V_p and
    V_s.

    Finally, it should be noticed that these conclusions only apply
for ultrasonic frequencies ($w \approx$ 1 MHz). At the frequency of seismic waves
($w \approx$ 1 Hz) or during quasistatic elastic deformation ($w <<$ 1 Hz) the
effective elastic moduli of a partially-melted material will be rather
lower than those measured with the ultrasonic method. As has been pointed
out by many authors (*e.g.* O'Connell and Budiansky, 1977; Zener, 1948)
relaxation mechanisms in viscoelastic materials may be inhibited during
high frequency deformations and become operative at longer periods.

Chapter 13

EXPERIMENTAL ASPECTS

13.1   Introduction

In this chapter I will describe the specimen preparation, the
assembly and the experimental techniques used to obtain velocity measure-
ments of P- and S- waves through cores of finegrained granite in the
high-pressure, high-temperature apparatus built by Paterson (1970, 1977).
A special wide-bore furnace with a 24 mm diameter working space was
designed by Dr. M.S. Paterson to accommodate the specimen assembly.
The design of the arrangement is such that eventually measurements of
ultrasonic wave velocities can be made in three mutually perpendicular
directions under conditions of hydrostatic and non-hydrostatic stress.
Apart from two trial runs, these possibilities have not yet been explored,
all experiments described will be for an axial transducer arrangement and
for hydrostatic pressures.

13.2   Specimen preparation

The specimen material used is Delegate aplite, the fine grained
granitic rock described earlier in this thesis (Chapter 3). The ends of
cylindrical cores of 15 mm diameter and 20 mm length were ground and polished
to within 0.02 mm of parallelism. The specimens were then dried for at least
24 hours in a dessicator at 110°C, before they were sealed in thin walled
(0.25 mm) copper jackets with molybdenum endpieces and rings (Figure 13.1
and 13.2). In all wet experiments described, 0.7 weight percent of water
(1.8 volume percent at ambient conditions) was added to the specimens with
the following procedure. The dried specimens were immersed in water over-
night following evacuation to 10^{-2}- 10^{-3} torr as described in Section 3.7.2.
Between 0.3 and 0.4 weight percent water could be introduced into the
specimen in this fashion, indicating between 0.7 and 1.0 volume percent
initial accessible porosity. These values are in good agreement with the
0.8 percent accessible porosity obtained by the same method on smaller
specimens (Table 3.1). Extra water was added with a micropipette prior to
sealing to make the total amount of added water 0.7 weight percent in all
cases. Assembled specimens were weighed before and after each run to check
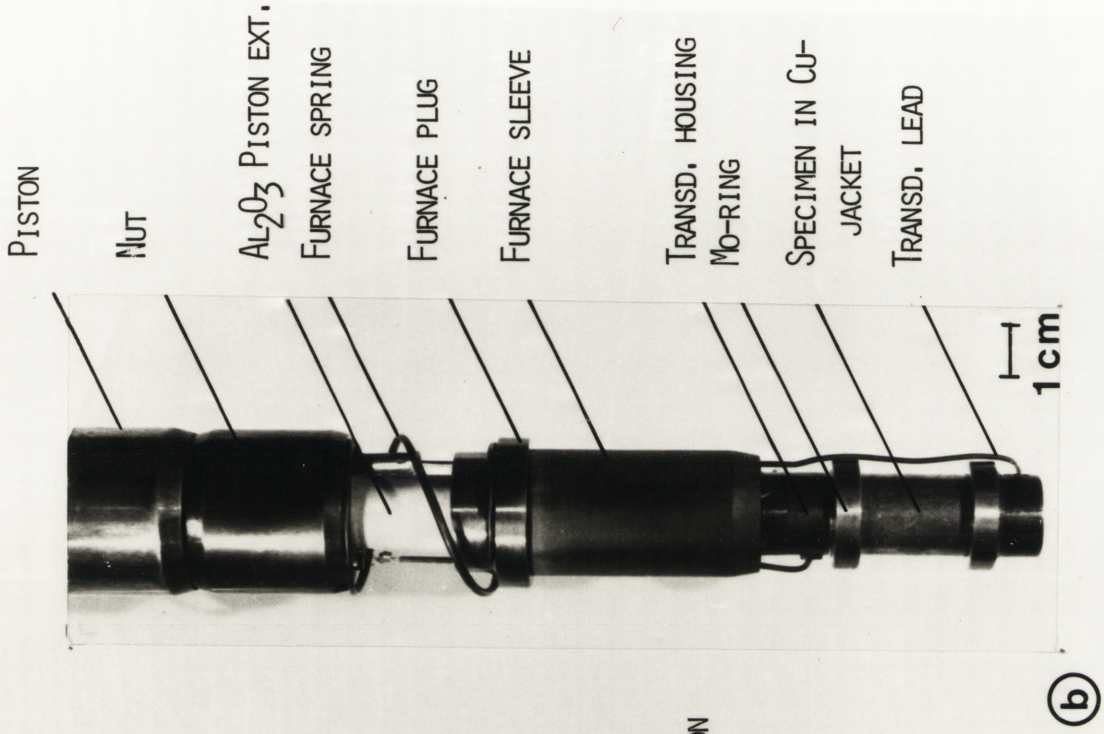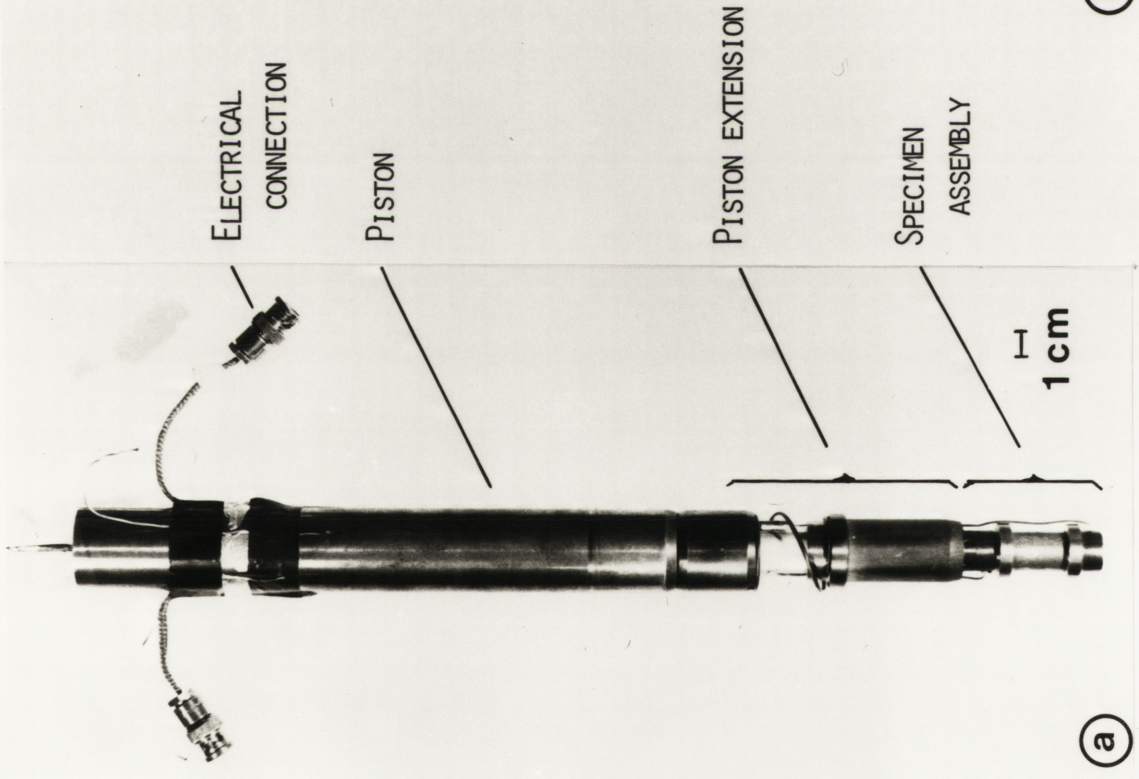for leaks and loss of water.

13.3 Assembly

Photographs of the piston and the assembly are shown in Figures
13.1-a and b. Many aspects of this arrangement are specific to the gas
apparatus used and need not be described fully here. Three main elements
may be discerned on the photographs: the specimen assembly proper, the
steel piston and the alumina piston-extension which is partly covered here
by a spring, a plug and a pyrophyllite sleeve, which are used to minimize
gas convection in the apparatus at high temperatures. The specimen is
situated between the molybdenum sealing rings and the transducers are
located inside the transducer housings on the other side of these rings.
Care has been taken to ensure insulation and shielding of the transducer
leads; all metal parts of the assembly except the inner wires of the
transducer leads and their connections are earthed.

The transducers are gold plated lithium niobate crystals ($LiNbO_3$),
36° rotated Y-cut for compressional mode, and 41° rotated X-cut for shear
mode generation and reception. The gas confining medium can enter the
transducer housing, and the $LiNbO_3$ crystals therefore operate under
conditions of high temperature and pressure, and an oxygen fugacity
determined by the presence of molybdenum and other metal parts in the
assembly and by impurities such as carbon which occur in the gas.

A detailed drawing of the specimen assembly proper is presented
in Figure 13.2. The upper half of this figure shows how the assembly is
attached to a hollow steel rod which provides a mechanical and electrical
connection with the piston (not shown in the figure) through the alumina
piston-extension. In the case of triaxial experiments the whole assembly
may be advanced onto the alumina anvil, but for hydrostatic experiments
it hangs on the piston, ~1-2 mm above the anvil. Transducer-housing,
location ring and specimen are held together with a simple system of two
studs and nuts. The same system is used to attach the lower transducer
housing to the specimen but this is not shown in the cross-section at
90° in the lower half of the diagram. Here it may be seen how the coaxial
transducer cable (1 mm outer diameter, copper inner wire, insulated with
MgO powder and sheathed with steel; Sodern, France), is brought into the
transducer housing through a small steel block fitting into a slot in the
wall of the housing. The active wire of the transducer lead is held
against the transducer with a mammiform alumina insulator, the nipple of
which fits into a central hole of a cusp-shaped molybdenum spring seated

Figure 13.1-a,b. Piston and specimen assembly for velocity
measurements.

(b)

PISTON

NUT

Al_2O_3 PISTON EXT.

FURNACE SPRING

FURNACE PLUG

FURNACE SLEEVE

TRANSD. HOUSING

MO-RING

SPECIMEN IN CU-JACKET

TRANSD. LEAD

1 cm

(a)

ELECTRICAL CONNECTION

PISTON

PISTON EXTENSION

SPECIMEN ASSEMBLY

1 cm

Figure 13.2   Specimen assembly. The upper half of the diagram
shows the connection of the specimen assembly to the
piston extension, and the nut and stud system with
which the transducer housing is attached to the
endpieces. The lower half of the diagram (at 90°)
shows how the transducer leads are brought into the
transducer housing and pushed against the trans-
ducers with a spring. The following features may
be recognized.

1. Specimen (15 mm diameter, 20 mm length).

2. Cu-jacket.

3. Mo-endpiece.

4. Mo-sealing ring.

5. $LiNbO_3$ transducer.

6. Mo-location ring for transducers.

7. Mo-housing for transducers.

8. Stud.

9. Nut.

10. Mo-connector piece.

11. Hollow steel rod linking up with piston.

12. Al_2O_3- piston extension.

13. Platinum, platinum-rhodium thermocouples.

14. Coaxial transducer lead (steel sheathed, MgO-
insulated copper wire, 1 mm outer diameter).

15. Steel block to fit in slot in transducer housing.

16. Bonding medium, silver paint.

17. Al_2O_3 insulator.

18. Mo-spring, cusp shaped.

19. Al_2O_3 - anvil.

20. Furnace wall.
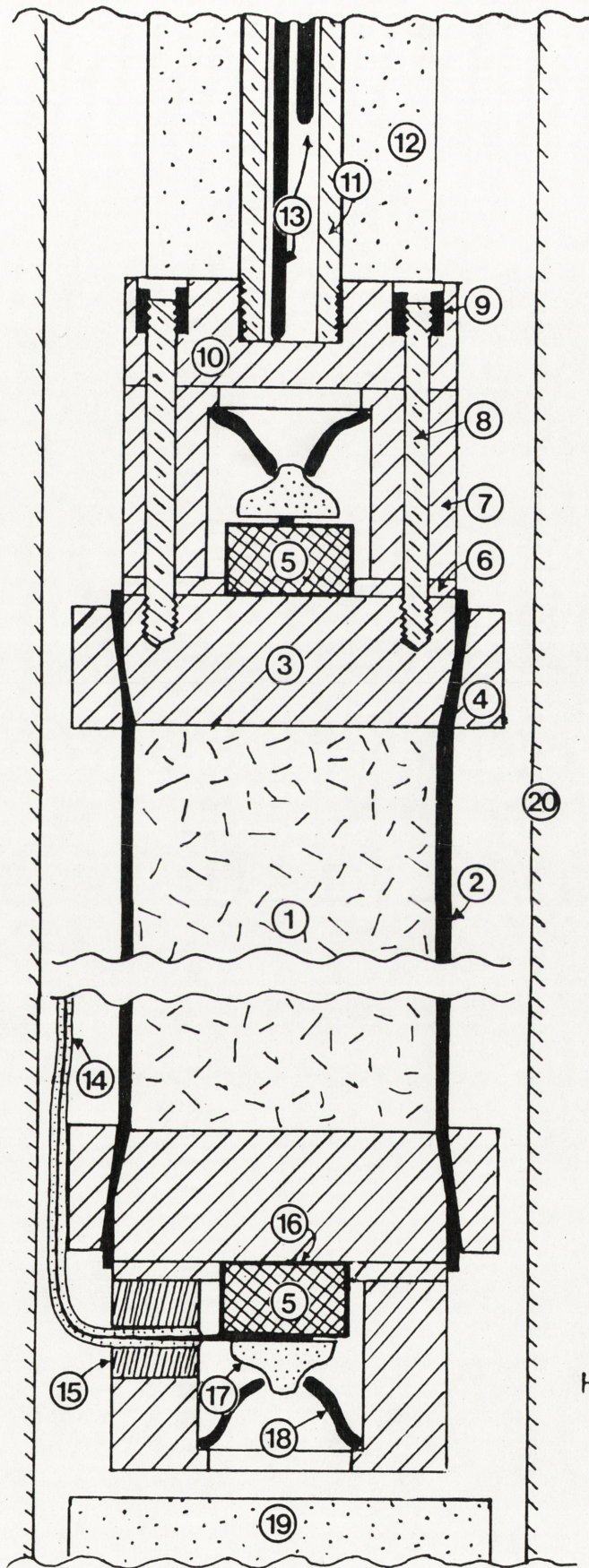
10 mm

on a ledge in the transducer housing. This spring is compressed when the nut and stud connection is tightened, ensuring at the same time that the transducers are pushed against the endpieces to aid the bonding medium (silver paint, Dupont Conductor Composition 4929).

Temperature is measured with the aid of two platinum, platinum-13 percent rhodium thermocouples positioned respectively 19 and 29 mm above the top of the specimen within the hollow steel rod. The temperature of these thermocouples, and the furnace settings required for a given constant temperature over the whole length of the specimen were calibrated with a hollow dummy specimen and a sliding thermocouple arrangement (see also Chapter 2.4). The low-pressure end of the thermocouples may be seen to emerge from the piston in Figure 13.1-a. It is estimated that the temperatures recorded in this part of the thesis are precise to within 15°C over the volume of the specimen.
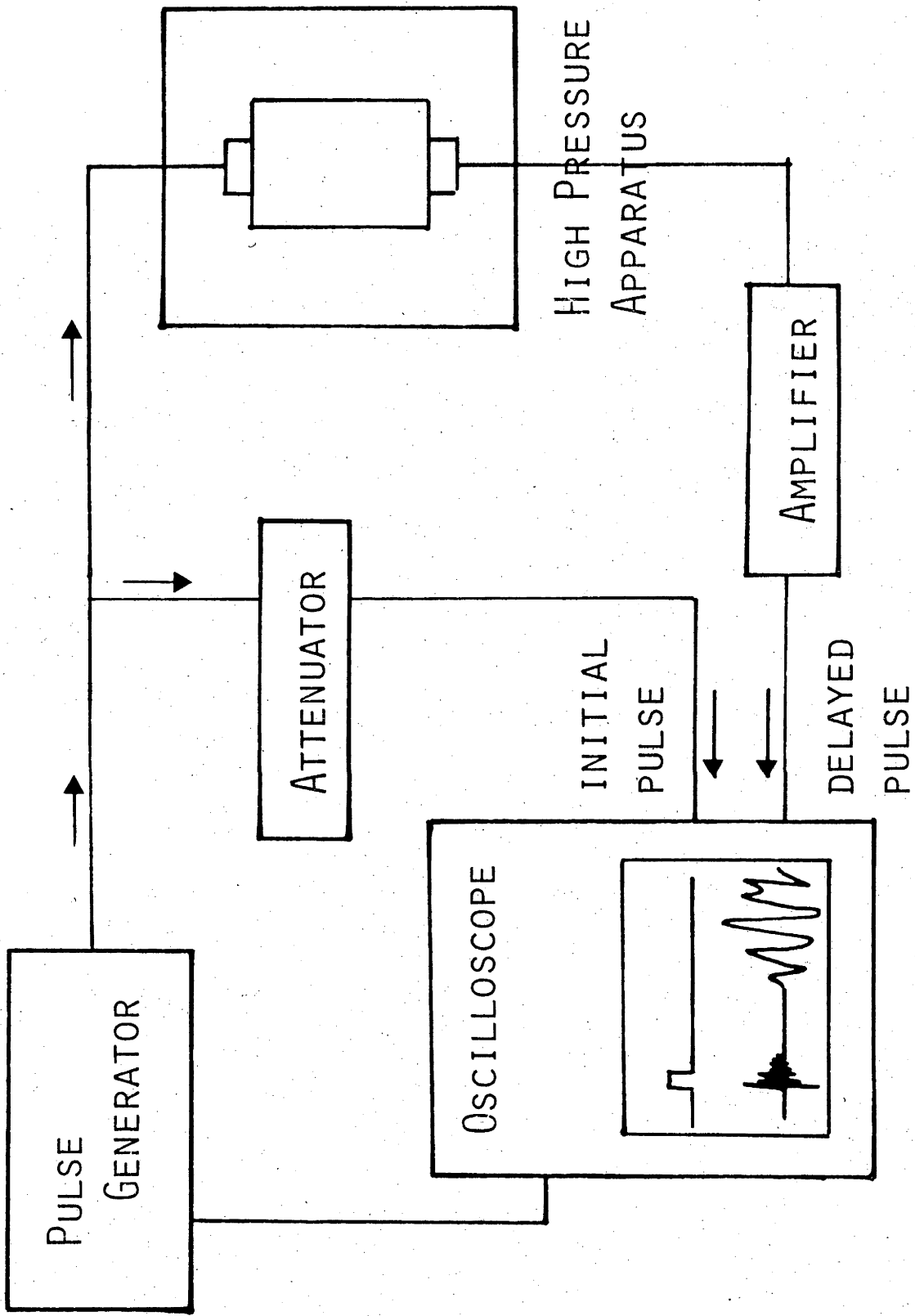
13.4   The pulse transmission method

A detailed description of the method used in the present experiments has been given by Liebermann *et al.* (1974). The system is shown schematically in Figure 13.3. Application of an electrical pulse to one of the piezoelectric transducers results in propagation through the sample of an acoustic pulse which is reconverted to an electrical signal by the receiving transducer. Simultaneous display of the applied pulse and the received signal (typically a few hundreths to a few tenths of a volt in amplitude) on an oscilloscope with a calibrated time base facilitates measurement of the total travel time of the acoustic pulse through the sample and the two endpieces. A negligibly small correction (- 0.05 μ sec) to the observed travel time is required to allow for electronic delays arising from the use of considerable lengths (~10 m) of 50 Ohm (5 nsec m^{-1}) coaxial cable.

13.5   LiNbO$_3$ transducers

The practical use of LiNbO$_3$ tranducers is restricted to lower temperatures than the Curie temperature of ~1200°C. Increased conductivity of the crystals at high temperatures and low partial oxygen pressure (P_{O_2}) results in less electrical energy being converted into compressional or shear mode waves at the generating transducer and less mechanical energy being converted into electrical signals at the receiving transducer. The results of Jorgensen and Bartlett (1969) for the temperature dependence of
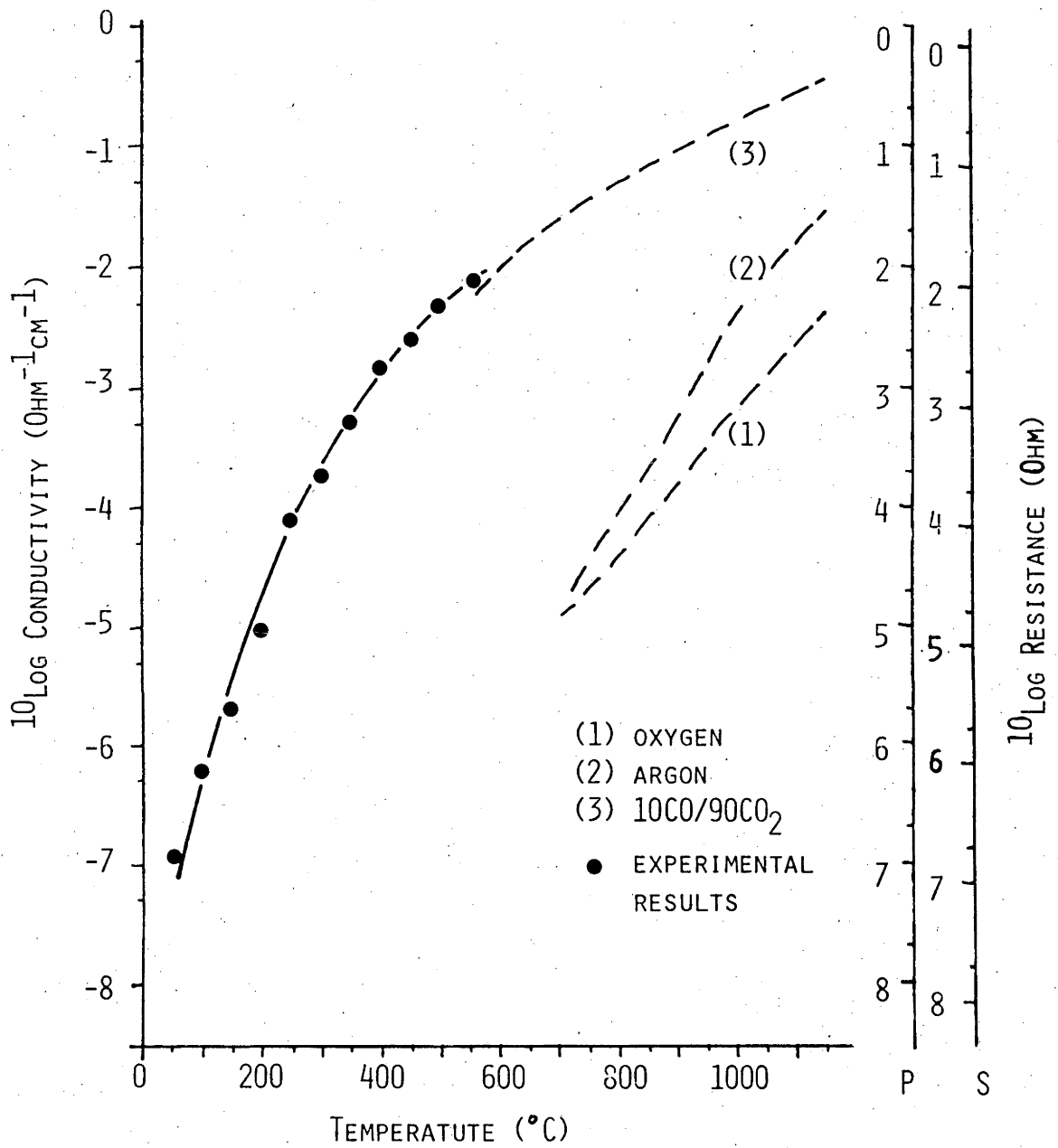
Figure 13.3   The time of flight system.

PULSE GENERATOR

ATTENUATOR

HIGH PRESSURE APPARATUS

AMPLIFIER

OSCILLOSCOPE

INITIAL PULSE

DELAYED PULSE

conductivity in $LiNbO_3$ are given for various gaseous environments in Figure 13.4. Conductivity values may be converted to resistances for the P- and S- transducers used in the present study by referring to the axes on the right hand-side of the figure.[1] From the results of Jorgensen and Bartlett for argon, it was initially expected that velocity measurements could be made in the present gas apparatus at temperatures well above $600°C$. A simple experiment at ambient conditions through a 20 mm long granite core, with 1000 Ohm resistors in parallel with the gold-plated faces of P-wave transducers to simulate electrical leakage at $900°C$ showed that a satisfactory signal could be obtained. It was found in the present experiments that the delayed signal becomes unrecognisable against the background noise if the transducer resistance decreases to ~100 Ohm. However, such values are reached at much lower temperatures ($500°C$ – $700°C$) in argon gas in the apparatus, than might be expected from the literature. The experimental results in Figure 13.4 indicate that the pressure medium has a P_{O_2} more similar to that of $10CO/90CO_2$ than that of argon as measured by Jorgensen and Bartlett. Extrapolation of their results (op.cit., Figure 4) to the lower temperatures for the present experiments suggests P_{O_2} values as low as 10^{-20} to 10^{-30}. The P_{O_2} of the commercial grade argon pressure medium is unlikely to be much less than 10^{-6}. This discrepancy is attributed to the presence of reducing agents in the furnace environment in the form of molybdenum and carbon.[2] The loss of resistivity of the transducers at high temperatures was found to be independent of confining pressure, and could not be completely reversed by decreasing the temperature at the end of a run. The velocity measurements to the highest temperature reported ($700°C$) were made with crystals used for the first time. After runs to high temperature, transducers had a black discolouring throughout, which could be removed by heating the transducers in air at $600°C$ for a few hours, and part of the lost resistivity could also be recovered in this fashion. These effects suggest that carbon may have entered the crystal structure of $LiNbO_3$. Alternatively, it is possible that the oxidation state of the transition metal Nb decreases locally inside the crystal, for instance through the
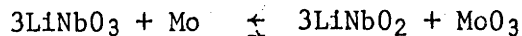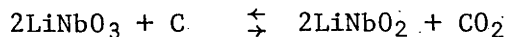
---

[1] $R = \frac{l}{C \cdot A}$, where R is resistance, C is conductivity, l is the height of the transducer and A its area. The offset between the axes for 1MHz P- and S- transducers is caused by a difference in height.

[2] A thin precipitate of carbon is often found on the specimen assembly (footnote continued on following page.)

Figure 13.4   The conductivity of $LiNbO_3$ as a function of temperature in various gaseous environments (after Jorgensen and Bartlett, 1969), and in the high pressure medium in the present apparatus. The resistance of P- and S- wave transducers may be read from the scales on the right-hand side of the diagram. The offset between the two scales is caused by differences in the height of P- and S- transducers.

reactions

$$2LiNbO_3 + C \; \underset{\rightarrow}{\leftarrow} \; 2LiNbO_2 + CO_2$$

$$3LiNbO_3 + Mo \; \underset{\rightarrow}{\leftarrow} \; 3LiNbO_2 + MoO_3$$

13.6 V_p and V_s measurements through molybdenum and granite

The travel times for P- and S- waves through specimens of granite were obtained from the total time of flight recorded on the oscilloscope by subtracting the delay time in the endpieces. The endpiece correction was obtained from separate calibration runs on a 32 mm long, unjacketed molybdenum dummy. In Figure 13.5 the observed V_p and V_s values over the temperature interval 20°C – 600°C at 300 MPa are compared with the Voigt and Reuss averages as calculated from single crystal data, for the compliances of molybdenum (Hearmon, 1969). The "molybdenum" used for parts in the present experiments is not 100 percent pure, but an alloy with 0.5 percent Ti, 0.15% C and 0.08 percent Zr(TZM). V_p is seen to follow the model calculations closely to 400°C beyond which it decreases more rapidly; the constant difference between the observed and calculated V_s values could suggest a systematic reading error. For all temperatures the differences with the models are less than 3 percent. It is not known to what degree the discrepancies are caused by differences in grade of molybdenum, by experimental error, or by differences between elastic wave propagation in the real poly-crystal and the assumptions of the model calculations. From the observed values the total delay time in the two endpieces (together 12 mm in length) is found to increase from 1.89 μsec to 1.95 μsec for P-waves between 20°C and 600°C and from 3.53 to 3.68 μsec for S-waves over the same temperature interval. These changes compare with the errors made in reading the total time of flight from the oscilloscope screen. Although small errors have thereby been introduced, I have used the same endpiece correction of 1.9 μsec for P-, and 3.6 μsec for S-waves for all temperatures. Similarly, the 0.05 μsec correction for delay in the coaxial cables (Section 13.4) has been omitted, and no correction has been made for the length changes in the

---

after runs to temperature exceeding 400°C. The O-rings used for pressure sealing in the top of the furnace and specimen assembly are the most likely source for carbon. A further improvement in design could reduce the temperature at the sealing rings, thereby preventing carbon releasing reactions. Alternatively a chemical buffering method may be attempted to control the P_{O_2} value of the pressure medium close to the transducers, so that velocity measurements at higher temperatures may be made in the present apparatus.

Figure 13.5-a, b. P- and S- wave velocities through molybdenum-
alloy (TZM) as a function of temperature. The
observations are compared with the Voigt and Reuss
averages as calculated from single crystal data for
pure molybdenum (Hearmon, 1969).
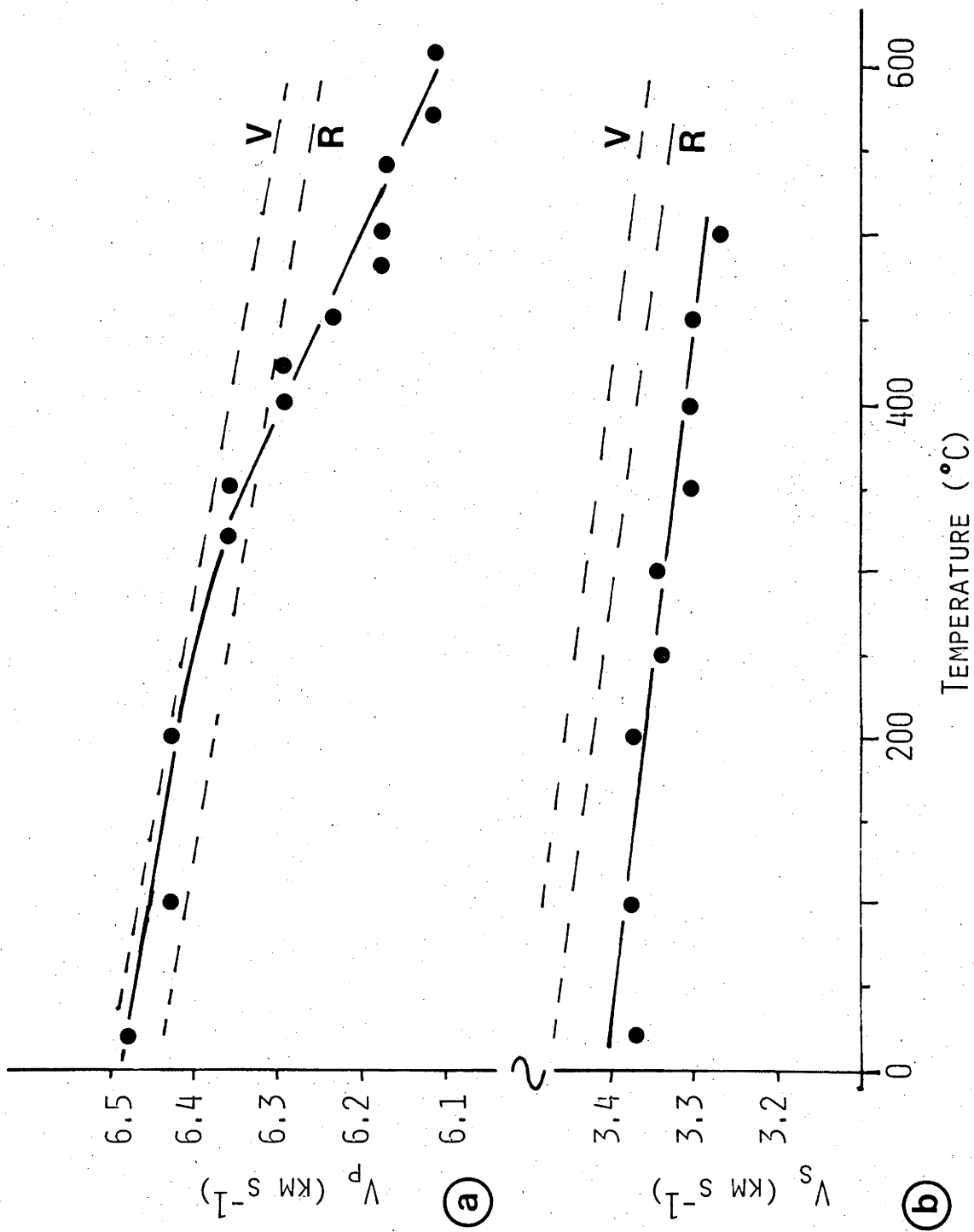
specimen with pressure and temperature. The measurements of compression and of thermal expansion at confining pressure of the specimen material (part II, Chapter 9) indicate that length changes are less than 1 percent of the original length over the pressure and temperature intervals studied.

An example of a P-wave signal is given in Figure 13.6-a. The lower signal is the initial pulse. The delayed signal is characterized by an initial period of 1.8 μsec of noise which is due to leakage despite the precautions taken to insulate and shield transducer leads in the system as much as possible. The first pulse of the delayed signal typically curves into a straight limb. I have adopted the practice of reading the travel time at the intersection of this straight limb with the abscissa. Travel times in such a figure can be read to within 0.05 μsec for good quality signals obtained at confining pressure and moderate temperature and to within 0.1 μsec for more diffuse signals at low confining pressure or high temperature. The difficulties encountered with S-wave signals are illustrated in Figure 13.6-b. Again there is leakage of the input signal, strongly recorded in the first 2 μsec and then leakage decays in a wavy form towards 8 μsec. The pulse generated by S-transducers has a weak P- component and conversion of S- to P-waves may occur at interfaces. From separate measurements of P-wave velocities at 100 MPa and high temperatures (Figure 14.3) it is expected that the first P-arrival will be around 6.7 μsec. Commonly the first P-arrival has a lower amplitude than subsequent arrivals (Figure 13.6-a), and in Figure 13.6-b, P-wave signals become only clearly visible at 7.6 μsec, which may also be partly due to interference with the leakage. The first S-wave arrival is read at the intersection of the first strong signal with the abscissa (arrow in the figure). Interference patterns prior to this S-pulse change with pressure and temperature as the amplitude and velocity of P-waves vary markedly with these parameters, while the S-signal experiences relatively small changes only. The factors outlined above indicate that for the short specimen length (20 mm), P- and S- components of the delayed pulse are insufficiently separated to make highly accurate measurements of V_s. Precision could be improved upon if longer specimens are used. Measurements were made consistently according to the methods described, it is estimated that absolute accuracy of the P- and S-wave velocities in the following chapter are not better than within ~3 percent, but small relative changes of ~1 percent in velocity are readily detected with the present arrangement.

Figure 13.6   Examples of P- and S- wave signals as displayed
on the oscilloscope screen, drawn after photographs.

a.   Signal for a P- wave through dry granite at 300 MPa
and 370°C. The lower signal is the attennuated input
signal (compare Figure 13.3).

b.   Signal for an S- wave through dry granite at 100 MPa
and 550°C. The first S- arrival is picked at
the arrow.

P_wave

0 1 2
μ sec

(a)

S_wave

0 2 4
μ sec
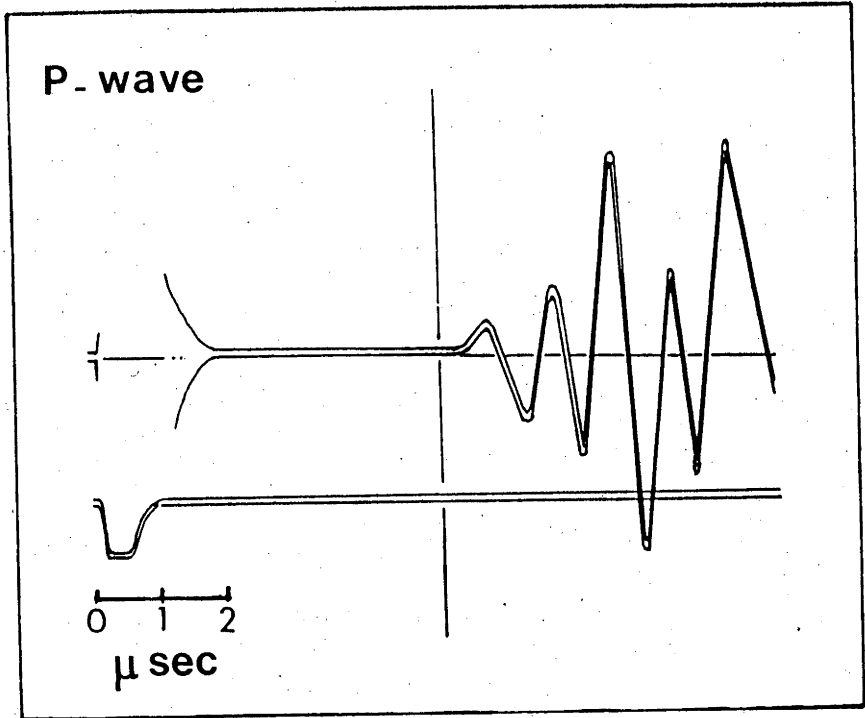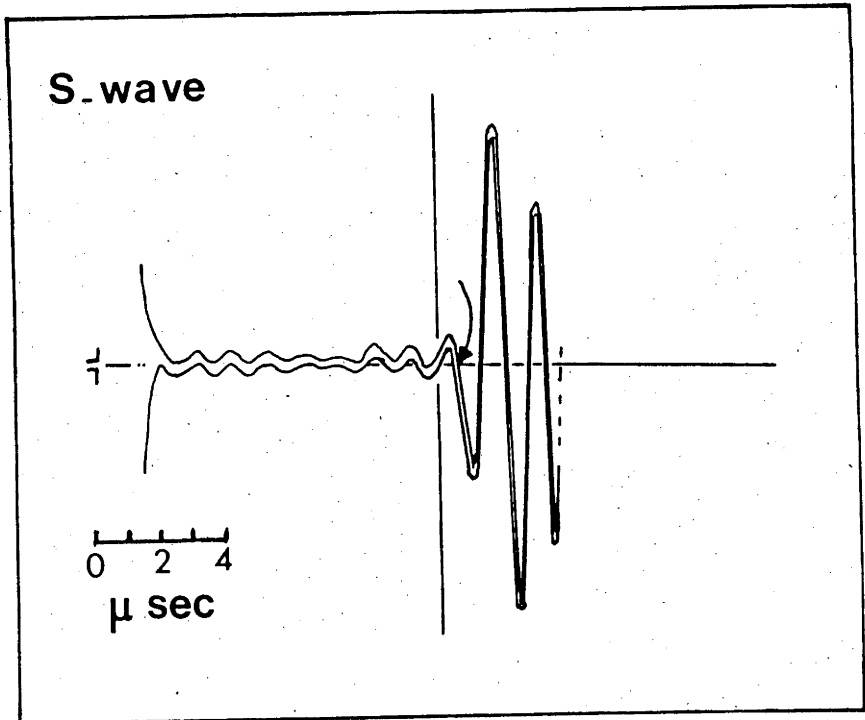
(b)

The quality of P-wave signals for specimens with added water was notably better than for dry ones at low confining pressures, and about the same at pressure and temperature. In the case of S-waves the conversion of S- to P- components is stronger with added water than in the dry case. Experiments have been performed with S-transducers at 100, 200 and 300 MPa, but interference of P- and S- components and leakage in the delayed signal was such that reliable V_s measurements could not be made. The uncertain results I have obtained would indicate absolute V_s values equal to those in the dry case, and no marked change in V_s with increasing pressure. Again, improvement could be obtained by increasing the specimen length.

Chapter 14

PRELIMINARY RESULTS AND DISCUSSION

14.1   Introduction

All of the measurements described in this chapter were obtained from runs on virgin cores of granite. Compressional − (V_p) and shear wave (V_s) velocities were determined during compression at room temperature, followed by measurements at constant pressure and increasing temperature. From the discussion in this chapter, it will be clear that measurements also have to be performed *after an initial cycle to high temperature,* to make direct comparison with observations of other workers possible. A few duplicate experiments reveal similar variations in V_p although the absolute values were found to vary somewhat (±2 percent of the average) at confining pressures above 25 MPa, but for lower pressures the differences were as large as ±3.5 percent of the average. The spread about the average has been indicated by bars in Figures 14.1 and 14.2. These differences reflect experimental uncertainties (Chapter 13.6) and perhaps a degree of specimen variability. Most results however are for individual runs, curves connecting data points have been fitted by eye.

14.2   Effect of compression at room temperature on V_p and V_s

The effect of increasing confining pressure to 300 MPa at room temperature on V_p for both dry and wet specimens of granite is shown in Figure 14.1. The dry results are in good agreement with previously reported values of V_p in granite (*e.g.* Nur and Simmons, 1969; Kern, 1978) The rapid increase in V_p over the first 100 MPa is ascribed to crack closure as discussed in Part II, Chapter 9. The initial increase in the wet case reflects perhaps the closure of some inaccessible cracks, but it seems more likely that complete saturation at atmospheric pressure has not been achieved by the specimen preparation method employed (Chapter 13.2). However, the application of pressure onto the jacket forces the extra water, which was added with a micropipette to the outside of the specimen, into any remaining accessible pore space, thereby achieving complete saturation at confining pressures above 25 MPa. Pore pressure is equal to confining pressure in the wet experiments. After the runs, free water was found inside the jacket on the surface of the specimens. The 0.7 weight percent added water is in excess of the amount that can enter accessible pore space, in

Figure 14.1 V_p in wet and dry granite during room temperature
compression to 300 MPa.   The represented results
for dry specimens are the average of 5 runs.   The
spread between these runs is largest for low
confining pressures as indicated by bars.

Figure 14.2 V_s in dry granite during room temperature compression
between 50 and 300 MPa.   The signal quality for lower
pressures was insufficient to make reliable measure-
ments.
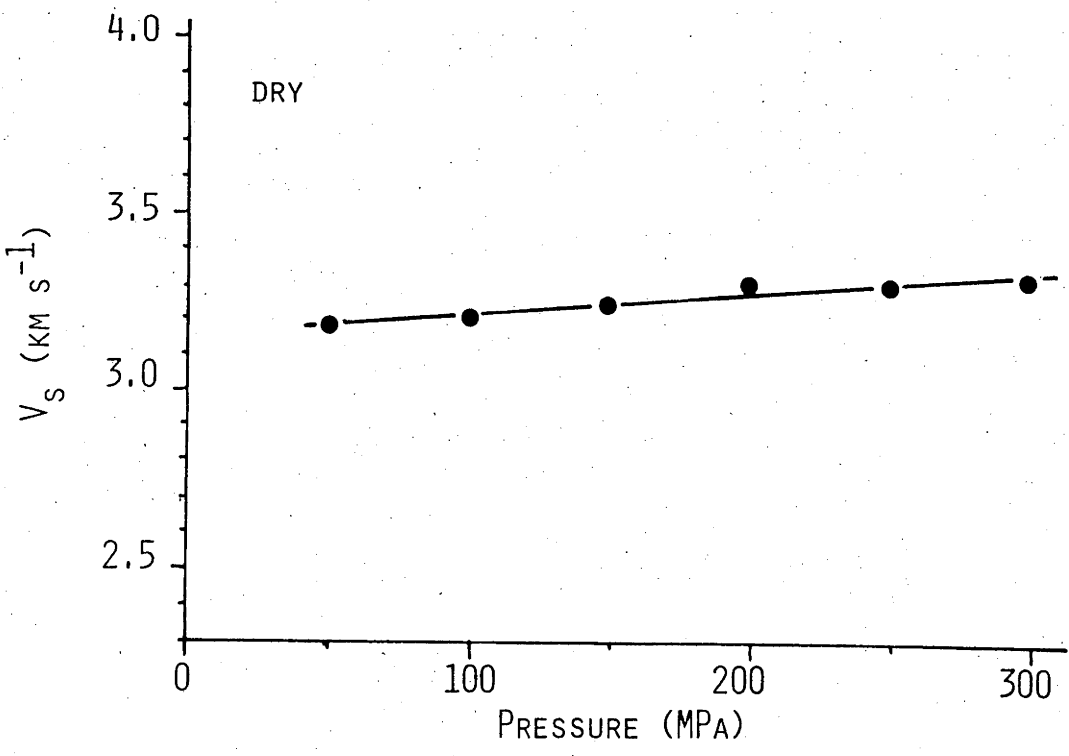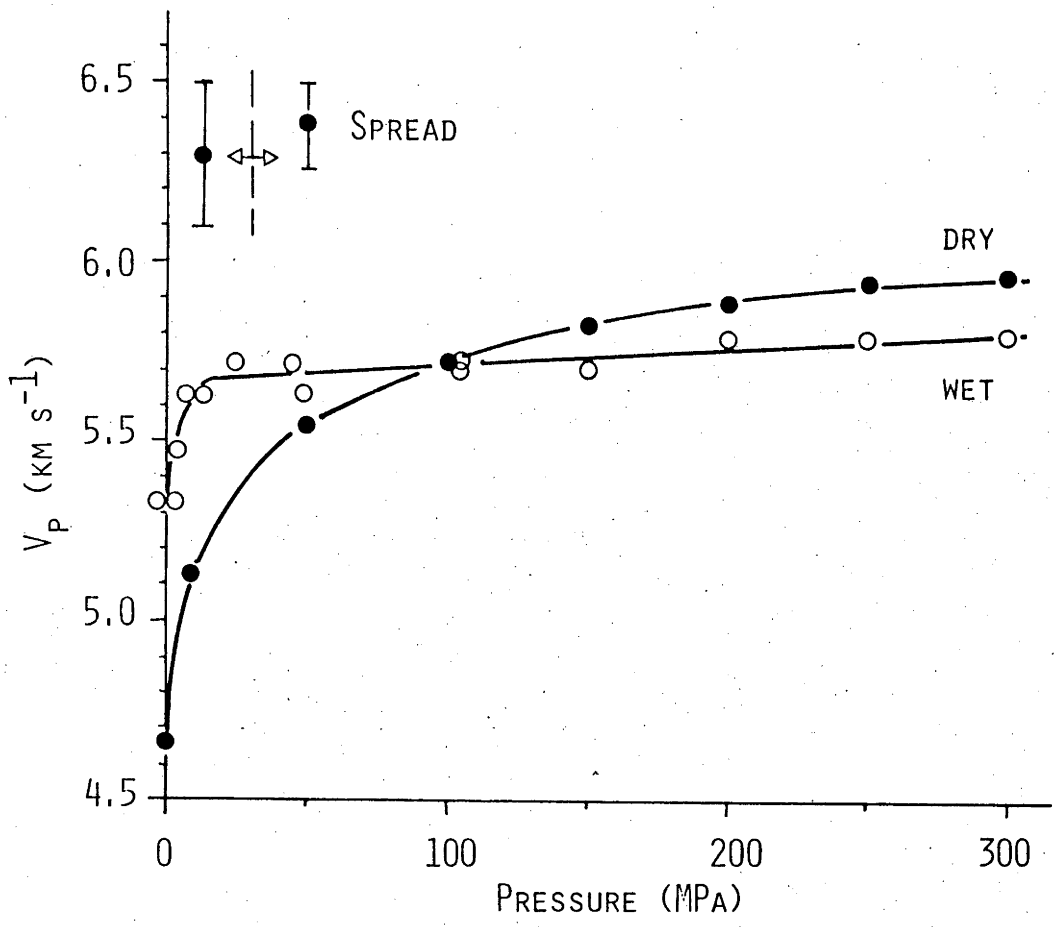
agreement with the results of Chapter 3.

At low confining pressure, saturation with water increases V_p appreciably (Figure 14.1), but at higher confining pressures (> 100 MPa), V_p is found to be less than in the dry case, for example by 3.5 percent at 300 MPa. Nur and Simmons (1969) found a larger difference of 10 percent between V_p in dry and V_p in wet Casco granite for conditions of equal pore pressure and confining pressure above 100 MPa. Such discrepancy between experimental results is likely to be caused by differences in the starting materials, particularly by differences in the pore geometry.

Reliable measurements of V_s could be obtained only on dry specimens of granite (see also Chapter 13.6). The results in Figure 14.2 indicate that V_s is less sensitive to confining pressure than V_p over the pressure interval studied, where it increases almost linearly. Simmons (1964) and Nur and Simmons (1969) demonstrated a large, non-linear increase in V_s through dry granite over the first 100 MPa pressure, comparable to the change observed in V_p. Theoretical models for the effects of cracks on the shear modulus also predict a large effect of crack closure in dry materials on V_s (e.g. O'Connell and Budiansky, 1974; see also Section 14.5.1). Such changes at low pressure could not be detected in the present experiments because of interference problems and the low amplitude of the first S-arrival at pressures less than ~50 MPa.

14.3   Effect of temperature and pressure on V_p and V_s in dry specimens

The changes in V_p and V_s through cores of dry granite at 100, 200 and 300 MPa, over the temperature range 20°C - 500°C are shown in Figure 14.3 and 14.4 respectively. In two experiments higher temperatures were reached with new transducers (see Chapter 13.5). The experiment for V_p at 200 MPa failed at low temperature: accordingly displayed results for 200 MPa have been derived by interpolation of results for 100 and 300 MPa as shown by the dashed line in the figure.

At constant confining pressure dV_p/dT in dry granite increases towards higher temperatures; for a given temperature above 200°C dV_p/dT is seen to be largest for the lowest confining pressure. Qualitatively these results agree fully with those of Kern (1978) for granite and granulite, but there are differences in the absolute values of V_p and dV_p/dT for any given pressure and temperature. The variation between the two data sets may reflect differences in composition and pore geometries of the respective

150.

Figure 14.3   The dependence of V_p in dry granite on temperature
for 100, 200 and 300 MPa. The black symbols for
300 MPa represent the average of 5 experiments, the
spread between these runs is indicated by a bar.
All other data for individual runs. The dashed
curve for 200 MPa has been interpolated.

Figure 14.4   The dependence of V_s in dry granite on temperature
for 100, 200 and 300 MPa. Notice the small tempera-
ture and pressure sensitivity up to 350°C, beyond
that temperature, V_s for 100 MPa decreases rapidly
to reach a minimum at 660°C which is associated
with the α-β transition of quartz in granite at this
pressure.
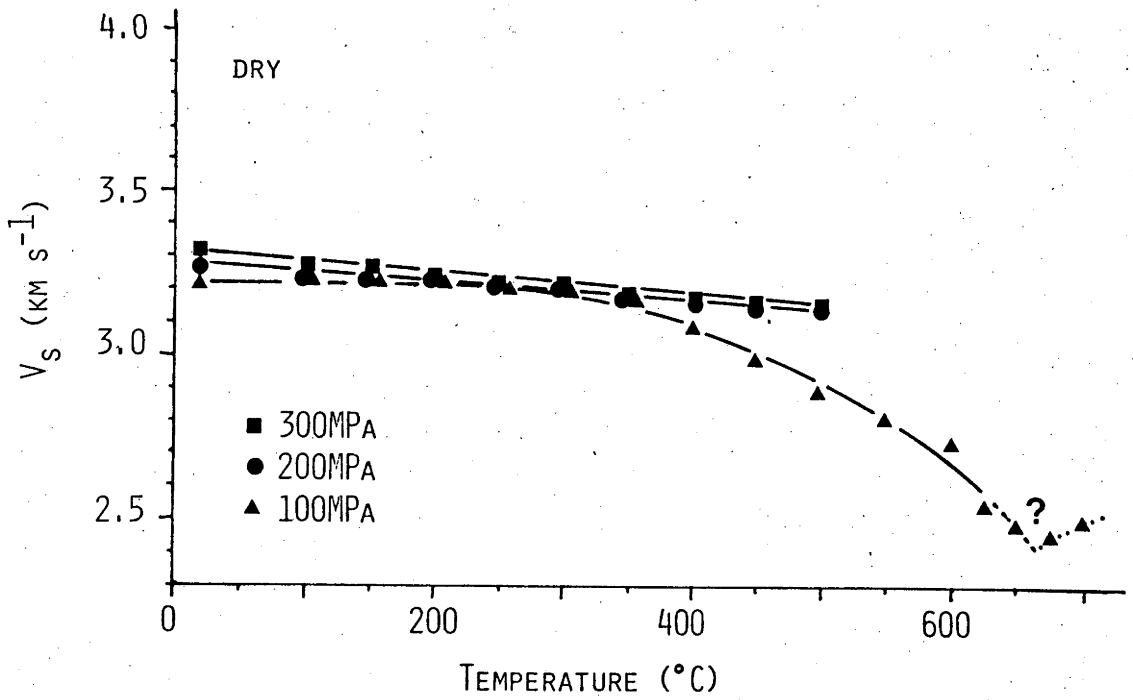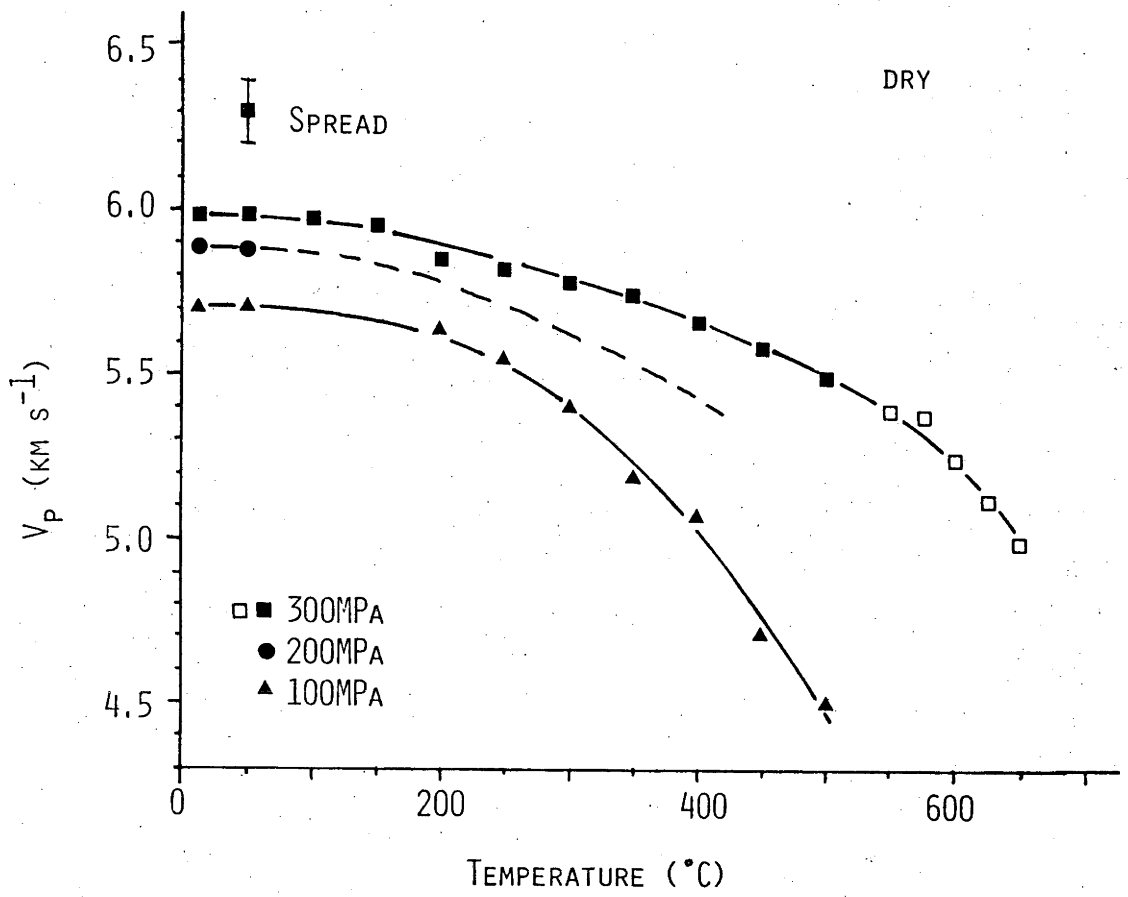
starting materials, differences in experimental error, as well as differences
in the experimental procedure. Discussion of the latter factor is postponed
to Section 14.5.2.

S-wave velocities in dry granite are seen to be relatively
insensitive to pressure, and to decrease by only a minor amount between 20°C
and 350°C. Beyond that temperature a marked effect is noted for V_s at 100
MPa, but not for 200 and 300 MPa over the intervals studied. The quality
of the signals in the 100 MPa run was good up to 600°C (Figure 13.6-b) -
beyond that temperature the signal deteriorated. The measurements performed
show an increase in V_s above ~660°C, placing the quartz α-β transition
temperature in granite at 100 MPa at about that value. This result is in
excellent agreement with that obtained from thermal expansion experiments
(Chapter 9), and that from ultrasonic V_p measurements at the same pressure
(Kern, 1978, in prep.). Kern (in prep.) also studied the change in V_s
through granite at 200 MPa and reports a small decrease from 3.50 km sec^{-1}
at 20°C to 3.41 km sec^{-1} at 500°C, followed by a marked drop to 3.16 km sec^{-1}
at ~660°C.

## 14.4   Effect of saturation with water on V_p at pressure and temperature

The results for V_p through specimens with 0.7 weight percent
added water at 100 and 300 MPa are compared in Figure 14.5 with those for
V_p through dry granite as obtained from Figure 14.3. First consider the
difference between the wet results at 100 and 300 MPa. At both pressures
the Terzaghi effective confining pressure on the aggregate is equal to zero
$(P_{confining} - P_{pore} = 0)$. Over the temperature interval 20°C - 300°C the
α-β transition temperature of quartz in granite is sufficiently far away to
make the influence on the elastic compliances and the thermal expansion of
the constituent minerals by the pressure difference negligible. This
argument and the measurements of compression and thermal expansion of wet
granite (Figure 9.1-a and 9.5), indicate that the elastic properties of the
constituent minerals, as well as the porosities in wet granite cannot be
very different between 20°C and 300°C for pressures of 100 and 300 MPa (a
small difference may arise from *inaccessible* pores being more closed at
high than at low pressure). It is concluded therefore that the differences
in V_p through wet granite between 20° C and 300° C at 100 and 300 MPa are
essentially controlled by changes in the compressibility of the water in the
accessible pores. This conclusion is supported by Figure 14.6-a,b, where
the ratio of V_p in wet rocks to V_p in dry rocks is compared with the com-

Figure 14.5   Comparison of the dependence of V_p on temperature
in wet and dry granite at 100 and 300 MPa. The
dry results are from Figure 14.3. It is not known
whether the increase in V_p between 100°C and 200°C
for 300 MPa in wet granite is reproducible.

Figure 14.6   Comparison of the effect of water on V_p in granite
at pressure and temperature with the compressibility
of water under the same conditions.

    a.   The ratio of V_p in wet specimens over V_p in dry
specimens as obtained from Figure 14.5

    b.   The compressibility of water calculated from
P-V-T data of Burnham *et al*. (1969).

NOTE: A similar correspondence is obtained if the
difference of V_p^{dry} and V_p^{wet} is compared with the
compressibility of water.
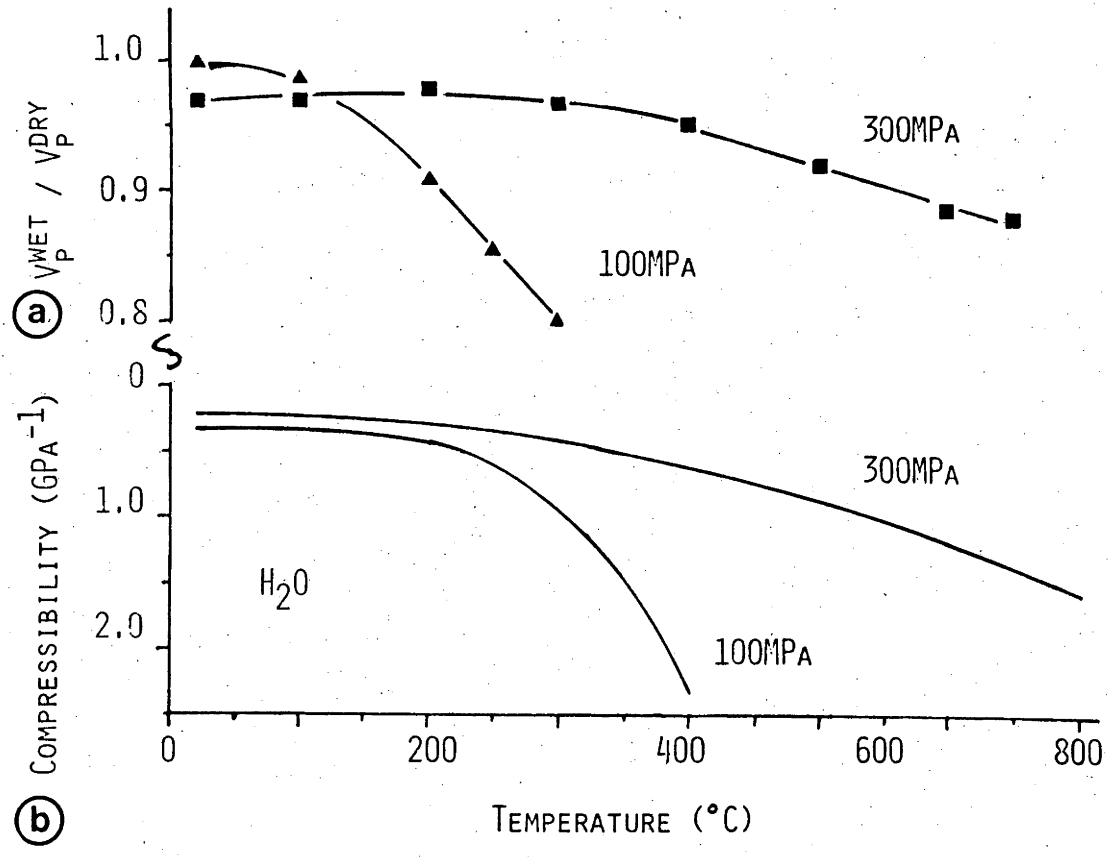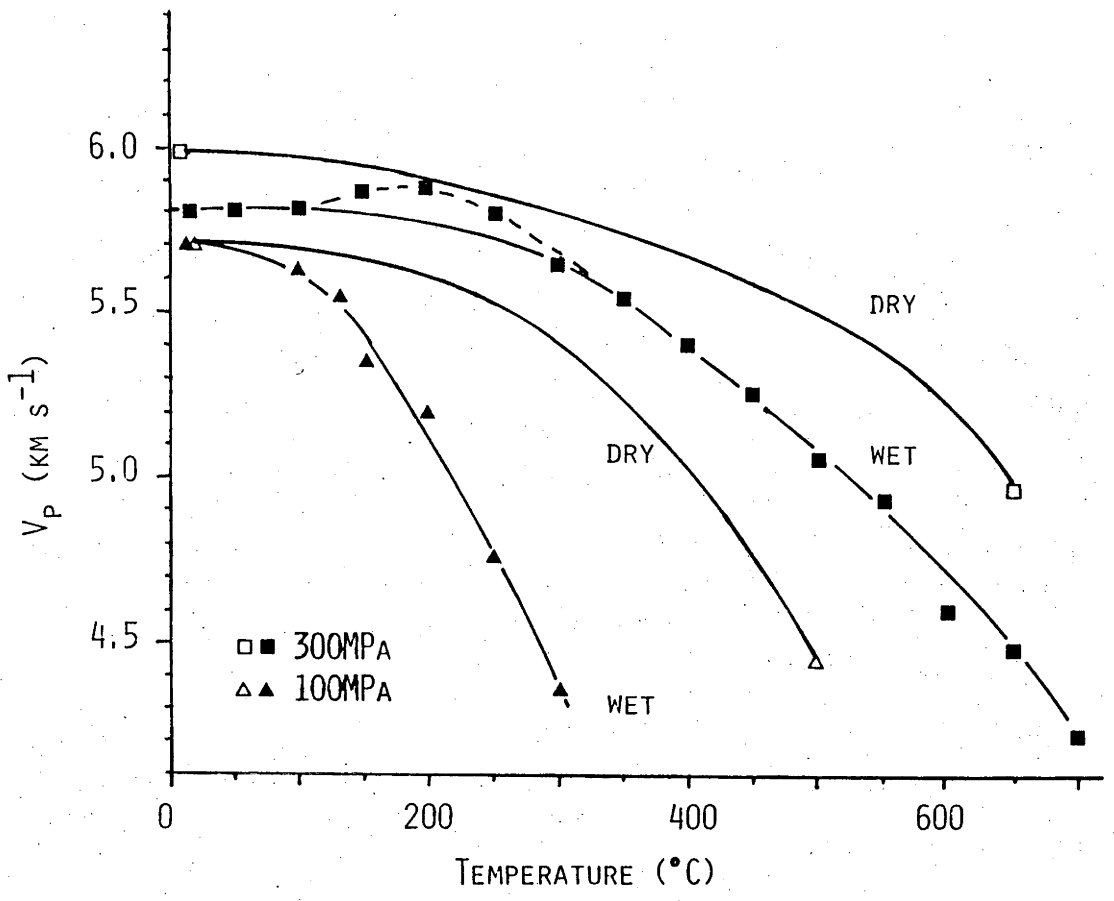
pressibility of water at pressure and temperature as calculated from the P.V.T. data for water (Burnham *et al.*, 1969).

The differences between V_p in wet and dry granite for a given temperature and pressure are caused by the presence of a compressible pore phase, as well as by differences in porosity. The latter factor is borne out by the thermal expansion measurements of Part II, where it was shown that the porosity is higher in the wet than in the dry cases (Chapter 9.4.4). Finally, it should be pointed out that there is no marked kink in the V_p-curves at 300 MPa below 700°C in Figure 14.5, indicating that the quartz α-β transition must occur at a higher temperature in both the dry and the wet specimens. The velocity measurements therefore lend support to earlier conclusions about the quartz α-β transition shift in wet and dry granite (Chapter 9.4.4 and Chapter 11.3.3).

14.5 The dynamic elastic parameters of dry granite at high pressure and temperature
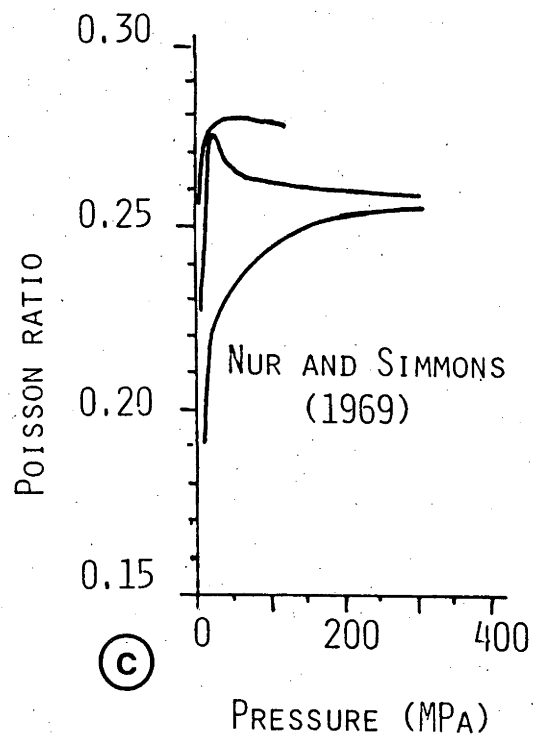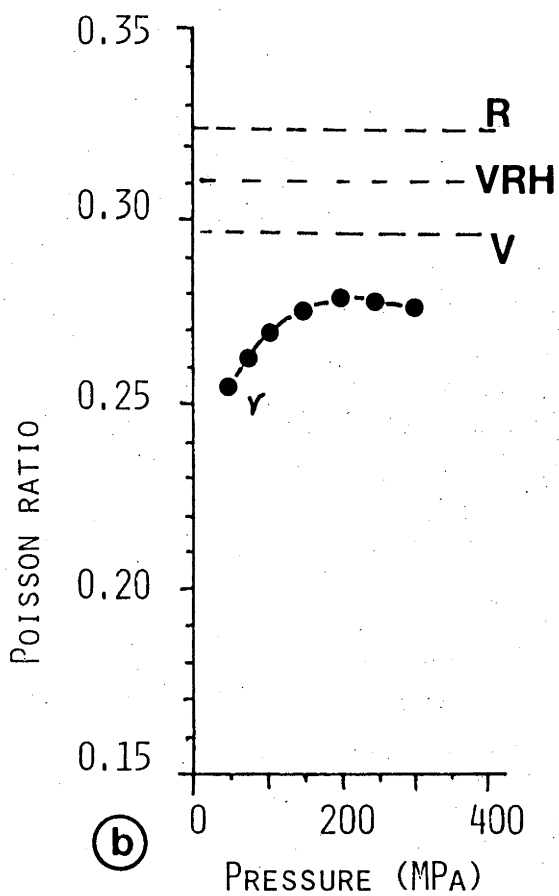
Assuming isotropic elastic behaviour with respect to the small deformations associated with the transmission of ultrasonically generated pulses one can calculate the dynamic elastic parameters of granite from a knowledge of V_p, V_s and density (Chapter 12.4). Values for the bulk modulus (K), the shear modulus (μ) and the Poisson ratio (v) are presented in Figures 14.7-a, b and 14.9-a, b for dry granite at confining pressures of 100, 200 and 300 MPa and between 20°C and 500°C. Other elastic parameters may be calculated from any two of K, μ, v (*e.g.* Jaeger, 1969, p. 57). Over the temperature pressure range of interest here, the specimen volume differs less than 2 percent from that at ambient conditions (Chapter 9). A constant density of 2.57 g cm^{-3} (Chapter 3.7.1) has been used for all calculations.

14.5.1 Room temperature compression

The results for K, μ and v during room temperature compression between 50 and 300 MPa are shown in Figure 14.7-a, b. The magnitudes of these elastic parameters, and their changes with pressure are in good agreement with previously published values (*e.g.* Birch, 1966).[1] The results of Nur and Simmons (1969) for the Poisson ratio of three different granites

---

[1] K obtained from length changes in static compression (Figure 9.1-a) varies between 14 and 40 GPa, the values obtained here are seen to be appreciably higher for confined specimens. The discrepancy is attributed to differences in strain-magnitude during static compression and during the transmission of a compressional pulse (for further discussion, see Simmons and Brace, 1965).

Figure 14.7-a-c. The dynamic elastic parameters of dry granite
during room temperature compression to 300 MPa. Also
indicated are the Voigt, Reuss, and Voigt-Reuss-Hill
averages calculated from single crystal data assuming
no pressure sensitivity for the elasticity of the
constituent minerals of granite over this small range
in pressure. The bulk modulus and the shear modulus
are indicated in Figure -a and the Poisson ratio in
Figure -b. For comparison Nur and Simmons' (1969)
results for Poisson ratio in three different granites
are shown in Figure -c.

(a)

MODULUS (GPA)

63 ↑ VRH   70 ↑ R

V

K

R
VRH
V

μ

PRESSURE (MPA)

(b)

POISSON RATIO

R
VRH
V

γ

PRESSURE (MPA)

(c)

POISSON RATIO

NUR AND SIMMONS
(1969)

PRESSURE (MPA)
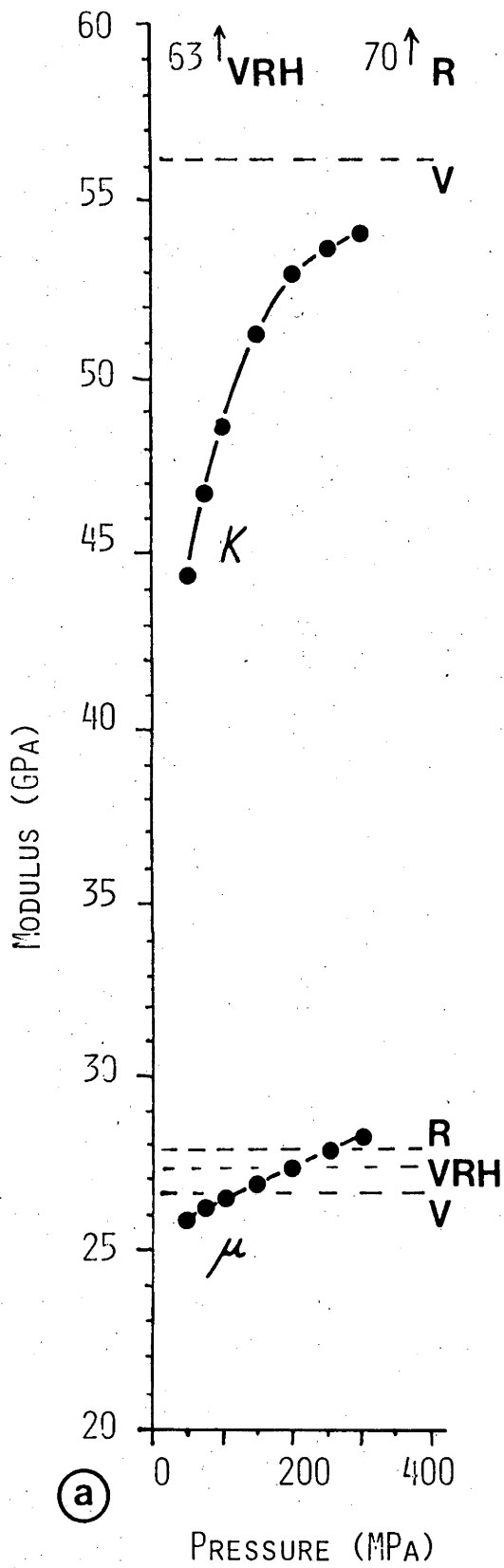
are shown in Figure 14.7-c for comparison.

The Voigt-, Reuss- and Voigt-Reuss-Hill averages for K, μ and v for hypothetical crackfree granite[1] are also shown in Figure 14.7. Despite its lack of physical significance compared to other more advanced averaging procedures (*e.g.* Watt *et al.*, 1976), I have taken the Voigt-Reuss-Hill average as a reference for comparison of the experimental data. The bulk modulus of the real material K increases non-linearly over the pressure interval studied from 70 percent to 85 percent of K_{VRH}, Poisson's ratio v from 81 to 88 percent of v_{VRH} with a maximum of 89 percent at 200 MPa. The shear modulus μ increases from 95 to 104 percent of μ_{VRH}, the latter percentage pointing to either experimental errors in the determination of μ or to deficiencies in the model calculation, because (trivially) the measured value cannot rise above the highest possible value. These experimental results are compared with O'Connell and Budiansky's self-consistent model[2] for the elasticity of cracked solids with open pores in Figure 14.8, which is drawn slightly modified after Figure 1 in O'Connell and Budiansky (1974). The measured

---

[1] Voigt averages have been calculated assuming no pressure sensitivity over the range studied with the normal equations for a crackfree composite (Watt *et al.*, 1976) which consists of equal fractions of quartz, plagioclase and K-feldspar. The moduli for these different minerals were obtained by:

   i.   for quartz taking the average of the values for room temperature Voigt-polycrystal-modulus for quartz as given by Simmons and Wang (1971, p. 332).

 ii.   for plagioclase and K-feldspar taking the Voigt averages of the elasticity data for single crystals of oligoclase and microcline as tabulated by Birch (1966, p. 147). The same procedures and the same references have been used to calculate the Reuss averages.

---

[2] The moduli of a cracked elastic material depend on porosity but may be the same for different porosities depending on the shape and the size of the pores. The quantity relating the modulus of the cracked solid to that of its uncracked counterpart is the *crack density* defined as:

$$\varepsilon \equiv \frac{2N}{\pi} \; <\frac{A^2}{P}> \, ,$$

where N is the number of cracks per unit volume, A the area of a crack and P its perimeter.

Figure 14.8   Comparison of the Voigt–Reuss–Hill averages for
K, μ and v with the observed values in terms of
the self-consistent model for the elasticity of
cracked solids with open pores of O'Connel and
Budiansky (1974, Figure 1). The present figure
is a slight modification, v_{VRH} = 0.31 has been
taken for the Poisson ratio of the matrix
(compare Figure 14.7-b).
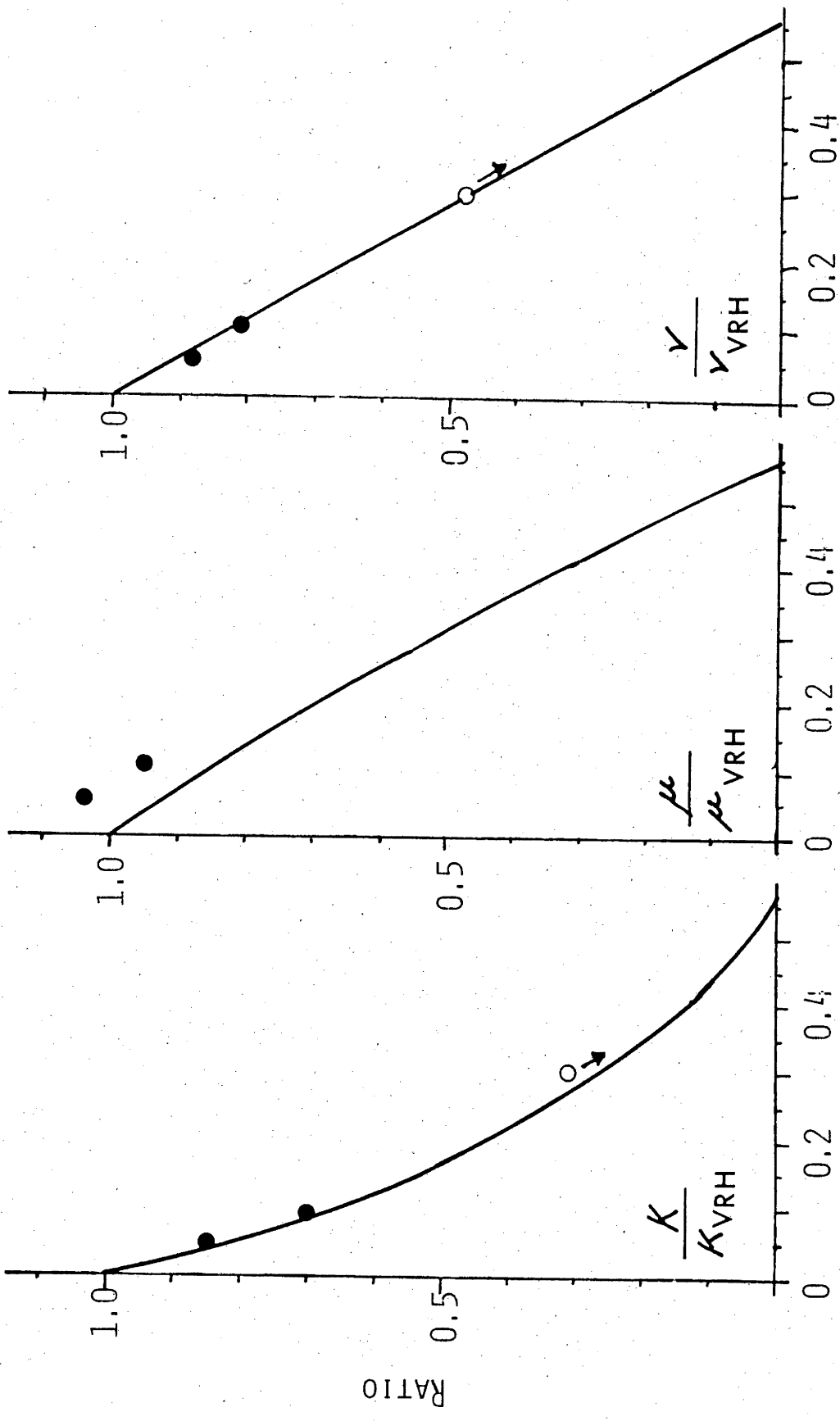
CRACK DENSITY PARAMETER ϵ

differences for K and v between 50 and 300 MPa fall close to the model results for a crack density decrease from 0.10 to 0.05, the change in μ is also consistent with the expected change over that interval in crack density, but the absolute values are too high as discussed earlier. Measurements of volume changes between 1 atmosphere and 300 MPa at room temperature (Chapter 9.4.1) indicate a decrease in *total porosity* from ~2.3 percent at 1 atmosphere to ~1.8 percent at 100 MPa, ~1.3 percent at 200 MPa and ~1.0 percent at 300 MPa, that is a decrease from approximately 2.0 percent porosity at 50 MPa to 1.0 percent between 50 and 300 MPa. An impression of the changes in the average shape of cracks may be obtained by assuming that each crack has a penny shaped, flat ellipsoidal form. From the relationship between the porosity ϕ and the crack density in the model, the change in the aspect ratio of the cracks may then be obtained from (O'Connell and Budiansky, 1974):

$$\frac{\phi}{\varepsilon} = \frac{4}{3} \pi < \frac{c}{a} > \qquad [1],$$

where $< \frac{c}{a} >$ is the average aspect ratio of the cracks, defined as thickness : width. It is concluded that the average aspect ratio of the cracks remains close to 5×10^{-2} during compression from 50 to 300 MPa. The K, μ and v values at pressures below 50 MPa have not been determined, but extrapolation of the present results to lower pressures and comparison with previously published results (Nur and Simmons, 1969) would indicate that at 1 atmosphere $K \leq 20$ GPa (corresponding to 32 percent of K_{VRH}) and $v \leq 0.15$ (corresponding to 48 percent of v_{VRH}). These estimates have been given by open symbols in Figure 14.8, they indicate that the crack density of the starting material must have been $\varepsilon \geq 0.3$ which compares favourably with estimates of crack densities in other granites at ambient conditions (O'Connell and Budiansky, 1974). From the initial total porosity of ~2.3 percent it is therefore estimated from [1] that the average initial aspect ratio at ambient conditions is less than ~1.8×10^{-2}. Comparison of O'Connell and Budianski's model with the velocity measurements and the compressibility measurements of the present study therefore leads to the following conclusions:

1. Between 1 atmosphere and 50 MPa approximately 0.3 percent of porosity is removed which is associated with an increase in the average aspect ratio of the pores from less than ~1.8×10^{-2} to ~5×10^{-2} and with

large increases in the dynamic elastic moduli of granite and the velocity of ultrasonic waves through it. Cracks with the lowest aspect ratios (the flattest) are closed over this pressure interval causing a large change in the average aspect ratio for a relatively minor change in porosity.

2. Between 50 and 300 MPa the average aspect ratio of the cracks remains constant at ~5 x 10^{-2} while the porosity decreases by half from ~2.0 percent to ~1.0 percent of the total volume. This points to a progressive closure of cracks whereby the thickness and the width of the cracks are reduced simultaneously by the same factor. The associated changes in the properties of granite are large, non-linear increases in K and V_p, smaller almost linear increases in μ and V_s, and non-linear increases in v in the manner shown in the figures. A progressive closure of cracks at constant crack-width would, according to the model, result in constant values for crack density, velocities and elastic moduli. The experiments clearly contradict such a possibility.

14.5.2 Temperature increase at confining pressure

The results for K, μ and v at 100, 200 and 300 MPa between 20°C and 500°C are shown in Figure 14.9-a, b. From arguments presented in earlier sections, the following conclusions may be derived. The temperature and pressure sensitivity of the dynamic elastic moduli of dry granite in experiments depends on two factors. The first factor is the pressure and temperature sensitivity of the elastic parameters of the constituent minerals, particularly for quartz when the α-β transition is being approached, resulting in decreasing values for K, μ and v of the granite. This effect is strongest for the run at 100 MPa where the α-β transition temperature of quartz in granite (~650°C, Chapters 9 and 11 and Section 14.3) is most nearly approached. The second controlling factor is the state of micro-cracking of the material. Microcracks cannot be completely closed by the confining pressures considered,   particularly not at the higher temperatures where differential thermal expansion of the constituent minerals tends to open cracks. This effect is again strongest for the run at 100 MPa, at 500°C. A small increase in Poisson ratio for 300 MPa over the first 200°C is observed, which could possibly reflect the decrease in porosity over that temperature interval noted from the thermal expansion experiments (Chapter 9.4.3). According to the model of O'Connell and Budiansky (1974), (Section

Figure 14.9-a-c.   The dynamic elastic parameters of dry granite as
a function of temperature for 100, 200 and 300 MPa.
The bulk modulus and the shear modulus are shown in
Figure -a and the Poisson ratio in Figure -b.
K and v at 200 MPa depend on the interpolation for
V_p at that pressure (Figure 14.3).   For comparison
the Poisson ratios of granite determined by Fielitz
(1971, 1976), Spencer and Nur (1976) and Kern (in
prep.) have been given in Figure -c.
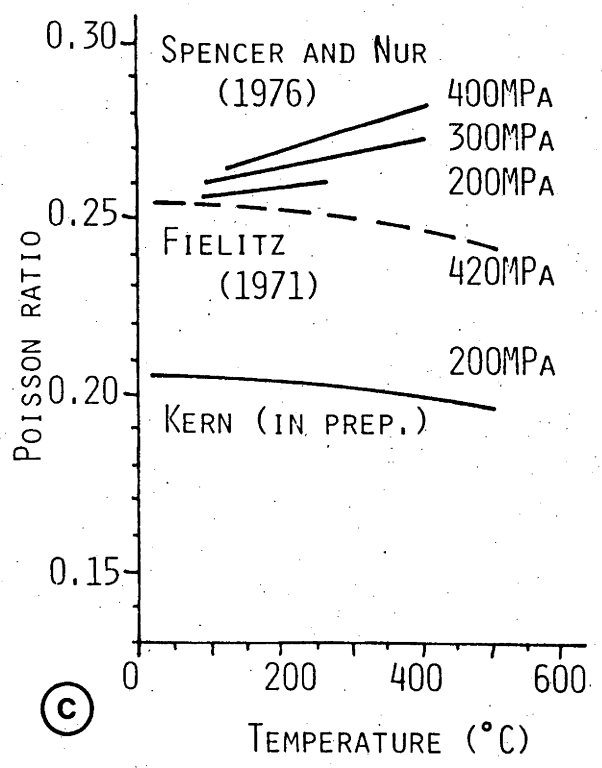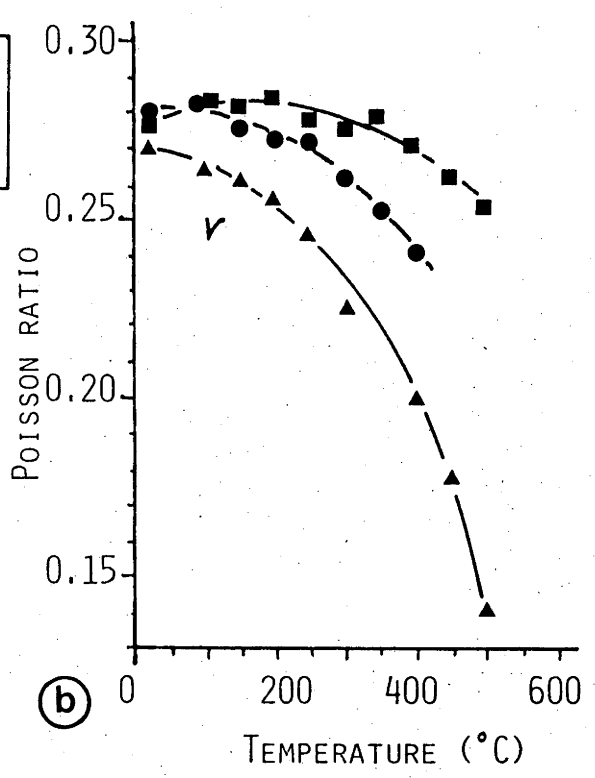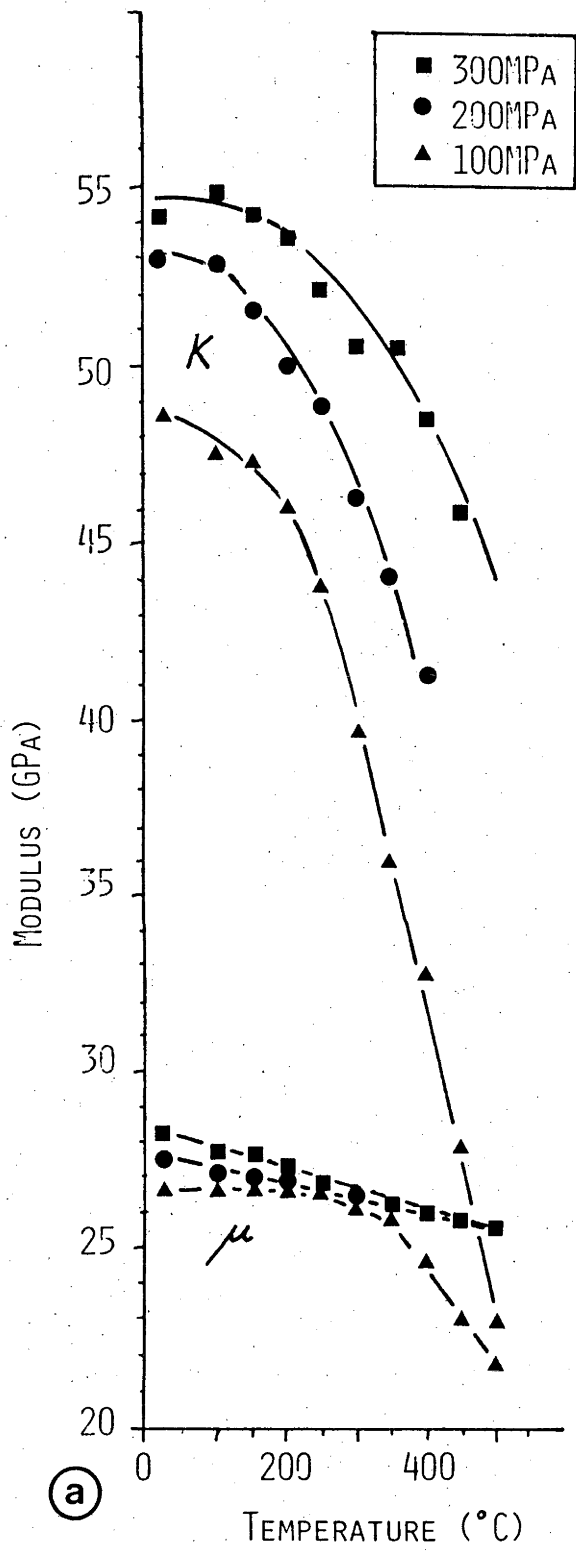
14.5.1), small changes in porosity should affect the moduli at 300 MPa
(where total porosity is lowest), more than at 200 and 100 MPa. The
Poisson ratio is not found to increase for the lower pressures.

The results of the present study for Poisson ratios are compared
with the results of Fielitz (1971, 1976), Spencer and Nur (1976) and
Kern (in prep.) in Figure 14.9-b and c. There is considerable discrepancy
between the various data sets, both in the absolute values of v and in its
variation with temperature (see also Chapter 12.4). Absolute differences
are likely to be influenced by the starting materials and the experimental
errors in these studies. The precision with which relative changes in V_p and
V_s, and therefore in v have been determined, is sufficiently high however
for all studies to postulate that the observed discrepancies in the trend
of v as a function of temperature are caused by differences in the experi-
mental procedures. A long quote from Spencer and Nur (1976) may serve
to clarify this conclusion:

> *"We wanted to examine the joint effects of temperature, external
> confining pressure, and internal pore water on sonic velocities
> in Westerly granite without the additional effects due to thermal
> microcracking. We found that there are large initial decreases
> in velocity during the first temperature cycle, which probably
> reflect thermal loosening at grainboundaries and the possible
> creation of new cracks. However, the velocities decrease little
> during subsequent, identical cycles, suggesting that there are only
> small increments of thermal damage after the first cycle. Following
> this observation, we adopted the practice of initially cycling each
> sample to the anticipated peak temperature, while at the lowest
> confining pressure, and proceeding with the tests on the operational
> assumption that subsequent thermal stress would have only minor
> effects on sonic velocities. "*

All results reported in the present study are for specimens compressed and
heated for the first time. Fielitz (1971, p. 951) also cycled to the
highest temperature first to obtain reversibility, Kern (priv. comm., 1979)
on the other hand used the same experimental procedure as followed by the
author. Heating a specimen of crystalline rock at moderate confining pressure
causes an increase in porosity, which is not completely reversed upon
subsequent cooling at the same pressure. The reversibility of the V_p and V_s
measurements of Fielitz and Spencer and Nur indicate that porosity changes

in subsequent heating cycles are reversible. Since the elastic moduli
of the constituent minerals of granite decrease with increasing temperature
it is concluded that porosity *decreased* upon heating in the experiments of
Spencer and Nur (1976), possibly by reclosing cracks formed by differential
thermal contraction during cooling after the first heating cycle. The same
effect is thought to operate in the experiments of Fielitz. It is not
known what causes the difference between his results obtained in a cubic
anvil apparatus and those of Spencer and Nur obtained in a gas apparatus.
The results of Fielitz at 420 MPa (Figure 14.9-c) compare favourable with
the 300 MPa data of the present study (Figure 14.9-b).

14.6 Concluding remarks

To determine the applicability of the results to the problems
of elastic wave transmission through the earth's crust it is mandatory that
a complete understanding of the data is obtained in terms of known changes
in the elastic properties of the constituent minerals and the known changes
in porosity of granite during the experiments. Care has been taken in the
previous sections to interpret the observed changes in V_p, V_s, K, μ and ν
in terms of these parameters as obtained from the thermal expansion measure-
ments of Part II and known single crystal data. It is for this reason that
I have preferred to measure velocity changes on specimens compressed and
heated for the first time, rather than follow the initial heating cycle
procedure adopted by other authors, because the changes in porosity with
temperature at confining pressure in subsequent cycles have not been deter-
mined.

Four factors make application of the experimental results for
V_p and V_s through granite at high pressure and temperature to the inter-
pretation of seismic velocity profiles through the crust difficult. They
will be discussed in turn below.

1. *Crack porosity in experiments.* As discussed previously in Chapter
    11.4, it is expected that – in the absence of a pore fluid – cracks
    will be closed in crustal rocks remaining at pressure and temperature
    for geological periods of time. In Part II it has been shown that
    the confining pressures of the experiments are insufficient to close
    all cracks in the specimen material, particularly at high temperatures.
    In this part of the thesis it has been shown that P- and S- wave
    velocities are sensitive to changes in the porosity, and that the

cracks cause the measured values of V_p and V_s to be lower than expected for a crack free granite.

2. *The quartz α-β shift in experiments.* Those unrelaxed elastic stress inhomogeneities which allow cracks to be open in granite under experimental conditions of high pressure and temperature, also cause the temperature of the α-β transition of quartz in granite to be "shifted" to higher values than for single crystals of quartz at the same confining pressure (Part II). For a given temperature and pressure (within the α-field of single crystals of quartz) the shift causes the values for V_p and V_s to be higher than they would be in the absence of such an effect. The effects of cracking and the quartz α-β shift are therefore opposite and it may not be concluded *a priori* whether the observed velocities are upper or lower limits for the velocities of seismic waves through dry granitic crust at the same pressure and temperature conditions. An argument presented in Chapter 11.4 would indicate that the effect of cracking in experiments dominates and that therefore the observed V_p and V_s values represent lower bounds.

3. *Geothermal gradients in nature.* In order to interpret seismic measurements of crustal P- and S- wave velocities, in terms of the experimental results, it is necessary that the geothermal gradient in the area is known, which is often not the case. Gradients range from 6°C km^{-1} [1] for very low grade, high pressure metamorphic areas to 100°C km^{-1} for areas with shallow contact metamorphism (Winkler, 1974). For stable continental shields the gradient ranges between 15°C and 25°C km^{-1}. By judicious choice of geothermal gradient one can explain constancy of velocities or velocity increases or decreases with depth in terms of the experimental data. Alternatively, if elasticity data for the constituent minerals of granite were available over the relevant pressure and temperature range, Voigt's model, Reuss' model and more sophisticated averaging procedures (Watt *et al.*, 1976) could be used to place bounds on the dependance of V_p and V_s

---

[1] Approximately 26 MPa increase in lithostatic pressure is associated with 1 km increase in depth in the crust.

through dry crack free granite at pressure and temperature. Observed seismic velocity profiles could then constrain the possible geothermal gradient of an area. There is however, a last factor which makes such an application difficult.

(4) *Composition of the crust.* Although dominant, granite and its gneissic counterparts are not the only rock types of the upper half of the continental crust. Sediments as well as basic igneous and metamorphic rocks, each with their own dependance of V_p and V_s on pressure and temperature (*e.g.* Fielitz, 1971, 1976) affect the observed velocities of seismic P- and S- waves through the crust.

The dynamic elastic behaviour of natural granite has been studied experimentally over a wide range of temperature and pressure, and the observed changes are fairly well understood in terms of variations of independently known physical parameters. The need for temperature and pressure derivatives of the elastic parameters and thermal expansion coefficients of the constituent minerals of granite has become clear in this study. Particularly for quartz, these properties have to be determined for simultaneous high pressure and temperature. Such measurements may readily be made on oriented cores of single crystals of quartz in the present apparatus.

Appendix 1

EXPULSION OF MELT FROM BETWEEN TWO CYLINDERS

Consider a cylindrical element consisting of two rigid cylinders of radius R with a melt film in between them (Figure A.1.1). This element is shortened in the z direction at a constant strainrate $\dot{\varepsilon}$ by pushing out the melt film with viscosity η and thickness h. For a total initial length of $2R$ the approach velocity V is given by:

$$V = 2\dot{\varepsilon}R \qquad\qquad (1)$$

The pressure in the fluid film is given as a function of the distance r from the z-axis by (Bowden and Tabor, 1950, p. 274):

$$p = \frac{3\eta V}{h^3} (R^2 - r^2) \qquad c.g.s. \qquad (2)$$

this is a parobolic function with $p_{max} = 3\eta V R^2 h^{-3}$ at $r = 0$, and $p = 0$ at $r = R$.

The differential stress σ on the cylinders needed to produce a constant approach velocity is equal to the average pressure in the fluid which can easily be shown to be half of the maximum pressure at $r = 0$, thus:

$$\sigma = p_{av} = \frac{3}{2} \frac{\eta V}{h^3} R^2 \qquad c.g.s. \qquad (3\text{-}a)$$

Now substituting (1) and equating R to half the grain size d we obtain:

$$\sigma = \frac{3}{8}\eta\dot{\varepsilon} \left(\frac{d}{h}\right)^3 = \frac{3}{8}\eta\dot{\varepsilon} \left(\frac{1}{\alpha}\right)^3 \qquad (3\text{-}b)$$

where α is the ratio of the melt film thickness to its diameter.

Appropriate values for the constant strainrate experiments on partially-melted Delegate aplite at 800°C are $\eta = 10^4$ Pascal seconds (see Chapter 7.3.4) $d = 1$ mm and $3 \times 10^{-6} \leq \dot{\varepsilon} \leq 3 \times 10^{-4} s^{-1}$. The stresses needed to expell melt films from grainboundaries perpendicular to the stress are calculated from (3-b) for different thicknesses and strainrates and given in Table A.1.1.

Figure A.1.1   Geometry considered for melt expulsion.
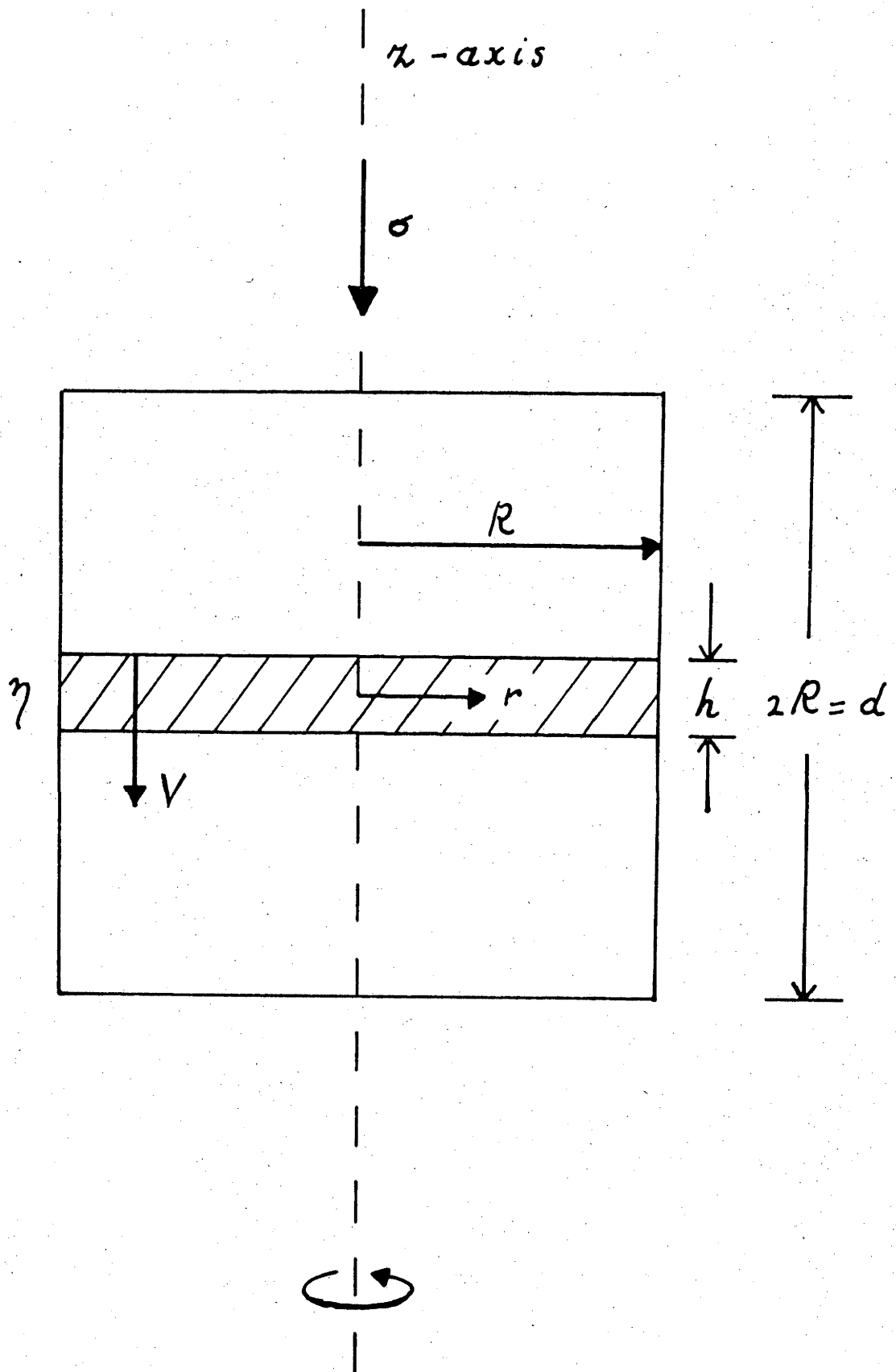
Table A.1.1   Stresses as a function of fluid film thickness and strainrate.

h	Stress (MPa)		
10μ	1	0.1	0.01
1μ	1000	100	10
0.1μ	10^6	10^5	10^4
$\dot{\varepsilon}(s^{-1})$	3×10^{-4}	3×10^{-5}	3×10^{-6}

Appendix 2

DILATANCY IN A CLOSE-PACKED HARD SPHERE MODEL

A.2.1 Case of equal spheres

Consider a hexagonal close-packed structure that is deformed by shortening normal to the hexagonal layers. The deformation is accommodated by a uniform increase in the spacing of the spheres within a layer, while the spheres in one layer remain in contact with those in adjacent layers as the layers move towards each other. It is sufficient to consider the changes in a prismatic primitive unit cell containing the equivalent of one sphere (Figure A2.1-a, b). The base of the unit cell is the 60° parallelogram bounded by the lines joining the centers of four initially contiguous spheres in a hexagonal layer and has an area $a^2 \frac{\sqrt{3}}{2}$ where a is the spacing of the spheres in this layer. The height h of the unit cell is equal to the distance $(\frac{3D^2 - a^2}{3})^{\frac{1}{2}}$ between adjacent layers, where D is the diameter of the spheres. The volume V of the unit cell is given by $\frac{a^2}{2} (3D^2 - a^2)^{\frac{1}{2}}$. Defining shortening strain as $\varepsilon = \frac{h_o - h}{h_o}$ and bulk dilatational strain as $\varepsilon_V = \frac{V - V_o}{V_o}$ (volume increase and length decrease being represented as positive strain), it can be shown that:

$$\varepsilon_V = 3\varepsilon - 6\varepsilon^2 + 2\varepsilon^3 \qquad (1),$$

or

$$\varepsilon_V \approx 3\varepsilon \qquad (1\text{-}a)$$

for small strains.

In general dilatational strain ε_V leads to an increase in porosity from an initial value of ϕ_o to:

$$\phi = \frac{\phi_o + \varepsilon_V}{1 + \varepsilon_V} \qquad (2),$$

in the present case this leads to

$$\phi \approx \phi_o + 3\varepsilon \qquad (2\text{-}a),$$

for small strains, where

$$\phi = 1 - \frac{\pi}{\sqrt{18}} = 0.26.$$

Figure A.2.1 Unit cell of the close-packed hard sphere model.

       a.   the undeformed state.

       b.   the deformed state.

       c.   normal force and shear force at the contact between two grains.

$$X$$
$$U \qquad T \qquad W$$
$$\frac{D}{2}$$
$$V$$
$$h_0 = D\sqrt{\frac{2}{3}}$$
$$P \to (S) \qquad \frac{D}{2} \qquad (S) \leftarrow R$$

(a)

$$a_0 = D$$

$$X$$
$$U \qquad T \qquad W$$
$$\frac{D}{2}$$
$$V \qquad h$$
$$P \to (S) \qquad \frac{D}{2} \qquad (S) \leftarrow R$$

(b)

$$a$$

$$T$$
$$F \qquad \frac{D}{2}$$
$$\alpha$$
$$\mu F \qquad h$$
$$P \qquad\qquad R$$

(c)

$$a/\sqrt{3}$$
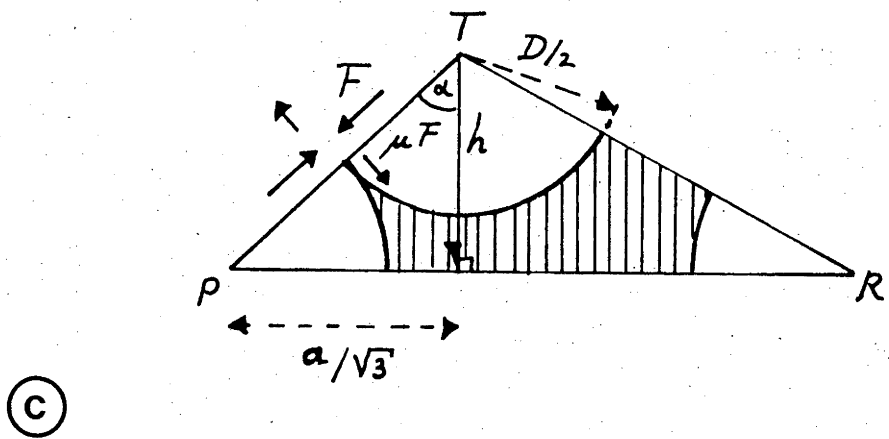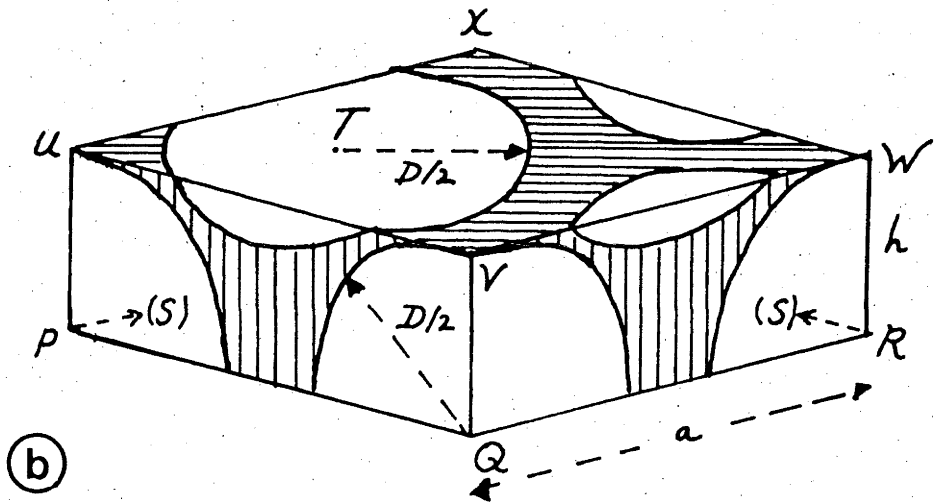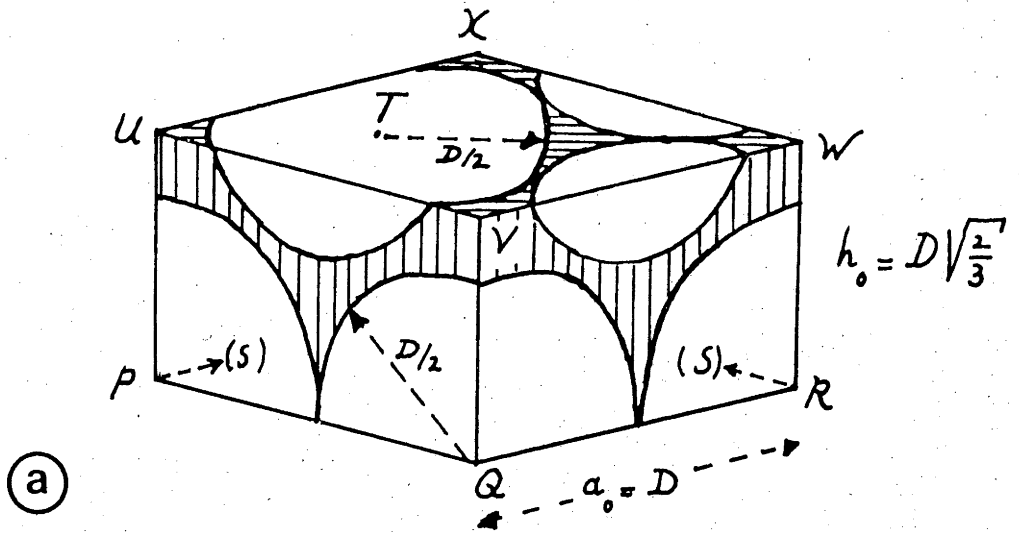
Correspondingly a bulk dilational strain ϵ_V involves a volumetric strain ϵ_p of the pore space given by:

$$\epsilon_p = \frac{\epsilon_V}{\phi_o} \qquad\qquad (3),$$

that is in the present case

$$\epsilon_p \approx 11.5\epsilon \qquad\qquad (3\text{-}a)$$

for small strains.

If the porespace is initially filled with a fluid of bulk modulus $\tilde{K}$ at pressure p and if movement of fluid in or out of the assemblage is prevented ("undrained case"), then the change in pore pressure Δp through dilatancy will be in general:

$$\Delta p = - \tilde{K}\epsilon_p \qquad\qquad (4),$$

or in the present case approximately

$$\Delta p \approx - 11.5 \tilde{K}\epsilon \qquad\qquad (4\text{-}a)$$

for small strains.

In order to bring about this deformation a compressive differential stress σ must be applied in the direction normal to the layers. By considering the balance of forces between the spheres within the unit cell, and assuming that the strains are small it will be shown below that if friction is neglected:

$$\sigma \approx - 4\Delta p \qquad\qquad (5),$$

or, by (4) and (3-a),

$$\sigma \approx 46\tilde{K}\epsilon \qquad\qquad (5\text{-}a).$$

With equation (5-a) we have now arrived at a stress-strain relationship for dilatancy hardening in the case of rigid spheres.

If frictional resistance to relative movement of spheres is taken into account, with a coefficient of friction μ at sphere contacts, then under the same assumptions as above the dilatancy hardening relation (5-a) is replaced by:

$$\sigma \approx 46\tilde{K}\epsilon \; \frac{1 + \mu/\sqrt{2}}{1 - \mu\cdot\sqrt{2}} \qquad\qquad (6),$$

if $\mu < \dfrac{1}{\sqrt{2}}$. The assemblage becomes rigid if $\mu \geq \dfrac{1}{\sqrt{2}}$.

The derivation of (5) and (6) is best understood by referring to Figures A.2.1-a, b and c. The undeformed and deformed unit cells are shown in Figures 1-a and b respectively.

Let the normal force between two contacting spheres be F and the shearforce at the contact μF (Figure A.2.1-c), then it is easily seen that the vertical component of the force between grains P and T is:

$$F^{PT}_{vert} = F \,(\cos\,\alpha + \mu\,\sin\,\alpha) \qquad (7),$$

and that the horizontal component of the force between P and T is given by:

$$F^{PT}_{hor} = F \,(\sin\,\alpha - \mu\,\cos\,\alpha) \qquad (8).$$

The total vertical force is made up of contributions from grains P, Q and S which are in contact with grain T, this force acts over the area of $PQRS$ such that the vertical differential stress

$$\sigma_{vert} = \sigma = \frac{3F \,(\cos\,\alpha + \mu\,\sin\,\alpha)}{\tfrac{1}{2}a^2 \,\sqrt{3}} \qquad (9).$$

The horizontal force F^{PT}_{hor} acts over the area of $QVXS$ and equal horizontal forces F^{QT}_{hor}, and F^{ST}_{hor} act over equal areas of $PSXU$ and $PQVU$ respectively. Thus the horizontal differential stress, which may be equated with $-\Delta p$ is given by:

$$\sigma_{hor} = -\Delta p = \frac{F(\sin\,\alpha - \mu\,\cos\,\alpha)}{h.a} \qquad (10).$$

Reworking (9) and (10) and remembering that $cotg\,\alpha = h\,\sqrt{3}/a$ (Figure 1-c) we obtain:

$$\sigma = -\Delta p \cdot 2cotg^2\alpha \cdot \frac{1 + \dfrac{\mu}{cotg\,\alpha}}{1 - \mu \cdot cotg\,\alpha} \qquad (11).$$

For small strains $h \approx D\,\sqrt{\dfrac{2}{3}}$ and $a \approx D$ such that $cotg\,\alpha \approx \sqrt{2}$, and (11) reduces easily to (5) and (6).

A.2.2 Case of unequal spheres

In order to gain some impression of the effect of having mixed sizes of spheres we now consider the case in which the spheres in alternating layers are reduced in diamters from D to d. Provided

$\dfrac{d}{D} \geq \sqrt{\dfrac{7}{3}} - 1$ or approximately 0.53, all previous contacts between spheres in adjacent layers are preserved, but the amount of relative displacement before the larger spheres in alternative layers make contact is reduced as this value of d/D is approached. Similar calculations show that now

$$\varepsilon_V = (4X^2 - 1)\varepsilon - 6X^2\varepsilon^2 + 2X^2\varepsilon^3 \tag{12}$$

or

$$\varepsilon_V \approx (4X^2 - 1)\varepsilon \tag{12-a}$$

for small strains, and

$$\sigma \approx 4X^2 (4X^2 - 1) \cdot \frac{\tilde{K}\varepsilon}{\phi_o} \tag{13}$$

for small strains neglecting friction, or

$$\sigma \approx 4X^2(4X^2 - 1) \cdot \frac{\tilde{K}\varepsilon}{\phi_o} \cdot \frac{1 + \mu/X\sqrt{2}}{1 - \mu \cdot X\sqrt{2}} \tag{14},$$

for small strains with friction :

$$\mu < 1/X\sqrt{2},$$

where

$$\phi_o = 1 - \frac{\pi}{\sqrt{18}} \cdot \frac{1 + (\frac{d}{D})^3}{2X},$$

and

$$X^2 = \frac{3}{8}(1 + \frac{d}{D})^2 - \frac{1}{2}.$$

The stress-strain relationship (14) has the form

$$\sigma \approx C \cdot \frac{\tilde{K}\varepsilon}{\phi_o} \cdot f \tag{14-a},$$

where C is a geometrical factor depending on the d/D ratio, and f is a friction factor depending on μ and d/D. Some values for C, ϕ_o, and f for various d/D and μ, and the values of μ for which the assemblage becomes rigid are given in Table A.2.1.

Table A.2.1   The dilatancy hardening relationship (14-a) for the case
              of equal and unequal spheres.

d/D	c	ϕ_o	$\mu=0$	f 0.3	0.5	limiting μ
1.0	12	0.26	1	2.1	4.6	0.71
0.7	3.1	0.35	1	1.9	3.2	0.93
0.55	1.0	0.32	1	1.8	2.8	1.12

Appendix 3

ELASTIC DEFORMATION OF A HERTZIAN CONTACT

In order to illustrate the elastic deformation of grains with curved grainboundaries in contact with one another, we consider the geometry of Figure A.3.1. Two ideally elastic grains are touching one another on a circular area perpendicular to the loading direction z on spherical contacts with a radius of curvature R. The grains are symmetrical about the z-axis and have a radius r away from the contact and an initial height r each. Let the radius of the contact area be a if a force F is applied. Then the "macroscopic" stress on the grains is given by:

$$\sigma_{macr} = \frac{F}{\pi r^2} \tag{1},$$

and the average contact stress by

$$\bar{\sigma}_{contact} = \frac{F}{\pi a^2} \tag{2}.$$

Let the shortening of this unit element be h for an applied force F such that the strain of the element is given by (Figure A.3.1-a):

$$\varepsilon = \frac{h}{2r} \tag{3}.$$

The fundamental Hertzian equations relating the contact radius a, the shortening h and the contact stress as a function of distance ρ from the z-axis (Figure A.3.1-a) to the applied force F and the elastic constants E (Young's modulus) and v (Poisson Ratio) of the material are (e.g. Landau and Lifshitz, 1959):

$$a = F^{1/3} \cdot \left(\frac{D \cdot R}{2}\right)^{1/3} \tag{4},$$

$$h = F^{2/3} \cdot \left(\frac{2D^2}{R}\right)^{1/3} \tag{5},$$

and

$$\sigma_{contact} = \frac{3}{2} \frac{F}{\pi a^3} (a^2 - \rho^2)^{1/2} \tag{6},$$

where $D = \frac{3}{2} \left(\frac{1 - v^2}{E}\right).$

The following non-linear stress-strain relationships are derived from (1) - (6):

$$\sigma_{macr} = C \cdot \varepsilon^{3/2} \cdot \left(\frac{R}{r}\right)^{1/2} \cdot E \tag{7}$$

Figure A.3.1   Geometry considered for stress-strain relationship
                of two grains with a Hertzian contact.

    a.   radius of curvature larger than half the grain
          diameter. The radius of the contact area is a,
          and the distance from the center of the contact
          area is ρ $(o \leq \rho \leq a)$.

    b.   radius of curvature less half the grain diameter.

x-axis
F
r
h
2r
a
e
R
R
h
r

ⓐ

ⓑ
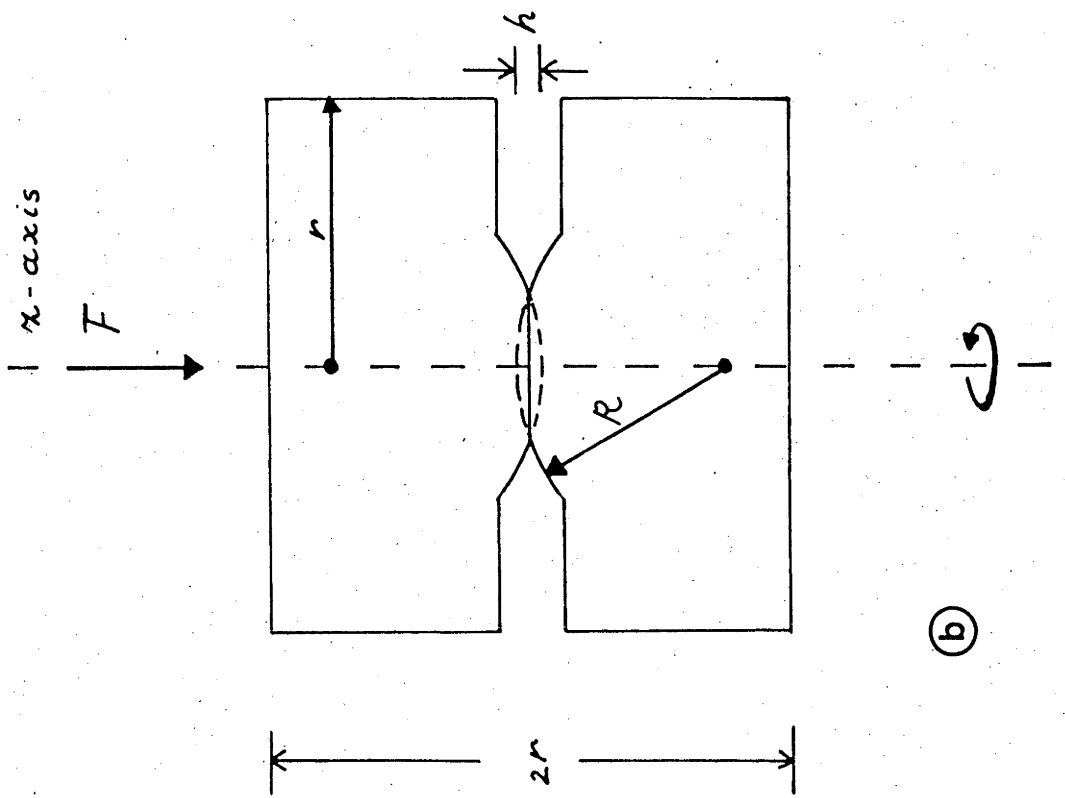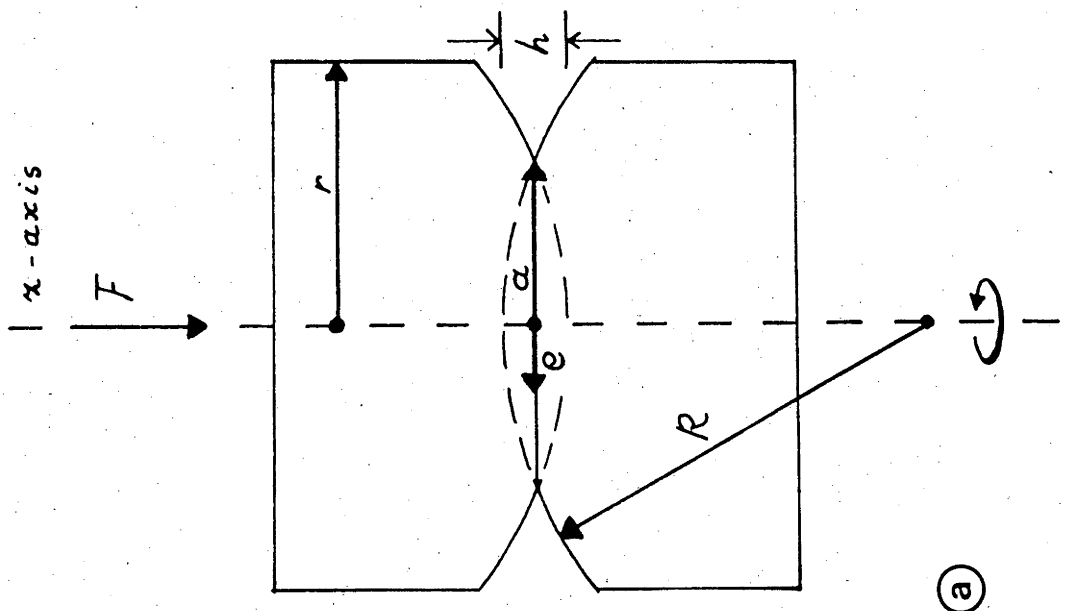
$$\bar{\sigma}_{contact} = C \cdot \epsilon^{1/2} \cdot (\frac{r}{R})^{1/2} \cdot E \qquad (8),$$

and
$$\sigma_{contact}^{max} = \frac{3}{2} \bar{\sigma}_{contact} \qquad (8\text{-}a),$$

where $C = \dfrac{4}{3\pi(1 - v^2)} \approx 0.5$ for all reasonable values of the Poisson

ratio ($0.1 < v < 0.5$; Birch, 1966). The average stress at the contact
is related to the macroscopic stress by (7) and (8):

$$\bar{\sigma}_{contact} = \frac{\sigma_{macr}}{\epsilon} \cdot \frac{r}{R} \qquad (9),$$

irrespective of the elastic parameters of the material. In contrast,
the stress and strain for a flat contact are given by:

$$\sigma_{macr} = \sigma_{contact}$$
$$\epsilon = \frac{\sigma_{macr}}{E} \qquad (10).$$

A few numerical examples are worked out below.

For a macroscopic differential stress of 10 MPa, and a
reasonable Young's modulus for the minerals in granite of $E = 100$ GPa
(Birch, 1966) it is calculated from (7) that the elastic strain for
spherical grains ($\frac{R}{r} = 1$) is $\epsilon \approx 3.4 \times 10^{-3}$. For the corresponding case
of a flat contact the strain is given by (10) : $\epsilon \approx 10^{-4}$, that is more
than thirty times less. For lower stresses this factor is higher, and
for higher stresses it is lower than 34, reflecting the non-linearity of
the stress-strain relationship of a Hertzian contact.

A large stress concentration at the contacts is indicated by
equations (8) and (9). For example, in the case of spherical grains
considered above, the average contact stress will be ~1.85 GPa, 185 times
higher than the macroscopic stress of 10 MPa. The elastic strength of
dry single crystals of quartz in compression at 800°C and 300 MPa
confining pressure is of the order of 2 GPa (Dr. K.R.S.S. Kekulawala,
priv. comm.). Thus, since the maximum contact stress is 1.5 times as
high as the average contact stress (8-a), two contacting spherical quartz
grains will tend to break under these pressure temperature conditions
at macroscopic differential stresses as low as 10 MPa. From equation (9)
it may further be seen that fracture of the grains will occur for still

lower values of macroscopic stress if the radius of curvature of the contact is smaller than half the diameter of the grains ($\frac{r}{R} > 1$), as in Figure A.3.1-b. But fracture will occur at a higher macroscopic stress than 10 MPa, if the radius of curvature of the contact is larger than half the grain diameter ($\frac{r}{R} < 1$), as in Figure A.3.1-a.

References

Anderson, D.L., Minster, B., Cole, D.: The effect of oriented cracks on seismic velocities. *J. Geophys. Res.* *79*, 4011-4015 (1974).

Arndt, N.T.: Ultrabasic magmas and high-degree melting of the mantle. *Contrib. Mineral. Petrol.* *64*, 205-221 (1977).

Arzi, A.A.: Critical phenomena in the rheology of partially melted rocks. *Tectonophysics* *44*, 173-184 (1978-a).

Arzi, A.A.: Fusion kinetics, water pressure, water diffusion and electrical conductivity in melting rock, interrelated. *J. Petrol.* *19*, 153-169 (1978-b).

Ashby, M.F., Verrall, R.A.: Micromechanisms of flow and fracture, and their relevance to the rheology of the upper mantle. *Phil. Trans. Roy. Soc. Lond.* A *288*, 59-95 (1977).

Auten, T.A., Gordon, R.B.: Compressive creep rates of partially melted Al-Ga alloys. *Metallurg. Trans.* *6A*, 584-586 (1975).

Auten, T.A., Gordon, R.B., Stocker, R.L.: Q and mantle creep. *Nature* *250*, 317-318 (1974).

Ave'Lallemant, H.G., Carter, N.L.: Syntectonic recrystallization of olivine and modes of flow in the upper mantle. *Geol. Soc. Am. Bull.* *81*, 2203-2220 (1970).

Bamford, D., Crampin, S.: Seismic anisotropy - the state of the art. *Geophys. J. Roy. astr. Soc.* *49*, 1-8 (1977).

Barrière, M.: Flowage differentiation: limitation of the "Bagnold effect" to the narrow intrusions. *Contrib. Mineral. Petrol.* *55*, 139-145 (1976).

Bayuk, Ye. I., Tedeyev, R.V.: The longitudinal wave velocity in rock samples under the simultaneous action of high pressure and temperature. *Izv. Earth Phys.* *8*, 63-70 (1974).

Berger, A.R., Pitcher, W.S.: Structures in granitic rocks : a commentary and a critique on granite tectonics. *Proc. Geol. Ass.* *81*, 441-461 (1970).

Biot, M.A.: Nonlinear and semilinear rheology of porous solids. *J. Geophys. Res.* 78, 4924-4937 (1973).

Birch, F.: The velocity of compressional waves in rocks to 10 kilobars, Part I. *J. Geophys. Res.* 65, 1083-1102 (1960).

Birch, F.: Compressibility; elastic constants. *In: Handbook of physical constants (S.P. Clarke, Jr., ed.). Geol. Soc. Am. Mem.* 97, 97-173 (1966).

Bottinga, Y., Weill, D.F.: Densities of liquid silicate systems calculated from partial molar volumes of oxide components. *Am. J. Sci.* 269, 169-182 (1970).

Bottinga, Y., Weill, D.F.: The viscosity of magmatic silicate liquids : a model for calculation. *Am. J. Sci.* 272, 438-475 (1972).

Bowden, F.P., Tabor, D.: The friction and lubrication of solids, Part I. *pp. 337, Oxford : Clarendon Press (1950).*

Brace, W.F.: Some new measurements of linear compressibility of rocks. *J. Geophys. Res.* 70, 391-398 (1965).

Brace, W.F., Martin, R.J.: A test of the law of effective stress for crystalline rocks of low porosity. *Int. J. Rock Mech. Min. Sci.* 5, 415-426 (1968).

Brand, E.W.: Some observations on the control of density by vibration. *p. 121-132 in: Selig, E.T., Ladd, R.S., eds. (1973).*

Brown, G.C., Fyfe, W.S.: The production of granitic melts during ultra-metamorphism. *Contrib. Mineral. Petrol.* 28, 310-318 (1970).

Bulau, J.R., Waff, H.S.: Mechanical and thermodynamic constraints in partial melts (in prep.) See also: Waff, H.S., Bulau, J.R.: Equilibrium fluid distribution in an ultramafic partial melt under hydrostatic stress conditions (in prep.).

Burnham, C.W.: Viscosity of a water-rich pegmatite melt at high pressures (abs.). *Geol. Soc. Am. Spec. Paper* 76, 26 (1964).

Burnham, C.W., Holloway, J.R., Davis, N.F.: Thermodynamic properties of water to 1000°C and 10,000 bars. *Geol. Soc. Am. Spec. Paper* 132 (1969).

Büsch, W., Schneider, G., Mehnert, K.R.: Initial melting at grainboundaries, Part II: Melting in rocks of granodioritic, quartzdioritic and tonalitic composition. *Neues Jahrb. Mineral. Monatsh.* 8, 345-370 (1974).

Castro, G.: Liquefaction of sands. *Harvard Soil Mech. Ser.* 81, *Harvard University, Cambridge, Mass.* (1969).

Chong, J.S., Christiansen, E.B., Baer, A.D.: Rheology of concentrated suspensions. *J. Appl. Polymer Sci.* 15, 2007-2021 (1971).

Christensen, N.I.: Compressional wave velocities in possible mantle rocks to pressures of 30 kilobars. *J. Geophys. Res.* 79, 407-412 (1974).

Coe, R.S., Paterson, M.S.: The α-β inversion in quartz : A coherent phase transition under nonhydrostatic stress. *J. Geophys. Res.* 74, 4921-4948 (1969).

Cooper, H.W., Simmons, G.: The effect of cracks on thermal expansion of rocks. *Earth Planet. Sci. Lett.* 36, 404-412 (1977).

Cornforth, D.H.: Prediction of drained strength of sands from relative density measurements. *p. 281-303 in Selig, E.T., Ladd, R.S., eds.* (1973).

Daly, R.A., Manger, G.E., Clark, S.P., Jr.: Density of rocks. *In: Handbook of physical constants. (S.P. Clark, Jr. ed.). Geol. Soc. Am. Mem.* 97, 19-26 (1966).

Dickin, E.A.: Influence of grain shape and size upon the limiting porosities of sands. *p. 113-120 in Selig, E.T. Ladd, R.S., eds.* (1973).

Durham, G.N., Townsend, F.C.: Effect of relative density on the liquefaction susceptibility of a fine sand under controlled-stress loading. *p. 319-331 in Selig, E.T., Ladd, R.S., eds.* (1973).

Eshelby, J.D.: The determination of the elastic field of an ellipsoidal inclusion and related problems. *Proc.Roy.Soc.London A* 241, 376-396 (1957).

Fielitz, K.: Elastische Wellengeschwindigkeiten in verschiedenen Gesteinen unter hohem Druck und bei Temperaturen bis 750°C. *Zeitschr. f. Geophys.* 37, 943-956 (1971).

Fielitz, K.: Compressional and shear wave velocities as a function of temperature in rocks at high pressure. *In: Explosion Seismology in Central Europe (P. Giese, C. Prodehl, A. Stein, eds.), p. 40-44. Berlin - New York : Springer Verlag* (1976).

Frank, F.C.: On dilatancy in relation to seismic sources. *Rev. Geophys.*
3, 485-503 (1965).

Gallagher, J.J., Jr., Friedman, M., Handin, J., Sowers, G.M.: Experimental
studies relating to microfracture in sandstone. *Tectonophysics*
21, 203-247 (1974).

Goetze, C.: A brief summary of our present day understanding of the
effect of volatiles and partial melt on the mechanical properties
of the upper mantle. *In: High pressure research, applications
in geophysics (M.H. Manghnani, S. Akimoto, eds.), p. 3-23. New York:
Academic Press (1977).*

Goetze, C., Kohlstedt, D.L.: Laboratory study of dislocation climb and
diffusion in olivine. *J. Geophys. Res.* 78, 5961-5971 (1973).

Griggs, D.T.: Hydrolytic weakening of quartz and other silicates.
Geophys. J. Roy. astr. Soc. 14, 19-31 (1967).

Hart, E.W.: Constitutive relations for the nonelastic deformation of
metals. *Trans. ASME, J. Eng. Mater. Tech.* 98, 193-202 (1976).

Hart, E.W., Li, C.Y., Yamada, H., Wire, G.L.: Phenomenological theory :
A guide to constitutive relations and fundamental deformation
properties. *In: Constitutive Equations in Plasticity (A.S. Argon,
ed.) p. 149-197. Cambridge, Mass. : MIT Press, (1975).*

Hearmon, R.F.S.: The elastic constants of non-piezoelectric crystals.
*In: Landolt-Bornstein Tables, Vol. II, new series, group III
(K.H. Hellwege, ed.), p. 1-39. New York : Springer Verlag (1969).*

Hobbs, B.E., Means, W.D., Williams, P.F.: An outline of structural geology.
pp. 571, New York, London, Sydney, Toronto : John Wiley and Sons (1976).

Hoffmann, C.: Granite intruding into granodiorite : An example from the
Damara belt, South West Africa. *Geol. Rundschau* 66, 465-477 (1977).

Holubec, I., D'Appolonia, E.: Effect of particle shape on the engineering
properties of granular soils. *p. 304-318 in Selig, E.T., Ladd, R.S.,
eds. (1973).*

Hulme, G.: The interpretation of lava flow morphology. *Geophys. J.Roy. astr.
Soc.* 39, 361-383 (1974).

Jaeger, J.C.: Elasticity, fracture and flow. *pp. 268, London, Methuen & Co., Science Paperbacks (1969).*

Jaeger, J.C., Cook, N.G.W.: Fundamentals of rock mechanics. *2nd ed., pp. 585, London: Chapman and Hall (1976).*

James, K., Ashbee, K.H.G.: Plasticity of hot glass-ceramics. *Progress Mat. Sci. 21, 1-59 (1975).*

Jeffrey, D.J., Acrivos, A.: The rheological properties of suspensions of rigid particles. *Am. Inst. Chem. Eng. J. 22, 417-432 (1976).*

Johannes, W.: Melting of plagioclase in the systems Ab-An-H_2O and Qz-Ab-An-H_2O at P_{H_2O} = 5 kbars, an equilibrium problem. *Contrib. Mineral. Petrol. 66, 295-303 (1978).*

Johnson, A.M.: Physical processes in geology. *pp. 577, San Francisco : Freeman, Cooper and Company (1970).*

Jorgensen, P.J., Bartlett, R.W.: High temperature transport processes in lithium niobate. *J. Phys. Chem. Solids 30, 2639-2648 (1969).*

Karabelas, A.J.: Particle attrition in shear flow of concentrated slurries. *Am. Inst. Chem. Eng. J. 22, 765-771 (1976).*

Kern, H.: The effect of high temperature and high confining pressure on compressional wave velocities in quartz-bearing and quartz-free igneous and metamorphic rocks. *Tectonophysics 44, 185-203 (1978).*

Kern, H.: Effect of high-low quartz transition on compressional and shear wave velocities under high pressure (in prep.).

Kern, H., Fakhimi, M.: Effect of fabric anisotropy on compressional-wave propagation in various metamorphic rocks for the range 20°C - 700°C at 2 kbars. *Tectonophysics 28, 227-244 (1975).*

Kern, H., Karl, F.: Eine dreiaxial wirkende Gesteinspresse mit Heizvorrichtung. *Bergbauwissenschaften 16 (3), 90-92 (1969).*

Komar, P.D.: Mechanical interactions of phenocrysts and flow differentiation of igneous dikes and sills. *Geol. Soc. Am. Bull. 83, 973-988 (1972-a).*

Komar, P.D.: Flow differentiation in igneous dikes and sills: profiles of velocity and phenocryst concentration. *Geol. Soc. Am. Bull. 83, 3443-3448 (1972-b).*

Komar, P.D.: Phenocryst interactions and the velocity profile of magma flowing through dikes or sills. *Geol. Soc. Am. Bull.* <u>*87*</u>, *1336-1342* *(1976)*.

Koster van Groos, A.F.K., Ter Heege, J.P.T.: The high-low quartz transition up to 10 kilobars pressure. *J. Geol.* <u>*81*</u>, *717-724 (1973)*.

Kroenke, L.W., Manghnani, M.H., Rai, C.S., Fryer, P., Ramananantoandro, R.: Elastic properties of selected ophiolitic rocks from Papua New Guinea : Nature and composition of oceanic crust and upper mantle. *In:* *The Geophysics of the Pacific Basin and its margin (G.H. Sutton, M.H. Manghnani, R. Moberly, eds.).* *Am. Geophys. Union Monogr.* <u>*19*</u>, *407-421 (1976)*.

Kushiro, I.: Changes in viscosity and structure of melt of $NaAlSi_2O_6$ composition at high pressures. *J. Geophys. Res.* <u>*81*</u>, *6347-6350 (1976)*.

Kushiro, I., Yoder, H.S., Jr., Mysen, B.O.: Viscosities of basalt and andesite melts at high pressures. *J. Geophys. Res.* <u>*81*</u>, *6351-6356* *(1976)*.

Kuster, G.T., Toksöz, M.N.: Velocity and attenuation of seismic waves in two-phase media. *Geophysics* <u>*39*</u>, *587-618 (1974)*.

Ladanyi, B.: Discussion of W.F. Brace and R.J. Martin's paper "A test of the law of effective stress for crystalline rocks of low porosity". *Int. J. Rock Mech. Min. Sci.* <u>*7*</u>, *123-124 (1970)*.

Lambe, T.W., Whitman, R.V.: Soil mechanics. *pp. 553, New York - London - Sydney - Toronto : John Wiley and Sons (1969)*.

Landau, L.D., Lifshitz, E.M.: Theory of elasticity. *pp. 134, London - New York - Paris - Los Angeles : Pergamon Press (1959)*,

Liebermann, R.C., Ringwood, A.E., Mayson, D.J., Major, A.: Hot pressing of polycrystalline aggregates at very high pressure for ultrasonic measurements. *Proc. 4th Int. Conf. High Pressure, Kyoto, 495-502, 1974*.

Martin, R.J.: Time-dependent crack growth in quartz and its application to the creep of rocks. *J. Geophys. Res.* <u>*77*</u>, *1406-1419 (1972)*.

Mehnert, K.R.: Migmatites and the origin of granitic rocks. *pp.393, Amsterdam - London - New York : Elsevier Publishing Company (1968)*.

Mehnert, K.R., Büsch, W., Schneider, G.: Initial melting at grainboundaries
        of quartz and feldspar in gneisses and granulites. *Neues Jahrb.*
        Mineral. Monatsh. *4*, 165-183 (1973).

Meissner, R., Fakmimi, M.: Seismic anisotropy as measured under high-
        pressure, high-temperature conditions. *Geophys. J. Roy. astr. Soc.*
        49, 133-143 (1977).

Montgomery, C.W., Brace, W.F.: Micropores in plagioclase. *Contrib. Mineral.*
        Petrol. *52*, 17-28 (1975).

Morgenstern, M.: Maximum entropy of granular materials. *Nature* *200*,
        559-560 (1963).

Murase, T., McBirney, A.R.: Properties of some common igneous rocks and
        their melts at high temperatures. *Geol. Soc. Am. Bull.* *84*, 3563-3592
        (1973).

Murrell, S.A.F., Chakravarty, S.: Some new rheological experiments on
        igneous rocks at temperatures up to 1120°C. *Geophys. J. Roy. astr.*
        Soc. *34*, 211-250 (1973).

Murrell, S.A.F., Ismail, I.A.H.: The effect of temperature on the strength
        at high confining pressure of granodiorite containing free and
        chemically-bound water. *Contrib. Mineral. Petrol.* *55*, 317-330 (1976).

Nicolas, A., Poirier, J.P.: Crystalline plasticity and solid state flow
        in metamorphic rocks. *pp. 444, London - New York - Sydney - Toronto :*
        John Wiley and Sons (1976).

Nur, A., Simmons, G.: The effect of saturation on velocity in low porosity
        rocks. *Earth Planet. Sci. Lett.* *7*, 183-193 (1969).

Nur, A., Simmons, G.: The origin of small cracks in igneous rocks.
        Int. J. Rock Mech. Min. Sci. *7*, 307-314 (1970).

O'Connell, R.J., Budiansky, B.: Seismic velocities in dry and saturated
        cracked solids. *J. Geophys. Res.* *79*, 5412-5426 (1974).

O'Connell, R.J., Budiansky, B.: Viscoelastic properties of fluid-saturated
        cracked solids. *J. Geophys. Res.* *82*, 5719-5735 (1977).

Paterson, M.S.: The ductility of rocks. *In: Physics of strength and*
        plasticity (A.S. Argon, ed.) p. 377-392. Cambridge, Massachusetts :
        M.I.T. Press (1969).

Paterson, M.S.: A high-pressure, high-temperature apparatus for rock deformation. *Int. J. Rock Mech. Min. Sci.* *7*, 517-526 (1970).

Paterson, M.S.: Nonhydrostatic thermodynamics and its geologic applications. *Rev. Geophys. Space Phys.* *11*, 355-389 (1973).

Paterson, M.S.: Experience with an internally heated gas-medium deformation apparatus to 500 MPa. *2nd Int. Conf. on High Pressure Engineering, Brighton, 1975. Pub. by The Institution of Mechanical Engineers (1977).*

Paterson, M.S.: Experimental rock deformation : The brittle field. *pp. 254 Berlin - Heidelberg - New York : Springer Verlag (1978).*

Raleigh, C.B., Paterson, M.S.: Experimental deformation of serpentinite and its tectonic implications. *J. Geophys. Res* *70*, 3965-3985 (1965).

Ramananantoandro, R., Manghanani, M.H.: Temperature dependence of the compressional wave velocity in an anisotropic dunite : Measurements to 500°C at 10 kbar. *Tectonophysics* *47*, 73-84 (1978).

Riecke, E.: Ueber das Gleichgewicht zwischen einem festen, homogen deformirten Körper und einer flüssigen Phase, insbesondere über die Depression des Schemlzpunktes durch einseitige Spannung. *Ann. Phys.* *54*, 731-738 (1895),

Robie, R.A., Bethke, P.M., Toulmin, M.S., Edwards, J.L.: X-ray crystallographic data, densities, and molar volumes of minerals. *In: Handbood of physical constants (S.P. Clark, Jr., ed.). Geol. Soc. Am. Mem.* *97*, 27-73 (1966).

Roscoe, K.H., Schofield, A.N., Wroth, C.P.: On the yielding of soils. *Géotechnique* *8*, 22-53 (1958).

Roscoe, R.: The viscosity of suspensions of rigid spheres. *British J. Appl. Phys.* *3*, 267-269 (1952).

Rutter, E.H.: The effects of strain-rate changes on the strength and ductility of Solenhofen limestone at low temperatures and confining pressures. *Int. J. Rock Mech. Min. Sci.* *9*, 183-189 (1972).

Sabatier, G.: Influence de la teneur en eau sur la viscosité d'une rétinite, verre ayant la composition chimique d'un granite. *Compt. Rend.* *242*, 1340-1342 (1956).

Scarfe, C.M.: Viscosity of basic magmas at varying pressure. *Nature Phys. Sci.* *241*, 101-102 (1973).

Schlue, J.W., Knopoff, L.: Shear wave anisotropy in the upper mantle of the Pacific basin. *Geophys. Res. Lett.* *3*, 359-362 (1976).

Scholz, C.H.: Static fatigue of quartz. *J. Geophys. Res.* *77*, 2104-2114 (1972).

Selig, E.T., Ladd, R.S., eds.: Evaluation of relative density and its role in geotechnical projects involving cohesionless soils. *ASTM Spec. Tech. Publ.* *523*, 1-510 (1973).

Shaw, H.R.: Obsidian – H_2O viscosities at 1000 and 2000 bars in the temperature range 700°C to 900°C. *J. Geophys. Res.* *68*, 6337-6343 (1963).

Shaw, H.R.: Comments on viscosity, crystal settling, and convection in granitic magmas. *Am. J. Sci.* *263*, 120-152 (1965).

Shaw, H.R.: Rheology of basalt in the melting range. *J. Petrol.* *10*, 510-535 (1969).

Shaw, H.R.: Viscosities of magmatic silicate liquids : An empirical method of prediction. *Am. J. Sci.* *272*, 870-893 (1972).

Shaw, H.R.: Diffusion of H_2O in granitic liquids. Part I. Experimental data. Part II. Mass transfer in magma chambers. *In: Geochemical transport and kinetics (A.W. Hofmann, B.J. Giletti, H.S. Yoder, Jr., R.A. Yund, eds.), p. 139-170. Washington : Carnegie Institution* (1974).

Shaw, H.R., Wright, T.L., Peck, D.L., Okamura, R.: The viscosity of basaltic magma : An analysis of field measurements in Makaopuhi lava lake, Hawaii. *Am. J. Sci.* *266*, 225-264 (1968).

Simmons, G.: Velocity of shear waves in rocks to 10 kilobars, 1. *J. Geophys. Res.* *69*, 1123-1130 (1964).

Simmons, G., Brace, W.F.: Comparison of static and dynamic measurements of compressibility of rocks. *J. Geophys. Res.* *70*, 5649-5656 (1965).

Simmons, G., Wang, H.: Single crystal elastic constants and calculated aggregate properties : A handbook. *p. 370, Cambridge, Mass. : M.I.T. Press* (1971).

Skinner, B.J.: Thermal expansion. *In: Handbook of physical constants (S.P. Clark, Jr., ed.).* Geol. Soc. Am. Mem. *97*, 75-96 (1966).

Smith, C.S.: Grains, phases and interfaces: an interpretation of microstructure. *American Institute of Mining and Metallurgical Engineers. Technical publ.* *2837* *(Class E)*, 1-37 (1948).

Sparks, R.S.J., Pinkerton, H., MacDonald, R.: The transport of xenoliths in magmas. *Earth Planet. Sci. Lett.* *35*, 234-238 (1977).

Spencer, J.W., Jr., Nur, A.: The effect of pressure, temperature and pore water on velocities in Westerly granite. *J. Geophys. Res.* *81*, 899-904 (1976).

Sprunt, E.S., Brace, W.F.: Direct observation of microcavities in crystalline rocks. *Int. J. Rock. Mech. Min. Sci. Geomech. Abstr.* *11*, 139-150 (1974).

Stewart, R., Peselnick, L.: Velocity of compressional waves in dry Franciscan rocks to 8 kbar and 300°C. *J. Geophys. Res.*, *82*, 2027-2039 (1977).

Stocker, R.A., Ashby, M.F.: On the rheology of the upper mantle. *Rev. Geophys. Space Phys.* *11*, 391-426 (1973).

Terzaghi, K., Peck, R.B.: Soil mechanics in engineering practice. *pp. 729, New York - London - Sydney : John Wiley and Sons (1967).*

Tullis, J., Yund, R.A.: Experimental deformation of dry Westerly granite. *J. Geophys. Res.* *82*, 5705-5718 (1977).

Van Wazer, J.R., Lyons, J.W., Kim, K.Y., Colwell, R.E.: Viscosity and flow measurement. *pp. 406, New York : Interscience (1963).*

Waff, H.S.: Pressure-induced coordination changes in magmatic liquids. *Geophys. Res. Lett.* *2*, 193-196 (1975).

Walsh, J.B.: The effect of cracks on the uniaxial elastic compression of rocks. *J. Geophys. Res.* *70*, 399-411 (1965).

Wang, H.F., Simmons, G.: Microcracks in crystalline rock from 5.3 km depth in the Michigan basin. *J. Geophys. Res.* *83*, 5849-5856 (1978).

Warren, N., Anderson, O.L.: Elastic properties of granular materials under uniaxial compaction cycles. *J. Geophys. Res.* *78*, 6911-6925 (1973).

Watt, J.P., Davies, G.F., O'Connell, R.J.: The elastic properties of composite materials. *Rev. Geophys. Space Phys.* *14*, 541-563 (1976).

Whitney, J.A.: The effects of pressure, temperature, and X_{H_2O} on phase assemblage in four synthetic rock compositions. *J. Geol.* *83*, 1-31 (1975).

Winkler, H.G.F.: Petrogenesis of metamorphic rocks (3rd ed.). *pp. 320, Berlin - Heidelberg - New York : Springer (1974).*

Yoder, H.S., Jr.: Generation of basaltic magma. *pp. 265, Washington D.C.: National Academy of Sciences (1976)*.

Youd, T.L.: Factors controlling maximum and minimum densities of sands. *p. 98-112 in Selig, E.T., Ladd, R.S. eds., (1973).*

Zener, C.: Elasticity and analasticity of metals. *pp. 163, Chicago, Illinois : University of Chicago Press (1948).*